Universidade de Aveiro Departamento de Engenharia Mecânica
2017

Ana Margarida Ramos Bola

Proposta de Teste Pré-Clínico Para Aferir o Desempenho Biomecânico de Próteses do Ombro

Proposal of a Pre-Clinical Test to Assess the Biomechanical Performance of Shoulder Prostheses

Tese apresentada à Universidade de Aveiro para cumprimento dos requisitos necessários à obtenção do grau de Doutor em Engenharia Mecânica, realizada sob a orientação científica do Professor Doutor António Manuel de Amaral Monteiro Ramos, Professor Auxiliar do Departamento de Engenharia Mecânica da Universidade de Aveiro e do Professor Doutor José António de Oliveira Simões, Professor Associado com Agregação da Universidade de Aveiro.

Apoio financeiro da FCT através da bolsa SFRH/BD/71162/2010

Ao Pedro e à Matilde, por todo o amor, apoio e alegria.

o júri

presidente

Doutor Artur Manuel Soares da Silva
Professor Catedrático do Departamento de Química da Universidade de Aveiro

Doutor João Orlando Marques Gameiro Folgado
Professor Associado do Instituto Superior Técnico, Lisboa

Doutor Mário Augusto Pires Vaz
Professor Associado da Faculdade de Engenharia da Universidade do Porto

Doutor João Manuel da Costa Ferreira Torres
Professor Auxiliar Convidado da Faculdade de Medicina da Universidade do Porto

Doutor Jorge Augusto Fernandes Ferreira
Professor Auxiliar do Departamento de Engenharia Mecânica da Universidade de Aveiro

Doutor António Manuel de Amaral Monteiro Ramos
Professor Auxiliar do Departamento de Engenharia Mecânica da Universidade de Aveiro

agradecimentos

Em primeiro lugar gostaria de expressar o meu sincero agradecimento ao meu orientador, Professor Doutor António Manuel de Amaral Monteiro Ramos, por todo o apoio e incentivo que me ofereceu. Ao Professor Doutor José António de Oliveira Simões, que também orientou o trabalho de investigação, o meu agradecimento pela sua disponibilidade. Aprendi muito convosco.

Ao Dr. José Manuel Lourenço agradeço a amabilidade e simpatia com que nos recebeu no seu consultório, a rapidez com que me ajudou sempre que necessitei e a disponibilidade imediata e desinteressada com que se deslocou a nossa casa para realizar a artroplastia experimental.

Ao Enfermeiro Ricardo Nóbrega, da BIOMET Portugal, agradeço os implantes facultados bem como todo o material cirúrgico necessário para realizar a artroplastia. Agradeço ainda a sua ajuda durante a realização da mesma.

Ao Engenheiro António Festas, pela sua disponibilidade sempre que solicitado.

A todos os amigos que fiz no grupo de Biomecânica e no grupo GRIDS, que me acolheram, ensinaram, ajudaram e distraíram, tantas vezes! Obrigada!

Finalmente agradeço aos meus familiares e amigos mais próximos, pela compreensão e ânimo que sempre me ofereceram.

palavras-chave

Teste pré-clínico, articulação glenohumeral, prótese anatómica, modelos *in vitro*, modelos de elementos finitos

resumo

A comercialização de uma prótese requer o cumprimento de regulamentos e normas que garantam a segurança de utilização da mesma. No entanto, diversas próteses têm sido retiradas do mercado devido às elevadas taxas de insucesso que apresentam, sendo este um forte indicador da falta de testes adequados que permitam uma avaliação mais rigorosa do seu desempenho e eficácia. Deste modo, o principal objetivo desta tese de doutoramento consistiu no desenvolvimento de um ensaio pré-clínico capaz de aferir o desempenho biomecânico de próteses do ombro. Para o efeito, numa primeira fase foi utilizado um modelo multi-corpo do ombro intacto contendo todos os grupos musculares com vista a identificar e caracterizar os que mais contribuem para o movimento de abdução de 90°, sendo eles o deltoide, o infraespinhal, o supraespinhal e o subescapular. Foram construídos dois modelos *in vitro* recorrendo a estruturas ósseas compósitas do úmero e da escápula. No modelo intacto foram consideradas as cartilagens e o ligamento glenohumeral inferior e no modelo implantado foi utilizada uma prótese anatómica não cimentada (Comprehensive® Total Shoulder System) e um pino central de fixação da componente da glenoide revestido com metal poroso. Rosetas de extensometria foram utilizadas para medir as extensões sofridas pelas estruturas ósseas quando posicionadas a 90º de abdução e sob carregamento. Foram desenvolvidos modelos de elementos finitos (EF) do ombro intacto e implantado que replicam os modelos *in vitro*. Os modelos de EF foram sujeitos aos mesmos cenários de carregamento que os modelos *in vitro.* A comparação entre as deformações determinadas numericamente e experimentalmente permitiu a validação dos modelos de EF.

A distribuição de tensões e deformações no interior das estruturas ósseas, determinadas com o modelo de EF do ombro implantado, estão de acordo com as observações clínicas presentes na literatura. Isto indica que, de uma forma geral, o modelo de EF desenvolvido prevê o comportamento do osso na presença de uma prótese e pode ser considerado um teste pré-clínico para avaliação do desempenho de implantes do ombro. Para verificar que o teste pré-clínico desenvolvido é sensível a pequenas diferenças no design dos implantes e que pode ser utilizado para prever o desempenho de próteses, foi utilizado um novo pino central de fixação em polietileno. A distribuição de tensões e de deformações determinadas através do modelo de EF usando o novo pino de fixação estão (mais uma vez) de acordo com as observações clínicas, o que confirma que o modelo de EF desenvolvido pode ser utilizado na avaliação pré-clínica de outros implantes do ombro, permitindo analisar o seu desempenho antes da utilização clínica.

keywords

Pre-clinical test, glenohumeral joint, anatomical prosthesis, *in vitro* models, finite element models

abstract

Prosthesis commercialization requires the compliance of regulations that ensure the safe use of prosthesis. However, several prostheses have been withdrawn from the market due to their high failure rates, which is a strong indicator of the lack of suitable pre-clinical tests that allow a more rigorous evaluation of its performance and effectiveness. Thus, the main objective of this doctoral thesis consisted in the development of a pre-clinical test capable of accessing shoulder prosthesis performance. For this purpose, a multi-body model of the intact shoulder containing all muscle groups was used in the first stage in view to identify and characterize those that most contribute to the 90º abduction movement, being them the deltoid, the infraspinatus, the supraspinatus and the subscapularis. Two *in vitro* models were constructed using composite bone structures of the humerus and of the scapula. In the intact model the cartilage and the inferior glenohumeral ligament were considered and in the implanted model a non-cemented anatomical prosthesis (Comprehensive® Total Shoulder System) and a central post in porous metal for glenoid fixation were used. Strain gage rosettes were used to measure the deformation suffered by the bone structures when positioned at 90º abduction and subjected to loading. Finite element models (FEM) of the intact and implanted shoulder, that replicate the *in vitro* models, were developed. The FEM were subjected to the same loading scenarios as the *in vitro* models. The comparison between the strains determined numerically and experimentally allowed FEM validation.

Stress and strain distribution inside the bone structures, determined with the FEM of the implanted shoulder, agree with the clinical observations present in literature. This indicates that, in a general way, the developed FEM predicts bone behavior in the presence of a prosthesis and may be considered a pre-clinical test to evaluate shoulder implants performance. To verify that the pre-clinical test developed is sensitive to small differences in implant design and that can be used to predict shoulder prosthesis performance, a new central fixation post in polyethylene was used. Stress and strain distributions determined using the FEM with the new fixation post are (once again) in agreement with clinical observations, confirming that the developed FEM can be used for the pre-clinical evaluation of other shoulder implant designs, allowing to analyze their performance before clinical use.

Contents

List of Acronyms

3D	Three-Dimensional
AAR	Average Aspect Ratio
AH	Anterior Humerus
AR	Aspect Ratio
CAM	Computer Aided Manufacturing
COR	Centre of Rotation
CPR	Cumulative Percent of Revision
CT	Computer Tomography
DOF	Degrees Of Freedom
DSEM	Delft Shoulder and Elbow Model
DSM	Delft Shoulder Model
EMG	Electromyography
EU	European Union
FE	Finite Element
FEM	Finite Element Model
GH-JRF	Glenohumeral Joint Reaction Force
H	Height
HA	Hemiarthroplasty
HDPE	High-Density Polyethylene
IGHL	Inferior Glenohumeral Ligament
LHBT	Long Head of Biceps Tendon
MRI	Magnetic Resonance Imaging
PCSA	Physiologic Cross Sectional Area
PE	Polyethylene
PMMA	Polymethylmethacrylate
RLL	Radiolucent Lines
ROM	Range of Motion
RTV	Room Temperature Vulcanization
SD	Standard Deviation
SMR	Shoulder Modular Replacement
TSA	Total Shoulder Arthroplasty
UHMWPE	Ultra-High Molecular Weight Polyethylene
WOOS	Western Ontario Osteoarthritis of the Shoulder

Introduction

The shoulder joint arises from the close relationship between the humeral head and the glenoid cavity. Due to the small contact area between these two bone structures this is the most moveable joint of the human body, requiring a high muscular control to be stable.

The combination between a high instable joint and a high physical activity – observed over the last decades in the adult population – has led to the rise of shoulder trauma and of joint replacement with prostheses. This procedure is known as shoulder arthroplasty and is one of the last resources in the treatment of many shoulder pathologies.

In general, shoulder arthroplasty divides into two major categories: anatomic arthroplasty and inverted arthroplasty. Currently, the use of anatomic and inverted prostheses is well established and each concept is used in the treatment of a specific group of diseases. Moreover, the surgical procedures adopted have allowed the achievement of some success. Nevertheless, the advantages and disadvantages of both solutions still needs proper scientific validation and depends on the associated pathologies.

Despite the relative success of shoulder arthroplasty, prostheses continue to present problems, mainly related with the glenoid implant and less with the humeral implant. More specifically, the most common complications are related with the ease with which glenoid component loosens from bone, known as glenoid loosening.

To overcome implant-related problems, many designs have been developed and even though the European Union (EU) has established specific directives (93/42/EEC) to regulate and ensure the safety of implants, prostheses that have been recalled from market due to high failure rates are still a reality, such as the Comprehensive Reverse Shoulder® withdrawn in February 2017 by Zimmer Biomet. This and other cases corroborate our conviction that EU directives are not evaluating prostheses efficiency, but only their safety. Due to the implications that this problem has on public health, it is essential to understand and evaluate the causes of failure of shoulder prosthesis to find the most reliable solutions.

Thus, the main objective of this PhD thesis was to develop and propose a numerical pre-clinical test to predict short and long-term performance of anatomical shoulder prosthesis before entering the market.

The pre-clinical test developed is based on a finite element model (FEM), validated both experimentally and with clinical data. For the experimental validation, an experimental model, using synthetic bone structures, was developed. The synthetic bone structures replicate well the behaviour of real bone and allow the generation of qualitative and quantitative information appropriate to the proposed objectives. With the FEM is possible to investigate different bone/implant interfaces and analyse the stress/strain patterns of bone structures and of the implants used in the study.

The specific objectives of this study were the following:

- To develop experimental models of the intact and implanted shoulder joint (that is, with prostheses), using composite bone structures;
- To develop FEM of the intact and implanted shoulder joint;
- To validate the FEM using the experimental models developed;
- To analyse the different bone/implant interfaces in the implanted model;
- To correlate the numerical results with the clinical predictions available in literature;
- To purpose a numerical pre-clinical test that can predict short- and long-term performance of shoulder implants.

The thesis, excluding this introduction, is organized into seven chapters. Chapter 1 begins with an extended presentation of shoulder anatomy, related pathologies and biomechanics. Shoulder arthroplasty, the several implants and fixation techniques are presented, as well as an overview of some arthroplasty registers with the goal of presenting the worldwide importance of the aspect under study.

Chapter 2 is dedicated to the modelling of shoulder muscle actions with the AnyBody Modelling System. The muscle recruitment and inverse dynamic problem are presented and the intact shoulder model is used to determine the most important muscles in shoulder abduction, as well as the muscle forces employed by each muscle to perform the referred movement. A reduced model of the intact shoulder is purposed.

In Chapter 3, the shoulder simulator developed in this thesis and the experimental models of the intact and implanted shoulder are presented. The *in vitro* models were built with synthetic bone structures of the humerus and scapula, the intact model comprise also the cartilage and the inferior glenohumeral ligament, whilst the implanted model comprises the Comprehensive Total Shoulder System (Biomet©) provided by Biomet Portugal.

Chapter 4 is focused on the development of the FEM of the intact and implanted shoulder and on their validation using the experimental data acquired and presented in Chapter 3. The chapter starts by presenting an overview of the existent shoulder models and of the general finite element modelling process. A detailed presentation of the development of the intact and implanted models is given, as well as of the mesh sensitivity analysis performed using the humeral bone structure and the humeral cartilage.

In Chapter 5 the numerical results are correlated with the clinical predictions available in literature. The clinical outcomes of the glenoid component and of the humeral component were presented for state-of-the art components and CT-scans available in literature were analysed for this purpose. The stress/strain distribution on the intact shoulder joint is analysed and the behaviour of the glenoid and humeral cartilage is also presented. The short-term post-operative scenario previewed by the FEM is compared with the clinical findings and the long-term post-operative previsions are also presented to evaluate the evolution of stress/strain behaviour and implant micromotions.

In Chapter 6 a polyethylene central fixation post is analysed with the pre-clinical test and compared with the previous results obtained for the titanium central fixation post. The purposed pre-clinical testing procedure is summarized.

The conclusions and future developments are presented in Chapter 7.

Chapter 1

Shoulder Articulation and Arthroplasty

Due to the complexity of the glenohumeral joint, this chapter describes an overview of the shoulder anatomy, its pathologies and biomechanics. It is expected that the reader can become familiar with some important concepts related with this joint.

1.1 The Shoulder

1.1.1 Anatomy

The shoulder is composed of three bones: the clavicle, the scapula and the proximal extremity of the humerus (Figure 1.1). The clavicle is in front of the torso, being the only bone connection between the torso and the upper limb. The scapula is approximately triangular, placed on a postero-lateral aspect of the thoracic cage; its main features are the acromion and the coracoid process. Together, the clavicle and the scapula form the shoulder girdle. Regarding the humerus, its main structures are the humeral head and the greater and lesser tubercles [1].

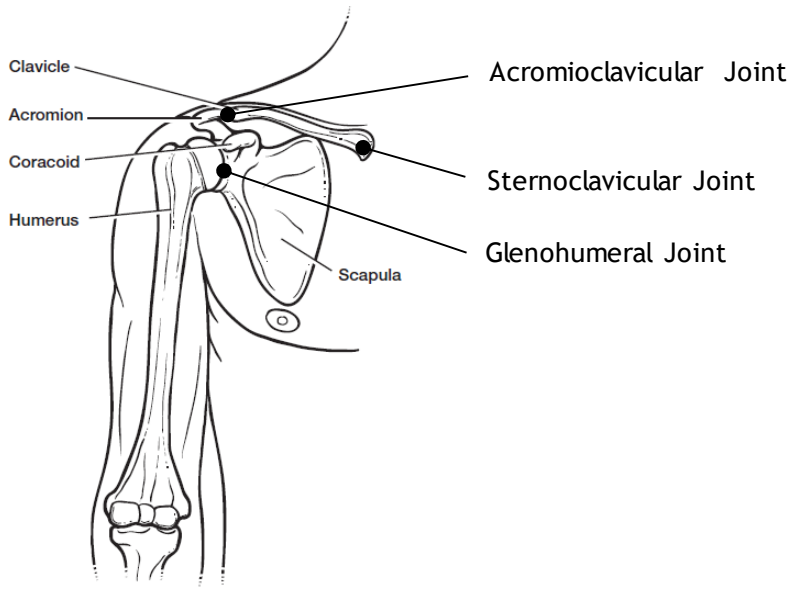

Figure 1.1. Shoulder bones and anatomical joints at the right arm. Adapted from [2].

Shoulder bones interact with each other by means of three anatomical joints (sternoclavicular joint, acromioclavicular joint and glenohumeral joint) and of a functional joint (scapulothoracic joint [1]).

The sternoclavicular joint is formed by the proximal end of the clavicle – clavicular part closest to the trunk – and the articular cavity of the manubrium (at the sternum), along with

a small part of the first rib cartilage, as represented in Figure 1.2 (A). This is the only joint attaching the upper extremity to the axial skeleton [3] and its articular cavity is surrounded by four ligaments: the anterior and posterior sternoclavicular ligaments, and the interclavicular and costoclavicular ligaments. Despite all studies, the classification of this joint gathers no consent between the scientific community, since some authors consider it as a plane-type synovial joint [1] and others as a saddle-type synovial joint [4]. Nevertheless, all agree that it has three degrees of freedom and a wide range of movements, mainly in the antero-posterior and longitudinal directions, with some rotation also possible.

Regarding the acromioclavicular joint, it is classified as plane-type synovial [5] and is established between the clavicle lateral end and the acromion medial margin, as shown in Figure 1.2 (B). Surrounding it is an articular capsule reinforced by the superior and inferior acromioclavicular ligaments, covering the joint superior and inferior parts, respectively. With three degrees of freedom, this articulation allows movements in the antero-posterior and longitudinal directions, as well as some axial rotation. The coracoclavicular ligament, identified in Figure 1.2 (B), is one important accessory ligament supporting the upper limb weight on the clavicle, keeping it correctly positioned. The sternoclavicular and acromioclavicular joints hold the shoulder girdle bones with each other and with the trunk, and the combined movements between these articulations cause a high degree of freedom of the upper limb.

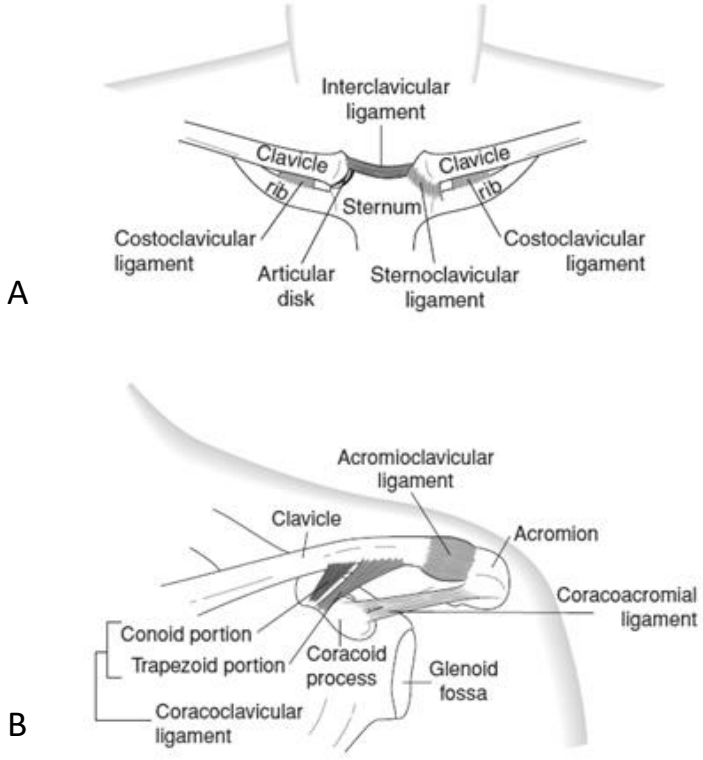

Figure 1.2. (A) sternoclavicular joint; (B) acromioclavicular join and their ligaments. Adapted from [6].

Between the humeral head and the small glenoid cavity is the glenohumeral joint, represented in Figure 1.3. This is the human joint with the highest mobility and, hence, less stability. Considered the main articulation of the shoulder – and therefore called the shoulder joint – it consists of a spherical head in one bone extremity, and a socket in the other bone extremity. It is classified as a synovial ball-and-socket joint [4].

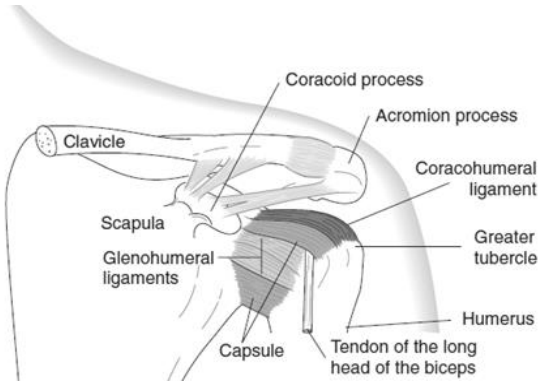

Figure 1.3. The glenohumeral joint and their ligaments. Adapted from [6].

The right coronal section of the glenohumeral joint is represented in Figure 1.4 (A). It shows that the superficial area of the humeral head is three to four times bigger than that of the glenoid with which it articulates. The glenoid is also lesser curve than the humeral head, and this fact allows the humerus to move linearly through it and to have some rotational movement. In the glenoid borders, there is a ring of fibrocartilage (the labrum) which deepens the cavity, making the joint more stable. The labrum is formed by the tendon of the biceps brachii long head and by the glenohumeral ligaments.

In addition to the glenohumeral ligaments, the other major shoulder ligaments are the coracoacromial ligament, forming an arched structure for humeral head protection (see Figure 1.2 (B)); the coracohumeral ligament, which strengthens the superior part of the articular capsule (see Figure 1.3); and the transverse humeral ligament, that contains the tendon of the biceps brachii long head [4]. Overall, the glenohumeral ligaments, the coracohumeral ligaments and the muscles crossing the joint stabilize the shoulder.

As stated before, the scapulothoracic joint is a functional joint, as it has no usual joint characteristics and it depends on both the acromioclavicular and sternoclavicular joints. Since the scapula is attached to the lateral end of the clavicle via the acromioclavicular joint, and the clavicle is attached to the axial skeleton by the sternoclavicular joint, any scapular movement on the thorax produces movement at either the acromioclavicular and sternoclavicular joints or at both [5].

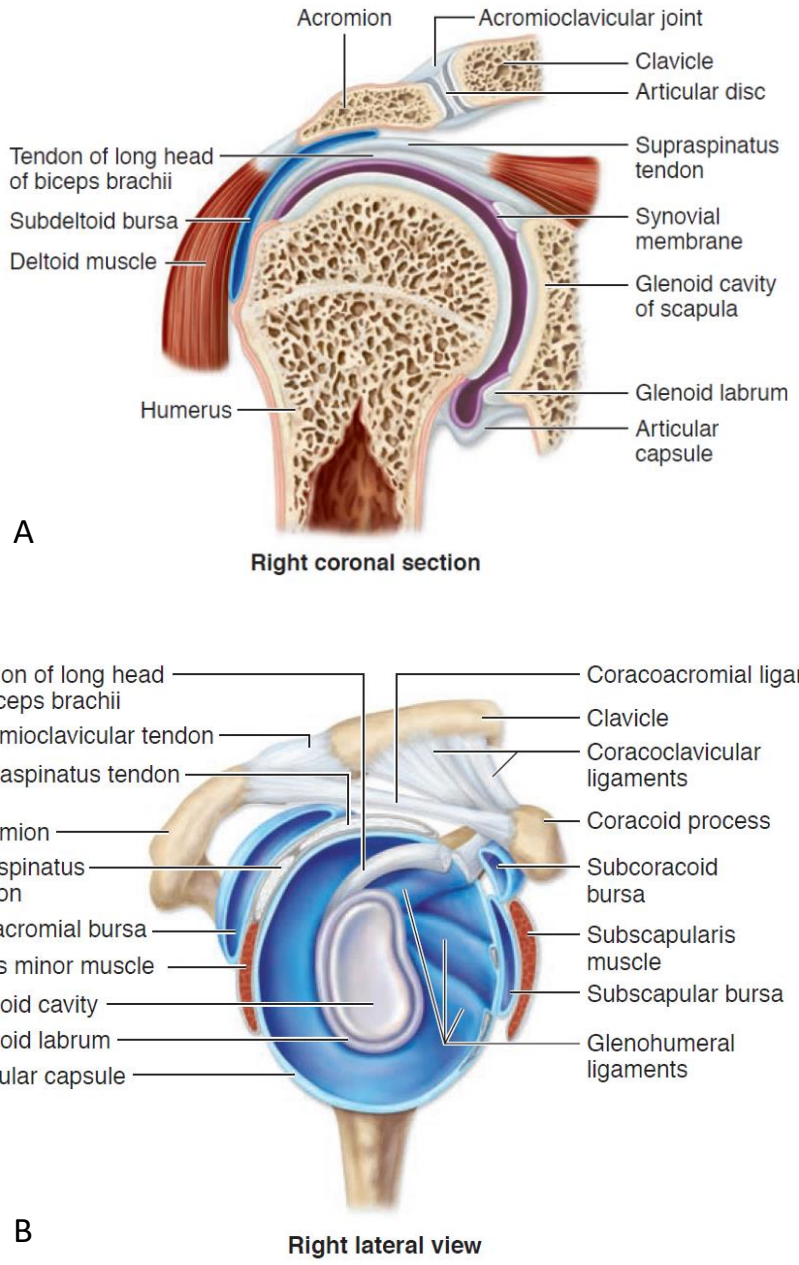

Figure 1.4. (A) Right coronal section and; (B) right lateral view of the glenohumeral joint. Adapted from [4].

The shoulder muscles, in Figure 1.5, are classified as scapulothoracic or glenohumeral, depending on their function. The scapulothoracic muscles control the shoulder girdle motion, originating at the axial skeleton and inserting at the clavicle and scapula. The trapezius, rhomboideus major and minor, levator scapulae, serratus anterior, pectoralis minor and subclavius belong to this group. The glenohumeral muscles cross the glenohumeral joint and control the arm. In this group are the deltoideus, coracobrachialis, teres major, subscapularis, supraspinatus, infraspinatus, teres minor, pectoralis major, latissimus dorsi and the biceps brachii and triceps brachii long heads.

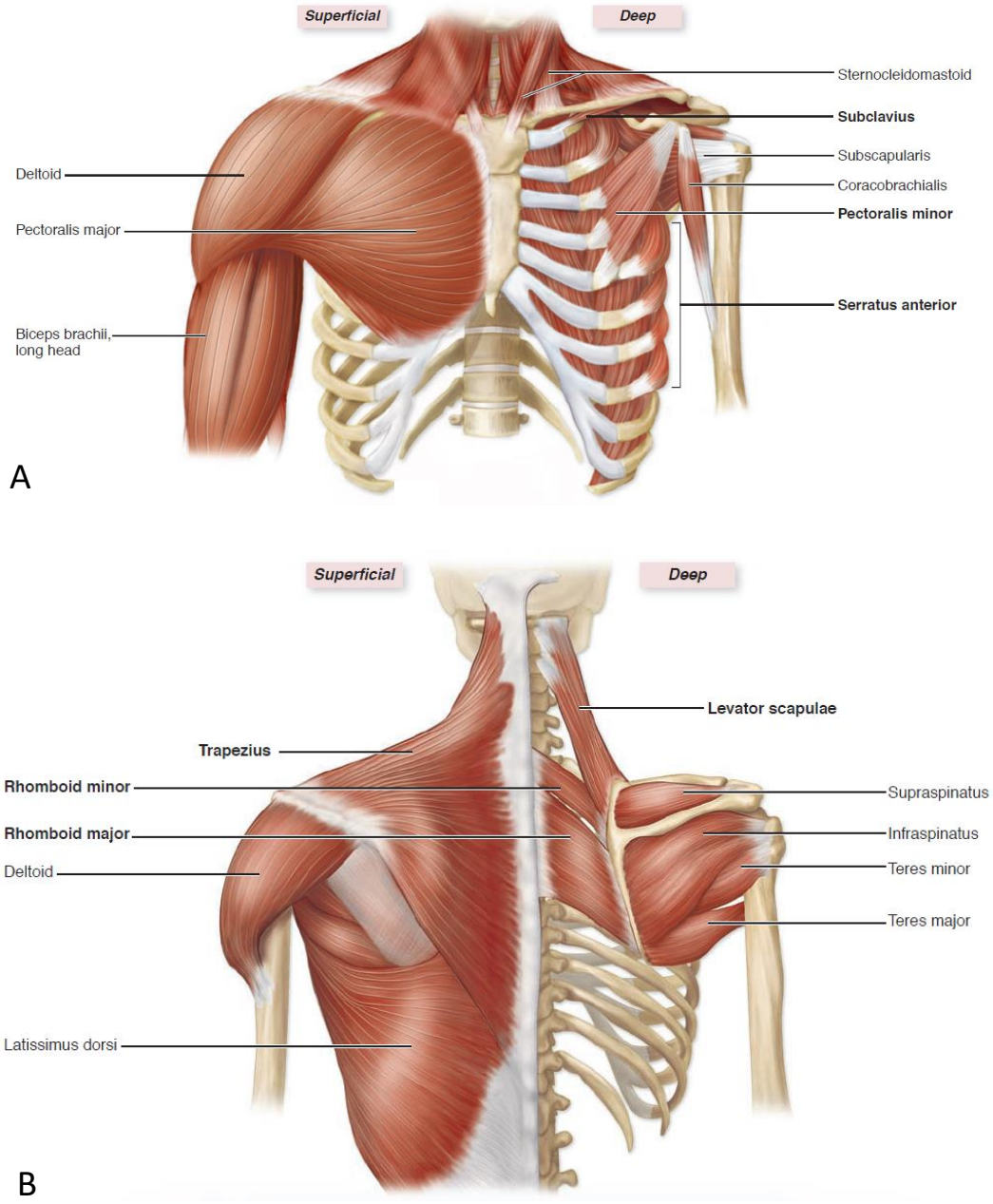

Figure 1.5. Glenohumeral and scapulothoracic muscles (in bold). Anterior (a) and posterior (b) views. Adapted from [7].

Pectoralis major and latissimus dorsi are the most important attachments of the arm to the trunk, originating at the axial skeleton and inserting at the humerus. The subscapularis, supraspinatus, infraspinatus and teres minor form the rotator cuff, illustrated in Figure 1.6. Along with the deltoideus, these are the most important muscles of the shoulder, as they unite the scapula to the humerus and supply strength and stability to the glenohumeral joint [7]. Their origin and insertion sites and main actions are gathered in Table 1.1.

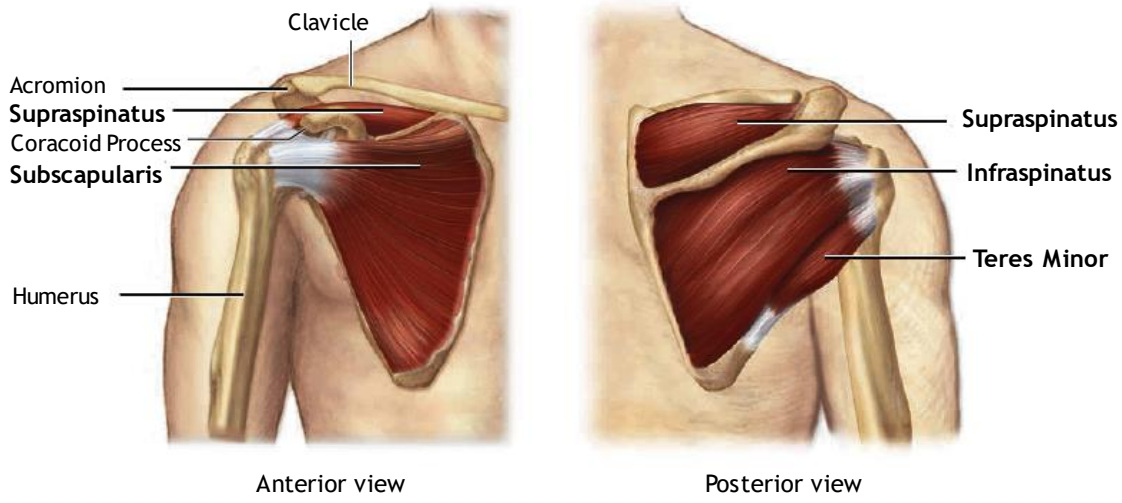

Figure 1.6. Rotator cuff muscles. Adapted from [7].

Table 1.1 - Features of the most important muscles of the shoulder complex [7].

Muscle	Origin (O) and Insertion (I)	Actions
Deltoideus	O: acromial end of the clavicle; acromion and scapular spine; I: all fibres insert in humeral tuberosity	Anterior fibres: flex and medially rotate the arm; Middle fibres: prime movers of arm abduction; Posterior fibres: extend and laterally rotate the arm.
Subscapularis	O: subscapular fossa of the scapula; I: lesser tubercle of the humerus.	Medially rotates the arm
Supraspinatus	O: supraspinatus fossa of the scapula; I: greater tubercle of the humerus;	Abducts the arm
Infraspinatus	O: infraspinatus fossa of the scapula; I: greater tubercle of the humerus.	Abducts and laterally rotates the arm
Teres minor	O: upper dorsal lateral border of the scapula; I: greater tubercle of the humerus.	Abducts and laterally rotates the arm

1.1.2 Pathologies

The pathologies of the shoulder joint mostly found are osteoarthritis and rheumatoid arthritis. Osteoarthritis, also known as degenerative arthritis, is frequently found in the elderly population and is characterized by the breakdown of articular cartilage, causing bone to rub against bone during arm movement, making the joint stiff and painful. The growth of bony spikes and swelling of the synovial membrane, surrounding the joints, are also characteristics of this disease [4]. Rheumatoid arthritis typically affects woman in their young and middle ages. This autoimmune disorder starts with synovial membrane inflammation; lately the articular cartilage and bone become eroded, and the scar formed ossifies, immobilizing the joint. Besides pain and joint swelling, muscle weakness and osteoporosis are also present, as well as problems related with the heart and blood [4].

Humeral fractures are also common, being normally subdivided into categories, according with its severity [8]. Concerning humeral dislocations, there are two main types: anterior humeral dislocation and partial humeral dislocation. Application of an enforced shoulder abduction, along with a lateral rotation, leads to anterior humeral dislocation, causing the humeral head to move out of the glenoid fossa in the anterior direction. Partial humeral dislocation happens when the muscles are unable to hold the humeral head in the glenoid fossa, which is known as glenohumeral subluxation. This muscular paralysis, associated with the force of gravity and with arm weight promotes humeral dislocation [1].

Regarding shoulder disorders related with muscles, a tear of the rotator cuff with loss of glenohumeral cartilage and alterations of the glenohumeral joint, leading to humeral head instability, is characteristic of rotator cuff tear arthropathy. The upward movement of the humeral head causes subacromial impingement, where the rotator cuff muscles, the long head of the biceps and the subacromial bursa are compressed between the acromial arch, the humeral head and the coracoacromial ligament during overhead activities, causing pain [1]. The humeral head movement will eventually erode the anterior part of the acromion, as well as the acromioclavicular joint. Furthermore, the incorrect placement of the humeral head may lead to glenoid erosion in such an extent that the coracoid becomes eroded too.

There are other chronic conditions causing pain at the shoulder, like tumour, osteonecrosis, or the Hill-Sachs defect, but all present small incidence rates.

1.1.3 Biomechanics

With the objective of better describing human movement, the body is divided in eight parts with the help of three fixed planes: sagittal plane, frontal plane and transverse plane. Each one is perpendicular to the other and all intersect at the centre of gravity. The sagittal plane (or medial) divides the body into right and left parts. A body structure closer to it is called medial, and one far from it is called lateral. The frontal plane (or coronal), divides the body into anterior and posterior parts (or front and back parts, respectively). Lastly, the

transverse plane (horizontal or cross-sectional) divides the body into superior and inferior parts (or upper and lower parts, respectively) [9].

There are also three main axes of movement: sagittal, frontal and vertical. The sagittal is included on the sagittal plane and movements around it occur on the frontal plane. On its turn, frontal axis is included on the frontal plane, and movements around this axis occur on the sagittal plane. Finally, the vertical axis is determined by the intersection of the frontal with the sagittal plane and movements around this axis occur on the transverse plane [9].

The glenohumeral joint has six degrees of freedom that allow superior member orientation in relation to the three planes of movement, but if the glenohumeral joint is stable, small translations can be neglected [3]. Shoulder movements comprise four groups: flexion, extension and hyperextension in the first group; abduction and adduction in the second; lateral and medial rotation in the third and horizontal abduction and adduction in the fourth [9] (Figure 1.7).

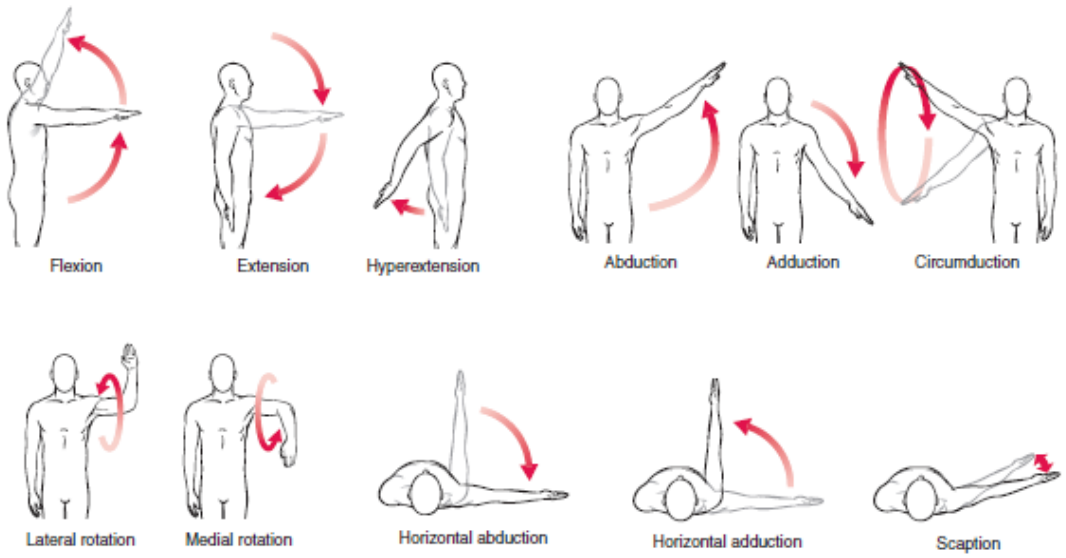

Figure 1.7. Shoulder joint motions. Adapted from [9].

Shoulder complex range of motion (ROM) is still a question of debate in the scientific community [10]. Nevertheless, there is consent that humerus movement is restricted if kept in neutral or medial rotation, since in abduction there is impingement of the greater tubercle on the coracoacromial arch, only avoided by humeral lateral rotation. Nevertheless, it is generally accepted that flexion/extension and abduction/adduction have about 180° of motion, with nearly 45° of hyperextension. Regarding lateral/medial rotation, 90° of amplitude is possible, while only about 30° of horizontal abduction and 120° of horizontal adduction [9]. Despite the importance of maximum ROM, daily living activities are

performed without making use of such a wide range, as attested in several studies [11, 12].

The existing relationship between glenohumeral and scapulothoracic joints is still a topic of discussion [13, 14]. Thanks to different measuring techniques, motions studied, or type and number of subjects involved, comparison of conclusions between the several studies is a difficult task. Nonetheless, it became clear that for the first 30° of elevation, glenohumeral joint motion is very inconsistent and during the last 60° the contribution of both glenohumeral and scapulothoracic joints is equivalent. The classic study of Inman *et al.* [15], that analysed 2D radiographs in order to document scapular position, shows an overall ratio of 2:1 between humeral and scapular movement. This is known as shoulder rhythm or scapulothoracic rhythm and it is still accepted as correct by the scientific community.

Abduction and flexion of the glenohumeral joint present many biomechanical affinities. In the case of abduction, the deltoideus and the supraspinatus muscles are the prime movers, whilst in flexion the anterior deltoideus fibres are the ones controlling movement. Like in many other cases, the deltoideus muscle force $(\overrightarrow{F_D})$ is composed of a translational $(\overrightarrow{F_{Dt}})$ and a rotational component $(\overrightarrow{F_{Dr}})$. In the case of the arm hanging at the side, the translational component is the largest one, as the scheme of Figure 1.8 (A) shows, meaning that most of the deltoideus force causes superior translation of the humeral head and only a small force causes humeral rotation. Consequently, the translational force applied to the humerus does not serve to its stabilization. Therefore, if the translational force component is not opposed, impact of the humeral head on the coracoacromial arch will occur [5].

Since to produce movement the deltoideus force must exceed that of gravity, it becomes clear that another arrangement of forces needs to be added to the system, to counterbalance the effect of the translational component and to avoid impingement. This function is attributed to infraspinatus, subscapularis and teres minor, whose lines of action are exposed in Figure 1.8 (A). When the resultant force of these muscles $(\overrightarrow{\sum F})$ is divided into its translational $(\overrightarrow{F_t})$ and rotational $(\overrightarrow{F_r})$ components (see Figure 1.8 (B)), it becomes clear that the rotational force component compresses the humeral head against the glenoid fossa, also causing the humerus to rotate. On the other hand, the translational component is mandatory in the process of joint stabilization, since it almost cancels the translational force component of the deltoideus muscle, consequently working to avoid impingement [5].

Concerning supraspinatus muscle, belonging to the rotator cuff, it does not counterbalance the deltoideus translational force component $(\overrightarrow{F_{Dt}})$ because its own translational force component $(\overrightarrow{F_{SPt}})$ has the same direction as $\overrightarrow{F_{Dt}}$, as represented in Figure 1.9. However, this muscle is an effective glenohumeral joint stabilizer, since its rotational part generates a strong compressive force against the scapula. Furthermore, this component has a large moment arm capable of generating almost completed range of motions of the joint and, with the assistance of gravity, it is able to stabilize the glenohumeral joint [5].

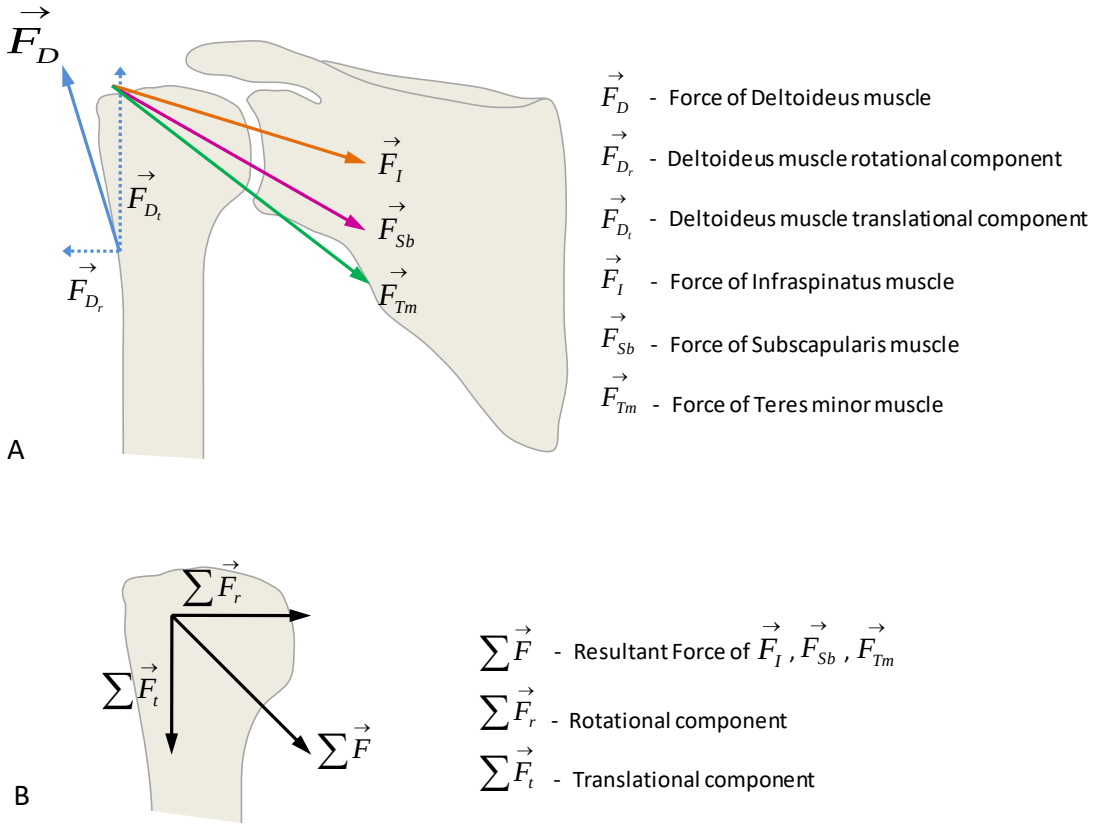

Figure 1.8. a) Lines of action of muscles deltoideus, infraspinatus, subscapularis and teres minor. b) Resultant force of three cuff muscle forces. After [5].

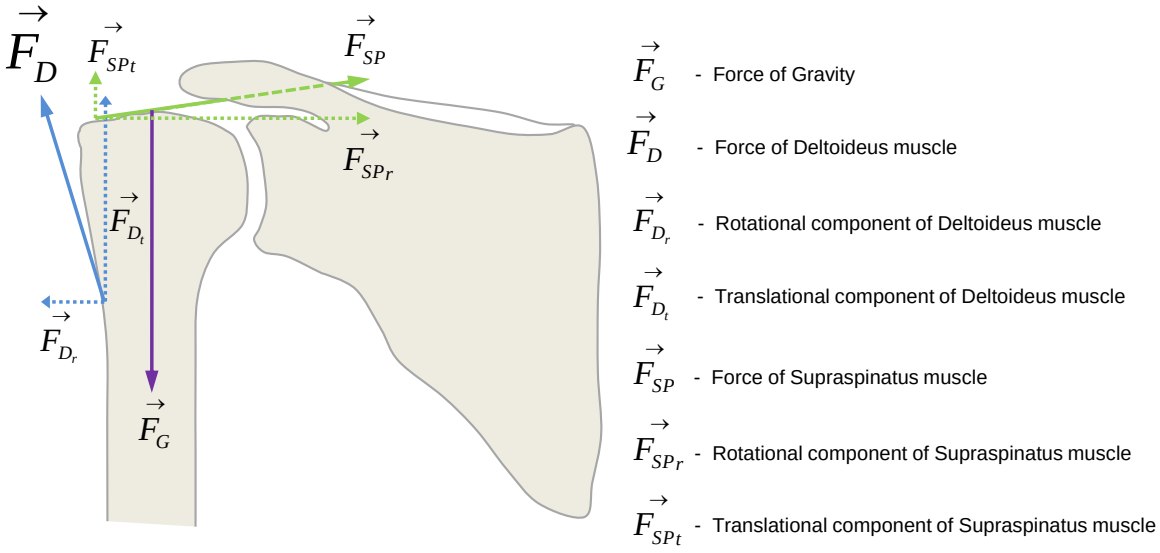

Figure 1.9. Lines of action of the deltoideus, supraspinatus and the force of gravity. After [5].

Besides the rotator cuff muscles and the deltoideus, the biceps muscle long head is also considered an important player in glenohumeral joint stability. This happens because of its superior position at the glenohumeral capsule, and its connections with the remaining reinforced structures. Consequently, the biceps long head works in centring the humeral head in the glenoid fossa, reducing possible humeral dislocations [5].

A free body diagram of arm elevation is represented in Figure 1.10.

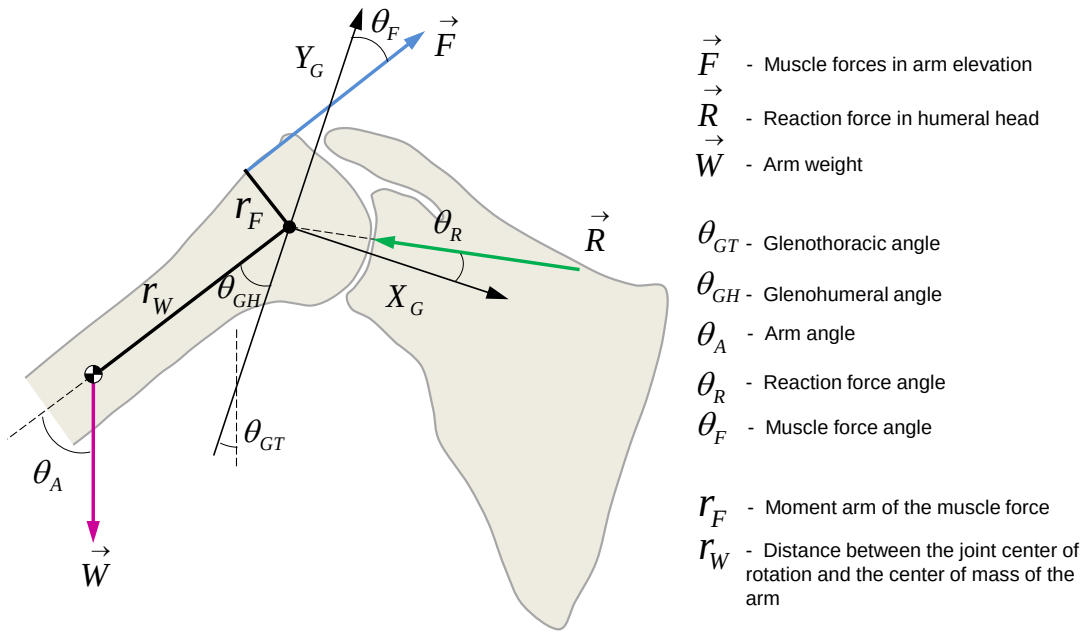

Figure 1.10. Free body diagram of arm elevation [3].

The glenohumeral joint is considered a ball-and-socket joint and its centre of rotation coincides with the centre of the humeral head. According with the diagram, the weight of the arm ($\vec{W}$), muscle forces ($\vec{F}$) and force reactions ($\vec{R}$) are considered and friction ignored. Furthermore, force reaction ($\vec{R}$) is considered to pass in the centre of rotation, not contributing to moment. As the diagram suggests, x-axis (X_G) is perpendicular to the articulation surface. Bearing in mind only the contribution of the deltoideus and supraspinatus, the moment around the centre of rotation and force equilibrium equations become as follows:

$$W \sin(\theta_A)\, r_W - F_D r_D - F_S r_S = 0 \qquad \text{Eq. 1.1}$$

$$\begin{cases} W \sin(\theta_{GT}) + F_D \sin(\theta_D) + F_S \sin(\theta_S) - R \cos(\theta_R) = 0 \\ W \cos(\theta_{GT}) + F_D \cos(\theta_D) + F_S \cos(\theta_S) - R \sin(\theta_R) = 0 \end{cases} \qquad \text{Eq. 1.2}$$

However, since the number of muscles acting on the shoulder is greater than the number of equations available in the system, the solution becomes indeterminate, as different muscle combinations can cause the same moment around the joint.

1.2 Shoulder Arthroplasty and Implants

Shoulder replacement with a prosthesis is the ultimate resource in the treatment of a shoulder pathology in view to restore its function. The medical procedure is known as shoulder arthroplasty, or shoulder replacement, and has had a great success, similarly with what is being observed with the knee and hip replacements [16].

The early history of joint replacement pays tribute to the pioneering work of Themistocles Gluck, who in 1890 performed the first total knee joint replacement on a 17-year-old girl suffering from tuberculous arthritis. The prosthesis was made of ivory and got an outstanding short-term success. However, due to continuous infections, it failed. Gluck reported in detail five other arthroplasties – 3 in the knee, 1 in the wrist and 1 in an elbow – and designed a few shoulder replacements [17]. Still, Gluck is not considered the pioneer of shoulder prosthesis, as he never published about its implantation in living human beings. On the contrary, the medical community acclaims Jules-Émile Péan to be the precursor of shoulder prosthesis, as he performed a shoulder arthroplasty, in 1893, on a 37-year-old baker suffering from tuberculous arthritis. The surgery was a success, but 2 years later the prosthesis (see Figure 1.11) was removed due to infections [18].

Decades have passed from the first shoulder arthroplasty procedure and ever since then, shoulder prosthesis concepts and implants have experienced tremendous developments.

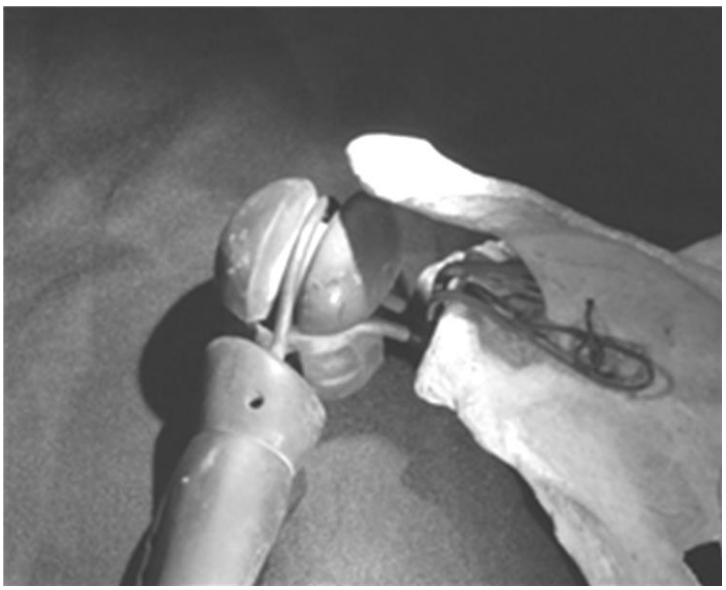

Figure 1.11. Total shoulder prosthesis, of Jules-Émile Péan [en.wikipedia.org].

1.2.1 Arthroplasty Concepts

1.2.1.1 Anatomical Shoulder Arthroplasty

Since 1893, few developments occurred in shoulder arthroplasty, but none had such an impact as the achievements of Doctor Charles Neer II, generally considered the father of modern shoulder arthroplasty [19].

The revolutionary work of Doctor Neer took place between 1953 and 1954, when he successfully implanted shoulder prostheses (see Figure 1.12) in 12 patients suffering from avascular necrosis, fracture dislocations and hypertrophic osteoarthritis. The published report of those results [20] became one of the most relevant articles in the history of shoulder arthroplasty. The articular part of the prosthesis had the shape of a normal humeral head and the superior edge was flattened to allow the settling of the prosthesis onto the greater tuberosity. At its neck there was a mechanism to add fixation and eliminate rotation; a hole placed at the neck served to hold the fragments of the tuberosity to the prosthesis in cases of recent fracture-dislocations [20]. The prosthesis was designed to only replace the articular surface of the humerus, so that the anatomy of the greater and lesser tuberosities, and their attachments, were disturbed as little as possible. It was built in vitallium alloy. This replacement is known as Hemiarthroplasty (HA)

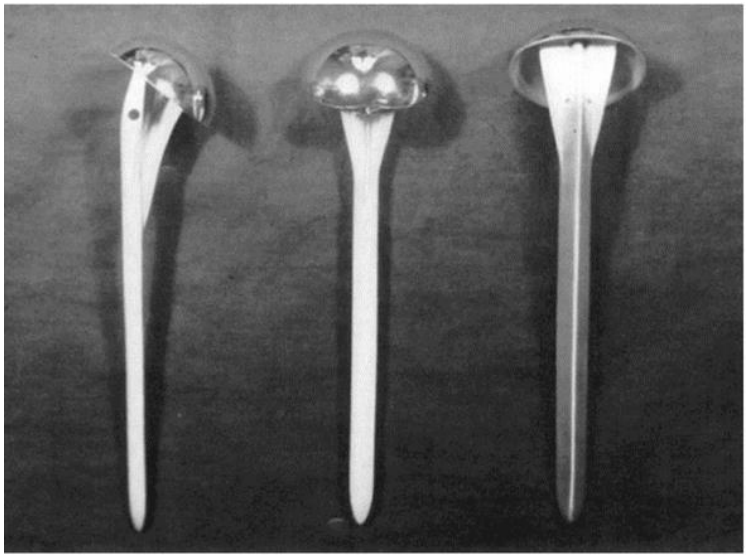

Figure 1.12. Small, medium and large models of Charles Neer replacement prosthesis [20].

Approximately 20 years later, Charles Neer brought to light the clinical outcomes of HA treatments, followed during an average of 6 years, on patients suffering from glenohumeral osteoarthritis [21]. The results were excellent, allowing substantial pain relief and improved ROM. Nevertheless, strength recovery was slow and some patients felt fatigue. On the same study [21], Neer reported on suitable initial results for the use of a glenoid prosthesis, along

with the humeral prosthesis, in 7 patients suffering from glenohumeral osteoarthritis. The glenoid component was made of high-density polyethylene (PE), fixed with acrylic cement in 6 cases and with no cement in 1 case. It had a keeled back and the radius of curvature matched the humeral head prosthesis. Neer termed the procedure Total Shoulder Arthroplasty (TSA), so establishing the beginning of the first generation of shoulder replacement. Despite the successful application of the glenoid component, there was not enough follow-up time to conclude on the results achieved.

Total Shoulder Arthroplasty and HA are well-tested procedures that offer pain relief and improved function in most cases [22, 23], except in certain cases of insufficient bone at the glenoid. In chronic pathologic conditions, such as rheumatoid arthritis, primary osteoarthritis with an intact rotator cuff and fracture sequelae, several outcome studies conclude that TSA is the best form of treatment [22, 24].

Pfahler *et al.* [24] compared the outcomes of 705 TSA and 469 HA in the treatment of fracture sequelae, rheumatoid arthritis, primary osteoarthritis, eccentric arthrosis, osteonecrosis and other etiologies. All patients had an Aequalis® Shoulder Prosthesis (Tornier, SA) and the period of follow up was 3.5 years, in average. The revision rate was higher for the HA group. For most the etiologies, both functional outcome and subjective outcome assessment were better for TSA than for HA. More specifically, TSA presented better results in the treatment of primary osteoarthritis, rheumatoid arthritis and sequelae after fracture. As for HA, it performed better in cases of osteonecrosis and instability arthritis. The authors did not found significant difference in the outcome results of TSA and HA in the treatment of eccentric osteoarthritis and cuff arthropathy. However, the evaluated cases were small to draw strong conclusions on this aspect.

Sandow *et al.* [22] showed that TSA seems to be better than HA in the treatment of osteoarthritis with an intact rotator cuff. At 6 months, 1 year and 2 years after surgery, patients treated with TSA had less pain, better ROM, improved joint function and better quality of life.

Conversely, the success of TSA is compromised when a massive rotator cuff is associated with glenohumeral arthritis [25], known as cuff tear arthropathy. However, HA has proven to be a valid surgical approach in the treatment of this pathology [26]. Zuckerman *et al.* [26] conducted a review on the outcome of 15 shoulders treated with HA for cuff tear arthropathy, where patients were followed during a mean of 28.2 months after surgery. Both the active forward elevation and active external rotation increased, as well as the ability to complete daily-living activities. Pain relieve was also majorly improved and 87% of patients were satisfied with surgery outcomes.

Regardless of the good results achieved so far with shoulder replacements, surgeons need to be careful in the treatment of shoulder pathologies in patients under 50 years old, as it was observed that observed that almost half of the young patients undergoing a shoulder arthroplasty were unsatisfied with the outcome results [27].

1.2.1.2 Reverse Shoulder Arthroplasty

As referred before, in damaged glenohumeral joints with severe complications at the rotator cuff, the treatment with TSA is not successful and the use of HA requires some restrictions. To try to overcome this, constrained hinged or reverse prosthesis designs were developed, but complication rates were high and glenoid loosening, fracture and pain were recurrent. Because of the challenges this type of arthroplasty presented, many began to explore a different type of system: the reverse ball-and-socket design. However, the majority resulted in poor functional improvement of shoulder motion, being abandoned [28].

French surgeon Paul Grammont understood that all prosthesis available at the time caused the same mechanical malfunction: weakness of the middle deltoideus lever arm at abduction. Therefore, Grammont concluded that when the rotator cuff is not active, the key is to strengthen the abduction component of the middle deltoideus and lessen its elevation component responsible for loosening and stress at the glenoid [29]. This is possible through the insertion of a prosthetic ball in the glenoid cavity and a socket in the humerus, as illustrated in Figure 1.13.

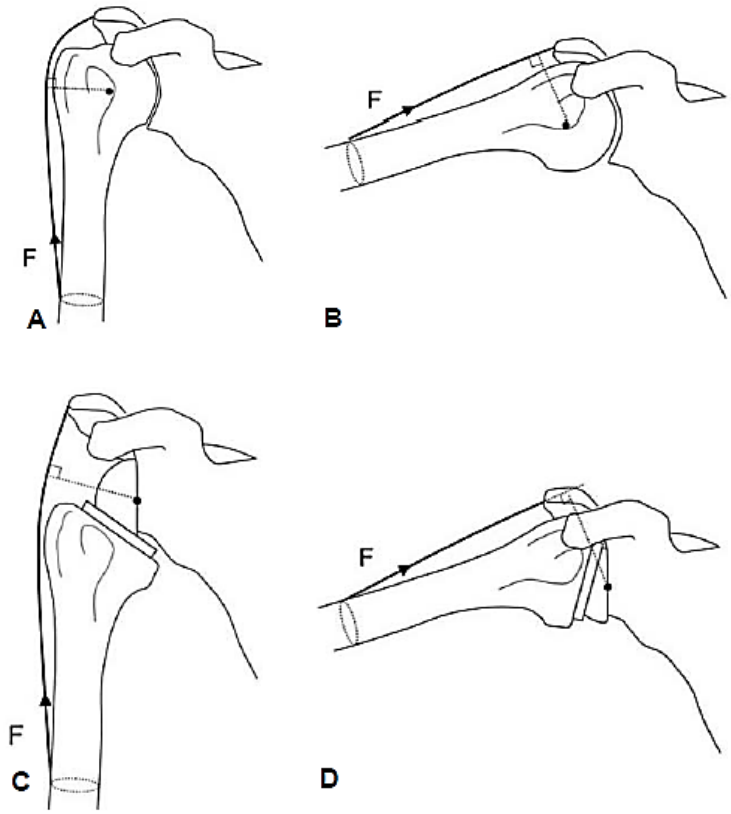

Figure 1.13. Rotation centre and position of the humerus and of the deltoideus in an intact (A, B) and implanted (C, D) shoulder. Arm at the side (A, C) and in abduction (B, D). Adapted from [30].

With the use of a prosthetic ball on the scapula, the centre of rotation of the glenohumeral joint is deviated medially (see Figure 1.13 C, D), which eliminates the lever arm applied to the glenoid, preventing loosening. The abduction component is strengthened due to the lowering of the centre of rotation.

The first modern version of Grammont reverse prosthesis had a ceramic glenoid component, consisting on 2/3 of a sphere with no neck. Its rotation centre was on a medialized location facing the glenoid and there was a concave monoblock cone of polyethylene on the humeral side. Both components were cemented to the glenoid and to the humerus, respectively [29]. After some attempts, the Grammont reverse concept gained significant importance when Grammont *et al.* [31] reported the successful treatment of 8 patients. Six months after surgery all were pain free, but their function varied between 100° and 130° of elevation.

After several modifications to the design of the Grammont reverse prosthesis, the Delta III (DePuy International Ltd, Leeds, England) was established and it has proven to be effective in the treatment of complicated cases for the past 20 years [32, 33]. The first version of the Grammont prosthesis and the Delta III are presented in Figure 1.14.

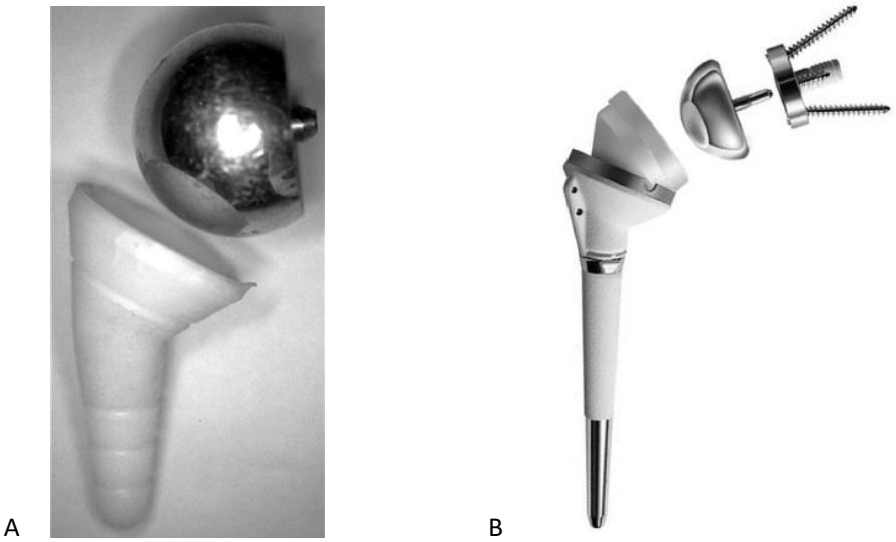

Figure 1.14. a) Grammont reverse prosthesis, known as Trompette [29]. b) Delta III reverse prosthesis, DePuy International Ltd, Leeds, England [34].

Some short-term review studies of patients treated with a reverse prosthesis acknowledge the good, or excellent, early results of the treatment in most cases. Sirveaux *et al.* [35] examined the outcome of 80 Delta III inverted prosthesis, at a mean of 44.5 months after surgery, for the treatment of glenohumeral osteoarthritis with massive rotator cuff. At follow-up, 96% of patients had slight or no pain and improvement of activity and mobility

was evident. Regardless of the good early results, some complications were observed, such as loosening of the glenoid component (6.3%), unscrewing of the glenosphere (8.8%) and scapular notching (63.4%). The survivorship rate of the prosthesis was 88%, 72% and 29% at 5 years, 7 years and 8 years after surgery, respectively. The authors categorised the early results as promising, but advice that the prosthesis should be used only in elderly patients that did not respond to other type of therapy and whose glenoid bone is adequate to support the glenoid component.

Boileau *et al.* [36] analysed the outcome of the Delta III reverse prosthesis used to treat cuff tear arthritis, fracture sequelae and revision arthroplasty, with a mean follow-up of 40 months. The procedure was successful in restoring shoulder function, mainly active elevation of the humerus, as also noted by Grassi *et al.* [37]. However, active rotation did not improve due to the prosthesis design. In the study of Boileau *et al.* [36], the reverse prosthesis had small reoperation rates in the treatment of cuff tear arthropathy. Regarding revision surgery with a reverse prosthesis, the functional outcomes were not as promising as the ones achieved in primary surgery and most the complications were registered in the revision arthroplasty cases.

Despite the fact that glenoid loosening is one major concern in total conventional prosthesis, in the study of Boileau *et al.* [36] this was not encountered. However, Grassi *et al.* [37], on their 6-year experience with a Delta III, found loosening on the glenoid component of 2 patients. Thus, care is mandatory when making conclusions on medium-term follow-up of arthroplasty procedures. Nonetheless, Boileau *et al.* [36] identified 3 main problems related with the design of the Delta III: acromial fracture, dislocation and scapular notching, which were also pointed by Grassi *et al.* [37]. Regardless of the relatively small differences between the studies mentioned, all concluded that patients were satisfied, or very satisfied, with the surgery outcome.

Meanwhile, reverse prostheses have been developed by other companies, and Frankle *et al.* [38] analysed the outcome of 60 Reverse Shoulder Prosthesis (Encore Medical, Austin, Texas). Cases of glenohumeral arthritis associated with severe rotator cuff injury were treated. The follow-up took place during 2.75 years. Even though there were some complications in 10 patients, more than half (68%) were very satisfied and 27% were satisfied. A mere 5% were disappointed. Overall, abduction and forward flexion increased and, at least in the short term, the authors consider the reverse approach to be encouraging.

Concerning Grammont design [33] (also known as Delta III) versus Frankle design [38] there are no significant conclusions about the level of adequacy of one treatment versus the other. Therefore, one cannot say which one is the best. Virani *et al.* [39] did a comparative study of glenoid bone/baseplate interaction for those two types of prosthesis (see Figure 1.15) using *in vitro* and finite element analysis methods: a strong correlation between the finite element model and the *in vitro* mechanical testing was clearly demonstrated. Both concluded that difference in baseplate motion was not significant between glenospheres

with larger centre of rotation (COR), compared with smaller COR offsets when tested in simulated high-quality bone.

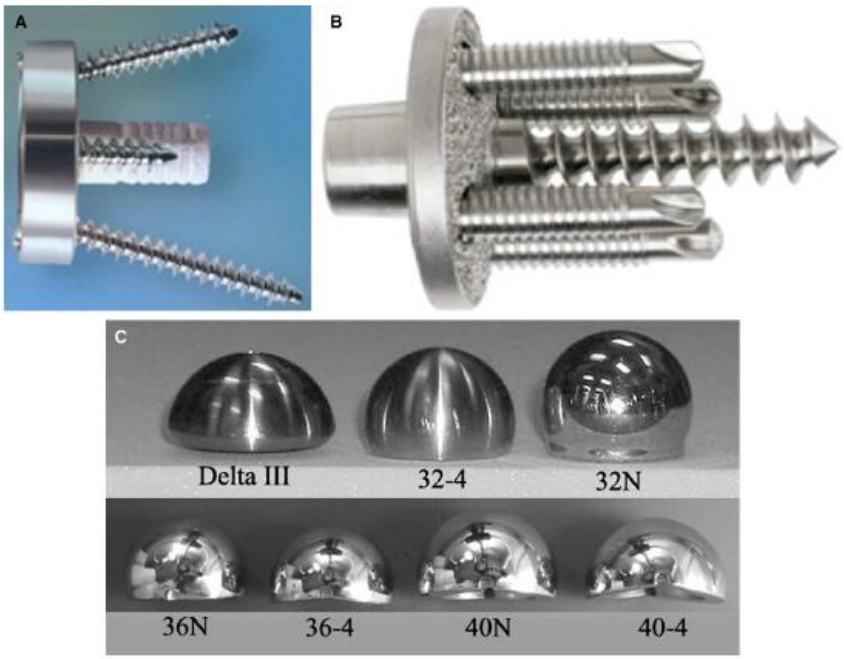

Figure 1.15. A: Baseplates and screws of the Delta III. B: Baseplates and screws of the Frankle design. C: Delta III glenosphere (36 mm diameter) and six different glenosphere sizes of the Frankle design. [39].

Besides all aspects related with reverse shoulder prosthesis, the studies are unanimous in what the ideal patient for such a procedure is. A patient suffering from primary rotator cuff tear arthropathy, primary osteoarthritis with a rotator cuff tear and a massive rotator cuff tear, and with more than 70 years of age, since this is a technically demanding procedure with high risk of complications [40, 41].

1.2.2 Implants

1.2.2.1 Humeral Component

After the first HA and TSA procedures were performed [20], Neer continued to develop the humeral component design. After some clinical studies [42], Neer *et al.* concluded that total shoulder prosthesis, capable of simulating the normal anatomy of the body, were of capital importance and the prosthesis was improved by the introduction of modular components. There were two humeral head sizes and three stem sizes available for each head. Five different glenoid components were also available, each with the same radius of

curvature of the humeral head. Figure 1.16 presents the new modular components that gave rise to the second generation of shoulder prosthesis.

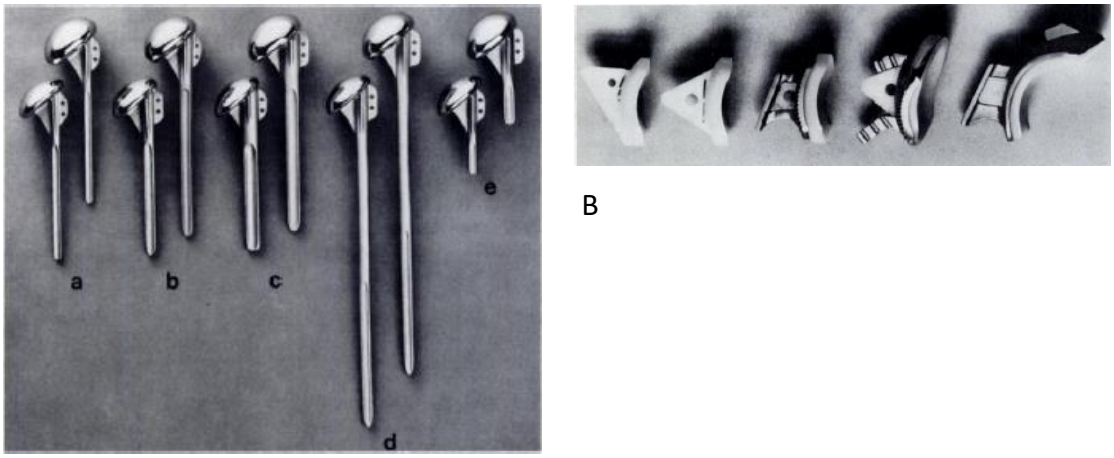

Figure 1.16. A: Humeral stem components. B: Keeled glenoid components. Adapted from [42].

Boileau and Walch thoroughly studied the proximal humerus anatomy and showed that its shape varies considerably amongst people [43]. They defended that the prosthesis available at the time did not considered this variability and that the humerus was being adapted to the prosthesis instead of the prosthesis being adapted to the humerus. Thus, the authors developed the first humeral prosthetic component that was both modular and adaptable to the bony anatomy of each patient (Figure 1.17). The studies of Boileau and Walch resulted on the third generation of shoulder prosthesis.

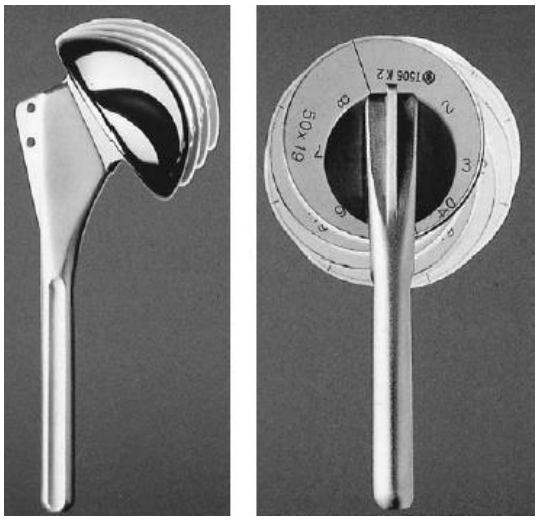

Figure 1.17. Aequalis (Tornier Inc., St. Ismier, France) shoulder prosthesis. Third generation of shoulder replacement [43].

With shoulder arthroplasty progress, the humeral stem has been suffering many changes, specially related with its size [44, 45]. Humeral resurfacing arthroplasty is characterized by bone stock conservation due to minimal resection of the humeral bone, because there is no intramedullary stem on the humeral component (Figure 1.18). Generally, contemporary resurfacing designs have a small central stem that promotes bone ingrowth, both at the stem and at the inner surface.

The quality and quantity of bone stock is mandatory for implant support and about 60% of the native humeral head is required for a successful procedure [46]. Humeral resurfacing eliminates complications associated with conventional stemmed implants, such as humeral fractures around the stem (periprosthetic fractures) and unnecessary blood loss during surgery. Thanks to bone conservation, it is easy to change to a standard stemmed component in a revision surgery, in case of needed. Humeral resurfacing, similar to that of the hip, is a real alternative to HA [47], as surgical procedure indications are the same for both treatments. Humeral bone preservation can make glenoid exposure a complicated process during surgery, and Mullett *et al.* [48] support that glenoid resurfacing should be avoided in this surgical procedure. If the articular damage of the glenoid is substantial, and a good glenoid exposure is difficult to achieve, humeral resurfacing should be abandoned in favour of a conventional total shoulder arthroplasty [49].

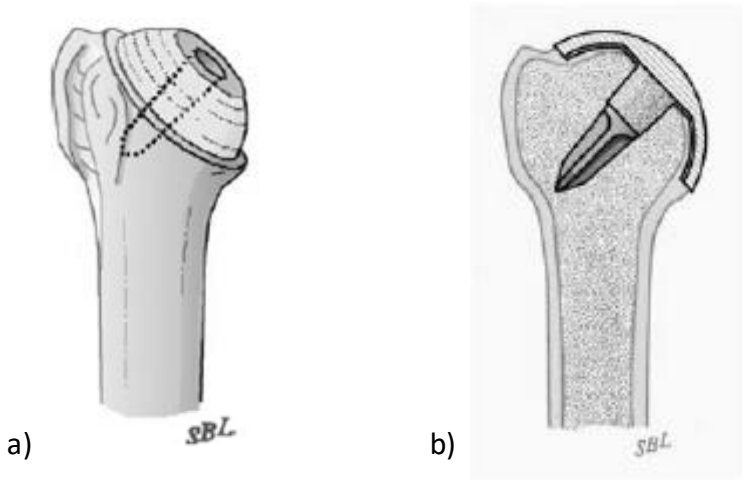

Figure 1.18. a) Scheme of the humerus showing the amount of resected bone for a humeral resurfacing procedure. b) Scheme of the humerus with a modern resurfacing implant. [47].

Clinical outcomes of modern humeral resurfacing arthroplasty are promising when compared to those of conventional shoulder arthroplasty [46, 50]. Patients have shown a better quality of live when using resurfacing arthroplasty compared to hemiarthroplasty [51]. The use of the resurfacing technique in young patients with a rotator cuff arthropathy (having an intact teres minor), provides an alternative with acceptable medium-term

outcomes (pain reduction but partial function increase) [52]. The resurfacing prosthesis also presents lower complication risks [46, 50].

Another new concept in shoulder replacement is stemless shoulder arthroplasty. Similar with humeral resurfacing arthroplasty, it has the goal of avoiding stem-related problems, of preserving a good bone stock quality in case of revision operation, to offer a simple revision surgery and, most importantly, to provide correct exposure of the glenoid component. In humeral resurfacing, major humeral bone head conservation is achieved, making it difficult to correctly expose and replace the glenoid. On the contrary, the stemless shoulder arthroplasty technique was designed to eliminate this main problem, since it relies on the same standard humeral neck cut (used for standard stem humeral prosthesis), allowing complete exposure and access to the glenoid for correct replacement [53]. This arthroplasty procedure has been in use for a little more than a decade and only a few prostheses are available, as well as a small number of clinical reports for 2 or more years of follow-up.

Churchill and Athwal [53] present a recent review paper on the existing designs and most significant reported outcomes, highlighting potential concerns of this new arthroplasty concept. At the short and early midterms, the available clinical reports allow to conclude that the anatomical stemless shoulder arthroplasty achieved clinical and radiographic outcomes like those of anatomical stemmed prosthesis. However, the available prostheses have different designs, and with such short evaluation is not possible to state which prostheses allow for better results.

1.2.2.2 Glenoid Component

The first glenoid component was introduced by Neer for the treatment of glenoid wear as a consequence of glenohumeral osteoarthritis [21] (see Figure 1.19, A). The Neer prosthesis had a keeled-back and was made of high-density polyethylene. Even though there are good clinical outcomes reported for the use of glenoid components, glenoid loosening has the focus when referring to implant-related factors that lead to arthroplasty failure and revision [54, 55].

To reduce this problem and achieve better long-term results, many modifications have been made to the glenoid component design and to the fixation techniques. In addition, other patient-related and technique-related factors influence glenoid implant loosening, such as preoperative shoulder pathology, glenoid wear, poor bone stock, glenohumeral stability and rotator cuff integrity; implant type, glenoid exposure, reaming instrument, humeral and glenoid prosthesis mismatch, wear of PE components, osteolysis, component mal-positioning and radiolucent lines (RLL) [56]. These aspects are well scrutinised on a complete review of Karelse *et al.* [57] on the main causes that influence glenoid loosening, focusing on implant-related factors, patient-specific factors and on surgical factors.

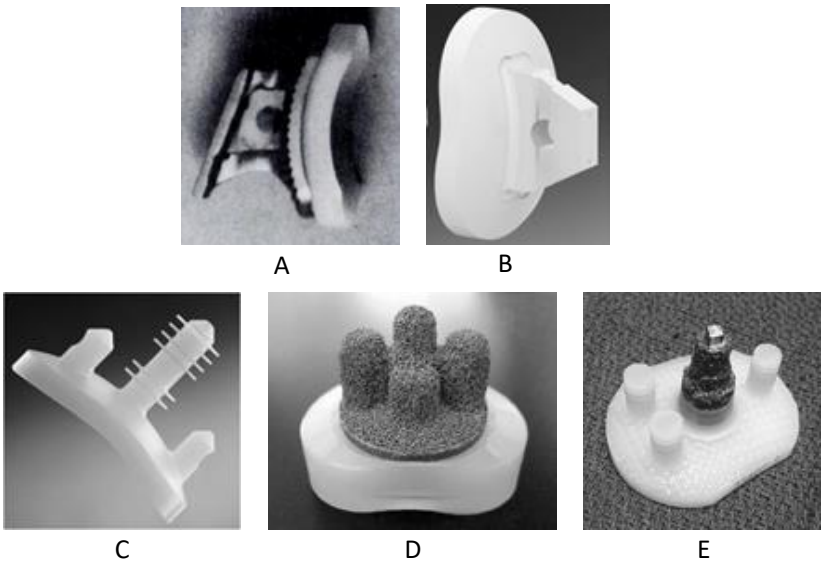

Figure 1.19. Different glenoid component designs. A: metal-backed, adapted from [42]; B: Aequalis PerFORM (Tornier); C: Affiniti CortiLoc (Tornier), adapted from [58]; D: Trabecular Metal Glenoid (Zimmer), adapted from [59]; E: Regenerex® Hybrid Glenoid (Biomet), adapted from [59].

The glenoid component has experienced many design modifications, such as pegged, all-polyethylene (all-PE) or metal-back, with or without porous coating and with appropriate features for cementing, non-cementing, hybrid or minimally cemented technique. More modern pegged glenoid components, as exposed in Figure 1.19 (C, D, E), have central pegs designed to provide bone ingrowth and biologic fixation. Regardless of all developments, not all resulted in smaller revision rates, nor in reduced incidence of glenoid loosening [59, 60]. There are several studies comparing the outcomes of the different glenoid designs [61, 62] and the majority claims that TSA with all-PE component is more successful than TSA with metal-backed component.

Boileau *et al.* [63] developed a study with the objective of comparing cemented all-PE with uncemented metal-backed components for a minimum follow-up of 3 years. Both components were from Aequalis Total Shoulder System (Tornier Inc., France). The study involved 40 shoulders with primary osteoarthritis, and each type of prosthesis was applied in 20 patients. The amount of radiolucent lines was higher on the cemented all-PE components (85%) than on the uncemented metal-backed components (25%). Of the 85%, 60% were observed immediately after surgery, and the remaining progressively with time, as were the radiolucent lines present on the uncemented metal-backed components. However, loosening was smaller on all-PE glenoids and considerably higher on metal-backed (20%), and was related with both component shift and osteolysis. Thus, despite being common, radiolucent lines around glenoid implants are not directly correlated with implant failure due to loosening, nor with need for revision. Boileau *et al.* [63] choose to abandon the use of metal-backed glenoids.

Gonzalez *et al.* [61] analysed 2657 TSAs in a complete literature review on the complications behind unconstrained shoulder prosthesis during a follow-up of 6 years (between 2 and 25 years). Glenohumeral instability was identified in only 11.6% of cases, while problems related with the glenoid represented 25.5% of all complications observed, being the majority related with glenoid loosening (24.0%). The authors distinguished between all-PE implants and metal-back implants, and acknowledged loosening in 13.6% and 16.7% of them, respectively. They defend that cemented all-PE glenoid implants should be the preferred in TSA.

Similar conclusions were made by Montoya *et al.* [62] on a recent study on the treatment of primary osteoarthritis with TSA with an uncemented glenoid implant (Univers metal-backed, Arthrex, Germany). The follow-up study took more than 5 years and 53 patients were observed. Even though initial clinical results improved considerably, glenoid loosening occurred at 9.4% of cases and revision rates were high (11.3% at 5.6 years after surgery). Considering these poor results, the glenoid prosthesis analysed was withdrawn from the market. Montoya *et al.* [62] claim to prefer cemented all-PE glenoid components in the treatment of glenohumeral osteoarthritis. Despite the superiority of all-PE glenoid components, these studies show that loosening and RLL continue to be a long-term problem related with TSA.

Adding to the conclusion that all-PE glenoid components are more successful than metal-backed, there are several studies favouring all-PE pegged implants then all-PE keeled implants [64–66]. This superiority is related with lower rates of RLL and lower failure risk.

Edwards *et al.* [65] did not find significant differences in the rate of radiographic lucent lines between pegged and keeled glenoid components immediately after surgery (0% and 15%, respectively). However, after an average follow-up of 26 months, the rate of lucent lines of keeled glenoids was higher than that of pegged glenoids (46% and 15%, respectively). This means that glenoid lucency progressed with time and it was more evident in keeled glenoids. The authors state that the lower rates of radiolucent lines may be related with the modern cementing technique used in the study, namely glenoid compaction and cement pressurization, as modern cementing techniques have shown to improve glenoid fixation and reduce the rate of RLL [67]. In a similar study by Gartsman *et al.* [66], the authors analysed the influence of glenoid design on postoperatively radiographic lucency on 43 patients suffering from primary glenohumeral osteoarthritis. A standard cementing technique was used. The authors found a 39% lucency rate in keeled glenoid components, against a very low 5% rate in pegged glenoid components.

Glenoid component designs have been focusing on solutions with minimum amount of cement, as it promotes thermal necrosis of adjacent bone, which may lead to component loosening [68]. A glenoid component design that is having great outcome results (Anchor Peg Glenoid, DePuy) has three cemented pegs at the periphery of the glenoid and an uncemented central peg that is larger than the others, having four spaced radial fins at its

extremity (see Figure 1.20). The glenoid prosthesis was first applied in a canine model, achieving good results concerning stability, bone ingrowth around the central peg and increased fixation strength over time (0, 3 and 6 months) [69]. The prosthesis was available for TSA in late 2001 and its clinical results are now being presented [70–73]. Some clinical and radiographic implant outcomes [70], performed at a minimum follow-up of 5 years, confirm improved longevity, RLL reduction and bone ingrowth at the central peg in 85% of cases.

Figure 1.20. Anchor Peg Glenoid (DePuy) [74]

At the core justification of glenoid loosening with time is humeral joint reaction force: if it is not centred at the glenoid fossa, excessive shearing forces will appear as the arm moves, leading to glenoid eccentric loading. This is known as the "rocking-horse", firstly described by Franklin et al. in 1988 [75]. This effects is more evident in cases of rotator cuff arthropathy, as the poor state of rotator cuff muscles promotes loosening of the humeral head and the absence of a centred reaction force. This effect is illustrated in Figure 1.22.

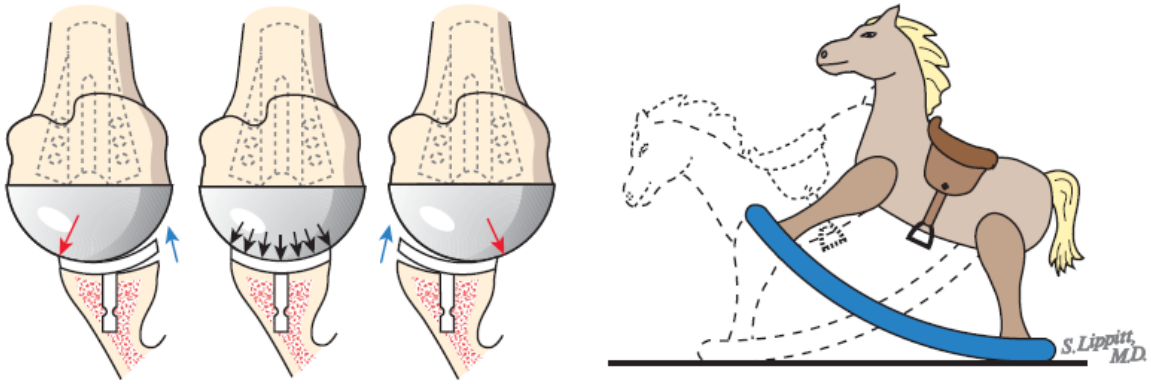

Figure 1.21. Rocking-hors effect illustration. The eccentric loading of the glenoid (red and blue arrows) exposes it to risk. Adapted from [76].

To avoid shearing forces, some authors have suggested the existence of small differences between the diameter of the glenoid and humeral head prosthesis [77, 78].

Anglin *et al.* [77] developed an experimental method to study glenoid prosthesis behaviour when subjected to rim loading. The authors analysed several features, concluding that roughened surfaces promote better bonding between bone cement and the prosthesis; that a curved-backed shape supports better the forces transmitted from the humeral head to the glenoid and, finally, that a less constrained prosthesis (with smaller glenoid rim slope) results in lesser tensile and compressive stresses in the underneath bone.

Wang *et al.* [78] analysed the biomechanical differences produced by three different glenoid designs: conforming, nonconforming and hybrid (conforming centre and nonconforming periphery). The authors concluded that changing only the periphery of the fully conforming design augmented the hypothesis of less rim loading, thus increasing joint stability. More recently, Zhang *et al.* [79] developed a finite element model that evaluated the glenoid prosthesis used in the experiments of Wang *et al.* [78]. During humeral head translation, the hybrid component suffered less stress at the periphery than the conforming design, being similar to that of the nonconforming. Conversely, all three designs had analogous shear stresses. Thus, the hybrid design has promising features to withstand wear and loosening.

These studies have shown that there must be a compromise between the radius of curvature of the glenoid and humeral head. At the one hand, more mismatch between them promotes less translational loads on the glenoid and, consequently, less risk of glenoid loosening with humeral translation. On the other hand, a higher conformity promotes stability and less contact stresses.

1.3 Fixation Techniques

Prosthetic component fixation, by cemented or uncemented techniques, is one of the major factors influencing shoulder arthroplasty success or failure.

The cementing technique promotes implant fixation to bone using polymethylmethacrylate bone cement (termed PMMA, or bone cement), as it fills the space between the implant and bone, creating a tight space to hold the implant against bone. Despite labelled a "cement", PMMA does not have adhesive properties and implant fixation depends on the mechanical interlock between its surface and the irregular surface of bone. Adding to the important function of implant fixation, PMMA is also used to transfer loads from the prosthesis to bone and to increase the load-carrying capacity of the system prosthesis/cement/bone [80]

Although the success rate of cemented arthroplasty procedure is rather good, it has several limitations. Perhaps the most critical of them is related with PMMA polymerization, since being an exothermic reaction it releases high quantities of heat (between 82° C to

86° C) into the circulating blood, the prosthesis, and the surrounding tissue, causing bone necrosis [81]. Other pitfalls related with PMMA cement are aseptic loosening due to PMMA mechanical weakness [81]; shrinkage of the cement when the temperature decreases as the polymerization is completed, which can compromise the bone/cement interface [80]; and difference between PMMA and adjacent bone stiffness.

Another important aspect that influences the long-term implant stability is the bonding strength and the degree of cement penetration into the surrounding bone (interface integrity). Wear particles released into bone and into the circulating blood are also a long-term concern and are indicated as initiators of biological reactions in aseptic osteolysis [82].

The uncemented fixation technique (or press-fit) was, in some extent, developed to eliminate the problems related with PMMA. Given that this new practice relies on biologic and mechanical bond capacities for fixation, implant surface is critical for a correct bonding and currently there are prosthesis with or without porous coating. In the prostheses without porous coating, the mechanical interlock is achieved without osseointegration. On the contrary, in porous coated prostheses, the mechanical fixation process is achieved in two stages: macro-interlock followed by micro-interlock through osseointegration, where bone tissue is formed in the coated surface.

When choosing a prosthesis, there are many factors that must be taken into consideration, such as patient's age, bone stock quality, related diseases (osteoarthritis, rheumatoid arthritis, rotator cuff arthropathy, etc.), fractures, existence of a previous arthroplasty and the surgeon's experience. According to William Levine and Steven Aviles [83], cemented humeral component should be used in humeral fractures and in cases of rheumatoid arthritis, because humeral loosening occurs more frequently in this pathology. Furthermore, press-fit humeral prosthesis seem to be more prone to loosening [61, 84]. Total shoulder arthroplasty revision due to implant fixation has fallen almost entirely on cement fixation failure of the glenoid component. Furthermore, there is no clear evidence of the superiority of press-fit humeral stem fixation against cemented fixation. For these reasons, Seitz *et al.* [85] adopted the cemented humeral stem fixation and uncemented trabecular metal anchorage of the glenoid component during a 10-year period. No cases of loosening and only one case of fracture of the glenoid component were registered. Sixty-six patients were followed during a mean of 4 years, with 95% survivorship rates. The authors clearly state that a combination between cemented humeral stem and trabecular metal anchorage of the glenoid component is the ideal fixation solution in TSA.

1.4 Shoulder Arthroplasty Registries

With shoulder arthroplasty development and the many shoulder prostheses available in the market, it is essential to identify which operational procedures and prostheses provide better results. In this sense, some countries tried to gather relevant information on the most

important aspects of every arthroplasty surgery performed at a joint. The main goal is to improve patients' quality of life and help to reduce surgery costs.

Most of the arthroplasty registers gather information like the hospital where the surgery took place, the patient data (age and gender), the side operated, the diagnosis and the reason for revision, the surgery technique, type of prosthesis and fixation procedures, along with other information. The aim is to trace each surgery so to establish its success or failure. Statistical analysis of the data allows to identify, for example, the most frequent aetiologies, the procedures mainly used, the implants with better acceptance and to determine the revision rates of each prosthesis. The identification of implants with the highest revision rates is crucial to withdraw them from the market. This has happened, for example, with the Shoulder Modular Replacement (SMR) consisting of a glenoid component (metal glenoid with polyethylene liner) and a humeral component (humeral head and stem). The glenoid component, named SMR L2 Metal Back Glenoid Component, was discontinued by Lima Orthopaedics after the Australian National Joint Replacement Registry concluded that it presented higher than expected revision rates (https://www.tga.gov.au/alert/smr-l2-metal-back-glenoid-component-used-shoulder-replacements, accessed 29/July/2017). Another example is the Comprehensive Reverse Shoulder System (Zimmer Biomet) that was recalled from market in December 2016 after presenting high fracture rates (https://www.fda.gov/MedicalDevices/Safety/ListofRecalls/ucm541862.htm, accessed 29/July/2017).

Establishing a working arthroplasty register with reliable scientific information is a difficult task and not all countries that tried were successful. Besides, years are needed before a register can gather enough data for relevant statistical conclusions [86]. The oldest arthroplasty register is the Swedish Arthroplasty Registry, established in 1975. Shoulder registers are relatively new and are only a few, but they already provide insights into the procedures with more success and the best prostheses available in the market. In the next sections, some of the most relevant and well-established registers will be revised.

1.4.1 The Swedish Shoulder and Elbow Arthroplasty Registry (1999 - 2011)

The Swedish Shoulder Arthroplasty Registry and the Swedish Elbow Arthroplasty Registry were created in January first 1999 [87], following the footsteps of the hip and knee Swedish Arthroplasty Registries. Starting as independent, they later merged into a single registry, covering about 90% of all shoulder and elbow arthroplasties made in Sweden [88], with nearly all hospitals participating. Its purpose is “to improve surgical techniques and selection of implants and identify individual risk factors” [87]. The life-quality self-evaluating questionnaires at the one-year, five-year and ten-year follow-up with the patient is the measurement tool for shoulder arthroplasty success. In cases of shoulder osteoarthritis, the Western Ontario Osteoarthritis of the Shoulder Index (WOOS Index),

recently adapted to the Swedish reality [89], is used. Another questionnaire used is the EuroQol-5D (https://euroqol.org/, acceded in 14/June/2017), a standardized instrument that aims at quantifying health outcome in many different treatments.

The registered primary shoulder arthroplasties made in Sweden, between 1999 and 2011, reached 9172 reports, represented in the column graph of Figure 1.22 [90]. From the first to the second year, the growth rate was of 28%, presenting smaller variations the following years. Between 2004 and 2011, primary arthroplasties escalated, reaching 1127 occurrences that represented a 125% increase.

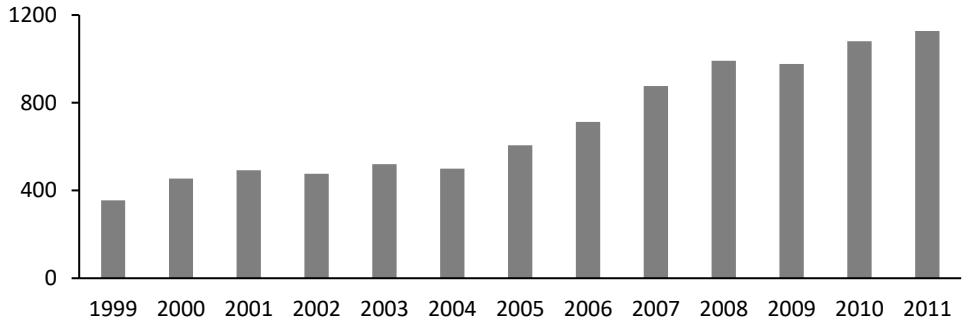

Figure 1.22. Registered primary shoulder arthroplasties made between 1999 and 2011 [90].

From all arthroplasties registered, 63% were hemiarthroplasty. Anatomical total shoulder holds 26%, and exceeded HA in 2011, as presented in the graph of Figure 1.23. It is interesting to notice that the use of both TSA and reverse shoulder arthroplasty (RSA) has seen a significant increase since 2004. TSA augmented 446%, whilst RSA augmented 841%.

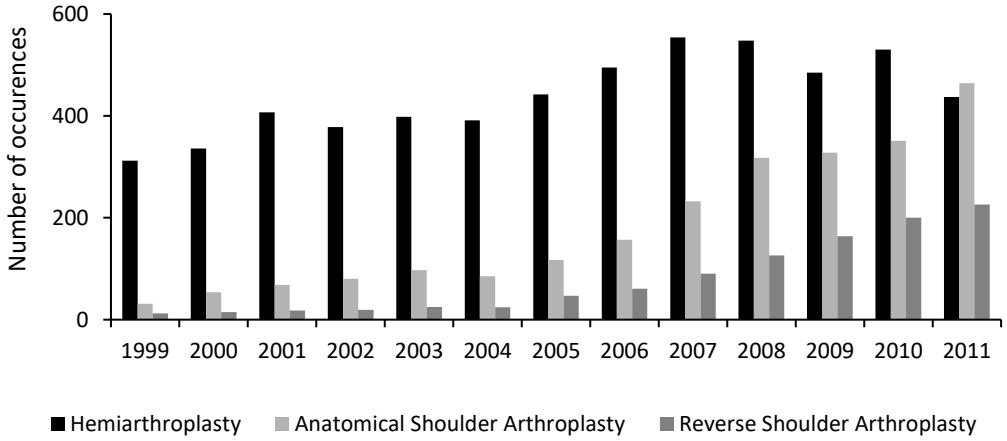

Figure 1.23. Type of arthroplasty procedures made between 1999 and 2011 [90].

According with the available reports, the main causes of HA relate to degenerative/post-traumatic conditions, or with fractures of the proximal humerus. The first with higher incidence throughout the years. In HA, traditional stemmed prosthesis is the most used (79% of all cases). Short stem prostheses are also used, but with a rate of only 17%. There are other options for HA, as the bipolar and head resurfacing, but are rarely used.

Considering the five-year follow-up outcomes of the WOOS index, it is better to perform a TSA than a HA in cases of osteoarthritis or rheumatoid arthritis. In cases of rheumatoid arthritis, the WOOS index reached 63% for HA and 70% for TSA. In the case of osteoarthritis, the WOOS index was 70% for HA and 85% for TSA [90].

The use of the reverse shoulder prosthesis in the treatment of more complex cases has increased during the last five to ten years, and it is mostly used to treat a rotator cuff arthropathy (49% of cases) [90]. Its use has seen a high growth since 2006, as the graphs of Figure 1.24 show. Cases of osteoarthrosis (11%), rheumatoid arthritis (9%), acute factures (15%) and sequels after facture (16%) also benefit from this procedure.

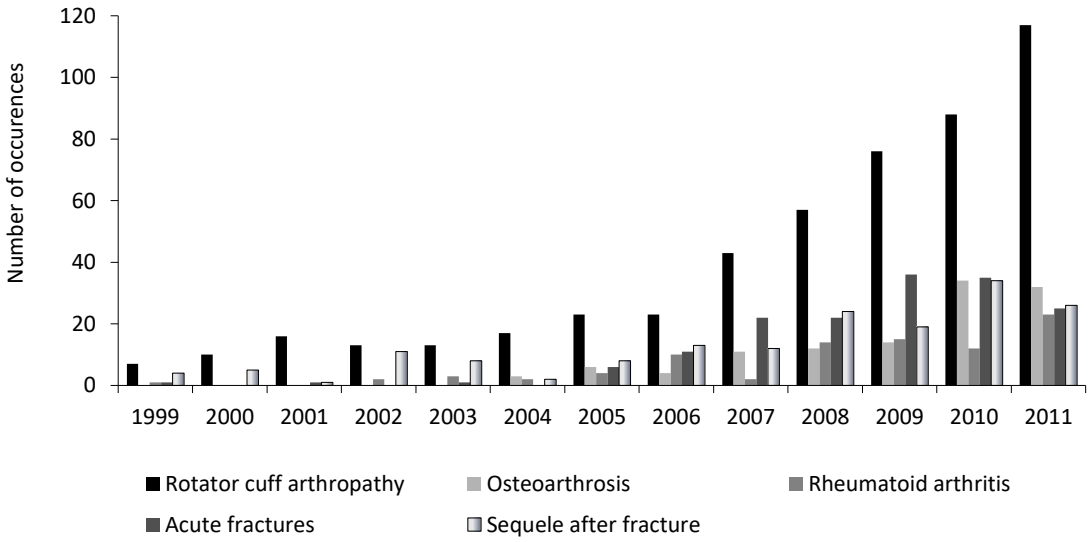

Figure 1.24. Pathologies treated with reverse prosthesis between 1999 and 2011 [90].

Regarding the reasons for revision, the existing reports reveal that the majority is due to instability of the prosthesis (20.7%) and glenoid erosion (16.5%), as exposed in the graph of Figure 1.25. The other two main pathologies that lead to revision are Infection (6.7%) and pain (6.3%) [91]. The reports also demonstrate that reverse shoulder prosthesis accounts for 44% of all revisions, and this number increased since 2004.

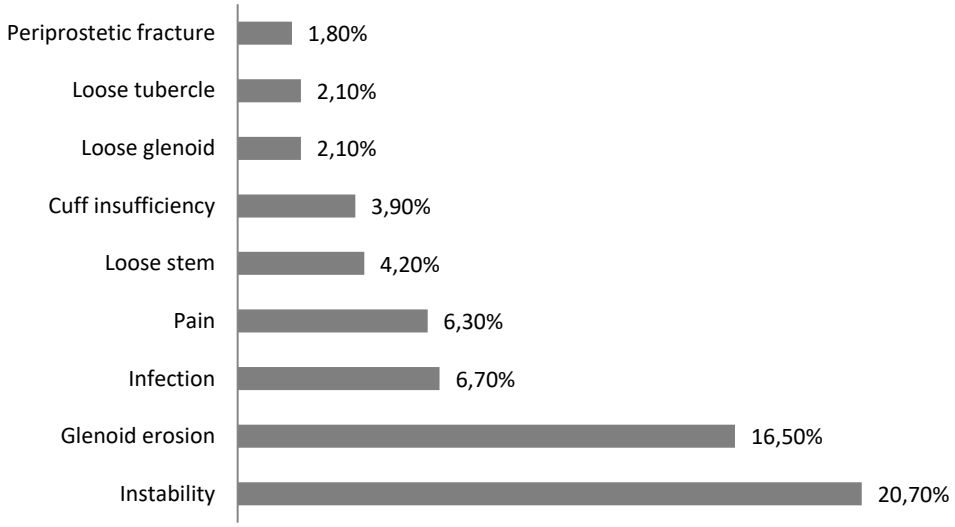

Figure 1.25. Reasons for revision of a prosthesis [91].

Besides information on the diagnosis, type of procedures, or reasons for revision, an arthroplasty register is also concerned with the shoulder implants used in each surgery. The main objective is, on the one hand, to identify the prostheses with better results and, on the other hand, to identify those less adequate in the treatment of shoulder pathologies. The purpose is that the best prostheses are preferred and the worst withdrawn from the market. In this sense, the register provides the revision burden of each of the prosthesis used in Sweden.

The register, reflecting eight years of experience, revealed that the Bipolar concept has the highest revision burden (14.3%), that the Delta-3 reverse prosthesis has revision rates of 8.1%, and the Global prosthesis of 5.5% (see Figure 1.26). Regarding the prosthesis with the lowest revision rates, Anatomical/Sulzer, Tornier Fx and Copeland have rates of 1.4%, 1.1% and 0.6%, respectively. Still, according with the reports [91], the prosthesis mostly used in Sweden, until 2006, were Bigliani-Flatow (694 surgeries, 2.6% revision rate), 3M-Modular (594 surgeries, 3.5% revision rate) and Nottingham (534 surgeries, 2.2% revision rate). In terms of design concepts, total shoulder prostheses have the lowest revision burden of all surgeries (1.1%), followed by hemiarthroplasty, with 2.5%. The reverse concept presents revision rates of 4.8% and the bipolar concept of 10.2%.

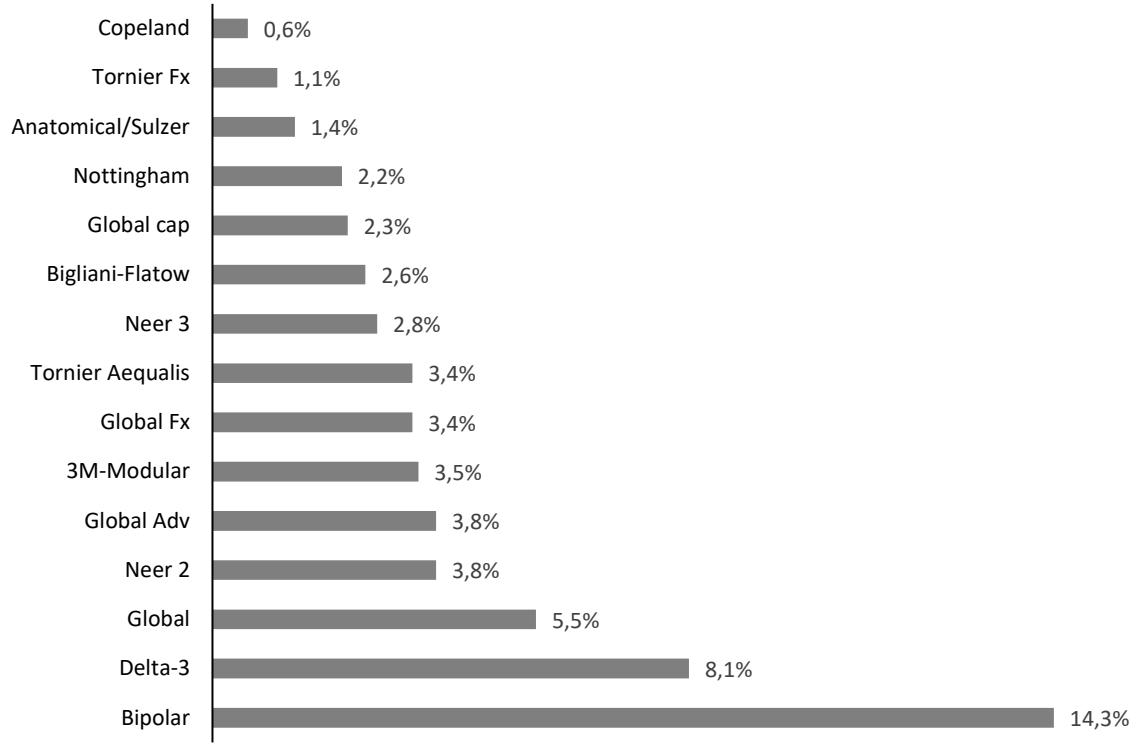

Figure 1.26. Reoperation Burden of the shoulder prosthesis used in Sweden [91].

1.4.2 Australian Orthopaedic Association National Joint Replacement Registry (2008 - 2015)

The Australian Orthopaedic Association National Joint Replacement Registry was established in 1999 with the purpose of improving and maintaining the quality of care of those who submit to a joint replacement surgery. Evidence on hip, knee, shoulder, elbow, wrist, ankle and spinal disc replacement is collected and the information available is very detailed.

The Australian registry categorizes shoulder replacement into three main groups: primary partial, primary total and revision replacement. Subsequently, primary partial and primary total replacements split into classes, depending on the type of prosthesis used. In the primary partial replacements group are partial resurfacing, hemi resurfacing, hemi mid head, hemi stemmed and humeral ball. In the primary total replacements group are total resurfacing, total mid head, total conventional and total reverse. The revision replacements group has fewer sections: minor replacements, major partial replacements and major total replacements [92].

The present output focuses on total conventional shoulder replacements. This group includes glenoid replacement combined with humeral replacement with a stemmed component and humeral head component. This is normally called total anatomic shoulder replacement. In 2014, the procedures increased 6.0% when compared with 2013, having

increased 70.9% since 2008. Primary total shoulder replacement is the most common of all shoulder procedures (see Figure 1.27) with 80.9% of the cases reported in 2014. In between these years, primary partial shoulder replacement decreased from 32.6% in 2008 to 9.2% in 2014. The rate of revision procedures has been around 10% all over the years [92].

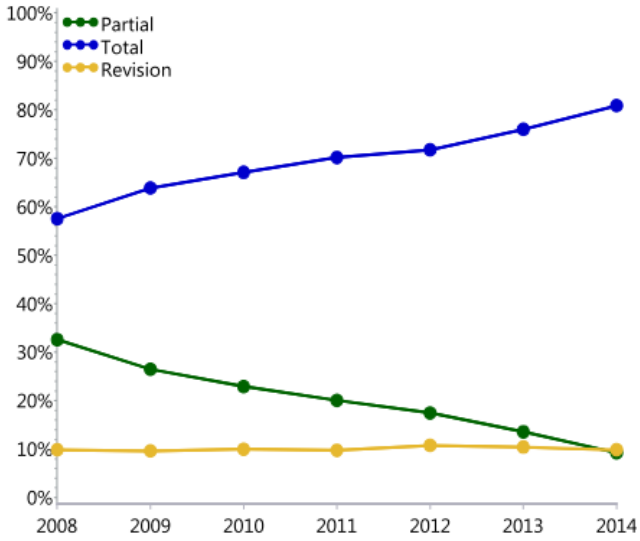

Figure 1.27. Arthroplasty procedures made in Australia between 2008 and 2014 (proportion of shoulder replacement by category) [92].

Primary total shoulder replacement is used in the treatment of osteoarthritis (69.6% of cases), rotator cuff arthropathy (17.3% of cases) and fracture (7.6% of cases). The diagnosis less frequently treated are rheumatoid arthritis (2.3%) and osteonecrosis (1.3%). These procedures are mostly performed in females (62.4%) with an average of 74 years old.

In 2014, total reverse replacement accounted for half (50.8%) of all primary total replacements, whilst total conventional for 46.7%. At seven years of follow up, the cumulative percent revision for total conventional was of 9.4%, and for total reverse was of 5.4%. The reports allow us to observe that between 2008 and 2010, total conventional was the procedure mostly used; and between 2012 and 2014 this tendency changed and the use of total reverse procedure increased.

Osteoarthritis has an eight-year cumulative percent revision of 10.5% for primary total conventional shoulder replacements. At five-year follow up, fracture has the highest cumulative percent revision (11.5%), and rheumatoid arthritis the lowest (4.5%), as shown in Figure 1.28.

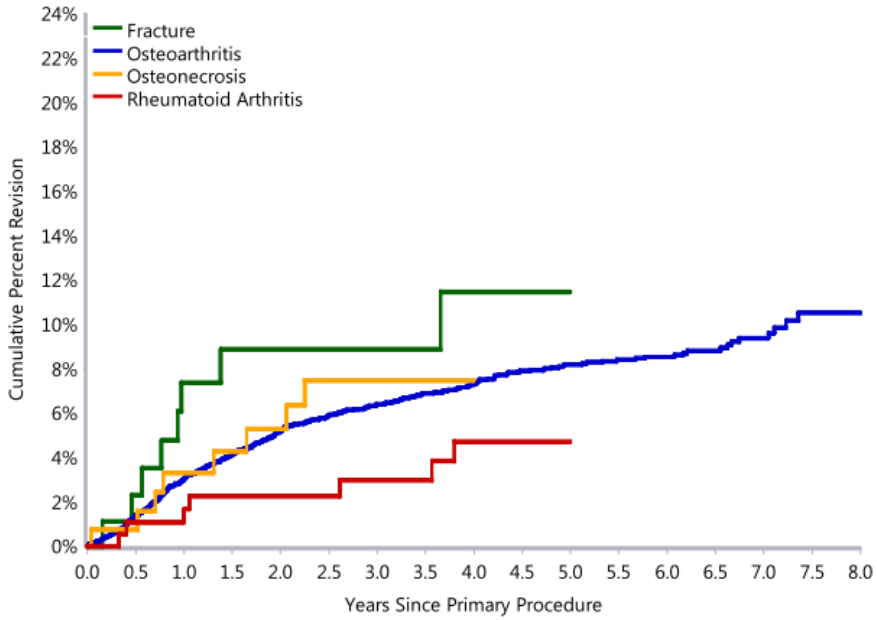

Figure 1.28. Cumulative percent revision of primary total conventional shoulder replacements. Adapted from [92].

Still regarding revision of a primary total conventional shoulder replacement, the most common reason is instability/dislocation, accounting for 26.4% off all revisions. Rotator cuff insufficiency comes next, with 20.7% of cases, and loosening with 16.5% (see Figure 1.29). In Australia, most the revisions are of humeral component (55.6% of cases) and only 8.7% of cases are revisions of the glenoid component.

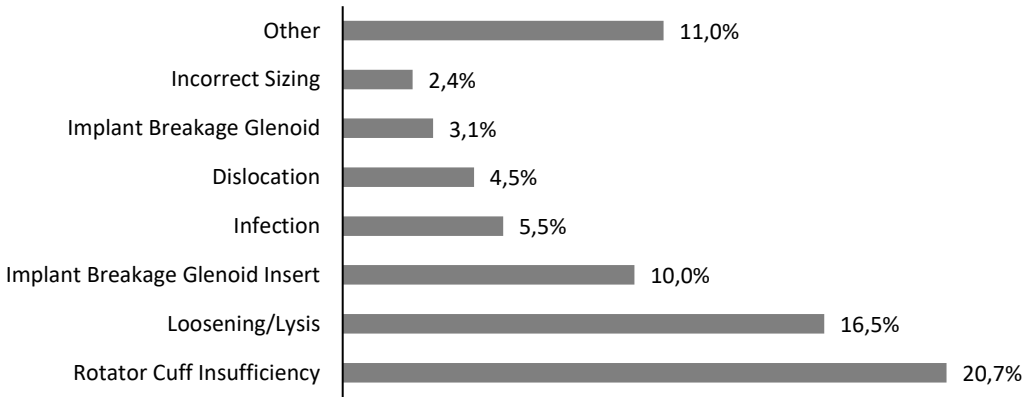

Figure 1.29. Reasons for revision of primary total conventional shoulder replacements [92].

The Australian Registry presents, in its annual report [92], the 10 humeral stem and glenoid prostheses most used in primary total conventional shoulder replacements, since 2008. In the graphs of Figure 1.30 we present only the three mostly used since 2011. The preferred for the humeral stem were GLOBAL AP® Shoulder Arthroplasty System (DePuy Synthes), SMR™ Modular Shoulder System (Lima Corporate), Aequalis® Shoulder System (Tornier). The preferred for the glenoid component were Global (DePuy Synthes), Aequalis (Tornier) and SMR (Lima Corporate). In 2014, these humeral stem prostheses and glenoid prostheses represent 98.2% and 98.9% of all primary total conventional shoulder replacements, respectively.

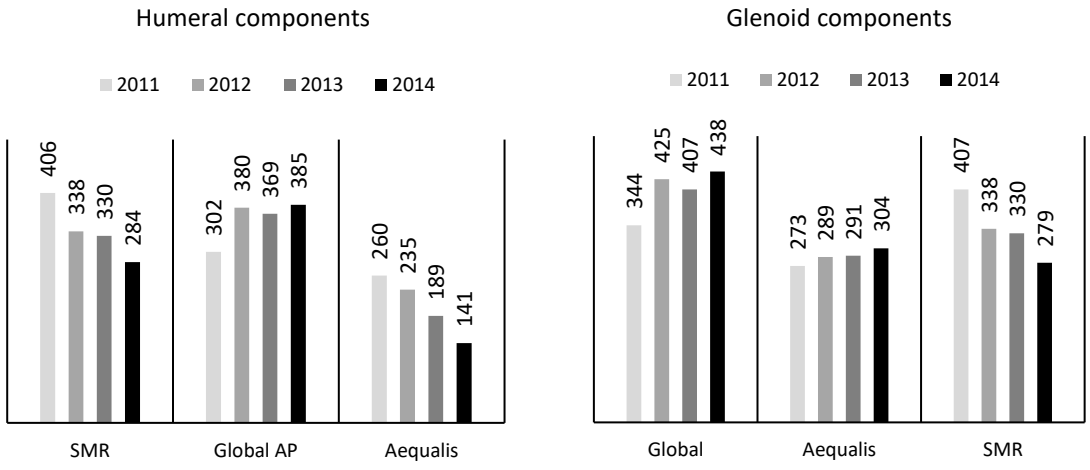

Figure 1.30 - The three humeral stem and glenoid prostheses most used, in primary total conventional shoulder replacement, from 2011 to 2014, in Australia [92].

The fixation type adopted is also an important aspect to evaluate. The Australian registry distinguishes four fixation procedures: all cemented, all cementless, humeral cementless with glenoid cemented and humeral cemented with glenoid cementless. These last two are known as hybrid. In 2014, 67.8% of all primary total conventional shoulder procedures used the hybrid fixation humeral cementless, which has been the mostly used ever since. All cementless procedures are the second mostly adopted, with a rate of 25.8% observed in 2014. All cemented fixation procedures present less than 15% of cases all over the years and the hybrid humeral cemented has an even lower frequency.

Due to its completeness, the Australian registries can draw conclusions related only with osteoarthritis, the main diagnosis of primary total shoulder replacement. For this diagnose, the cementless fixation presents the highest revision rates (4.38%) when compared with the cemented technique (0.97%) and with the hybrid (glenoid cemented) (0.82%) technique. Concerning the glenoid prosthesis, the registries conclude that 69.6% of glenoid

components are all polyethylene and these present lower revision rates (0.84%) when compared to the metal backed glenoid designs with modular (4.82%) or fixed (1.72%) inserts. When comparing the rate of revisions between pegged and keeled all polyethylene glenoids, the registers concludes that there are no significant differences between the two, and that their rate are low (0.841% and 1.01% respectively) [92].

From the registry data, it became evident that many the prosthesis available in the Australian market have similar outcomes. However, the registry could identify other prostheses that present revision rates higher than what was expected. In the case of total conventional shoulder prosthesis, the humeral/glenoid combination SMS/SMR L1 and Vaios/Vaios present revisions rates of 2.7% and of 10.2%, respectively, but were still in use. Moreover, the registry also identified humeral/glenoid combinations that were no longer in use, like SMR/SMR L2 (7.84%) and Univers 3D/Univers 3D (5.71%) [92].

1.4.3 The New Zealand Joint Registry (1999 – 2014)

The New Zealand Joint Registry gathers information on arthroplasty since 1999. It includes data on hip, knee, ankle, shoulder and elbow arthroplasties, but also on lumbar and cervical disc replacements.

Regarding the shoulder, 6 331 primary procedures were registered since the year 2000 (see Figure 1.31) and its amount increases every year, with 7.2% increase over 2013 and 557% increase over the entire 15 years of the register. Of all primary procedures, 38% are total conventional shoulder replacements, 32% are reverse shoulder replacements, 25% are hemiarthroplasty replacements, and the remaining are total resurfacing replacements and humeral sphere replacement (one case). The use of the reverse shoulder prosthesis began to increase in 2004, and already dominates, counting for 56% of procedures in 2014. Concerning patients undergoing surgery, the majority (64.5%) are females, expect in partial resurfacing arthroplasty, where males represent 64.4% of cases [93].

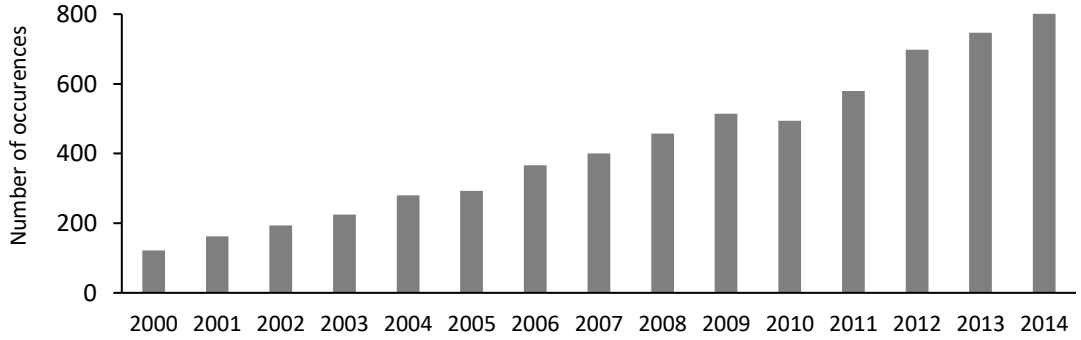

Figure 1.31 – Primary shoulder arthroplasties performed in New Zealand between 2000 and 2014 [93].

Osteoarthritis is the diagnosis mostly treated (53.7%), followed by cuff tear arthropathy (19.8%) and acute fractures of the proximal humerus (10.4%). Rheumatoid arthritis, post old trauma, avascular necrosis, post recurrent dislocations and other inflammatory conditions are also treated. This conclusions are in accordance with the registries of other countries [90].

The prosthesis mostly used between the years 2010 and 2014 are discussed in [93]. Considering the prosthesis for conventional shoulder replacements, SMR has dominated the preferences all four years, but its use saw a small increase rate from 2013 to 2014. The use of Global prosthesis has diminished since 2010, while the use of Global AP increases from 2011 to 2012, but has been diminishing ever since. Still regarding conventional prosthesis, the use of Aequalis had a high growth rate from 2013 to 2014. Regarding the prosthesis for the reverse replacements, the Delta Xtend Reverse is the mostly used. However, its use diminished from 2013 to 2014, while Aequalis Reversed augmented its presence in 2014.

Regarding primary arthroplasties revision, many patients are females (56%) with an average of 70.0 years of age. Pain, dislocation/instability, sub acromial cuff impingements and glenoid loosening are the four main reasons for revision, as shown in the graph of Figure 1.32. Uncemented glenoid prosthesis, that represent 34.8% of all glenoid fixation procedures, presents a revision rate of 2.2%. On the contrary, cemented glenoids have a revision rate of only 0.5%. The revision rate for partial resurfacing of the humeral head is the highest (2.3%). Total shoulder anatomical, reverse and hemi replacements presents small revision rates of 1.0%, 1% and 1.1%, respectively [93].

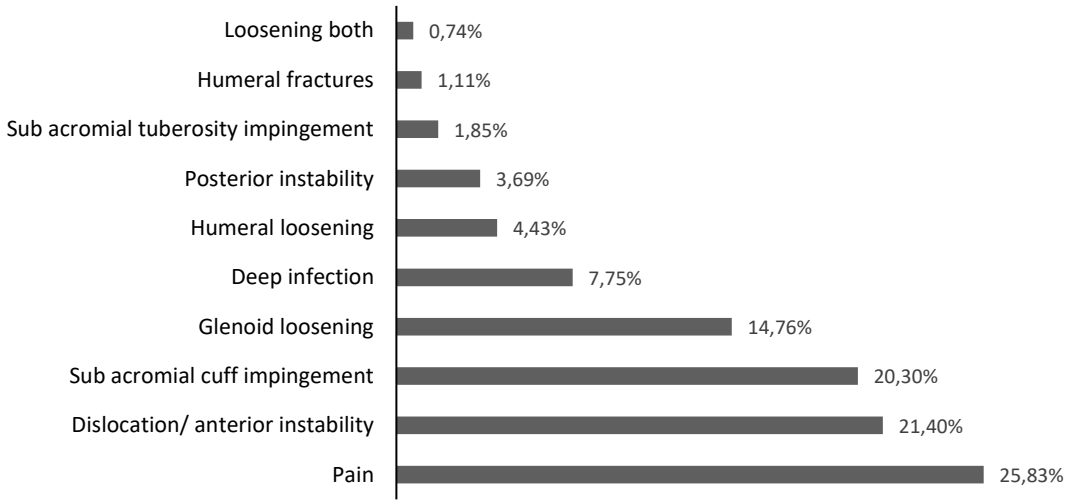

Figure 1.32 – Reasons for revision of primary shoulder arthroplasties in New Zealand [93].

1.4.4 National Joint Registry for England, Wales and Northern Ireland (2012 – 2015)

The National Joint Registry for England, Wales and Northern Ireland, established in 2003, extended its data collection in 2012 to include the shoulder and elbow joint replacements. It also implemented a pilot study on the Patient Reported Outcomes Measures for shoulder replacements. The data is collected at six months post-operatively.

From 1 April 2012, until 31 December 2014, 11.399 primary shoulder replacements were recorder. Of all primary surgeries, 36.2% were reverse shoulder replacements, and 29.4% were total anatomical replacements. Hemiarthroplasty and resurfacing hemiarthroplasty had 15.4% and 13.8% of cases, respectively, while resurfacing total arthroplasty only 5.2%. The mean age of patients undergoing primary surgery was of 73 years old, being that woman were the majority (71.6%) [94].

The reasons for primary shoulder replacement are in accordance with those of other countries, with osteoarthritis and cuff tear arthropathy the most frequent (58.5% and 23.7%, respectively). Each of the other pathologies has a frequency of less than 8%.

Osteoarthritis was treated mainly with total shoulder replacement, resurfacing total arthroplasty and resurfacing hemiarthroplasty, while cuff tear arthropathy was treated with reverse shoulder arthroplasty in more than half of cases (see Figure 1.33) [94].

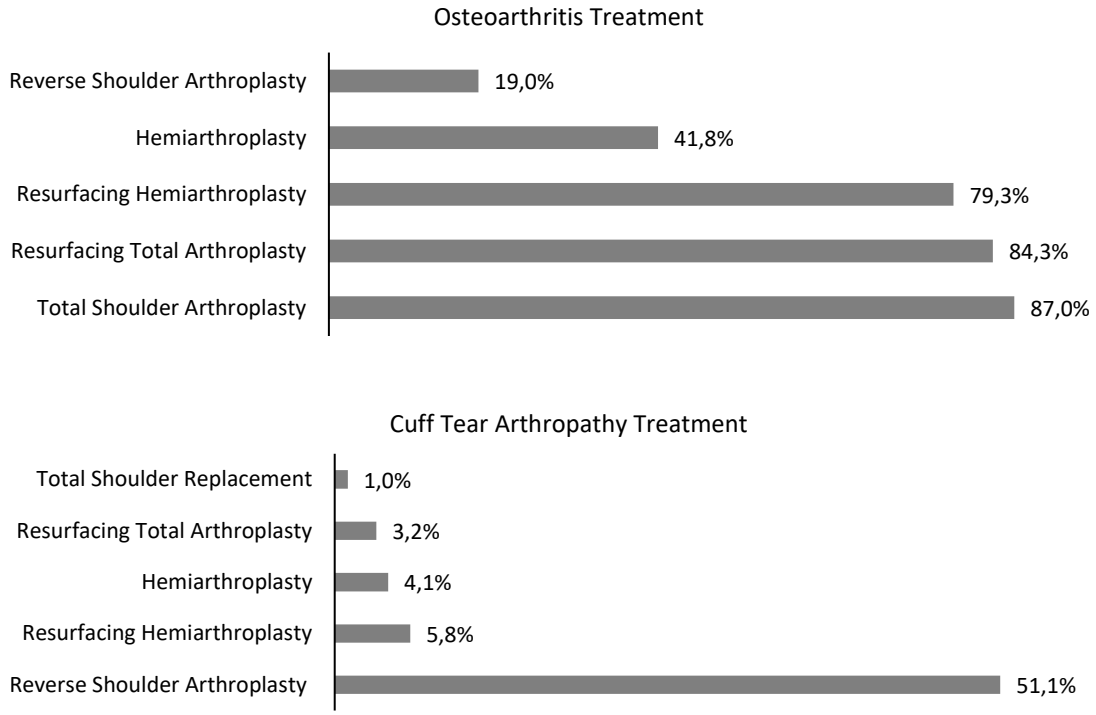

Figure 1.33. Procedures used in the treatment of osteoarthritis and cuff tear arthropathy [94].

The overall cumulative percentage of revision after a primary shoulder replacement, at 1.2 and 2.5 years, was of 1.1% and 2.4%, respectively. At 2.5 years, hemiarthroplasty and resurfacing hemiarthroplasty have the highest estimates (approximately 3.5%), closely followed by reverse shoulder arthroplasty (approximately 3%). The smaller cumulative percentage of revision are of total shoulder replacement and resurfacing total arthroplasty.

The five main reasons for revision of a primary shoulder procedure are instability, cuff insufficiency, infection, conversion from hemiarthroplasty to total arthroplasty and aseptic loosening, as exposed in Figure 1.34. The revision procedures preferred are reverse shoulder arthroplasty (60%) and total shoulder replacement (22.4%), [94].

Figure 1.34. Reasons for revision of primary shoulder arthroplasty in England, Wales and Northern Ireland [94].

1.4.5 The Portuguese Arthroplasty Registry (2009 - 2013)

The Portuguese Arthroplasty Registry, officially created in April 2009, was an idea of the Portuguese Society of Orthopaedics and Traumatology. The registry faces problems because not all hospitals adhered to it, and because there seems to be a lack of interest of many arthroplasty surgeons, major players in this process. This leads to low registration rates (only 57% in 2010, [95]) and poor conclusions. Still, we make a general evaluation related to shoulder arthroplasty.

The majority of shoulder replacement surgeries were performed in females (77% of cases in 2011 [95]), which is in accordance with what is observed in other countries [92]. In 2013, the diagnosis mostly treated was recent fracture (30 surgeries), followed by centred and decentred osteoarthrosis (17 surgeries each) and by rotator cuff tear (15 surgeries). In 2010, 50% of surgeries were hemiarthroplasty procedures and 31% were reverse arthroplasty procedures. This tendency was not maintained during 2011, with reverse arthroplasty chosen in 49% of cases and hemiarthroplasty in 32% of them. This tendency was kept in 2013 [95]. This observation is in some agreement with other countries.

Concerning fixation types, cemented arthroplasty holds 64% of cases and uncemented arthroplasty the remaining 36% in both years. This is not in accordance with the Australian reality, where all cemented fixation procedures present less than 15% of all cases [92].

1.5 Designs in the Market

As the arthroplasty registers showed, there is a vast diversity of implant designs available in the market. Figure 1.35 presents the three anatomical and reverse concepts mostly used worldwide.

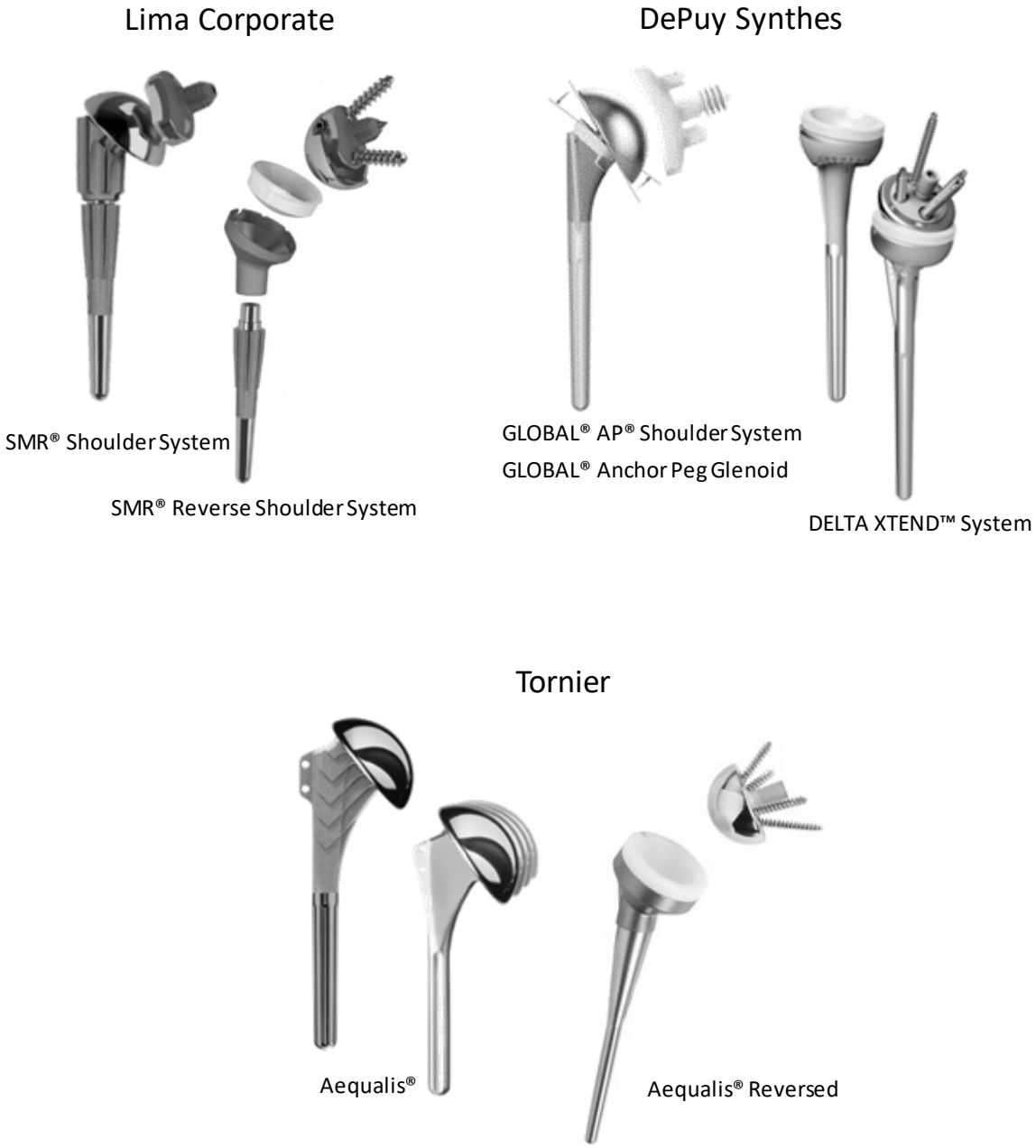

Figure 1.35. Anatomical and reverse prosthesis mostly used worldwide.

1.6 Conclusions

The glenohumeral joint has one of the most complex anatomy and biomechanics of all human joints. Adding to the high number of muscles and ligaments that compose it, the joint has a high degree of mobility and is a very instable mechanical system.

As with other joints, osteoarthritis is the pathology that mostly affects the shoulder and elderly women are the main target, typically treated with anatomical total shoulder arthroplasty (TSA). In cases of osteoarthritis associated with an intact rotator cuff, TSA seems to perform better than HA, but in cases of cuff tear arthropathy the HA procedure allows the achievement of superior results. Nonetheless, the reverse total shoulder arthroplasty (RTSA) is the procedure mostly used in the treatment of such severe condition.

Favard *et al.* [96] analysed, during a minimum follow-up of 8 years, the results and complications of TSA, RTSA and of HA. Of the 92 TSA evaluated, 28.5% had effective loosening, while there was suspicion of loosening in 17.4% of cases. On the RTSA group, effective loosening was present in only 3.4% of cases, whereas suspected loosening was present in 10% of cases. The study confirms the significant difference in glenoid loosening between TSA and RTSA in mid-term follow-up. This adds to the importance of studying the causes of glenoid loosening in TSA.

In a recent study, Kiet *et al.* [97] analysed the outcome results of shoulder arthroplasty in a clinical follow-up of nearly 2 years. Anatomical and reverse concepts were compared for glenohumeral arthritis and rotator cuff tear arthropathy, respectively. At the 2-year evaluation, major complication rates were low for the two procedures (15% for TSA and 13% for RTSA), as well as for the need of revision surgery. Patient-reported outcomes were also similar. The study demonstrates that TSA and RTSA may experience similar clinical outcomes closely after surgery.

During the last decades, there was an increasing conscience of the importance of bone on helping to achieve a successful surgery. In this sense, new arthroplasty concepts and component designs that try to preserve bone as much as possible have been developed. The humeral stem has become shorter [45, 53] and the glenoid component has been constructed only with polyethylene [71, 73], with polyethylene and a metal-backed component, or incorporating both polyethylene and metallic surfaces that promote bone ingrowth and ongrowth [98]. A big discussion around all-PE components and metal-baked components was observed and the majority of the authors agree that all-PE glenoid implants perform better than metal-backed implants [61, 62]. Furthermore, many also agree that all-PE pegged implants are preferred to all-PE keeled implants [64, 65].

Despite the encouraging results of the new implant designs, failure of the glenoid component continues to be one of the most common sources of arthroplasty revision. Moreover, if it is true that our current knowledge on this problem has increased over the last decades, it is also true that much more needs to be done [59, 60].

Globally, we have a clearer vision of shoulder arthroplasty importance by means of the shoulder arthroplasty registers of some countries. These reports allow us to conclude that anatomical total shoulder arthroplasty is the procedure mostly used and that there is a trend in the use of reverse shoulder arthroplasty in the treatment of more complicated cases, such as rotator cuff arthropathy.

With register comparison it is interesting to observe that in Sweden [90] HA is the procedure mostly used, but that it started to decrease with the increase of total anatomical and total reverse procedures around the year 2008. On the contrary, in Australia [92] the use of partial replacements (hemiarthroplasty included) was always inferior than the use of total anatomical and reverse replacements.

Since some reports are relatively new, not all allow us to conclude on the cumulative percent of revision (CPR) at 10-years after surgery. In Sweden, the CPR at 10-years is of 3.3% for osteoarthritic cases and of 4.8% for rheumatoid arthritis, whilst a smaller 2.4% at 10-years was observed for the total shoulder replacement [99].

In New Zealand, the overall CPR at 10-years was of 8.4%, being equal to 9% for total shoulder arthroplasty. In Australia, the CPR at 7-years equals 10.1% for conventional total shoulder arthroplasty in the treatment of osteoarthritis.

Chapter 2

Modelling of Shoulder Muscle Actions

2.1 Multibody Models

Over the last decades, several numerical shoulder models, with different degree of detail, have been developed. The simplest models found in scientific literature aim to represent shoulder's gross structure considering two or three rigid linkages to be connected by joints [100]. These are normally used in robotics, since the importance relays in equivalent kinematic shoulder structures and not on a realistic replica of the shoulder.

The modelling of human articulations began by focusing mostly on the hip and knee than on the shoulder. The main reasons that justify this fact are twofold. On the one side, hip and knee surgeries started long before shoulder surgeries did [101], which could have brought the necessity for hip and knee numerical models. On the other side, shoulder joint has a very complex anatomy that may have caused some reluctance on starting to develop sophisticated 3D numerical models.

Generally, numerical models can be grouped into musculoskeletal models and finite element models. The choice for one of them depends on the aspect under study. Musculoskeletal models, also called multi-body or rigid-body models, consist of rigid bodies connected between each other through kinematic constraints. Their goal is to study the functional capability of muscles. With respect to finite element models, they allow to study aspects such as bone deformation and strain response due to muscle activity.

Numerical models have been developed addressing different needs. Some focus on biomechanical principles to understand shoulder mechanisms [102, 103], others point their efforts in understanding shoulder behaviour in both daily living and working activities [104, 105]. Models reflecting possible structural changes [106, 107] are also of extreme importance, as they help to comprehend how shoulder performance is affected and how to enhance it. There are also models focused on strain behaviour as a result of muscle force [108, 109].

Since the present goal is to perform a numerical modelling of shoulder muscle actions, the musculoskeletal modelling approach was adopted. Over the last decades, some 3D musculoskeletal shoulder models have been developed, such as the Swedish Shoulder Model (1992) by Karlsson and Peterson [110], the Delft Shoulder Model (DSM) (1994) by van der Helm [111], the model developed by Garner and Pandy (2001) [112], the Newcastle Shoulder Model (2003) by Charlton [113], the model developed by Holzbaur (2005) [114] and the Waterloo Shoulder Model (2007) by Dickerson *et al.* [115].

The model developed by van der Helm is probably the most well-known three-dimensional musculoskeletal model that aimed to describe the function of shoulder's morphological structures [111, 116]. Being very detailed, it includes the sternoclavicular joint, the acromioclavicular joint and the glenohumeral joint, all modelled as spherical joints. The clavicle, scapula, sternum and humerus are also modelled, as well as three extra capsular ligaments and muscles. The complex mechanism between these morphological

structures has seven degrees of freedom: four at the shoulder girdle and three at the humerus. The modelling of all those anatomical structures was accomplished with the use of finite elements of simple geometry (truss elements, hinge elements and beam elements) in a computer program tailored for the dynamic analysis of multi-body systems. Kinematics of the shoulder mechanism was expressed in terms of the motion of the generalized coordinates. Positions and motions of the bone segments, and the external loads, were chosen as input variables to the model. Forces generated by the active elements (muscles and joints), muscle lengths and moments arms were the calculated outputs through an inverse-dynamic system. In the DSM there is an indeterminate system to solve to determine muscle forces and four optimization criteria were investigated [111]:

a) Minimization of the sum of quadratic muscle forces:

$$minimize \sum (F)^2 \qquad \text{Eq. 2.1}$$

b) Minimization of the sum of quadratic muscle stresses:

$$minimize \sum \left(\frac{F}{PCSA}\right)^2 \qquad \text{Eq. 2.2}$$

where PCSA is the physiologic cross sectional area of each muscle.

c) Minimization of the sum of quadratic muscle forces, normalized to the maximal muscle force $F_{i\,max}$, which in turn depends of the PCSA and length of the muscle:

$$minimize \sum \left(\frac{F}{F_{i\,max}}\right)^2 \qquad \text{Eq. 2.3}$$

d) Minimization of the maximal muscle stress in the entire mechanism:

$$minimize\ max\left(\frac{F_1}{PCSA_1}, \frac{F_2}{PCSA_2}, \dots, \frac{F_i}{PCSA_i}, \dots, \frac{F_N}{PCSA_N}\right) \qquad \text{Eq. 2.4}$$

Van der Helm pointed out weaknesses of each optimization criteria listed above: the results of criterion (a) are incorrect, since it does not account for muscle stress; results of criterion (b) are influenced by muscles with large moment arm, since those are favoured mathematically; the disadvantage of criterion (c) is related with the optimum length of the muscles, which is not known for *in vivo*; the last optimization criterion (d) is numerically unstable.

Although none of the studied criteria provides acceptable results, criterion (b) was the preferred. The calculated force-time curves were then compared to surface electromyography (EMG) signals in view to qualitatively validate the model [116]. Comparisons show acceptable agreement in the timing of muscle activations, but EMG amplitude cannot be used for direct validation of musculoskeletal model because EMG does not directly measure muscle forces.

The original DSM [111] was later modified to consider the elbow, being renamed Delft Shoulder and Elbow Model (DSEM). The elbow data are in part presented in a recent work of Nikooyan *et al.* [117], where the musculoskeletal model of the shoulder and elbow is presented. Muscle dynamics was also introduced in the shoulder model as a constraint of the optimization process on the maximum acceptable muscle force [118]. Another modification employed is related with the objective function used in the optimization system. Originally, minimization of the squared muscle stress was preferred (Eq. 2.2), but an energy-based objective function has been implemented [119], leading to more realistic predictions of muscle activation.

In a general way, musculoskeletal models are grouped into forward or inverse dynamic models [120]. Forward dynamic models are a cause/effect type of system: when force is applied on a skeleton, its motion can be predicted. So, forces work as input and motion is the output. However, when studying human movement, the opposite happens: motion is the measured variable and muscle forces are the unknowns. Thus, motion is the input and forces are the outputs. To calculate them, the sum of moments acting on a joint is computed by solving the equations of motion established. Afterwards, muscles whose combination produce the calculated joint moments are selected. Given the many muscles available in the human body this is an indeterminate system, as different muscle combinations can cause the same moment. This computational challenge is known as muscle redundancy and has already been studied [121, 122].

2.2 Muscle Recruitment in Inverse Dynamic Problems

In inverse dynamics, muscle redundancy is solved by formulating an optimization problem to recruit the best muscle combination between the existent. Mathematically we have to [123]:

Eq. 2.5

$$\underset{\mathrm{f}}{\text{Minimize}}\; G(\mathbf{f}^{(\mathrm{M})})$$

Subjected to

Eq. 2.6

$$\mathbf{C}\mathbf{f} = \mathbf{d}$$

Eq. 2.7

$$0 \leq f_{\mathrm{i}}^{(\mathrm{M})} \leq N_{\mathrm{i}} \quad , \quad \mathrm{i} \in \{1, \dots, n^{(\mathrm{M})}\} \quad ,$$

where G is the criterion chosen for the muscle objective function and is stated in terms of muscle forces $\mathbf{f}^{(\mathrm{M})}$. Furthermore, G is minimized with respect to all unknown forces in the problem: muscle forces $\mathbf{f}^{(\mathrm{M})}$ and joint reactions $\mathbf{f}^{(\mathrm{R})}$.

The optimization problem constraints are stated in Eq. 2.6 and Eq. 2.7. The first is the dynamic equilibrium equation, where **C** is the coefficient-matrix for the unknown forces; **f** is the matrix containing all unknown forces in the problem (muscle forces and joint reactions); and **d** is a matrix with all known applied loads and inertia forces. This equation means that whatever solution found must balance the external forces. Regarding Eq. 2.7, it states that muscles can only contract to exert force ($f_{\mathrm{i}}^{(\mathrm{M})} \geq 0$) and have its capacity limited by its strength ($f_{\mathrm{i}}^{(\mathrm{M})} \leq N_{\mathrm{i}}$). The question that remains with no correct answer is related with knowing what objective function mimics the strategy of the central nervous system when recruiting muscles for the many activities performed by the body. Muscle stress [124] and muscle energy consumption [119] are some examples.

According to Damsgaard *et al.* [123], the polynomial criterion is the most popular form of the objective function and has been used in several studies [125, 126], having the following mathematical expression:

Eq. 2.8

$$G\left(\boldsymbol{f}^{(M)}\right) = \sum_{\mathrm{i}=1}^{n^{(M)}} \left(\frac{f\mathrm{i}^{(M)}}{N\mathrm{i}}\right)^{p}$$

In Eq. 2.8, $f\mathrm{i}^{(M)}$ is the muscle force of muscle i, Ni is the strength of the muscle and the ratio between the two is known as muscle activity.

Another popular objective function largely used [127, 128] has the goal of minimizing the maximal muscle activity [129] and it is mostly known as the min/max formulation. It has the subsequent form:

Eq. 2.9

$$G\left(\mathbf{f}^{(\mathrm{M})}\right) = min\left(max\left(\frac{f\mathrm{i}^{(M)}}{N\mathrm{i}}\right)\right)$$

2.3 Critical Movement at the Shoulder Joint

Numerical simulations need validation through the comparison of the numerical results with experimental data. Nowadays, it is possible to measure *in vivo* contact forces and contact moments on the shoulder joint thanks to an instrumented shoulder prosthesis, with telemetric data transmission, developed by Westerhoff *et al.* [130]. The instrumented prosthesis was placed in four patients so to perform the characterization of glenohumeral joint contact loads for some activities of daily living [131]. It was observed that even though force measurements were reproducible for each patient, correlation between patients was difficult due to differences in anthropometry, weight and age. Still, the study allowed the authors to present some advices regarding activities to avoid after a shoulder arthroplasty. These included exercises such as manoeuvring a weal with one hand or lifting and lowering a weight with stretched arm.

Since the studied activities were not standardized movements, and were not repeatable amongst patients, Bergmann *et al.* [132] studied *in vivo* glenohumeral joint forces during abduction and forward flexion, hoping to obtain more consistent conclusions. The six patients involved in the study received the instrumented implant due to osteoarthritis. In all cases the rotator cuff muscles allowed glenoid preservation. Patients had distinct weights, heights, ages and physical abilities. The authors observed that arm elevation with an additional external load of 2.0 kgf increases the Glenohumeral Joint Reaction Force (GH-JRF). This increase is more pronounced in abduction than in forward flexion, as expressed in Figure 2.1 (A). On the other hand, fast arm motion decreases forces measured at the joint: -20% in abduction and -19% in forward flexion without external load. Furthermore, patients were not able to perform slow abduction with an external load of 2.0 kgf for more than 90°. Regarding joint moments, they vary even more than forces, as Figure 2.1(A and B) suggest.

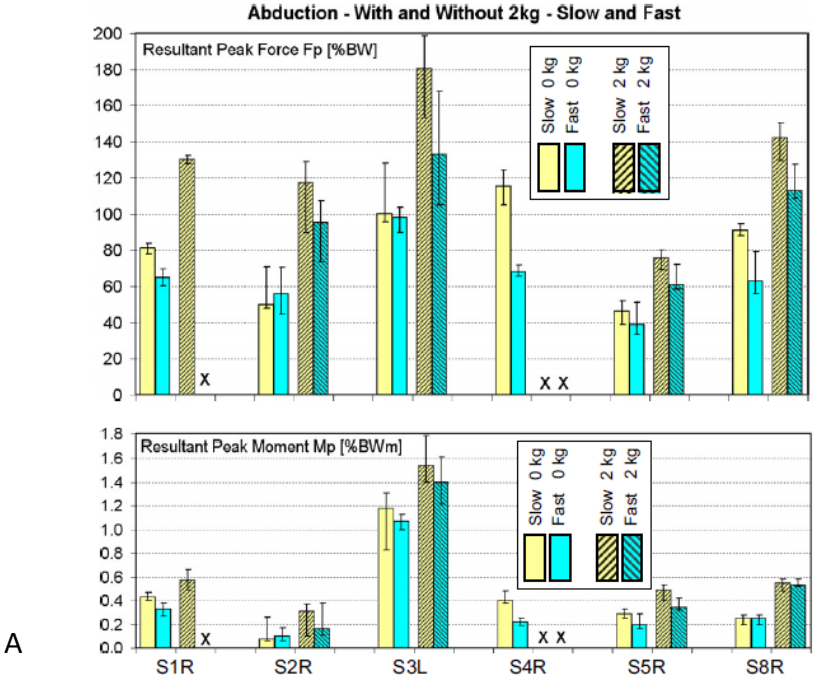

A

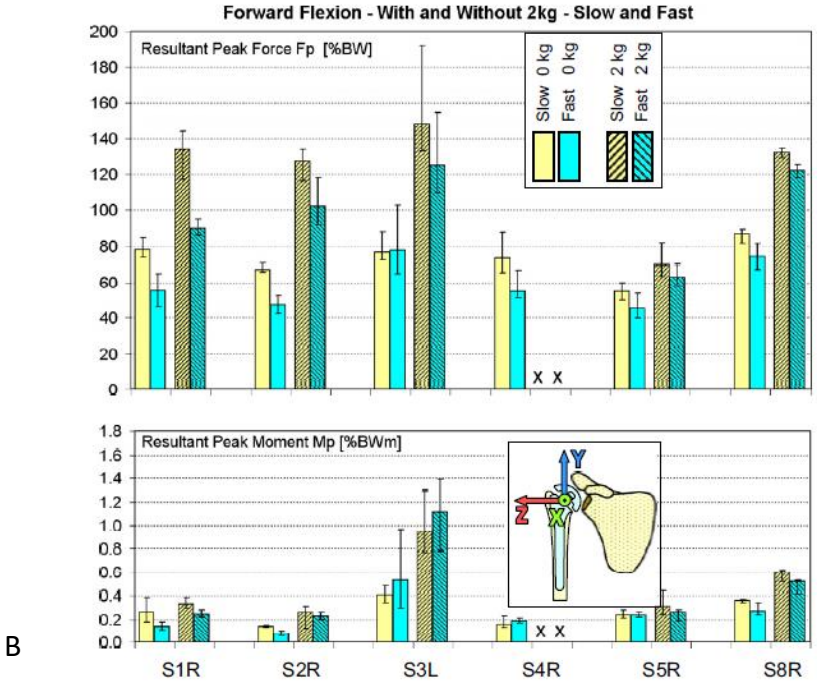

B

Figure 2.1. Resultant peak forces and peak moments for abduction (A) and forward flexion (B), with and without load, in slow and fast motion. SiR – Subject i Right shoulder; SiL – Subject i Left shoulder. Adapted from [132].

The graphs in Figure 2.2 show the GH-JRF obtained with the instrumented prosthesis for a 90° arm abduction/adduction and for a 120° arm flexion/extension, over time, without external load (https://orthoload.com/database/, accessed in May 2013). Despite the small difference in movement extent between abduction and flexion, the graphs illustrate that GH-JRF is higher for 90° abduction than for 90° flexion. The GH-JRF for the same movements as before, but for distinct loading cases, is represented in the graphs of Figure 2.3. The results allow the confirmation that GH-JRF increases with external load increase.

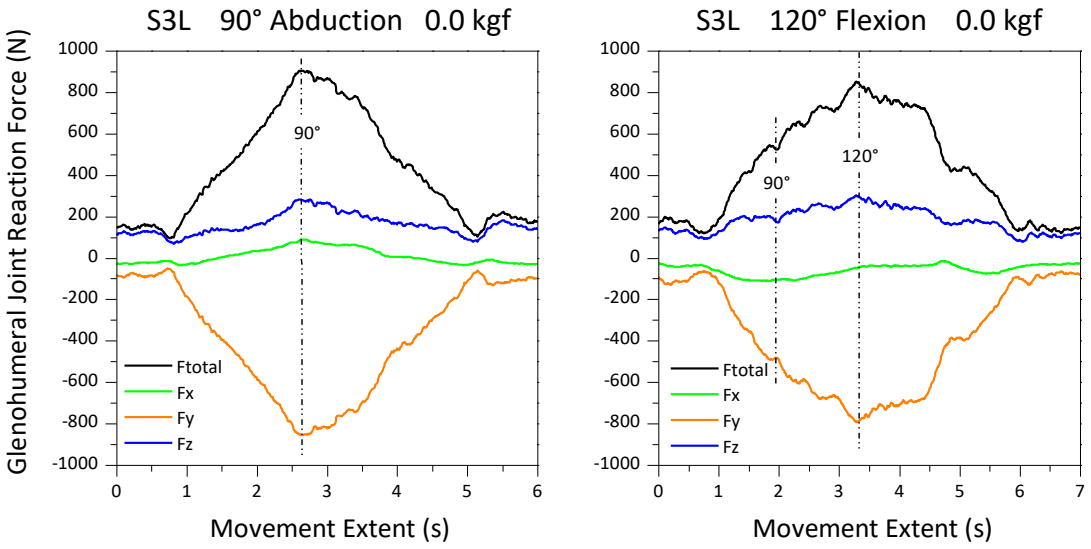

Figure 2.2. Results obtained with the instrumented shoulder prosthesis for abduction and forward flexion without external load. Subject S3L (L: left arm). (https://orthoload.com/database/).

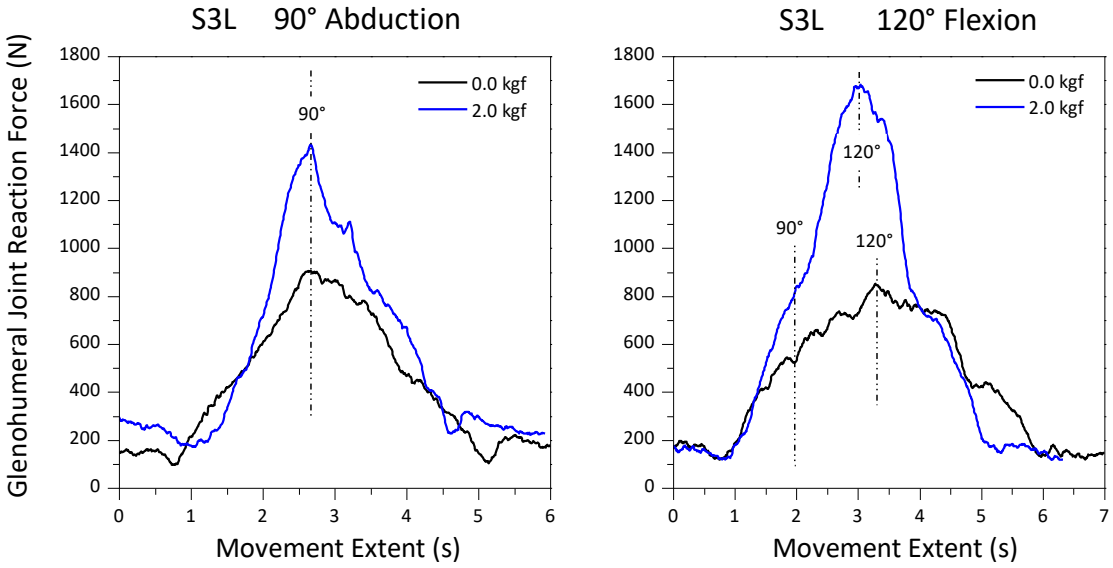

Figure 2.3. Comparison between the GH-JRF in abduction and in forward flexion with and without external load. Patient S3L (L: left arm). (https://orthoload.com/database/).

Bergmann *et al.* [132] concluded that the most severe testing conditions were recorded during 90° slow abduction and forward flexion with an external load of 2.0 kgf on the hand. These testing conditions represent critical movement in the shoulder joint.

As the present goal was to numerically characterize shoulder motion in a critical movement, a 90° slow abduction was the movement chosen to study. Thus, a reconstruction of the experiments of Bergmann *et al.* [132], on *in vivo* glenohumeral joint loads during forward abduction, were developed using of AnyBody™.

2.4 AnyBody™ Modelling System

The AnyBody™ Modelling System (version 5.0.0 (2014) [Computer software]. Aalborg, Denmark: AnyBody™ Technology. Available from http://www.anybodytech.com), from now on called AnyBody™, is a software specifically developed for musculoskeletal modelling. We used it to perform the numerical characterization of shoulder muscle actions.

AnyBody™ allows the analysis of body models with many muscles and degrees of freedom [123]. The modelling is accomplished by a text-based input, with a specially developed object-oriented language, called AnyScript. AnyBody™ uses inverse dynamic analysis and muscle redundancy is solved by formulating an optimization problem (see section 2.2). A standard rigid-body model is available for simulations (amongst other models) and Hill-type muscles are implemented in the standard model.

Muscle properties involved in a simulation are a major aspect to consider in inverse dynamics and thus muscle modelling is a very important feature to comprehend. In AnyBody™ there are three distinct muscle models that can be used with three different muscle types. The most elementary muscle model only needs information regarding the force that the modelled muscle performs in a static position at its optimum length. This force is usually considered to be proportional to the PCSA of the muscle. Another muscle model available incorporates a muscle and a tendon, which are the contractile and the linear-elastic elements, respectively. The muscle strength is proportional to its current length and to the velocity with which it contracts. Consequently, when its length decreases, or the contraction velocity increases, the muscle weakens. The Hill type muscle model is the last one available in AnyBody™ and is a very detailed model that considers numerous muscle properties. It has the drawback of requiring physiological parameters that are not easy to find or estimate and it is also very sensitive to model specifications [133].

Regarding muscle types, the simplest is the via-point muscle, where the muscle being modelled passes through a minimum of two points: one in its origin site (origin-point) and another in its insertion site (insertion-point). Muscles are always rigidly fixed to these points and, thus, forces transferred from the muscle to the origin-point and insertion-point are always in a longitudinal direction. In addition, muscles are not rigidly fixed to other

points that may exist between the origin-point and the insertion-point. Accordingly, the direction of the transferred forces to these other points depends on the angle formed by the muscle on the two sides of each of these points. Points created by the user can be attached to a segment (rigid body) or to the model global reference frame.

Another muscle type available in AnyBody™ is the wrapping muscle, easier to handle than the former. As its name suggests, the muscle wraps around surfaces (like bones) while having one origin point and one insertion point. If the surfaces in which the muscle wraps are blocked for any reason, then the muscle slides easily and with no friction over them.

The third and last muscle type is a more general class of muscle, and less physiological, that works as an actuator in anything the user wishes to measure with an algorithm (a full description of the way muscles are built can be found in the software tutorials, available in https://www.anybodytech.com/fileadmin/AnyBody/Docs/Tutorials/_template/FrontPage/FrontPage.html).

2.4.1 Intact Shoulder Model

The AnyBody™ Shoulder Model of the repository v.1.3.1 was used. It is constructed based on data and modelling premises of the Delft Shoulder Model [111, 116] (as described in 2.1) and simulates an average European male (75 kg of weight; 1.80 m of height). The model has 118 Hill-type muscle units linked to bones using tendons. Muscles are divided into several segments. The number of segments per muscle for scapulothoracic and glenohumeral muscles are stated in Table 2.1.

Table 2.1. Muscles of the shoulder included in the original AnyBody™ shoulder model.

	Shoulder Muscles	Muscle Segments		Shoulder Muscles	Muscle Segments
Scapulothoracic Muscles	Levator Scapulae	4	Glenohumeral Muscles	Latissimus Dorsi	5
	Rhomboid Major	3		Pectoralis Major	10
	Rhomboid Minor			Deltoideus	12
	Trapezius	12		Coracobrachialis	6
	Pectoralis Minor	4		Teres Major	6
	Serratus Anterior	6		Triceps Brachii	6
	Subclavius	*Not considered*		Biceps Brachii	2
				Subscapularis	6
				Supraspinatus	6
				Infraspinatus	6
				Teres minor	6

The glenohumeral capsule and all its ligaments are not simulated and the most important joints of the shoulder are modelled as spherical and in view of accounting for glenohumeral stability, muscle recruitment considers that the reaction force is directed always into the glenoid fossa. This means that muscle combinations allowed are the ones that generate resulting forces inside the glenoid.

A comprehensive computational reconstruction of the experiments of Bergmann *et al.* [134], for a 45° shoulder abduction of a patient that received an instrumented shoulder implant, was developed by Rasmussen *et al.* [135] (algorithm available in AnyBody™). The authors tried to obtain the same glenohumeral joint contact forces measured by the instrumented implant. Their goal was to validate the AnyBody™ intact shoulder model by comparing *in vivo* with computed glenohumeral joint reaction forces. Consequently, a force measurement tool that reads forces in the humeral coordinated system, similarly to the instrumented shoulder prosthesis, was implemented in the algorithm.

The joint coordinate system used is based on recommendations of the International Society of Biomechanics [136] and is depicted in Figure 2.4. It is set at the centre of the implant head and moves with the arm. The positive x-axis points anteriorly and abduction takes place around it, parallel to the humeral axis is the y-axis, the positive z-axis points in the lateral direction and forward flexion acts around it. When left-shoulders are used, the raw position data is mirrored with respect to the sagittal plane, that is z = - z.

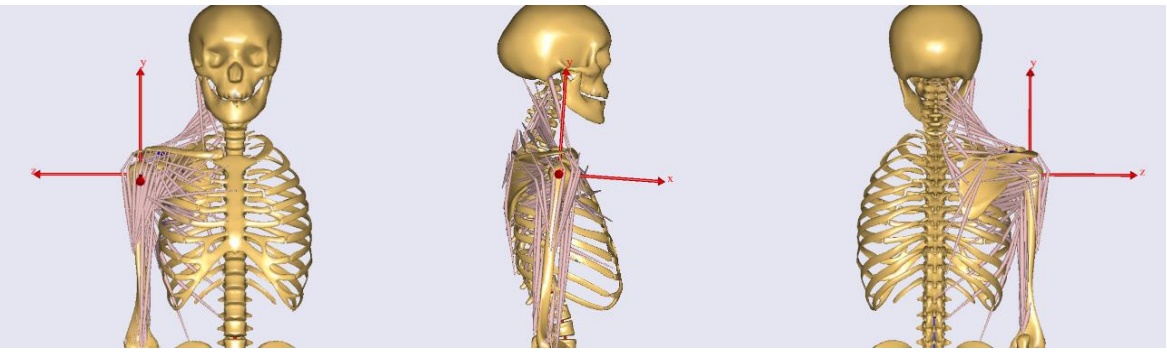

Figure 2.4. Joint coordinate system.

GH-JRF obtained by Rasmussen *et al.* [135] were similar to the experimental ones [134], but the value of the joint forces calculated depends much on the muscle recruitment criterion implemented. The algorithm developed did not considered the shoulder rhythm (relationship between glenohumeral and scapulothoracic joints regarding arm elevation). Later, the shoulder rhythm was formulated [137] with the objective of making the shoulder representation more realistic. This improvement has allowed a better replica of the results of Bergmann *et al.* [134] on a 45° abduction.

In the present study, the algorithm of Rasmussen *et al.* was used. Since AnyBody™ allows to choose shoulder rhythm, this feature was added. The algorithm was also modified to take into account a 90° arm abduction/adduction and also to match movement extent (14 s), weight (101 kg) and height (1.61 m) of subject S1R that participated in the experiments of Bergmann *et al.* [132].

Arm movement is governed by a sine function, as stated in Eq. 2.10, where P is the position of the arm, A and w the movement amplitude and angular frequency, respectively, t its extent and ø the phase:

$$P = Asin(wt + ø) \qquad \text{Eq. 2.10}$$

In the case of a 14 s movement extent, the arm reaches its highest position at 7 s with an angular frequency of 0.224 rad/s. Its angular position during movement is presented in graph of Figure 2.5.

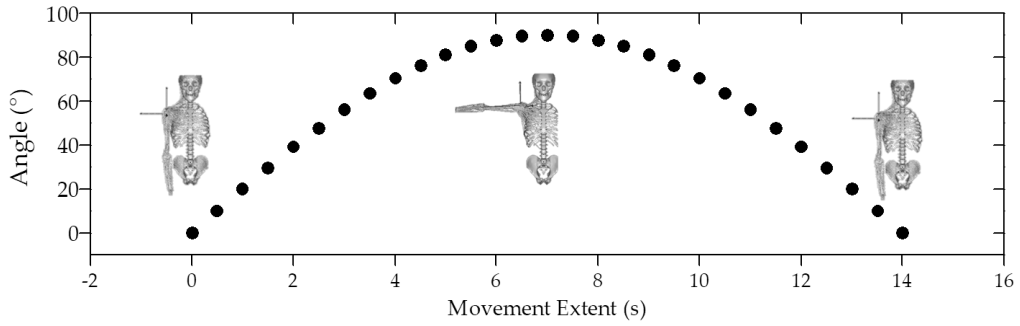

Figure 2.5. Arm angular position during a 90° abduction.

2.4.1.1 90° Abduction without External Load

Numerical simulations of abduction without external load were developed considering quadratic muscular recruitment (p = 2 in Eq. 2.8). As the quadratic criterion penalizes large terms in the sum, it was expected that the load would be distributed between several muscles, rather than in a minimum number of them. Since linear recruitment (p = 1 in Eq. 2.8) is non-physiological, it was not considered in the analysis.

Muscle activity was also determined, since it is a measure of muscle force relative to its strength (f / N). It also shows which muscles participate actively in movement and how much active a muscle is as the movement progresses. It is essential to be aware that muscle activation above 1 is non-physiological and this fact also helps in the process of choosing a muscular recruitment suited for a certain activity.

The numerical results were compared with the experimental ones (https://orthoload.com/database/, accessed in May 2013) and are represented in graphs G1 and G3 of Figure 2.6. GH-JRF measured with the instrumented implant (see graph G1 of Figure 2.6) increases throughout abduction, reaching its peak at nearly 7 s of movement. The arm is then adducted and GH-JRF decreases.

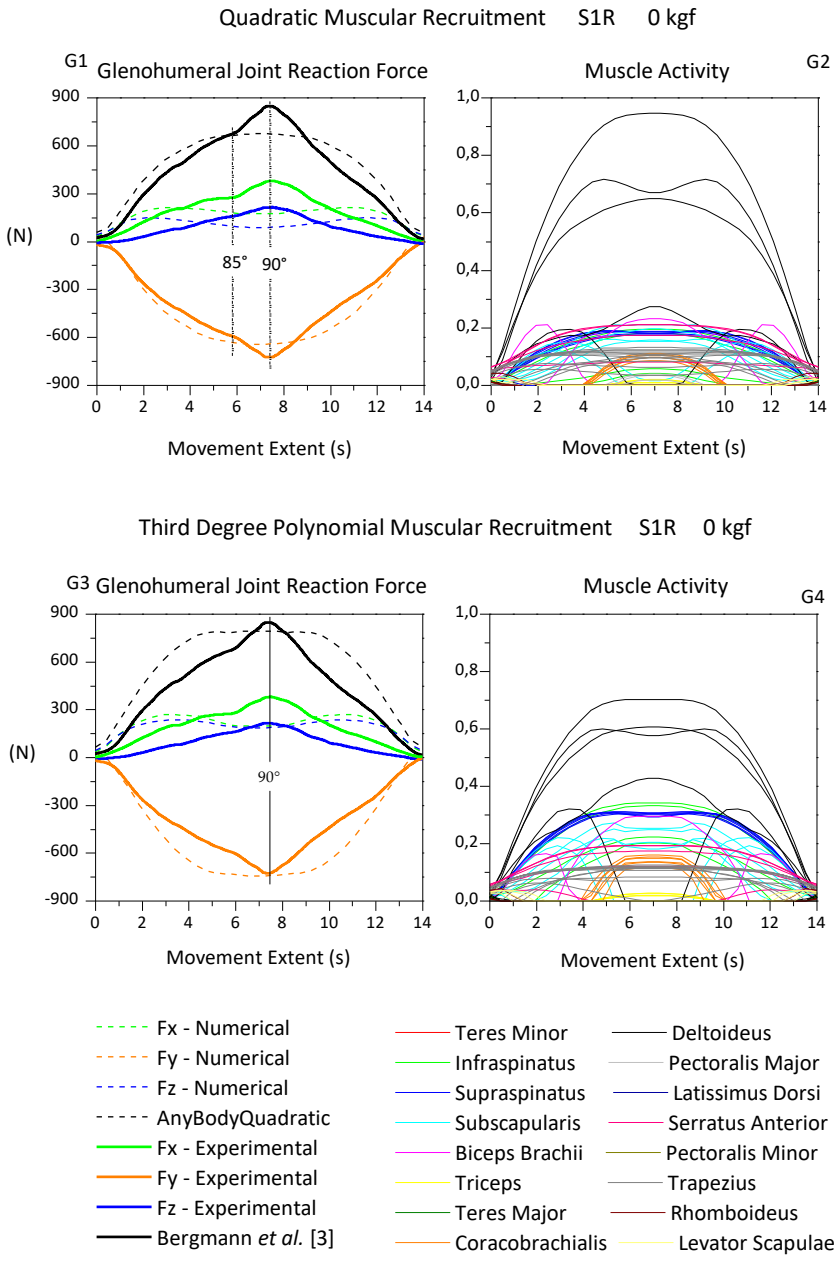

Figure 2.6. Glenohumeral Joint Reaction Force and Muscle Activity during 90° abduction in the frontal plane. No external load applied. Comparison between the numerical results for quadratic and third degree polynomial recruitments and the results of Bergmann *et al.* [132].

GH-JRF numerically determined is comparable to the experimental results from the beginning of abduction (0°) until 85°, failing to reproduce the experimental results up to 90°, as expressed in graph G1 of Figure 2.6. This happens because numerical components F_x and F_z do not mimic the behaviour of F_x and F_z components of the instrumented prosthesis. Regarding F_y, it acceptably reproduces the experimental results during the entire movement. In summary, the maximum value measured by the prosthesis is underestimated by the quadratic recruitment.

The numerical simulations were performed considering the third-degree polynomial muscular recruitment, shown in graph G3 of Figure 2.6. The GH-JRF numerically determined has similar trend with the GH-JRF measured, but a plateau appears between 4.5 s and 9.5 s (corresponding approximately to 75°). With this recruitment criteria, the components F_x and F_z have an almost equal behaviour between each other, which is not observed with the experimental measurements. Nevertheless, F_{total} at 90° is closer to the experimental results: 793 N in the numerical simulation and 847 N with the experiments, a 6% deviation relating to the experimental results.

Muscle activity over time is represented in graphs G2 and G4 of Figure 2.6. For both muscle recruitment types, muscle activity of each segment is smaller than 1, meaning that the arm moves without muscle overloading. For the quadratic recruitment (graph G2, Figure 2.6), three of the six muscular segments of the deltoideus scapular part are the most active through the entire abduction. When a third-degree polynomial recruitment is applied, two other scapular segments of the same muscle increase their activity.

The same happens mainly with the supraspinatus, infraspinatus and subscapularis, belonging to the rotator cuff. So, it has been verified that muscle recruitment function of higher degree increases muscle segments activity, increasing also the interaction between them.

None of the two criteria studied clearly describes the experimental results with high accuracy. The quadratic recruitment falls at representing GH-JRF at high angles; while the GH-JRF determined with the third-degree polynomial recruitment are higher than the experimental results for small angles, but closer to them in higher angles. Nonetheless, the results can be considered adequate.

2.4.1.2 90° Abduction with External Load

Numerical simulations were performed considering loads of 0.5, 1.0, 1.5 and 2.0 kgf to validate the shoulder model in use, despite the fact that Bergmann *et al.* [132] only made experiments with no load or with 2.0 kgf.

With an external load of 0.5 kgf, GH-JRF determined for a quadratic muscular recruitment (see graph G1 of Figure 2.7) followed the same trend as the obtained with no load. With load increasing, so the muscle activity increased, and one of the most active

muscle segments of the deltoideus has now its activity equal to 1, as shown in graph G2 of Figure 2.7. Since this is not a physiological behaviour, there must be more synergism between muscles, and a third-degree polynomial recruitment was employed. As expected GH-JRF behaviour and muscle activity were comparable to the ones obtained with no load applied, but the intensity increased (see graphs G3 and G4 of Figure 2.7). There was also an increased interaction between rotator cuff muscles, like in the previous loading case.

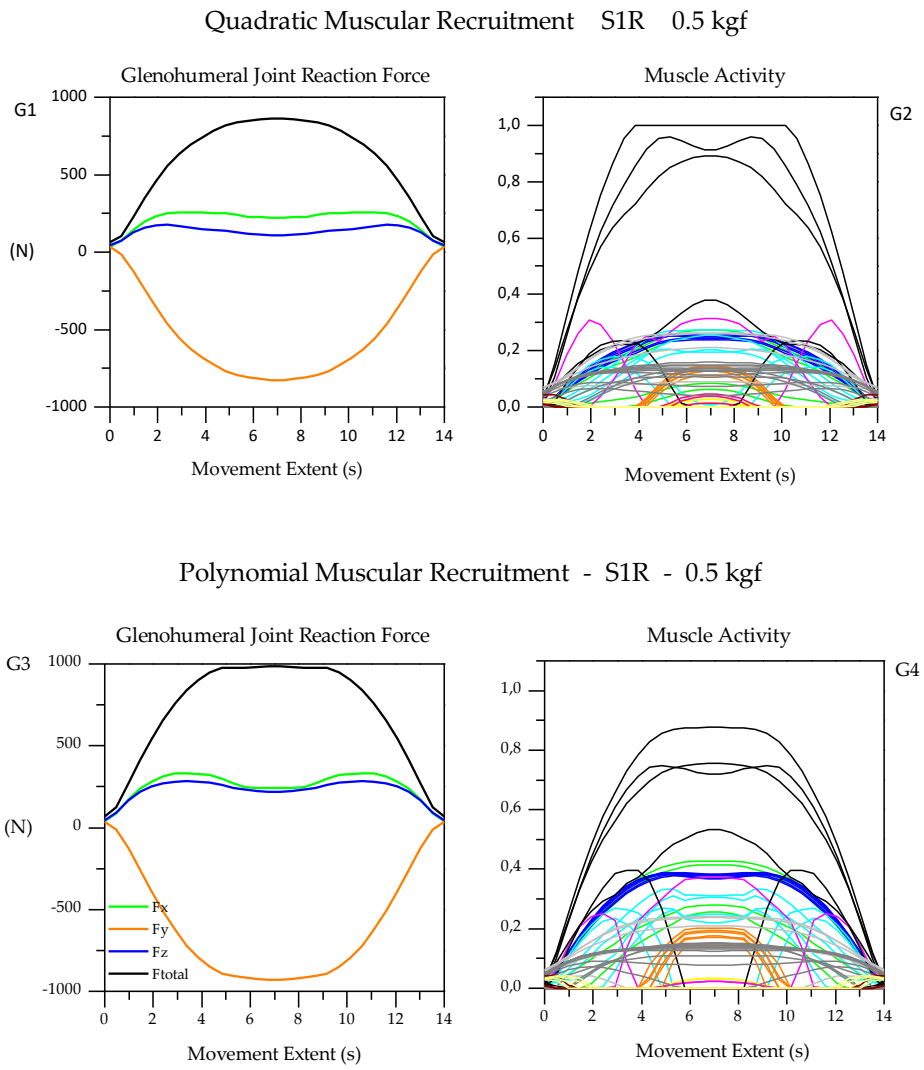

Figure 2.7 – Glenohumeral Joint Reaction Force and Muscle Activity during 90° abduction in the frontal plane. External load of 0.5 kgf. Comparison between quadratic and third degree polynomial recruitment.

Since for 0.5 kgf of external load the quadratic recruitment was not enough to obtain satisfying results, the same was expected to happen for 1.0 kgf, which was confirmed. For the third-degree polynomial recruitment, GH-JRF is similar in shape to the obtained earlier for the same recruitment, but its maximum value is higher and equal to 1188 N. Concerning muscle activity, it is equal to 1 for one deltoideus muscular segment during some movement extent, and consequently, a fourth-degree polynomial recruitment was employed. With this muscle recruitment strategy, force behaviour is again similar in shape with the obtained previously, and GH-JRF maximum equal to 1254 N. However, a small depression in F_{total} starts to appear as the abduction angle becomes elevated.

Concerning external loads of 1.5 kgf and 2.0 kgf, GH-JRF presents accentuated depression for motion at highest angles, being this behaviour similar for all recruitment types employed (fourth, fifth and min/max). In several muscle segments, muscular activity regarding the min/max muscular recruitment has very steep slopes (see graph G2, Figure 2.8) that do not seem to be physiological when compared with the maximum voluntary contraction determined by James Wickham *et al.* [138]. External loads of 1.5 kgf and 2.0 kgf did not present satisfying results and thus the subsequent studies were made considering an external load of 1.0 kgf, with a polynomial muscle recruitment of third degree. The referred muscular recruitment was chosen although muscle activity of a deltoideus muscular segment was equal to 1.

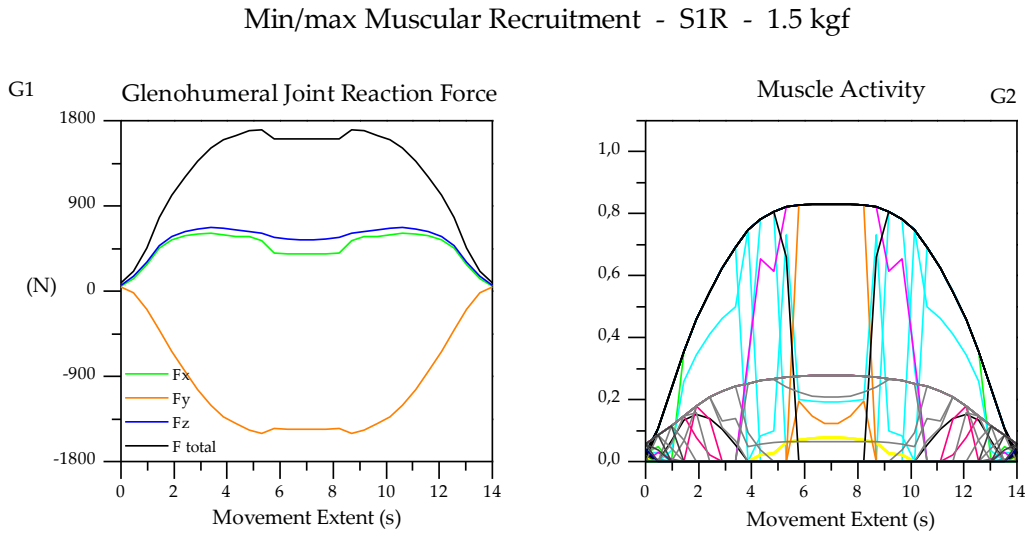

Figure 2.8. Glenohumeral Joint Reaction Force and Muscle Activity during 90° abduction in the frontal plane. External load of 1.5 kgf for the min/max recruitment.

Total muscle activity for the third-degree polynomial muscle recruitment (see Figure 2.9), shows that from the sixteen shoulder muscles only half contribute to abduction. The deltoideus is the one with higher activity, followed by the supraspinatus. Infraspinatus and subscapularis have similar behaviour until 70° of arm elevation, and it is interesting to notice that from all rotator cuff muscles, teres minor is the only one which is not relevant. Trapezius and levator scapulae are also active in arm elevation and have similar behaviour between each other. Regarding the biceps, its contribution does not have the same trend as the other muscles; and coracobrachialis only starts to act at 70° abduction.

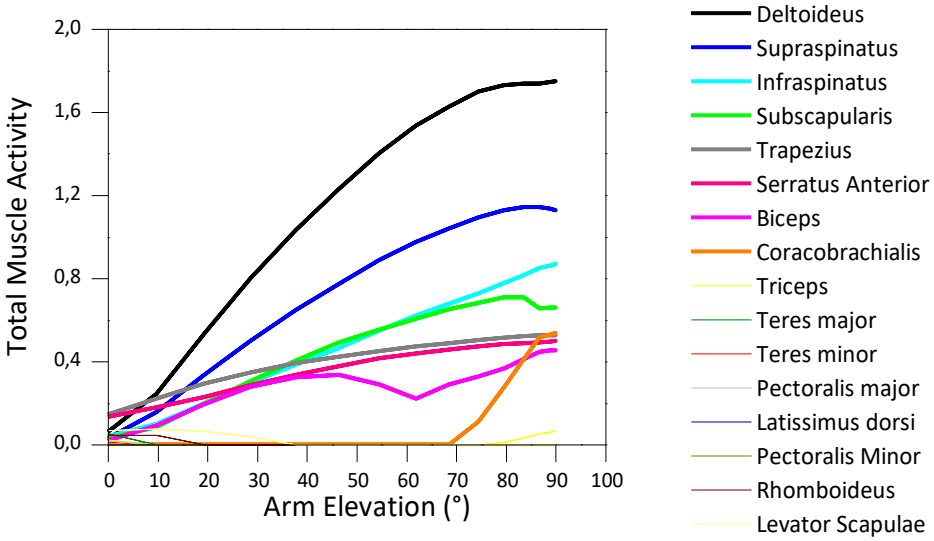

Figure 2.9. Total muscle activity for third degree polynomial muscle recruitment in different arm elevation angles.

Thus far, the study presented intended to accomplish a numerical characterization of shoulder muscle actions during a 90° arm abduction/adduction, since this movement was considered critical in shoulder joints by Bergmann *et al.* [132]. The most important muscles contributing to abduction were identified and results are in accordance with literature [138]. Before arm elevation started (0°), levator scapulae and trapezius had the highest activity (see Figure 2.9), which is in accordance with the results of James Wickham *et al.* [138] in their experimental study on the electromyographic activity of healthy shoulders.

GH-JRF without external load, is represented in Figure 2.10 as a function of arm elevation angle. Numerical results are compared with literature results.

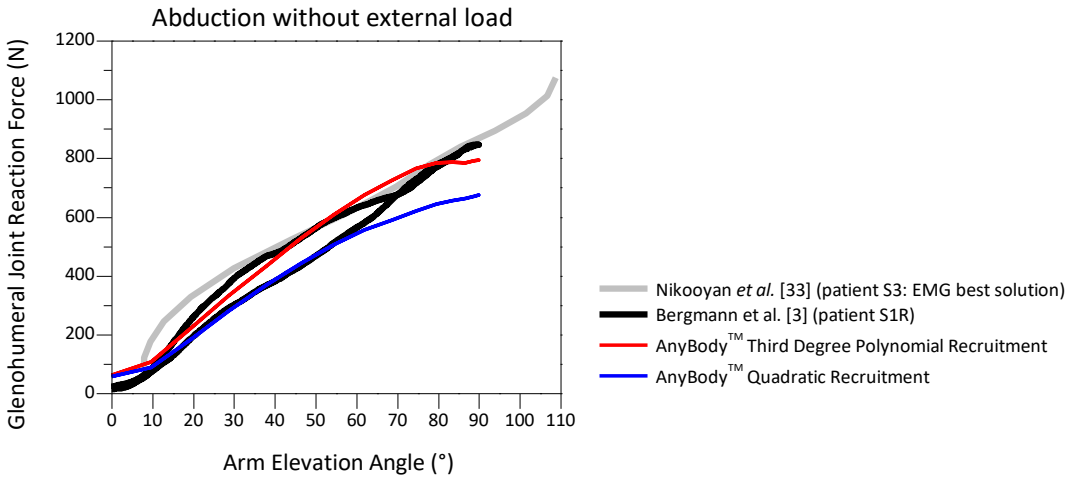

Figure 2.10. Comparison between numerical and literature results for abduction without external load.

Experimental data determined by Bergmann *et al.* [132] is not completely symmetric during abduction and adduction. GH-JRF calculated with a third-degree polynomial recruitment is closer to the experimental results in abduction. On the contrary, GH-JRF calculated with a quadratic recruitment is closed to the experimental results in adduction, especially between 60° and 0°.

The graph of Figure 2.10 also presents the results obtained by Nikooyan *et al.* [102], that developed a numerical shoulder model using electromyography (EMG) signals as model inputs. Their best solution is the combination of EMGs closer to their experimental results (with no external load). As exposed in the same figure, the GH-JRF determined with the third degree polynomial muscular recruitment is the one closer to the results of Nikooyan *et al.* [102] from 40° abduction.

With the objective of evaluating GH-JRF as the external load increases, joint reaction forces obtained considering the third-degree polynomial recruitment are represented in graph of Figure 2.11. The same graph also holds the experimental results of Bergmann *et al.* [132] obtained in the absence and in the presence of external load. It is important to notice that results for 2.0 kgf belong to a different patient (S2R: 91 kg, 1.68 m), since the one whose results had been used (S1R: 101 kg, 1.61 m) was not able to perform slow abduction with the highest load. This aspect is important since weight, height and the physical ability of a subject influences the loading [131, 132]. In addition to the anthropometric differences between individuals, they also suffer from osteoarthritis and, as Büchler *et al.* [139] demonstrated, osteoarthritic and normal shoulder present significant differences in shoulder biomechanics and, thus, in forces measured at the joint.

Overall, it was observed that as the external load increased the GH-JRF increased. Furthermore, abduction considering 2.0 kgf was accomplished during 10 s, and not 14 s as in the case of S1R. As observed [132], GH-JRF for slow movements is higher than for fast movements. Subsequently, despite the numerical results for 1.0 kgf are higher than experimental ones for 2.0 kgf, the speed with which motion is made must be considered.

Regardless of the differences in movement extent, bone quality or anthropometry data, experimental results obtained by Bergmann *et al.* [132] showed that GH-JRF always increased with the increase of abduction angle. No plateau was observed for the highest angles, as observed between 80° abduction in the numerical simulation (see Figure 2.11). Therefore, it can be assumed that AnyBody™ is underestimating GH-JRF for high angles.

Similarly to what Damsgaard *et al.* [123] observed, there are several muscle recruitment types adequate to be employed. This happens since the number of muscles available to carry the movement exceeds the necessary ones to drive the system degrees of freedom. This aspect makes it difficult to choose a muscular recruitment in detriment of other. Numerical results also depend on factors such as muscle decomposition, muscle path near the joint or the number of muscles modelled [121, 122].

Overall it was concluded that as the external load increases, the higher the GH-JRF and the more synergism must be employed between muscles to make them work together in a more efficient and physiological manner.

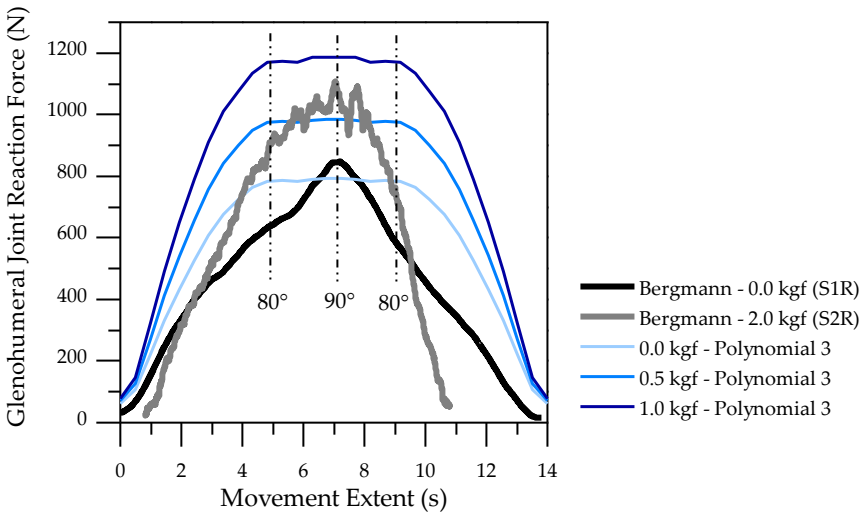

Figure 2.11. Glenohumeral Joint Reaction Force for different loading cases.

2.4.2 Simplified Model of the Intact Shoulder

The results obtained with the numerical model of the shoulder allow the identification of the most important muscles that contribute to abduction. It is possible to reduce the number of muscles and evaluate their influence in the biomechanical behaviour of the shoulder joint.

Kedgley *et al.* [140] developed an experimental setup to study the effect of muscle loading on the kinematics of abduction. Only the rotator cuff muscles and the deltoideus were considered. In this sense, the intact shoulder model was modified to only consider those muscles, but the dynamic equilibrium equations of AnyBody™ were not solved. Since muscles considered were only glenohumeral, one scapulothoracic muscle was added to the model, resulting in five different combinations to evaluate. Even so, all failed to develop a solution. Afterwards two scapulothoracic muscles were considered, but from the ten combinations possible, presented in Table 2.2, only combination B developed a successful solution. It includes the trapezius and the levator scapulae, posterior and anterior muscles, respectively. The remaining combinations tested failed to develop a solution because muscle segments considered are not enough to balance the dynamic equilibrium equations and because posterior and anterior muscles are needed to stabilize the arm.

Table 2.2. Combinations to evaluate the influence of scapulothoracic muscles.

Scapulothoracic Muscles		Muscle Combinations										
		[140]	A	B	C	D	E	F	G	H	I	J
Levator Scapulae	- *posterior muscle*	×	×	×	×	✓	×	×	✓	×	✓	✓
Rhomboid	- *posterior muscle*	×	×	×	✓	×	×	✓	×	✓	×	✓
Trapezius	- *posterior muscle*	×	×	✓	×	×	✓	×	×	✓	✓	×
Pectoralis Minor	- *anterior muscle*	×	✓	×	×	×	✓	✓	✓	×	×	×
Serratus Anterior	- *anterior muscle*	×	✓	✓	✓	✓	×	×	×	×	×	×

With the definition of the scapulothoracic muscles to consider (trapezius and serratus anterior), the rotator cuff was evaluated with the objective of understanding if all its muscles have the same importance in abduction. The combinations studied are in Table 2.3.

Table 2.3 - Combinations to evaluate the influence of the rotator cuff muscles.

Rotator Cuff Muscles	Muscle Combinations														
	B	C	D	E	F	G	H	I	J	K	L	M	N	O	P
Subscapularis – anterior muscle	✓	✓	✓	✓	×	✓	✓	×	✓	×	×	✓	×	×	×
Supraspinatus – posterior muscle	✓	✓	✓	×	✓	✓	×	✓	×	✓	×	×	✓	×	×
Infraspinatus – posterior muscle	✓	✓	×	✓	✓	×	✓	✓	×	×	✓	×	×	✓	×
Teres minor – posterior muscle	✓	×	✓	✓	✓	×	×	×	✓	✓	✓	×	×	×	✓
Model Output	ok	ok	ok	■	●	ok	■	●	■	●	●	■	●	●	●

■ - overloaded muscle configuration ● - error

Some conclusions can be drawn from the results:

- it is not possible to obtain good results without considering the supraspinatus, as solutions obtained overloaded the muscles to deliver some results;
- abduction is also not completed without the subscapularis, the only anterior muscle of the rotator cuff;
- carrying out the movement with just the subscapularis and the supraspinatus (model G) is conceivable because those are anterior and posterior muscles.
- All remaining models with only two rotator cuff muscles failed to develop a good solution.

The results obtained for models that delivered a solution, with or without muscle overloading, are represented in graph of Figure 2.12. Models H and E clearly overestimate the GH-JRF between 3.5 s and 10.5 s, corresponding to 65° abduction. Despite the absence of teres minor in model H, results of both models are equal, which confirms that this muscle is not mandatory in abduction movement. In models M and J, muscle configuration is overestimated in both, and GH-JRF behaviour is similar between the two. In the case of model M, only subscapularis is used, and in the case of model J, only teres minor is added. So, the same conclusion is as before: teres minor does not have much influence in abduction movement and can be ignored. Regarding models which developed a solution without muscle overloading (B, G, C, and D), models D and G have similar behaviour, and models B and C are analogous. As expected, the difference between models D and G, and B and C, is teres minor, only present in models D and B.

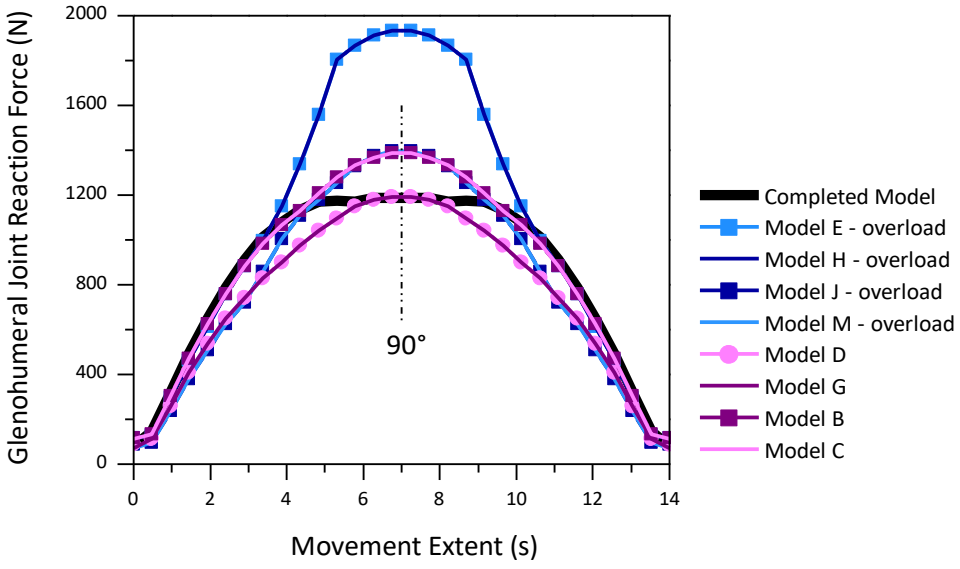

Figure 2.12. Glenohumeral Joint Reaction Force for different reduced models with external load of 1.0 kgf.

The completed model, with all shoulder muscles and considering the third-degree polynomial recruitment, is also represented in graph of Figure 2.12. As hypothesized before, AnyBody™ is probably underestimating GH-JRF for higher arm elevation angles. Accordingly, the reduced model to consider in the present analysis should be model C. It is very similar to the completed model, but without presenting a plateau at the higher degrees of arm movement.

The force each muscle segment performs to accomplish abduction as the arm is elevated is represented in graphs of Figure 2.13. From the six muscles of the model, the deltoideus is the one exhibiting the higher muscle force, especially five of the six scapular muscle segments. The next muscles with higher force is subscapularis, the only anterior muscle of the cuff. All its muscle segments contribute to motion. The trend of total muscle force of subscapularis is similar with both infraspinatus and supraspinatus (posterior muscles), differing only in magnitude. Thus, infraspinatus and supraspinatus balance the forces produced by subscapularis. Besides this, all muscle segments of supraspinatus participate equally in movement, which does not happen with infraspinatus and subscapularis.

In the case of serratus anterior, only four of the six segments are more active after 20° of arm elevation (> 15 N). For trapezius, all its segments have small contribution to movement (< 20 N) but all clavicular segments work together in an analogous fashion, which does not happen with the scapular muscular segments. Still, levator scapulae and trapezius have very similar behaviour throughout the entire movement extent, thus equilibrating each other since the first is an anterior muscle and the last a posterior one.

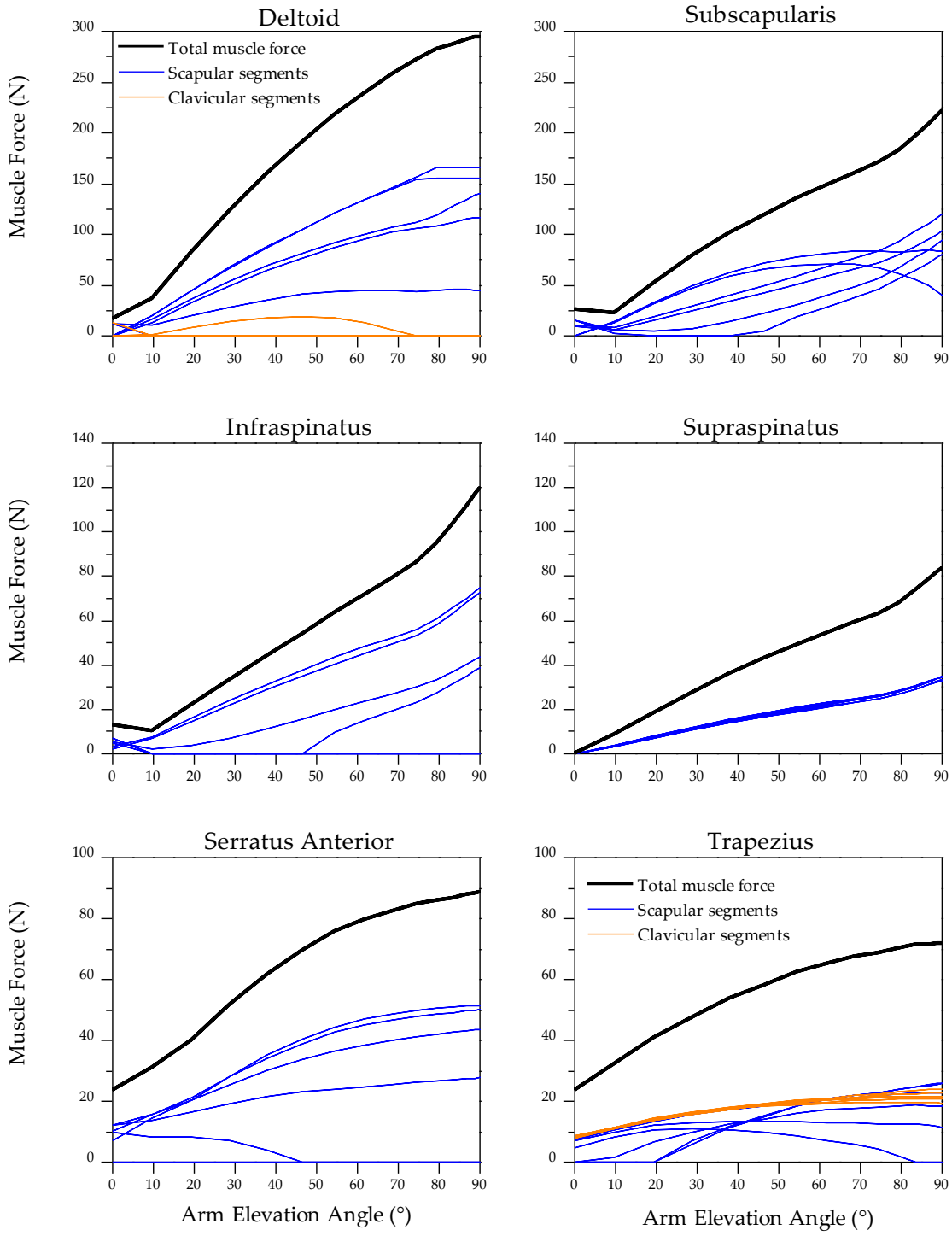

Figure 2.13. Force that each muscle segment of the reduced model performs to accomplish abduction/adduction during arm elevation

2.5 Conclusions

The main purpose of the study presented in this section was to determine the shoulder model with the minimum number of muscles (called the reduced model) able to mimic the behaviour of the completed shoulder model. Muscle forces as movement progresses were also characterized.

The reduced model obtained includes the deltoideus (glenohumeral muscle), subscapularis, supraspinatus and infraspinatus (rotator cuff muscles), trapezius and levator scapulae (scapulothoracic muscles). Results showed that the scapular segments of the deltoideus govern abduction, confirming why the middle deltoideus is considered the abduction prime mover [141]. Infraspinatus and supraspinatus (both scapular posterior muscles) serve to counterbalance the contribution of subscapularis (the only anterior muscle of the scapula) and thus they all contribute to glenohumeral stability.

Our results are in accordance with the ones of van der Helm [116], Favre *et al.* [103] and Yanagawa *et al.* [142], who determined that the deltoideus and the rotator cuff muscles are the most active during this movement. Nonetheless, in the work of Favre *et al.* [103], the muscles contributing to adduction (from 90° to 0°) are not the same as in abduction (from 0° to 90°) and this observation differs from ours. Several experimental studies [140, 143] aiming at investigating each shoulder muscle contribution in glenohumeral joint stability during arm abduction, also attribute especial importance to the deltoideus and rotator cuff muscles.

Regarding muscle force patterns predicted by AnyBody™, they are similar to the results of van der Helm [116], mainly for the deltoideus scapular part, for levator scapulae and for trapezius scapular part. Regarding force magnitude, results cannot be quantitatively compared because of the different amount of external load applied (1.0 kgf in our study and 0.750 kgf in van der Helm's [116]) and different anthropometric data used, which influences the loading [131, 132].

Chapter 3

Shoulder Simulator and Experiments

3.1 Overview of Existent Shoulder Models

The willingness of the adult population to have a healthier and longer life has made many to embrace a more active lifestyle and this fact alone may had led to an increase of shoulder problems. This growth has made the scientific communities to focus their attention on the shoulder joint with the goal of better understanding its biomechanical behaviour, both in the absence and in the presence of pathologies or prosthetic components.

Developing a precise biomechanical model of the shoulder is a difficult task. It involves three different bones that relate with each other by three anatomical articulations and comprises many muscles that control this intricate system. To try to simplify the complexity of the shoulder joint, many anatomical shoulder simulators focus their attention on the close relationship between the proximal humerus and the glenoid and consider a smaller number of muscles.

Several *in vitro* models of the glenohumeral joint have been developed, attempting to replicate the behaviour of the intact shoulder. Later, *in vitro* models of the implanted joint appeared, trying to evaluate the effects of the prosthesis on the biomechanics of the joint, but also with the goal of developing better prosthesis concepts. An overview of such models is provided next.

3.1.1 Intact Models

The glenohumeral joint accounts on soft tissues to keep a correct positioning of the humeral head inside the glenoid cavity. The majority of the *in vitro* systems are built with non-pathologic cadaveric structures [140, 144] and fewer with composite bone structures [145]. Generally, shoulder models consider a hanging humerus, activated in abduction by the external loads applied to the deltoideus and rotator cuff tendons.

Apreleva *et al.*[146] measured the glenohumeral joint reaction force of the full upper extremity of cadaveric specimens and studied the influence of the deltoideus and rotator cuff muscles in the abduction motion. The results obtained indicate that in all testing conditions the GH-JRF increases as the abduction angle increases, reaching peak values at nearly 90°. For the subsequent testing conditions the GH-JRF was:

- Equal force: (337 ± 88) N;
- Supraspinatus dominant: (365 ± 95) N;
- Deltoideus dominant: (315 ± 78) N;
- Supraspinatus paralysis: (279 ± 67) N;

The results also pointed out the importance of supraspinatus and deltoideus muscles to the magnitude of glenohumeral reaction forces, showing that debilitation of these muscles may lead to anomalous loading of the joint.

Bono *et al.* [144] showed that greater tuberosity fractures influence the joint mechanics and that higher forces are necessary to perform 90°abduction in case of fracture. Kedgley *et*

al. [140] studied the effect of different muscle-loading ratios on joint kinematics and concluded that the developed system allows repeatable motions. With the same experimental system, Kedgley *et al.* [147, 148] studied the effect of rotator cuff injury on shoulder joint kinematics and the behaviour of the humeral head during muscle loading. The system developed in [140] includes 6 pneumatic actuators that simulate the deltoideus muscle (anterior, middle and posterior sections), the supraspinatus, the infraspinatus/teres minor and subscapularis muscles. It is presented in Figure 3.1 to illustrate the complexity of *in vitro* shoulder models.

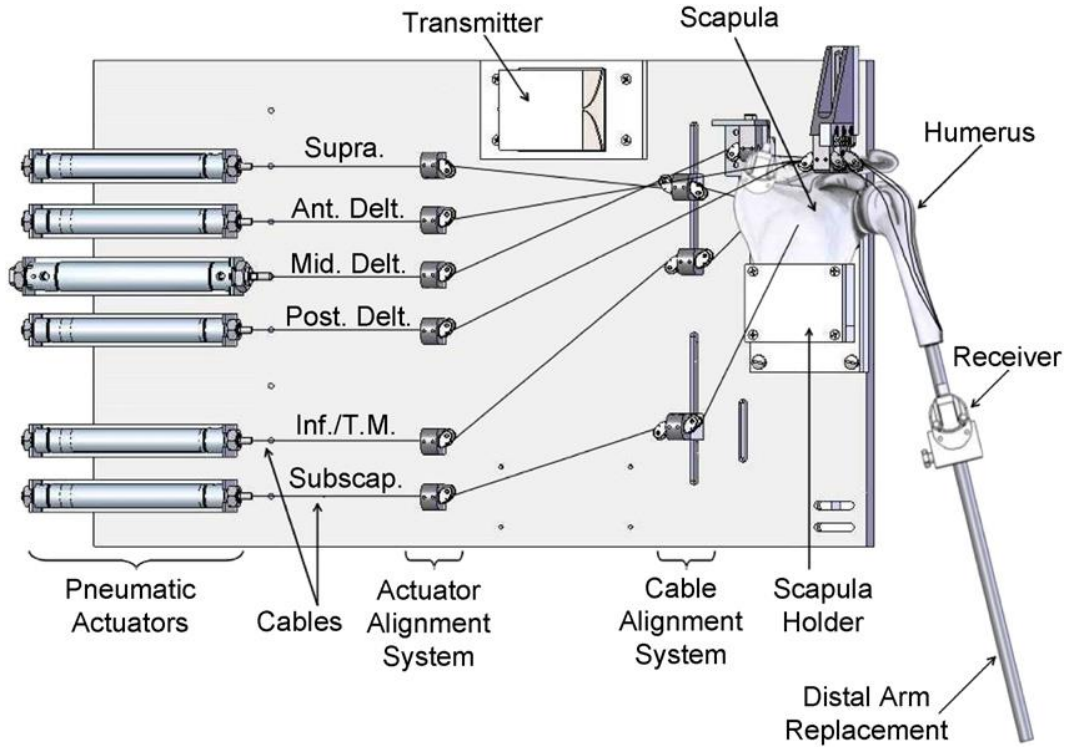

Figure 3.1. Shoulder testing apparatus, developed by Kedgley *et al.*[140].

Onder *et al.* [145] developed a simpler model with a composite humerus and a polyethylene glenoid and considered only the actions of the deltoideus and supraspinatus. Pneumatic muscles simulated the behaviour of the real muscles and load cells measured the applied forces of each muscle. In their experiments, the humerus was mechanically restricted, so that movement can perform only in a well-defined plane.

In the experimental setups reviewed, arm abduction is the mostly studied and although the glenohumeral movements are performed with the contribution of 18 muscles, the abduction and flexion can be performed only with the deltoideus and the rotator cuff. These have been the muscles considered in all *in vitro* models of the intact glenohumeral joint.

Several strategies are implemented for muscle force application, such as: different force ratios in several muscles [146], equal forces in all muscles [140, 146, 148], absence of forces in some muscles [146], force dependent on the physiologic cross-sectional area of each muscle [148] and force dependent on electromyography results [140, 148]. Commonly, muscle forces are applied by means of servo-hydraulic actuators [144, 146, 147] and of pneumatic muscles and weights [145].

Despite the valuable understanding on glenohumeral joints behaviour that these experimental systems provide, they were not designed for cycling loading, and this is considered a drawback of such systems when the objective is to evaluate the experimental performance of shoulder prosthesis. More recently, Baumgartner *et al.* [143] developed a robotic shoulder simulator able to perform repetitive and reproducible humeral movements. The system included a polyethylene glenoid and a metallic humerus, activated by electro-actuators, and includes the contribution of the scapular rotation to arm abduction. The deltoideus, supraspinatus, infraspinatus/teres minor and subscapularis were simulated. Despite the early encouraging results, the glenohumeral joint loads measured were lower than expected and the system presented some instability at high abduction angles.

A summary of the intact shoulder models previously reviewed is presented in Table 3.1.

Table 3.1. Intact shoulder models available in literature.

Authors	Model	Specimens	Muscles	Actuators	Goal of the study
Apreleva *et al.* [146]	Dynamic	Cadaveric	Deltoideus Rotator cuff	Servo hydraulic Hanging weights	Reaction forces at the glenohumeral joint
Bono *et al.* [144]	Dynamic	Cadaveric	Deltoideus Rotator cuff	Servo hydraulic	Effect of greater tuberosity fractures on joint kinematics
Kedgley *et al.* [147]	Static and dynamic	Cadaveric	Deltoideus Rotator cuff	Pneumatic	Effect of different muscle-loading ratios on joint kinematics
Onder *et al.* [145]	Dynamic	Composite humerus, polyethylene glenoid	Deltoideus Supraspinatus	Pneumatic	Simulate abduction
Baumgartner *et al.* [143]	Dynamic	Metallic humerus, polyethylene glenoid	Deltoideus, Rotator cuff	Electro actuators	Develop a simulator with a rotating scapula

3.1.2 Implanted Models

As with the in vitro intact shoulder models, the majority of the implanted models of the glenohumeral joint are built with cadaveric structures and consider more muscles than just the deltoideus and rotator cuff [149, 150]. The implanted models also consider servo-actuators [150, 151] and hanging weights [149, 152] to induce forces on the tendons of the simulated muscles. The main difference between the intact and the implanted shoulder models is, evidently, the presence of a prosthesis.

There are many experimental studies focused on glenohumeral biomechanical changes due to a TSA, with both anatomical prosthesis [149, 151] and reverse prosthesis [153, 154]. The majority uses cadaveric bone structures [149, 151] and fewer uses composite bone structures [155]. Generally, the studies focused on anatomical prosthesis study the effects that different designs or different prosthetic positioning have on bone/joint behaviour. This may be attributed to the fact that the biomechanics of an anatomic implanted joint is similar to that of a joint with no implant. On the contrary, the studies focused on the reverse prosthesis are still very focused in understanding the overall behaviour of the joint and surrounding muscles when subjected to a reverse arthroplasty, since its biomechanics is different from that of a joint with no implant.

Nyffeler *et al.* [152] studied the influence of glenoid version on humeral head displacement and on joint reaction forces. Total shoulder prostheses were implanted in healthy cadaveric shoulders, and glenoid version changed between more anteversion and more retroversion. The study clearly showed that any small change in glenoid version influences the loading behaviour of the glenoid component, ultimately leading to glenoid loosening.

Schamblin *et al.* [151] simulated overhead positions with cadaveric structures and studied the differences in the biomechanical performance of the joint before and after a TSA and before and after a bipolar HA. Joint reaction forces, contact areas, contact patterns and contact pressures were evaluated to identify potential causes of implant loosening. A 40 N force was applied to each rotator cuff muscle and to pectoralis major and latissimus dorsi muscles; while an 80 N force was applied to deltoideus muscle. The authors observed that after the TSA the posterior forces augmented considerably. Furthermore, when compared with the intact model, the contact patterns and pressures were greatly altered after the arthroplasty procedures. These observations may be an indicative of edge loading and rocking horse of the glenoid component, suggesting consequent loosening.

Jun *et al.* [149] studied how prosthetic humeral head shape influences rotational ROM and glenohumeral joint kinematics, comparing native humeral heads with non-spherical and spherical prosthetic heads. For the spherical humeral head, a prosthesis commercially available was used; for the non-spherical humeral head, a costume made prosthesis was produced, mimicking the anatomy of the native humerus. A total load of 200 N was applied to the experimental model. The study showed that not only the non-spherical humeral head

developed replicated accurately the humeral head anatomy, but it also replicated better the joint's rotational ROM and its kinematics. The experimental setup used in the study of Jun *et al.* [149] (see Figure 3.2) included the rotator cuff muscles, the deltoideus, the pectoralis major and latissimus dorsi muscles. The supraspinatus muscle was divided into anterior/posterior regions; the deltoideus muscle was divided into anterior/middle/posterior regions; and subscapularis, infraspinatus-teres minor, pectoralis major and latissimus dorsi muscles were divided into upper/middle/lower regions. The threads used to simulate the muscles were tied to the tendon insertions in one extremity and connected to the weights in the opposite extremity.

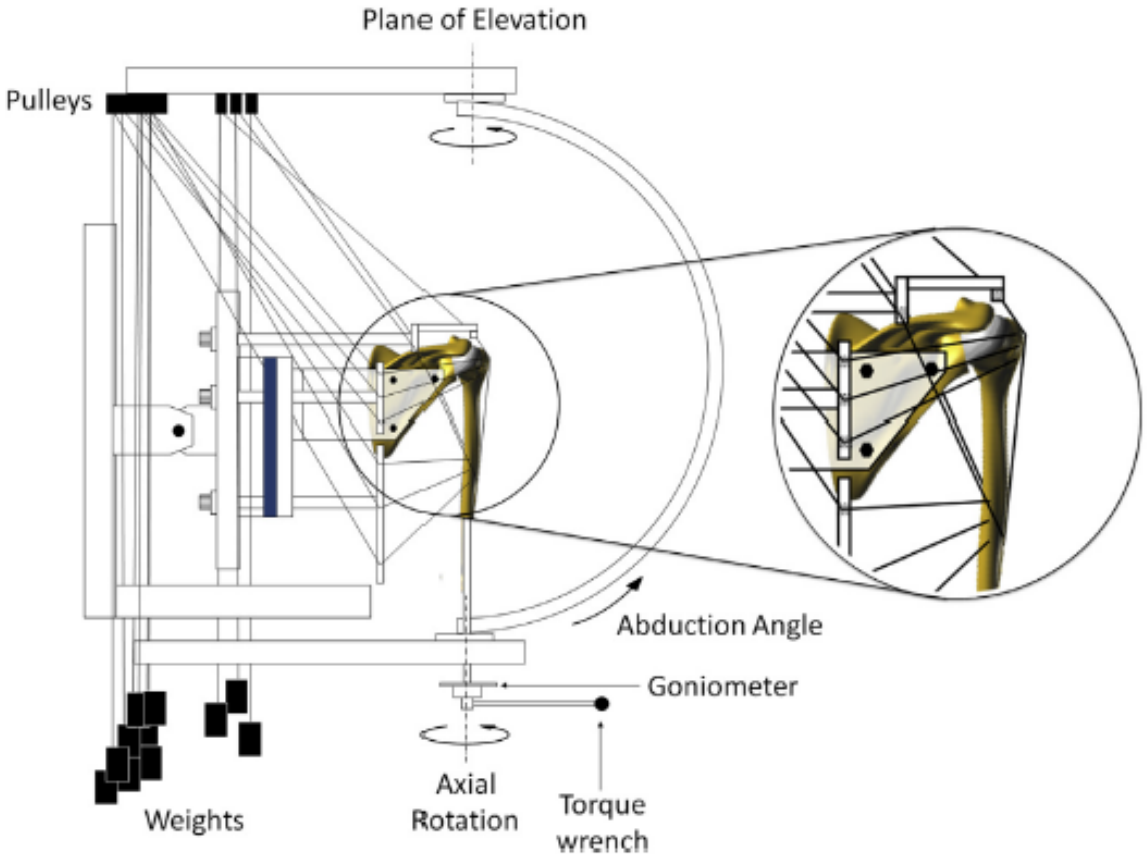

Figure 3.2. Shoulder testing apparatus, developed by Jun *et al.* [149].

Werthel *et al.* [150] focused their study on the glenohumeral muscle moment arms before and after implantation with a reverse shoulder prosthesis, through the evaluation of abduction, flexion and axial rotation. Unlike what has been observed with the previously referred studies, the study of Werthel *et al.* [150] uses cadaveric hemi-thoraces (see Figure

3.3), and tracks the 3D behaviour of the humerus, of the scapula and of the thorax. The model considers the anterior/middle/posterior deltoideus regions, the clavicular/sternal pectoralis major regions, and the infraspinatus, teres minor, latissimus dorsi and teres major muscles. Passive muscle forces were applied by means of pneumatic cylinders. The authors concluded that the presence of the reverse shoulder prosthesis notably altered the shoulder muscle moment arms, with the primary abductors, flexors and internal rotators suffering a major increase. On the contrary, the moment arm of the primary external rotators suffered a very accentuated decrease.

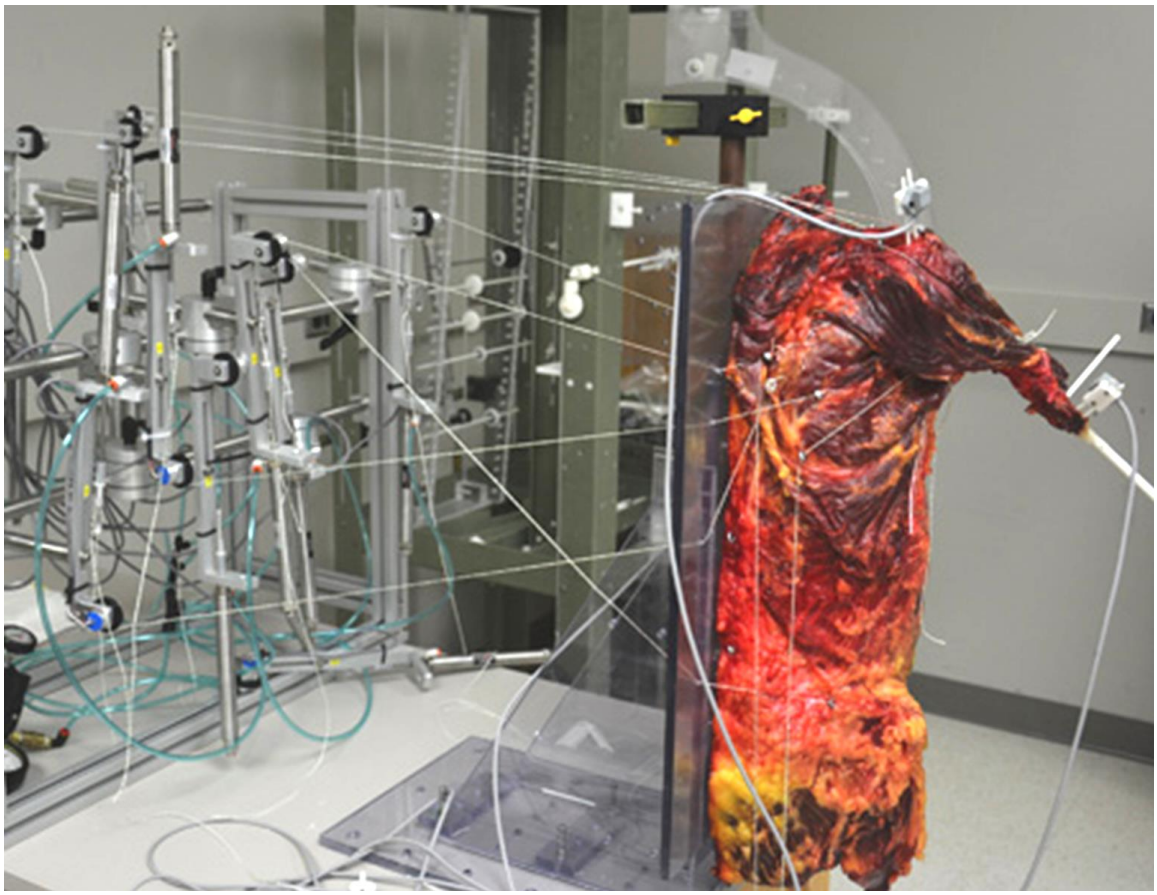

Figure 3.3. Shoulder testing apparatus, developed by Werthel *et al.* [150].

North *et al.* [155] studied the effects of reverse prosthesis design on the ROM, trying to relate it to prosthesis impingement. A shoulder simulator was developed with synthetic bone structures. The model included the anterior, middle and posterior deltoideus muscle. The authors concluded that the joint's ROM is not majorly affected by both implant diameter nor by glenosphere eccentricity. Krämer *et al.* [153] also focused their study on

implant impingement after a reverse shoulder arthroplasty, trying to establish the influence of both implant configuration and scapular anatomy. Cadaveric shoulders were mounted on a robot-assisted simulator, and internal rotation during abduction was simulated. The authors verified that implant selection is mandatory for an internal rotation free of impingement. However, the study was not conclusive regarding scapular anatomy, and it was not possible to establish its influence on internal rotation. In fact, some results contradict those of other [156], highlighting the importance of continuing to study the biomechanics of reverse prosthesis.

A summary of the implanted shoulder models previously reviewed is presented in Table 3.2.

Table 3.2. Implanted shoulder models available in literature.

Authors	Model	Specimens	Muscles	Arthroplasty	Actuators	Goal of the study
Nyffeler *et al.* [152]	Static	Cadaveric	Deltoideus Rotator cuff	HA	Weights	Influence of glenoid version on implant loosening
Schamblin *et al.* [151]	Static	Cadaveric	Deltoideus Rotator cuff Pectoralis major Latissimus dorsi	TSA Bipolar HA	Pneumatic cylinder	Identify potential causes of implant loosening
Jun *et al.* [149]	Static	Cadaveric	Deltoideus Rotator cuff Pectoralis major Latissimus dorsi	HA	Weights	Influence of prosthetic humeral head shape on range of motion and in joint kinematics
Werthel *et al.* [150]	Static	Cadaveric	Deltoideus Pectoralis major Infraspinatus Teres minor Latissimus dorsi Teres major	RSA	Pneumatic cylinders	Influence of reverse prosthesis on muscle moment arms
North *et al.* [155]	Dynamic	Synthetic	Deltoideus	RSA	Electric actuators	Influence of implant design on impingement
Krämer *et al.* [153]	Dynamic	Cadaveric	none	RSA	none	Influence of implant design and scapula anatomy on impingement

There are a great number of other experimental studies focusing only on questions related with the glenoid implant (anatomic) [157–160] since this is where most failure problems occur. These experimental setups normally do not include the action of muscle forces, but instead apply a corresponding reaction force directly into the glenoid. Consequently, those experimental setups are usually simpler than the ones reviewed before. There are also a few experimental studies focused mainly on the humeral component [161, 162].

Maurel *et al.* [163] studied the behaviour of cadaveric scapulae before and after implanted with a glenoid prosthesis. The glenoids were implanted with keeled or pegged polyethylene implants (cemented). Bone strains and implant displacements were measured. This work resulted on the first most complete dataset on strain distribution of intact and implanted scapulae. The scapulae were loaded with physiologic loads, simulating several positions of flexion and abduction motions. Furthermore, 500 N loads were also applied at nine exact loading points (glenoid/implant centre, glenoid/implant periphery). The results obtained indicate maximum strains between 60° and 120° of abduction (at the anterior and antero-superior regions) and anteflexion (at posterior and postero-superior regions). After implantation with a glenoid component, the strains measured tended to increase. However, tensile strains decreased at the postero-inferior glenoid region when the scapula was loaded in the antero-inferior loading point.

Diop *et al.* [164] studied the influence that the curvature radii difference between the glenoid and humeral components (known as glenohumeral mismatch) has on bone strains, on translational forces and on implant/bone displacements in an implanted scapula. Cadaveric scapulae, implanted with cemented keeled polyethylene implants were used. A constant 392 N preload was applied and 2.5 mm translations in the anterior, posterior, inferior and superior directions were performed. The study revealed that glenohumeral mismatch notably affects bone strains, relative implant/bone displacements and translational forces.

More recently, different cementing techniques have been compared in *in vivo* studies [157, 158] and micro-computed tomography has been used to characterize implant interfaces [158, 160]. However, none of these studies measured strain behaviour of the implanted scapulae.

3.2 In vitro Shoulder Models Developed

3.2.1 Intact Model

The *in vitro* intact shoulder model developed uses fourth generation composite bone structures, namely a left humerus and scapula, from Sawbones®, Pacific Research Laboratories, Inc. (Vashon Island, WA), as presented in Figure 3.4.

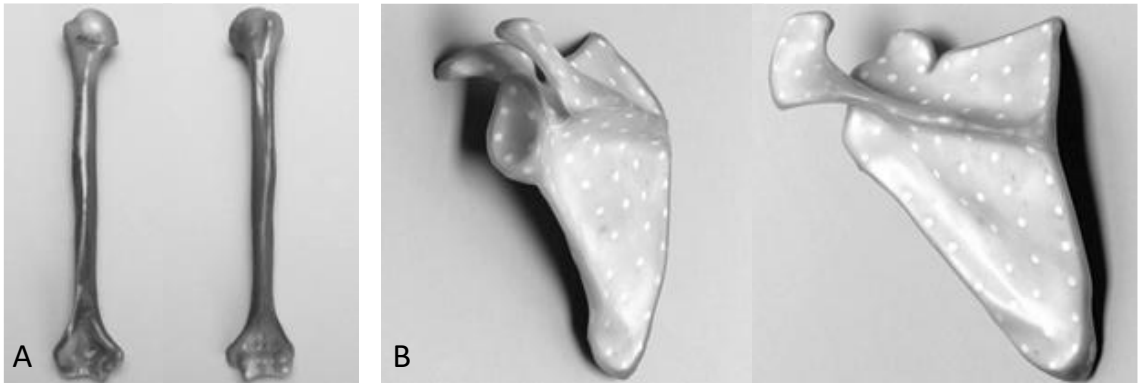

Figure 3.4. Fourth generation composite bone models from Sawbones® used in this work. Left humerus (A) and left scapula (B).

The cortical bone model is constructed with a mixture of fiberglass and epoxy resin, whereas the trabecular bone model is constructed with a rigid polyurethane foam [165]. This composite structure replicates well the mechanical behaviour of real bone, as their material properties are within the same range [166, 167].

The advantages of using synthetic bone structures, in place of cadaveric bone structures, are many. First, synthetic structures do not degrade, making their use a simple process. Second, synthetic bone structures are standard on the market and are reproducible [168]. This means that two composite bone structures have the same behaviour under the same testing conditions, making it possible to accomplish comparisons between similar studies. Generally, this is not the case for real cadaveric structures, as bone density and anatomical features are specific for each bone.

The inferior glenohumeral ligament (IGHL) was also included in the model, due to its importance in the abduction motion. An elastic part simulates the IGHL and its mechanical properties were determined through tensile testing ($v_{\text{tensile testing}}$ = 1 mm/min), as represented by the stress-strain curve in Figure 3.5. The elastic was 36 mm long ((36 × 23.6 × 1.2) mm) and suffered an elongation of 16.7 mm when the composite humeral bone was abducted from 0° to 90°. Thus, the elasticity modulus of the elastic equals approximately 3.5 MPa and that of the IGHL equals 3 MPa [169].

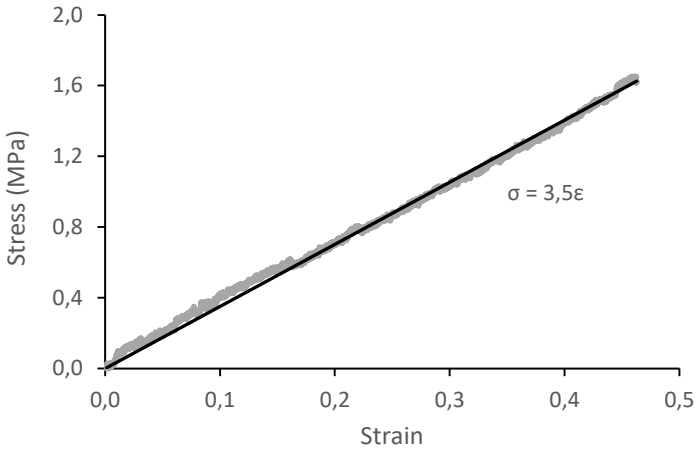

Figure 3.5. Stress-Strain curve for elastic characterization.

The developed intact shoulder model also considers the articular cartilage of the humeral head and of the glenoid cavity. To construct the humeral head cartilage, the composite humerus was scanned with a Roland PicZa 3D Laser Scanner (resolution (1.4 × 1.4) mm), and the external surface acquired was adapted with CATIA® (V5.21©Dassault Systèmes) [170]. Subsequently, the external geometry model of the humeral head was obtained and a volume generated. To create the cartilage of the glenoid cavity, a similar process was followed, but the scapula was scanned with a ZScanner 700 (Zcorporation). The CAD (Computer Aided Design) models of both cartilages were constructed assuming a constant thickness of 0.95 mm, being in accordance with literature [171] and with the average observed in different CT scans. The models developed are presented in Figure 3.6.

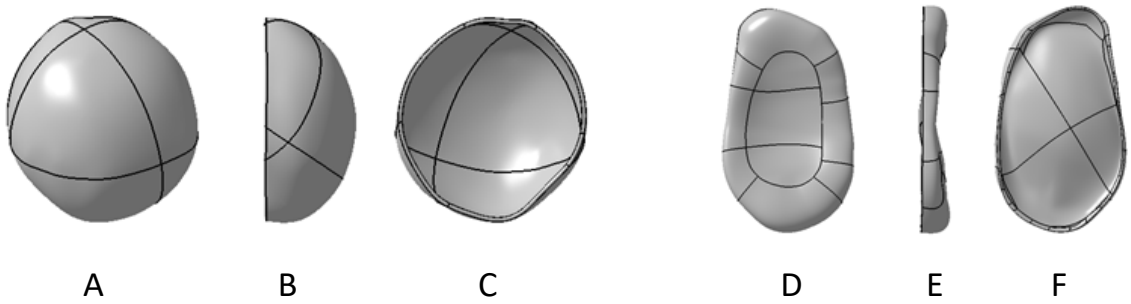

Figure 3.6. CAD models of the humeral cartilage (A, B, C) and of the glenoid cartilage (D, E, F) developed in the present study. Anterior (A, D), lateral (B, E) and posterior (C, F) views.

With the CAD models obtained, the molds were designed and manufactured via Computer Aided Manufacturing (CAM) (MIKRON VCE 500). Figure 3.7 illustrates the mold manufacturing process for the glenoid cartilage and Figure 3.8 shows the molds.

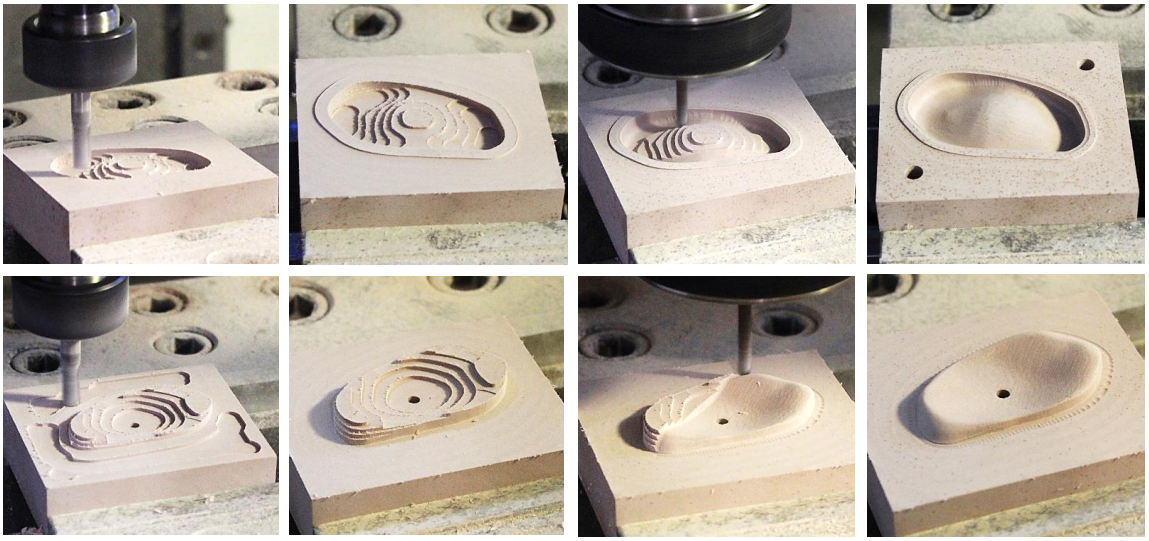

Figure 3.7. Mold manufacturing process for the glenoid cartilage model used in this work.

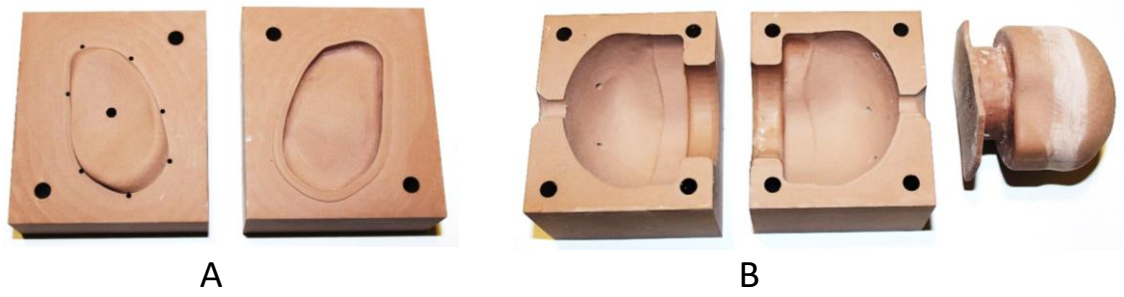

Figure 3.8. Molds of the glenoid (A) and humeral cartilage (B).

The cartilages were then produced through rapid prototyping, using room temperature vulcanization silicone technique (RTV). Figure 3.9 shows the cartilages obtained.

Figure 3.9. Molds of the glenoid (A) and humeral cartilage (B).

The most important muscles in abduction were previously identified with a multi-body model of the intact shoulder: deltoideus, subscapularis, infraspinatus, supraspinatus, serratus anterior and trapezius (see Chapter 2). However, for simplification of the experimental apparatus, the *in vitro* models developed (intact and implanted) did not consider the trapezius and the serratus anterior muscles. The intact shoulder model is represented in Figure 3.10, showing the composite bone structures, the muscles, the IGHL and the cartilages.

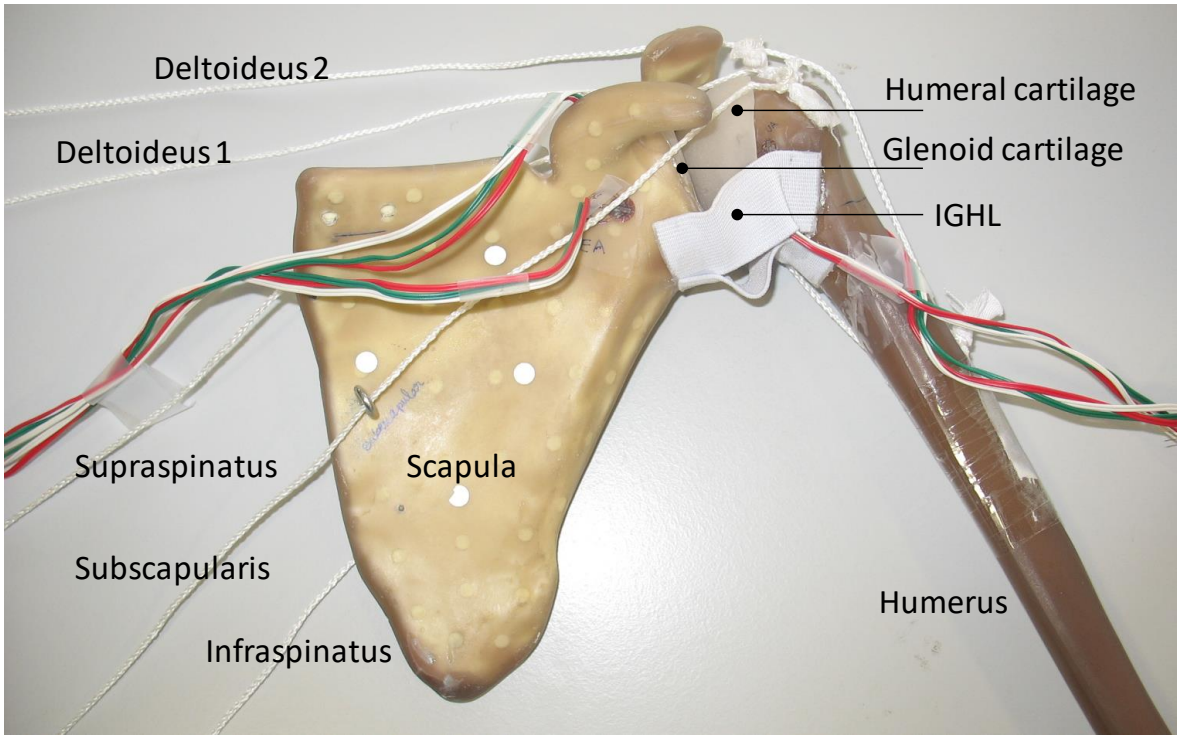

Figure 3.10. *In vitro* intact shoulder model developed in this work.

3.2.2 Implanted Model

As with the *in vitro* intact shoulder model, the *in vitro* implanted shoulder model was constructed with fourth generation composite bone structures from Sawbones® (see Figure 3.4). Since in a shoulder arthroplasty the IGHL suffers a tenotomy and is later re-sutured, its importance in abduction diminishes, especially in elderly patients, and for this reason we chosed not to add the IGHL in the implanted model.

The implant used in the study is a Comprehensive® Total Shoulder System, provided by BIOMET® Portugal, exposed in Figure 3.11 and in Figure 3.12. The Modular Hybrid® Glenoid Base is made of high-density polyethylene (HDPE) and has three outer pegs for glenoid fixation, designed to be implanted with bone cement. Other studies have proved

good stability, bone ingrowth and increased fixation with uncemented pegs with similar a design [58, 72]. At the glenoid base centre, there is a fit for the attachment of the central peg. A Regenerex® Modular Hybrid Peg was used, designed to be implanted without bone cement. The metallic peg is coated with porous titanium, which allows an improved pore structure, offering high levels of biologic fixation. The peg has a special design that promotes additional resistance to shear and axial forces on the face of the glenoid [172].

Regarding the humeral implant, it has three components (humeral stem, humeral head taper adaptor and Versa-Dial™ humeral head) all in titanium. The stem (mini length size) has a top-coated surface (0.75 mm thick on all sides [173]) to enhance fixation and the humeral head has a polished surface to reduce friction.

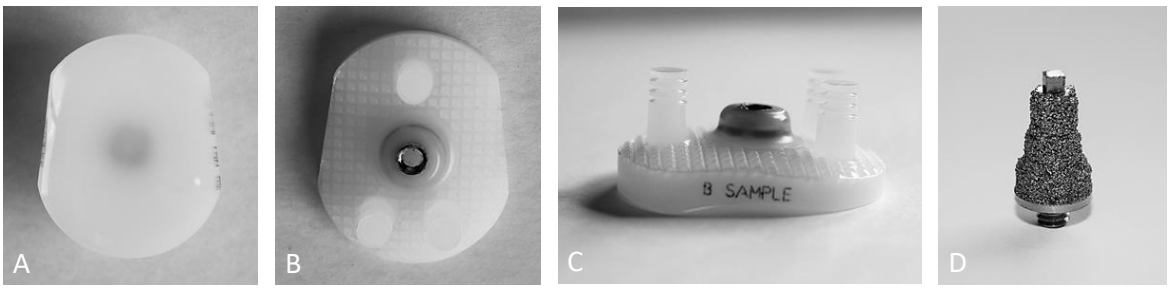

Figure 3.11. Modular Hybrid® Glenoid Base (A, B, C) and Regenerex® Modular Hybrid Glenoid Central Peg (D), of the Comprehensive® Shoulder System, BIOMET®.

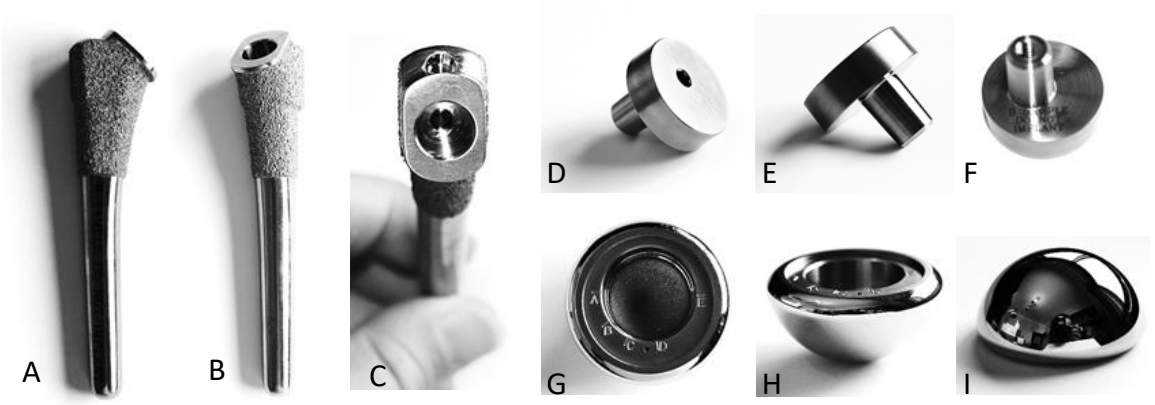

Figure 3.12. Mini Length Humeral Stem (A, B, C), Humeral Head Taper Adaptor (D, E, F) and Versa-Dial™ Humeral Head (G, H, I) of the Comprehensive® Shoulder System, from BIOMET®.

An experienced surgeon made the *in vitro* total shoulder arthroplasty in our laboratory, following the press-fit surgical technique, with adequate surgical instruments [173]. Figure 3.13 and Figure 3.14 illustrate the *in vitro* surgery of the humerus and scapula, respectively.

For the humerus composite structure, a pilot hole was bored into the humeral head, along the humeral shaft, and the humeral shaft was then reamed. The hole must be done medial to the rotator cuff attachment and lateral to the head of the articular surface (Figure 3.13, A). Afterwards, the humeral head was resected (Figure 3.13, B, C) at approximately 1 mm above the rotator cuff insertion site. In a real shoulder arthroplasty scenario, this would increase glenoid exposure. Humeral broaching was the next step (Figure 3.13, D), and it was done with a broach 2 to 3 mm smaller than the last reamer used. The broach is perfectly placed when the broach collar sits on the resected surface of the humeral head. The humeral head size was chosen using the resected humeral head for comparison, and its correct position was confirmed (Figure 3.13, E, F). After removing the humeral broach, the humeral stem was inserted into the canal (Figure 3.13, G) and the Versa-Dial™ Humeral Head inserted onto the stem and rotated to attain maximum coverage of the resected head surface. Figure 3.13, H shows the humeral prosthesis implanted.

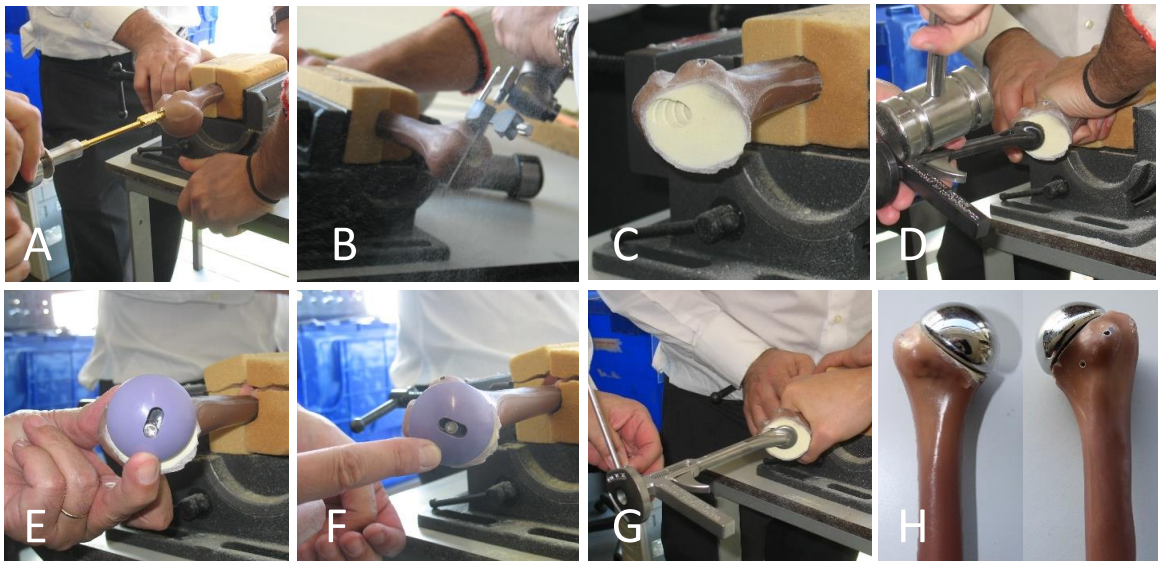

Figure 3.13. *In vitro* surgery of the humerus. Press-fit technique.

Regarding the composite structure of the scapula, an appropriate sizer was placed in the centre of the glenoid, with the wider side inferiorly (Figure 3.14, A). The centring hole was then drilled (Figure 3.14, B). A suitable size glenoid reamer was attached to the reamer shaft, and its centre was placed in the centre hole previously made. After that, the glenoid was reamed until a concentric glenoid surface shape was achieved (Figure

3.14, C). An anatomic drill-guide was chosen and placed in the glenoid cavity, and its centring peg matched the centre hole drilled before (Figure 3.14, D). With the drill-guide, the three outer peg holes (posterior-inferior, anterior-inferior, superior) were also drilled (Figure 3.14, E). With the help of the centre-peg-drill-guide (Figure 3.14, F), the central peg was drilled (Figure 3.14, G). Finally, the glenoid prosthesis was positioned in the cavity (Figure 3.14, H).

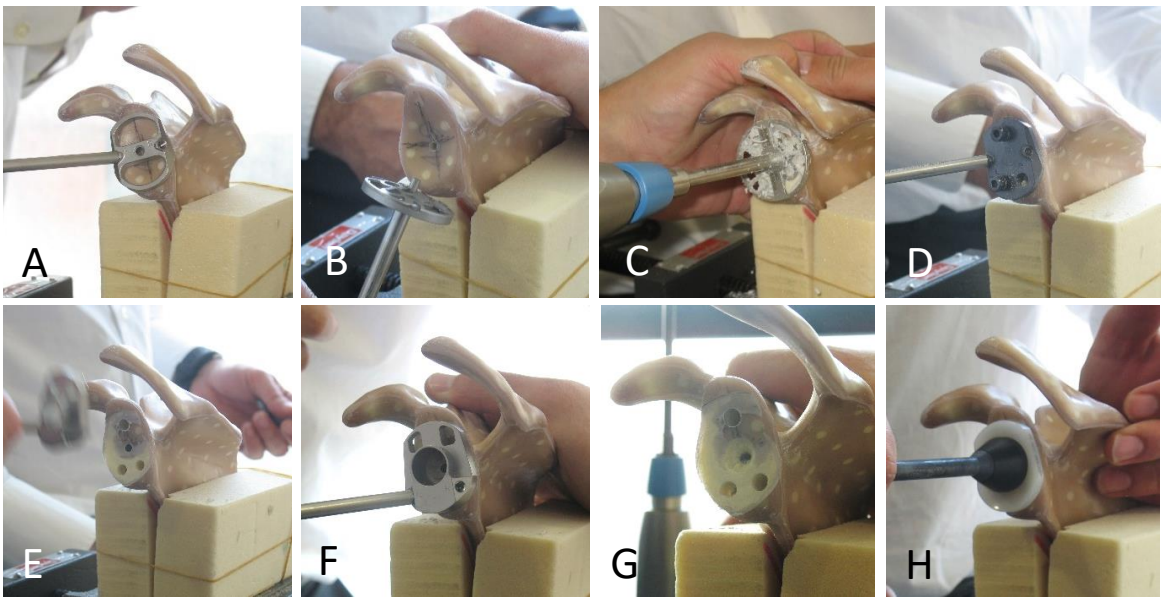

Figure 3.14. *In vitro* surgery of the scapula. Press-fit technique.

Prosthesis positioning is a key aspect for a successful arthroplasty procedure and the anatomical reconstruction of the joint is crucial for restoring mobility and limiting implant loosening. In the positioning of the humeral component, it is mandatory that the central drill stays aligned with the humeral shaft, so that the humeral prosthesis is correctly aligned with the bone structure. The humeral head cut is also important and it should be made so that the humeral head prosthesis can be adapted to better replicate the anatomical variations of the humeral bone, in both normal and pathologic conditions. When the humeral prosthesis is not correctly positioned, effects on ROM, kinematics and impingement are likely to happen [174].

In an experimental study made by Williams el at. [175], the authors evaluated the effect of articular malposition on the performance of the glenohumeral joint after a TSA. They pointed out that for minimum subacromial impingement and maximum glenohumeral motion to be observed, an anatomical reconstruction of the humerus may have an offset of 4 mm, at the most.

The biomechanical consequences of humeral component malpositioning after a TSA has also been studied using numerical models [176, 177], confirming that prosthetic position deviations lead to severe effects on the functional result and lifetime of the prosthesis.

In the positioning of the glenoid component, the ideal scenario would be prosthesis positioning in neutral version, with complete contact between implant/bone interfaces and bone stoke preservation. But because the glenoid vault is such a small and irregular bone structure, with various glenoid morphologies [178], this is not always the case [179]. In glenoid component fixation, the reaming of the glenoid surface is an important step towards neutral version of the component, and for achieving an improved surface for implant/bone interface contact. It is also essential that all fixation drills are performed as carefully as possible, so that the surrounding bone tissue can be preserved. When the glenoid component is not correctly positioned, humeral instability may be observed, and the glenoid component may suffer increased stress that can promote premature glenoid loosening [174]. Furthermore, the composite bone structures used in the experimental model of the shoulder here developed try to replicate the bone structure of most of the population in non-pathologic conditions. However, considerable differences in the shape of the proximal humerus [43] and of the glenoid cavity [180, 181] is a reality in both non-pathologic and pathologic patients. This fact needs to be addressed when designing a surgery strategy and when choosing proper prosthesis components.

The *in vitro* implanted shoulder model developed is exposed in Figure 3.15.

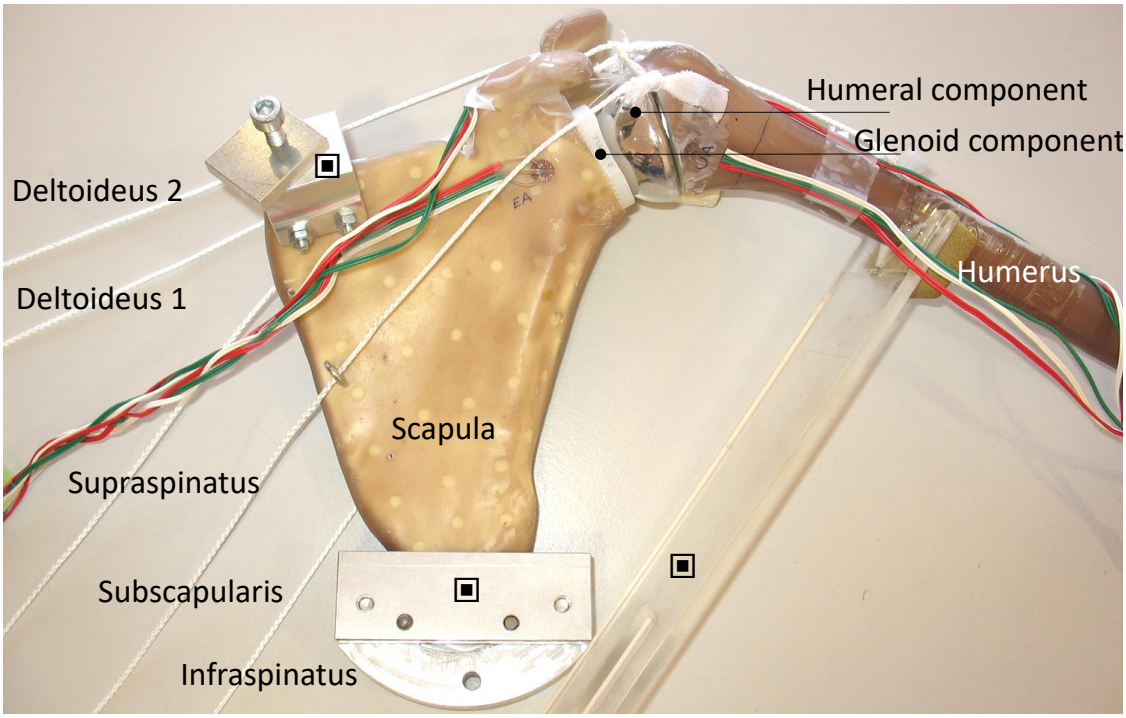

Figure 3.15. In vitro implanted shoulder model developed in this work. The structures indicated with the symbol belong to the experimental testing apparatus.

3.3 Experiments

3.3.1 Testing Apparatus

The static-dynamic shoulder testing apparatus developed is a new system constructed based on existing experimental shoulder models [140, 149] and is represented in Figure 3.16.

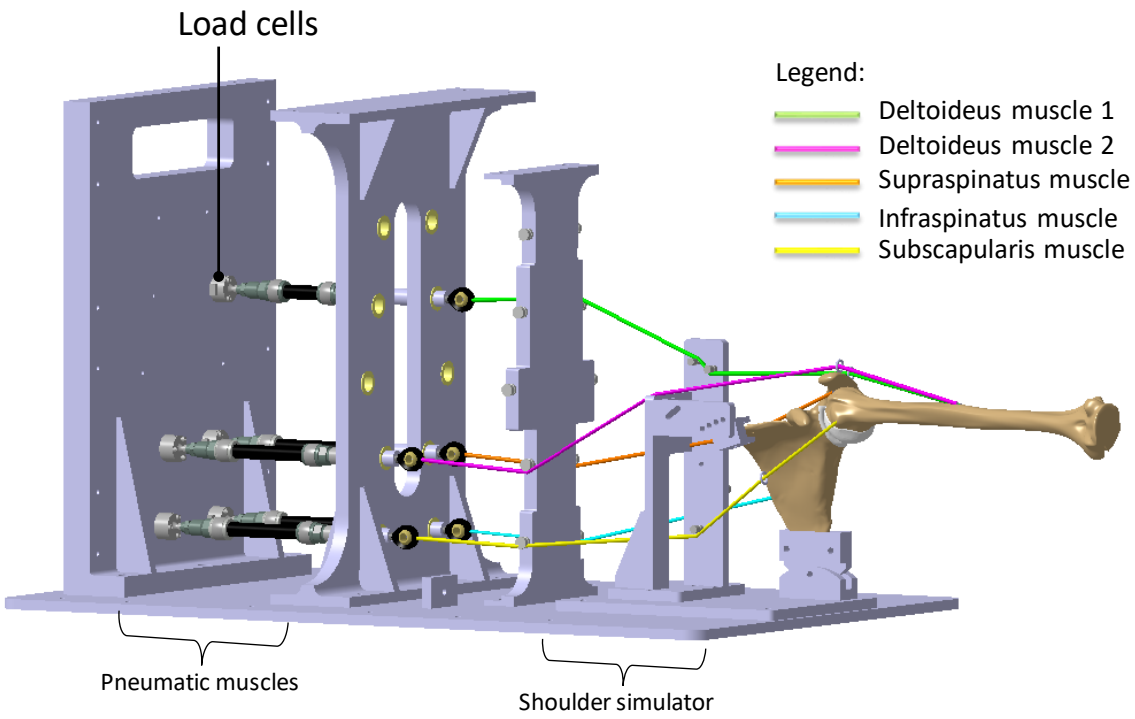

Figure 3.16. Simplified CAD model of the joint simulator with the shoulder testing apparatus designed.

The shoulder simulator was designed to replicate the glenohumeral joint in a static 90° abduction, since this is considered a critical position for the glenohumeral joint [132]. However, the developed system allows to position the joint in any desired abduction angle and to include the scapulothoracic rhythm. To hold the composite scapula, a specially constructed system fixes its inferior angle and its superior margin. The composite humerus is equilibrated by the muscle forces and by the external forces (not shown in Figure 3.16).

We later added an acrylic plate to the system to provide additional support to the composite humerus (see Figure 3.15). With the acrylic plate, we ensured the same humeral position in all trials. Despite reducing the degrees of freedom of the humeral bone structure, the acrylic plate allows it to move vertically in response to the external load and to the muscle actions. Furthermore, due to the small friction coefficient between the humeral head implant and the glenoid implant, the implanted shoulder model presents higher freedom than the intact shoulder model. Adding to this fact, the implanted model does not consider

the IGHL. Thus, to reduce the degrees of freedom of the implanted composite humerus, an extra support was glued to the acrylic plate and to the proximal humerus (see Figure 3.15).

The system considers two lines of action for the deltoideus muscle, simulated by two cables, since it produces the greatest amount of force. The rotator cuff muscles are considered as having one line of action each (that is, three cables). This strategy was previously adopted by others [140, 146]. Muscle directions were anatomically defined and two extremities of two cables were attached to the deltoideus tuberosity, while three extremities of three cables were attached to the corresponding origin site of each rotator cuff muscle. The remaining extremities were attached to pneumatic muscles (DMSP-10-40N-AM-AM and DMSP-10-80N-AM-AM, FESTO). The muscle forces were monitored by a real-time controller (NI c-RIO-9074, National Instruments) and were measured by load cells (U9B, HBM) placed in line with the pneumatic muscles, thus measuring the tension applied to each cable. A custom-written LabVIEW (National Instruments, Austin, TX, USA) program controlled the pneumatic muscles and displayed the measured forces.

The main structure holding the pneumatic muscles was previously developed to study the temporomandibular joint [182] and was adapted for the positioning of the shoulder.

To analyse the biomechanical response of the models to muscle and external forces, strain gage rosettes (45°) (KFG-3-120-D17-11 L3M2S: 3 mm size, and KFG-1-120-D17-11 L3M2S: 1 mm size, Kyowa Electronic Instruments Co.) were used to determine the deformation suffered by the composite structures. Two were glued on the glenoid (anterior and posterior regions) and two on the humerus (close to the greater and lesser tubercles) (see Figure 3.17 and Figure 3.18).

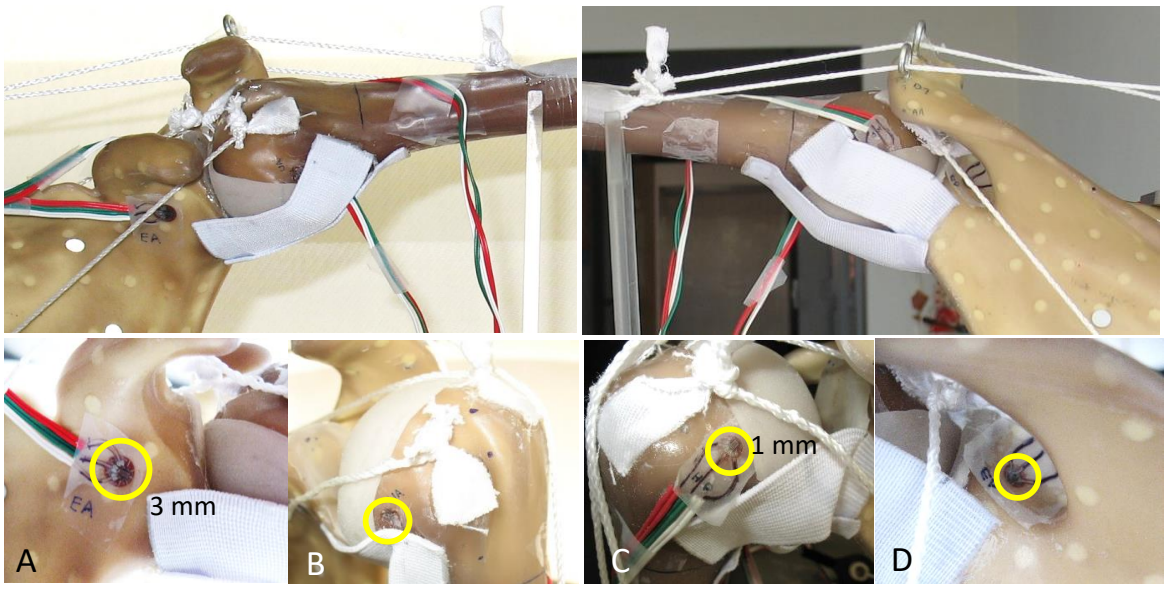

Figure 3.17. Positions of the rosettes (yellow circles) at the glenoid cavity (A, D) and humerus (B, C) in the intact model. Anterior view (A, B) and posterior view (C, D).

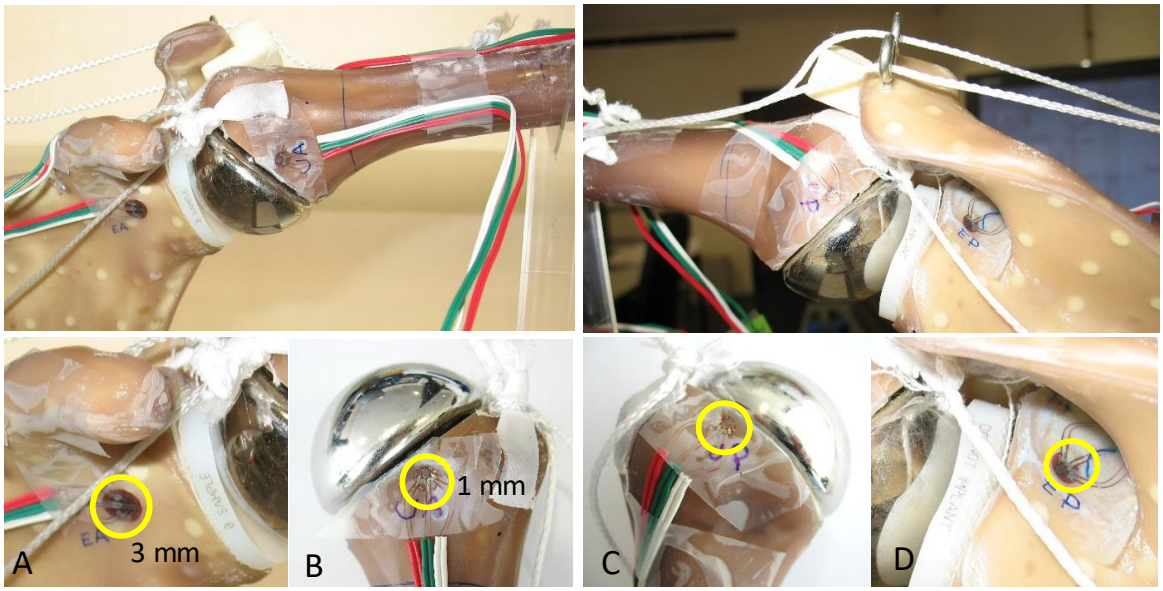

Figure 3.18. Positions of the rosettes at the glenoid cavity (A, D) and at the humerus (B, C) of the intact and implanted models (indicated by the yellow circles). Anterior view (A, B) and posterior view (C, D).

The rosettes were connected to a data acquisition system PXI-1050 (National Instruments, Austin, TX, USA), controlled by a LabVIEW application. The strains measured at each rosette (ε_1, ε_2 and ε_3) allow to determine the maximum principal strains according with Eq. 3.1 [183].

$$\varepsilon_{max/min} = \frac{1}{2}\left[\varepsilon_1 + \varepsilon_2 \pm \sqrt{2\{(\varepsilon_1 - \varepsilon_3)^2 + (\varepsilon_3 - \varepsilon_2)^2\}}\right] \quad \text{Eq. 3.1}$$

3.3.2 Applied Forces

The developed shoulder testing apparatus allows the use of diverse strategies for force application, like equal or different loads in all muscles or the lack of some of them, as in other shoulder simulators [146, 184].

In this study, muscle forces were previously determined with a multi-body model of the intact shoulder (see Chapter 2), that included the same muscles used in our experimental system. The developed multi-body model simulated an adult male (weight: 101 kg, height: 1.61 m) performing an abduction motion (from 0° to 90°) with an external load of 1 kgf in the hand. Knowing the height (H) of the simulated human body, the distance between the shoulder joint and the hand (x_0) was determined according to Eq. 3.2 [185]:

$$x_0 = 0.803\, H \quad \text{Eq. 3.2}$$

As the proposed experimental model only comprehends the scapula and the humerus, the external loads were applied on the extremity of the composite humeral bone, at a distance x_1 = 277 mm from the top of the humeral head. Since the mechanical system formed by the bones and by the external load is in equilibrium, an external force of 23.5 N (corresponding to an external weight of 2.350 kg) was applied at point x_1 to balance the muscle forces.

Because of pneumatic muscles features, it was not possible to apply 100% of the previously determined muscle actions and a 75% amount was considered, corresponding to an external weight of approximately 1.760 kgf. Table 3.3 indicates the muscle actions applied to the intact and implanted shoulder models.

Table 3.3. Muscle actions used in the experimental system.

Muscle Actions (%)	Muscle Forces (N)				
	Deltoideus 1	Deltoideus 2	Subscapularis	Infraspinatus	Supraspinatus
100	150	150	225	120	90
75	113	113	169	90	68

3.3.3 Testing Procedure

The structures were manually positioned on the experimental apparatus and the acrylic plate supported the humerus. With the shoulder structures correctly positioned, we gradually added the muscle forces to the muscle cables and the external weight to the humeral shaft. The same experimental protocol (Figure 3.19) was followed in each trial. To keep the humeral head correctly positioned, the rotator cuff muscles were the first to be actuated, until a certain muscle force was achieved in all three muscles. Afterwards, the deltoideus muscles were actuated until a defined muscle force value was reached. The external weight was then added to the system. This sequence was repeated until the muscle forces and external loads reached the expected values. The overall procedure was repeated, at least, seven times.

Because the humeral prosthesis confers more weight to the proximal humerus, thus changing the centre of rotation of the joint in the implanted model, it was mandatory to add a higher external weight to keep the implanted humerus performing a 90°. In this sense, instead of gradually applying the external forces, in the implanted model the humeral shaft was attached to the ground.

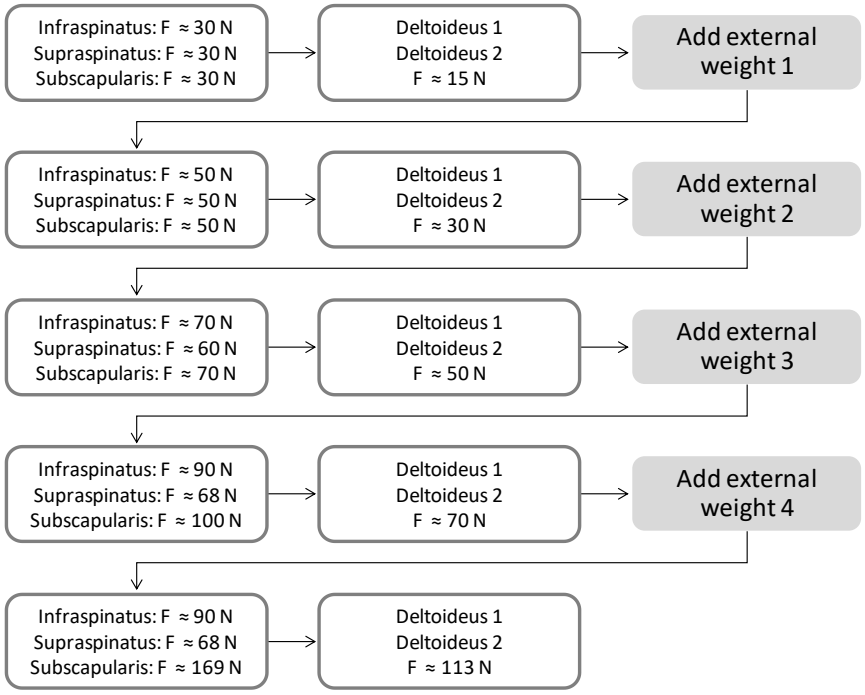

Figure 3.19. Experimental protocol used with the intact shoulder model.

3.4 Results

Principal strains were considered eligible if deviations from the average value were smaller than 15 %. However, in the intact model, the minimum principal strains at rosette AH (anterior humerus) had deviations from the average value between 19% and 29%; and in the implanted model, the maximum principal strains (at the same rosette) had deviations from the average value between 22% and 92%. For this reason, the trials considered eligible were the ones presenting the smaller number of deviations smaller than 15 %. Five trials from each model were chosen for the analysis.

The strain concentration in the cortical surface of a composite humerus and scapula, before and after implantation with a total shoulder prosthesis, were assessed in the present study and are represented in Figure 3.20 and Figure 3.21, respectively. The composite bones simulate the glenohumeral joint in a 90° abduction.

In the intact shoulder model, the higher principal strains were observed at the glenoid (see Figure 3.20). This may be related with the fact that the glenoid cavity has a smaller volume and smaller bone density than the humeral head. The most strained areas are at the posterior region of the glenoid cavity (rosette PS: $(353 \pm 28)\ \mu\varepsilon$) and the smallest at the anterior region of the humeral head (rosette AH: $(17 \pm 4)\ \mu\varepsilon$). The load is transferred posteriorly in the scapula and the contact centre is located posteriorly.

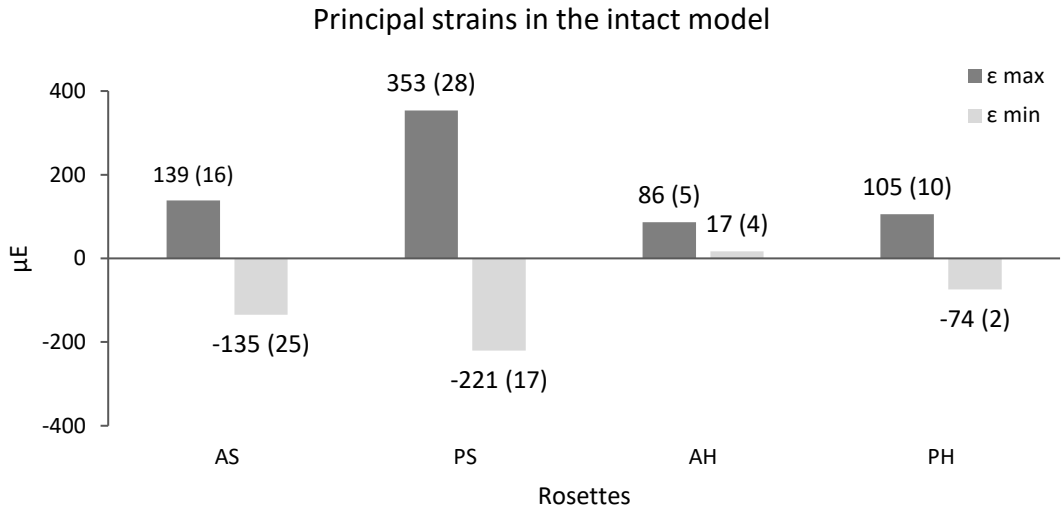

Figure 3.20. Mean principal strains and standard deviation (SD) at 90° abduction. AS/PS: Anterior/Posterior Scapula; AH/PH: Anterior/Posterior Humerus.

After implanted with a total shoulder arthroplasty, the glenoid cavity and the humeral head present similar principal strains (see Figure 3.21). Anteriorly and posteriorly, the glenoid cavity has maximum principal strains around 170 με, while at the anterior region of the humeral head this value is around 140 με. The highest strain concentration was measured at the anterior region of the glenoid cavity (rosette AS: (175 ± 10) με) and the smallest at the posterior region of the glenoid cavity (rosette PS: (-49 ± 3) με)). After the arthroplasty, the load is transferred by the anterior region.

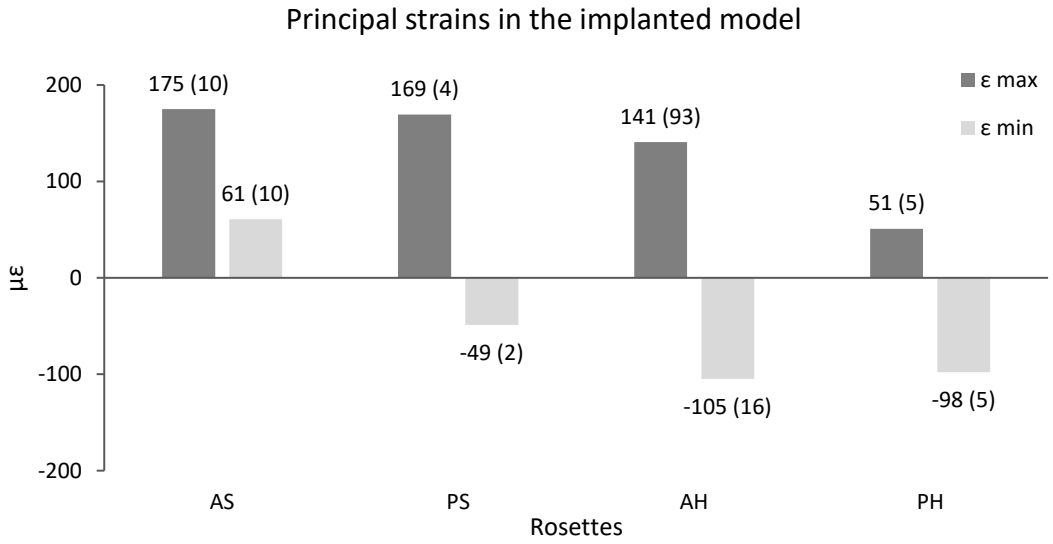

Figure 3.21. Mean principal strains and standard deviation (SD) at 90° abduction. AS/PS: Anterior/Posterior Scapula; AH/PH: Anterior/Posterior Humerus.

The glenoid cavity suffers mainly tensile strains in the anterior and posterior regions. However, in the posterior region (rosette PS) some compression is observed. Regarding the humeral head, the compressive and tensile strains are similar in both anterior and posterior regions. Standard deviations are generally small in both shoulder models, with the lowest value registered in the posterior region of the scapula: rosette PS (-49 ± 2) με. The highest value is observed in the anterior region of the humeral head: rosette AH (141 ± 93) με.

Near rosette AS, at approximately 7 mm, there is a hole which was made during the experimental arthroplasty procedure that may have some influence (border effect) in the strain measured at the rosette. Besides, the strain measured in rosette AH has a high degree of variability in all trials. This fact suggests other sources of error.

3.5 Discussion

To characterize the biomechanical behaviour of the intact and implanted glenohumeral joint we created a system for in vitro experiments. The intact shoulder model was constructed with composite bone structures, their cartilages, and with the IGHL, since it has a major importance in high amplitude movements. As for the implanted model, it considers the same composite bone structures and a Comprehensive® Total Shoulder System, from BIOMET®. The IGHL was not considered, since in real patients it suffers a tenotomy.

The intrinsic relationship between the glenohumeral muscles, the scapulothoracic muscles, and the soft tissues surrounding the joint determines glenohumeral motion in both intact and implanted shoulders. Furthermore, the forces that hold the joint in its correct place are continuously changing in magnitude and in direction, making it difficult to predict and to replicate in any experimental system.

As has been described, many muscle loading combinations allow the performance of shoulder abduction considering the muscles used in the present study (deltoideus, infraspinatus, supraspinatus and subscapularis) [146, 184]. However, *in vivo* loading scenarios are difficult to replicate.

The intact and implanted shoulder models developed permit to infer on the importance that the rotator cuff muscles, and the soft tissues surrounding the joint, have in keeping it stable. Disorders related with the rotator cuff, such as rotator cuff arthropathy, creates unstable scenarios on the shoulder, and in these cases the joint is more prone to dislocations.

The system constructed allows simulating several degrees of abduction, and the trials performed for the most critical condition revealed a good stability and confirmed the high freedom and instability that characterizes the glenohumeral joint. In both intact and implanted models, the applied forces were very similar to the expected ones (see Figure 3.22 and Table 3.3), although smaller (except for the supraspinatus muscle in the implanted model). The smallest and highest SD correspond to supraspinatus muscle in the intact and

implanted models ((67.1 ± 0.1) N and (68.9 ± 2.5) N, respectively). Overall, SD are higher for the implanted model, and this relates with the smaller friction coefficient between the glenoid and humeral head prosthesis components, that made the system less stable.

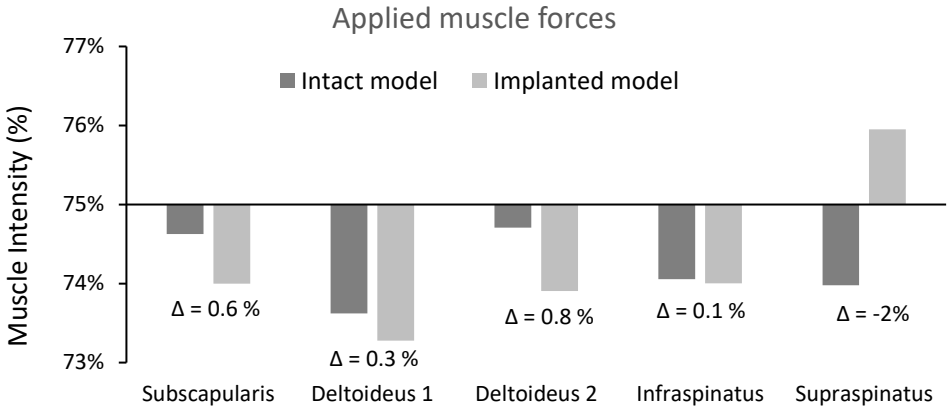

Figure 3.22. Percentage of muscle intensity applied in the intact and implanted models.

Table 3.4. Muscle forces applied in the intact and implanted models.

Muscle	Theoretical Muscle Forces [N] (75 %)	Average Muscles Forces (SD) [N]	
		Intact model	Implanted model
Deltoideus 1	113	110.9 (0.8)	110.4 (1.5)
Deltoideus 2	113	112.5 (1.4)	111.4 (2.0)
Subscapularis	169	168.1 (1.0)	166.7 (1.8)
Infraspinatus	90	88.9 (0.4)	88.8 (2.0)
Supraspinatus	68	67.1 (0.1)	68.9 (2.5)

As we manually apply the weights and the muscle forces, we observe some rotation of the humeral head in the intact model. We assume that those are possible of being reduced in the presence of the remaining soft tissues. Since in the implanted model the humerus was fixed with two supports, its rotations were smaller. The rotations suffered by the composite humerus, which are hard to control and influence the way the two bone structures interact with each other, influence the deformations of the system in each trial performed. Even so, the repeatability of the results was achieved with success. However, standard deviations

were higher in the implanted shoulder model, more specifically at the humeral head (rosette AH). Despite, we chose to keep the distal end of the humerus unconstrained to more accurately simulate the in vivo scenario.

With the experiments performed in this study we investigated the influence of total shoulder prosthesis on strain distribution at the cortical surface of the two bone structures. Figure 3.23 shows the comparison between the principal strains in the intact and implanted shoulder models. In the intact shoulder, the scapula suffers higher deformations than the humerus, but after a total shoulder arthroplasty, both bone structures present similar deformations. Maximum principal strains measured in the anterior region of both bone structures (rosettes AS and AH), augmented after prosthesis implantation, by a rate of 26% and 64%, correspondingly. On the contrary, the maximum principal strains in the posterior regions of both bone structures (rosettes PS and PH) diminished by a rate of 52% after prosthesis implantation. Therefore, after prosthesis implantation, tensile strains augmented in the anterior region of the model, and diminished in the posterior region. The minimum principal strains after prosthesis implantation diminished in the glenoid cavity, and augmented in the humeral head. The difference rates were higher than with the maximum principal strains.

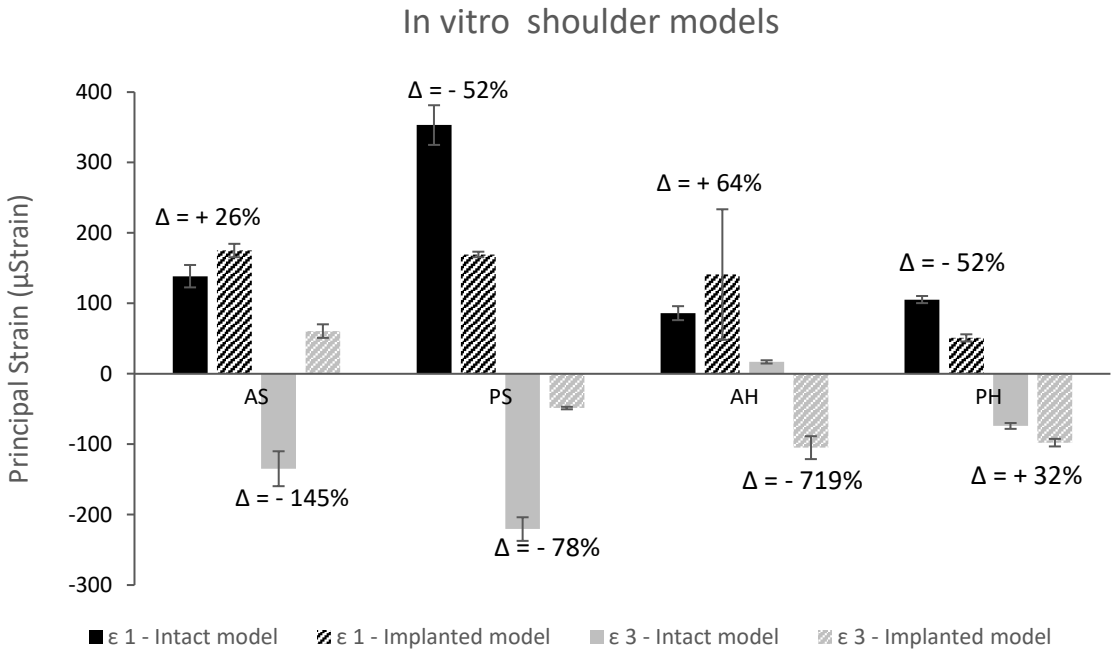

Figure 3.23. Comparison between principal strains at the intact and implanted models. AS/PS: Anterior/Posterior Scapula; AH/PH: Anterior/Posterior Humerus.

In the implanted model, the strain values were smaller than 200 με, and according to Roberts *et al.*[186], strains of less than 200 με are indicative of inappropriate stimulus, causing bone atrophy. Thus, the small strain values measured at the cortical surface suggest lower strain concentration for bone growth, which can lead to implant loosening, one of the main causes of implant failure of the glenoid component.

Comparing our results with those of literature is not straight forward, mainly because, as far as we know, no studies considering the shoulder joint analysed strain deformation, but instead focused on the global biomechanical characterization of the joint, before and after prosthesis implantation.

Thus far, the only studies considering the strain behaviour of the scapula are those of Maurel *et al.* [163] and of Diop *et al.* [164]. Nonetheless, they consider only the behaviour of the scapula when loaded in some exact locations (without considering the humerus) and no muscle actions were added to the experimental system. On the contrary, we analysed strain behaviour of the scapula and of the humerus due to their intrinsic relationship, and under muscle loading. Furthermore, we considered a press-fit implantation technique, and Maurel *et al.* [163] and Diop *et al.* [164] considered the cementing technique.

In the intact model, we observed that posterior glenoid has higher deformations (in tension and in compression). This is opposed to what Maurel *et al.* [163] observed in their intact scapula: during abduction, maximum principal strains were located mainly at anterior and antero-superior regions of the glenoid. This difference is related with the orientation of the loading and the amount of force applied in the two studies.

In the implanted model, we verified that at the anterior region (glenoid and humeral bone structures), tensile strains augmented after implantation of the prosthesis, having diminished in the posterior region. Regarding the compressive strains, they diminished in the glenoid cavity, and augmented in the humeral head. On the contrary, Maurel *et al.* [163] observed that after implantation there was a strong tendency of the strains to increase, decreasing only at the postero-inferior regions when an antero-inferior load was applied.

3.6 Conclusions

To build an experimental system that exactly replicates the anatomy and biomechanics of the glenohumeral joint is not an easy task, either due to the anatomy of the bone structures, as to the amount of soft tissue that compose the joint. Nevertheless, we developed an intact shoulder model and an implanted shoulder model that considers the most important muscles in abduction. Composite bone structures were used to build the shoulder, and an anatomical Comprehensive® Total Shoulder System was implanted in one composite model. The loading scenarios were defined by a multi-body model previously considered, and are in the range of forces applied in other *in vitro* shoulder simulators in literature.

The developed and implemented model for *in vitro* experimental testing allows the study of the glenohumeral joint in several degrees of abduction. The experimental tests for the most critical condition revealed the good stability of the intact and implanted shoulder models. The data obtained for the intact and implanted models will be used for a clearer understanding of the deformations suffered by the bone structures in a position considered critical for the shoulder. Furthermore, these results will contribute to the validation of a finite element model of the intact shoulder and of the implanted shoulder.

Chapter 4

Finite Element Models and Validation

4.1 Overview of Existent Shoulder Models

The finite element method is widely used in the simulation of biomechanical structures, which include complex geometries, interactions between structures and mechanical properties of bones.

The modelling of human articulations began by focusing mostly on the hip and knee than on the shoulder, and this may be due to clinical issues and to shoulder joint complexity. Despite the continuous increase in hip and knee arthroplasties [187], shoulder arthroplasty records are growing [188] and, by 2015, its demand was expected to exceed that of the hip and of the knee in the United States [189]. This growth has helped to turn the attention of researchers into the shoulder joint, as better prostheses are a demand to correctly provide pain relief and reduce revision surgery.

Developing an accurate finite element model (FEM) of the shoulder joint (intact and implanted) is a complex task, as it includes three bones, some articulations, cartilages and many muscles, as described before (see Chapter 1).

Generally, FEM are simplified, focusing their attention mainly on the connection between the humerus and the scapula bones, as these structures form the most important articulation of the shoulder complex: the glenohumeral joint. Simplification serves to facilitate the computational time when modelling of complex musculoskeletal structures, but at the expenses of differences between the numerical results and the real situation.

In this thesis, we developed two FE models of the shoulder joint. One corresponds to the intact condition, and the other to the implanted condition. The implant used was a Comprehensive® Total Shoulder System, provided by BIOMET® Portugal.

The FE models developed aim to be a replica of the experimental models of the intact and implanted shoulder, presented in Chapter 3. Validation was performed successfully. As far as we know, these are the first models considering the entire humeral and scapular structures, the action of the rotator cuff and deltoideus muscles, and of the inferior glenohumeral ligament and humeral and glenoid cartilages in the intact model; and of the anatomical shoulder prosthesis in the implanted model.

An overview of existent FEM of the intact and implanted shoulder joint is provided next.

4.1.1 Intact Models

Generally, FE models try to represent the intact shoulder joint using the scapula and the humerus as the two main bone structures. Their aim is to characterize the normal function of the joint and its stability, but also focus on the influence that certain deficiencies have on shoulder biomechanics.

Important differences between a normal and an osteoarthritic joint were proposed by Büchler *et al.* [139], and were in accordance with clinical findings. A case of supraspinatus deficiency was studied by Terrier *et al.* [190], suggesting that this insufficiency may cause

limitations in active abduction motion, and may promote degenerative glenohumeral changes in the joint.

Gerber *et al.* [191], using an automated muscle wrapping algorithm developed by Favre *et al.* [192], studied joint stability when in the presence of a larger critical shoulder angle (measured between the glenoid surface and the line linking the inferior glenoid rim and the lateral tip of the acromion [191]), which is known to be a strong indicative of future rotator cuff tears [193]. The study successfully demonstrates that larger critical shoulder angles lead to higher shear forces and smaller compression forces on the glenohumeral joint during abduction, causing joint instability.

Walia *et al.* [194] studied the effects that combined humeral head and glenoid bone defects have on joint stability. The study suggests that the presence of bony Bankart and Hill-Sachs defects reduces joint stability more than when only one defect is present. In this study, a compressive load was applied, with no muscles involved.

The reviewed studies [139, 190, 194–196] modelled the joint with realistic anatomical features, considering the intact shoulder stability to be achieved by means of muscles and of articular contact forces, which allows the humerus to move freely in the joint. Several methods were used to quantify joint stability. Favre *et al.* [196] considered the joint to be stable if the shear force necessary to dislocate the joint was less than a compressive load of $50\ N$. Büchler *et al.* [139] evaluated joint stability by analysing the centroid of the contact pressure, which must fall within the glenoid fossa, so that the joint can remain stable. In a similar way, Terrier *et al.* [190] evaluated joint stability by calculating the projection of the reaction force on the glenoid surface. These methods are similar, since stability is achieved when a model can keep the humeral head inside the glenoid cavity. Nevertheless, one cannot say which strategy is the best, and a standardization method should be proposed, so that studies can be properly compared.

One of the most robust 3D numerical models of the shoulder was developed by Favre *et al.* [195], and is characterized by the lack of pre-defined kinematic constraints. The authors developed an "integrated model" of the shoulder that is constituted by three distinct sub-models. In the first sub-model, the muscle path is determined for a certain position of interest [192]; in the second sub-model, knowing the muscle path and muscle length, the muscle forces which can equilibrate and stabilize the joint are determined [103, 197]; finally, the forces determined are applied in the third sub-model, to simulate joint contact and humeral head translation [196]. The model of Favre *et al.* [195] is a 3D FEM that includes anatomically precise representations of the scapula and of the humerus, including also the humeral and glenoid cartilage and the labrum. The study focuses on active glenohumeral stabilization considering the six DOF of the joint, and the equilibrium conditions are accomplished due to twenty-seven individual muscle segments. The study does not analyse strain distributions.

Normally, glenohumeral stability is accomplished mainly via the rotator cuff muscles, which are the active stabilizers of the joint. Thus, another concern regarding the shoulder is tears of the rotator cuff, a pathology that affects mostly the supraspinatus tendon. There are many FE studies that try to explore the mechanisms triggering rotator cuff tears [198–202]. The first being developed were 2D models [198, 199], usually considering the humeral head and the supraspinatus tendon. Later, more complex 3D FEM were developed, focusing on topics like muscle-strength reduction after a rotator cuff tear [200], or stress distribution in rotator cuff tendons [201, 202].

The other stabilizers of the glenohumeral joint, known as passive stabilizers, are the articular capsule and the labrum, which have been part of FE models. Some focus on the fundamental FE development of these structures [169, 203, 204], others on the study of stress/strain distribution [108, 109], or on the mechanical properties of the capsule [205].

Even though joint biomechanics as a whole is not taken into account in FEM focused on passive and active stabilizers, these models are important for a better knowledge of the mechanisms ruling these important structures. A summary of FEM of the intact shoulder is presented in Table 4.1.

Table 4.1. Review of finite element models of the intact shoulder.

Authors	Study goal	Components
Büchler *et al.* [139] 2002	Normal vs osteoarthritic shoulders	Scapula, humerus Subscapularis, supraspinatus, infraspinatus
Terrier *et al.* [190] 2007	Supraspinatus deficiency on joint stability	Scapula, humerus, cartilage Deltoideus, supraspinatus, subscapularis Infraspinatus/ teres minor
Adams *et al.* [200] 2007	Morphological changes to rotator cuff tendons after a rotator cuff tear	Scapula, humerus, cartilage Rotator cuff tendon
Seki *et al.* [202] 2008	3D stress distribution in the supraspinatus tendon	Humeral head, articular cartilage Supraspinatus Calcified and Non-calcified fibrocartilage
Favre *et al.* [196] 2012	Active glenohumeral stabilization	Scapula, humerus, cartilage, labrum 27 muscle segments
Walia *et al.* [194] 2013	Combined humeral head and glenoid bone defects on joint stability	Scapula, humerus, cartilage
Inoue *et al.* [201] 2013	Development mechanism of the rotator cuff tears on the supraspinatus muscle	Scapula, humerus Rotator cuff and deltoideus muscles
Hwang *et al.* [206] 2014	Superior humeral head motion due to rotator cuff tears and long head of biceps tendon (LHBT) loading	Humeral head, glenoid bone, cartilage Labrum, LHBT

4.1.2 Implanted Models

Finite element models have been widely used to study how TSA influences joint behaviour, analysing stress/strain distributions before and/or after prosthesis implantation, or at the implant/bone, bone/cement or implant/cement interfaces. Usually, FEM of implanted joints focus their attention on one bone structure at a time.

Glenoid loosening and wear are clinical issues largely affecting the implanted shoulder, and many FEM have been developed to address these problems. Parameters such as different loading positions and magnitudes [207–209], glenohumeral conformity [79, 207, 210, 211], several glenoid component designs [79, 209, 212–215], or issues related with component fixation [179, 207, 213] have been addressed.

On an early study, Mansat *et al.* [209] analysed how implant design, bone properties and load location influence the glenoid component survivor. An FE model of an osteoarthritic scapula was developed, and superior-anterior and superior-posterior centred loads were applied. A keeled and a pegged glenoid were used. The results indicated that eccentric loading increases stresses in the cement at the bone/cement interface. The study did not point for significant differences between the two designs, stating that the geometric and bone properties of the scapula have more influence than implant geometry on TSA success.

Similarly, Couteau *et al.* [207] compared the effect of centred and eccentric load on bone stresses, observing that at the bone/cement interface, eccentric loads can produce tensile and maximum shear stresses much higher than centred loads. These high strains may promote progressive loosening of the implant or of the cement mantle, which is in accordance with the findings of Mansat *et al.* [209]. Furthermore, issues related with component fixation were analysed by Couteau *et al.* [207]. The authors observed that a thin cement mantle promotes cement displacement in centred loads, while a thick cement mantle promotes stress shielding at the surrounding bone, which may lead to bone resorption in eccentric loads. This suggests that a compromise needs to be done regarding cement thickness, as not thin nor thick mantles are suitable for implant fixation.

Recently, the load transfer across a scapula before and after a TSA was studied by Patel *et al.* [208]. Two load magnitudes were considered, and several loading positions were compared. The study included a cemented pegged polyethylene glenoid component, and a non-cemented metal-backed component. The results suggest that eccentric and high-magnitude loads promote increasing stresses at the cement, and confirms that metal-back components reduce the load carried by the underlying bone, which is related with stress shielding. Patel *et al.* [216] performed another similar study, comparing normal with osteoarthritic shoulders (corrected and retroverted) implanted with a recent glenoid component. The study indicated that eccentric loads increase the stresses at the cement mantle, which is in accordance with others [207–209]. However, in the retroverted glenoid, the stresses in the bone/implant are less sensitive to the loading location.

In glenohumeral conformity studies [79, 207, 210, 211], the humeral bone is not always present [207, 211], being considered a rigid body by some authors [79, 210].

On their study on the mechanical behaviour of a scapula implanted with a glenoid component, Couteau *et al.* [207] also analysed the influence of glenoid conformity. Their results showed that less conformity leads to higher stresses on the prosthesis/cement interface, which relate with wear and loosening. Similar findings were observed by others [79, 210, 211].

Recently, Suárez *et al.* [211] analysed the influence of prosthesis conformity of a cementless glenoid component on bone/implant interface micromotions. They observed that as conformity decreases, the more susceptible the prosthesis is to the rocking-horse effect, because the contact pressure at the periphery of the prosthesis is very high. Furthermore, the authors observed larger interface micromotions with less conforming designs, and suggest that not only micromotions are higher, but can also be such that local bone ingrowth can be blocked.

Based on the experiments of Wang *et al.* [78], whom developed glenoid components with the strengths of both the conforming and nonconforming designs, Zhang *et al.* [79] evaluated the effects of several loading scenarios. Centred, transitional and periphery loading were chosen, demonstrating that periphery loading leads to the highest stresses at the glenoid component, and that those are most significant in the conforming design. The study showed that the new developed design is a suitable compromise between conformity and non-conformity, since it presents low glenoid component stresses when compressed at its periphery, and a larger contact area when compressed at the centre, indicating a low risk of wear and loosening.

Many examples of FEM of bone structures featuring implants are easily found in literature. Commonly, they study the influence of component designs, such as keeled *vs* pegged, metal-backed *vs* all-PE, with pegs or with conforming *vs* non-conforming *vs* hybrid design. Some focus also on the influence of the fixation procedure, such as more or less cement or different cement mantle thicknesses. However, as far as we know, there are no FEM of the implanted shoulder that consider the influence of the two prosthesis components, that is, of the humerus and of the glenoid. In the present chapter, we present and validate a FEM of the implanted shoulder considering both the humeral component and the glenoid component. A summary of some FEM of the implanted shoulder is presented in Table 4.2.

Table 4.2. Review of finite element models of the implanted shoulder.

Authors	Study goal	Components
Couteau *et al.* [207] 2001	Effect of eccentric loading, cement thickness and conformity on stress distribution	Scapula Glenoid component (keeled)
Terrier *et al.* [210] 2006	Effects of conformity	Scapula, humerus Rotator cuff muscles Humeral component Glenoid component (keeled, flat back) Cement layer
Suárez *et al.* [211] 2012	Effects of conformity in cementless implant	Bone substitute Glenoid component
Zhang *et al.* [79] 2013	Effects of conformity in different designs (conforming, nonconforming, hybrid designs)	Scapula Humeral component Glenoid component Cement layer
Patel *et al.* [208] 2014	Effect of load transfer after a TSA	Scapula (intact and implanted) Glenoid prosthesis Cement layer
Patel *et al.* [216] 2015	Effect of osteoarthritis on load transfer after a TSA	Healthy scapula Osteoarthritic scapula with 18° retroversion Osteoarthritic scapula with corrected retroversion to 6° Glenoid prosthesis Cement layer

4.2 Finite Element Modelling Process

A FEM of any biological structure requires geometric data acquisition, material property assignment, definition of boundary and loading conditions, and experimental validation. Over the next section, a summary of the techniques most used in the development of a FEM of the shoulder are discussed.

4.2.1 Geometric Data Acquisition

The most popular approach to obtaining geometric data of biological tissues is through medical imaging. To reconstruct bone structures, computed tomography scans (CT-scans) is the technique most used [217, 218], while to reconstruct the tendons and muscles more options are available, such as magnetic resonance imaging (MRI) [219], cryosection photos

[200], and also CT-scans [108, 203]. Even though CT-scans provide better images than MRI, there are small imaging differences between the several soft tissues in CT-scans, being difficult to identify the several ligaments and muscles.

In a few FE shoulder models [200, 210], the 3D geometry of muscles/tendons was reconstructed, although simplified. More recently, Webb *et al.* [220] developed an accurate 3D representation of the deltoideus and rotator cuff muscles, demonstrating the importance of 3D muscle description when studying shoulder movement. Nevertheless, this is computational expensive and requires long simulation times, even to study simple motions.

The majority of FE shoulder models consider force vectors instead of real muscles [79, 211, 221]. Still, some represent the muscles/tendons as a group of line segments [191, 192], using a higher number of segments for muscles with larger attachment sites.

Regarding the cartilage and labrum, their geometric reconstruction is difficult to accomplish using medical imaging, despite some encouraging results [222, 223]. To overcome this reality, several strategies have been used. Gatti *et al.* [204] applied a Boolean operation between two medical images, as follows: a CT-scan of a structure is obtained first; then a component is resected (i.e. the labrum); afterwards, a new CT-scan from the structure is obtained; finally, a Boolean operation is performed with both CT-scans. This allows the reconstruction of the resected component (i.e. the labrum).

Manual reconstruction of soft tissues considering the available anatomical data (e.g. thickness) is also a strategy adopted by some [190, 196]. Others [139, 201, 224] admit that the space between the humeral head and the glenoid cavity (observed in CT-scans) is filled with cartilage and consider that half of the gap distance corresponds to the cartilage thickness of each bone structure.

Glenohumeral ligament geometry has also been obtained via CT-scan for FE modelling [169, 203]. However, ligaments are less frequently added to shoulder models.

4.2.2 Material Property Assignment

Material property assignment of biological structures involves complex mathematical descriptions, which ideally should account for the anisotropy, viscoelasticity and non-homogeneous behaviour of anatomical structures. Nevertheless, the reality is that several simplifications are adopted when describing the material behaviour of shoulder structures.

Generally, the humerus and the scapula are considered as rigid bodies [194, 206], or as homogeneous, linear elastic and isotropic materials [196, 225], having high Young's modulus due to the high stiffness they present. However, with the increasing use of medical images for geometry reconstruction of bone tissue, strategies were developed to take advantage of the information collected in such images.

In CT-scans, an image is displayed in a grayscale (representing CT numbers, also called

Hounsfield values), that correlate with the apparent density of bone [226]. Consequently, in many recent FE models of the shoulder [212, 227, 228], bone density is derived from CT data, therefore considering bone as a non-homogeneous, linear elastic, isotropic structure. Issues related with material-mapping strategy in CT-scans have been object of several studies [225, 229].

Regarding the muscles/tendons, early studies consider them as linear elastic materials [190, 202]. However, this simple representation is not ideal to represent such complex structures, and recently they were modelled as incompressible, hyperelastic, transversely isotropic materials by Webb *et al.* [220]. Other constitutive models have been used, such as the linear elastic orthotropic material model [200], the exponential hyperelastic incompressible law [139, 210] or, more recently, a nonlinear stress-strain curve, accounting only for the passive behaviour of the muscles/tendon [201]. Weiss *et al.* [230] presents a systematic review of constitutive modelling aspects of ligaments.

The majority of the intact shoulder models include geometrical representations of articular cartilage, that has been modelled with Neo-Hookean hyperelastic incompressible properties [194, 196], with isotropic elastic properties [204, 206], with linear elastic properties [190, 201], and also considered as rigid [200], although less frequently. Nevertheless, other models are proposed [231, 232] in an attempt to better describe the tension-compression response and viscous effects of the complex mechanical behaviour of cartilage.

4.2.3 Boundary Conditions

The clear majority of the FE models of the intact and implanted shoulder assume several simplifications, such as the modelling of less bone structures, and consequently of less articulations, or the use of less muscles and tendons. As a result, boundary and loading conditions have to be applied in order to replicate the influence of the missing structures [79, 194, 196, 201]. Moreover, if a FEM tries to replicate an experimental apparatus, the boundary and loading conditions have to be added accordingly [200, 206, 211].

Despite the efforts, the external conditions applied to the problems are not fully capable to describe the real physiologic conditions of the shoulder complex. To try to overcome this, Favre *et al.* [196] suggested a different approach, and developed a 3D numerical model of the shoulder that is characterized by boundary conditions that are progressively eliminated until the humeral head is free to rotate and translate inside the glenoid cavity. The authors developed an "integrated model" of the shoulder that is constituted by three distinct sub-models. In the first sub-model, the muscle path is determined for a certain position of interest [192]; in the second sub-model, knowing the muscle path and muscle length, the muscle forces (which can equilibrate and stabilize the joint) are determined [103, 197];

finally, the forces determined are applied in the third sub-model, to simulate joint contact and humeral head translation [196]. The model developed by Favre *et al.* [195] is a 3D FEM that includes anatomically precise representations of the scapula and of the humerus, including also the humeral and glenoid cartilage and the labrum. The study focuses on active glenohumeral stabilization considering the six DOF of the joint, and the equilibrium conditions are accomplished exclusively via twenty-seven individual muscle segments.

4.2.4 Model Validation

Because of simplifications assumed in the development of any FEM, it is fundamental to validate it against experimental data, so that we can rely on the numerical results obtained. However, in a review made by Burkhart *et al.* [233] on recommendations for bone tissue modelling, 39% of the studies did not present validation data and 42% were not adequately validated, as many present only qualitative assessment of their results, comparing them with reported data available on literature; while only 57% validated their results against own experimental data.

In what concerns the shoulder joint, the majority of the validated FEM correspond to the ones of individual structures, such as the humerus [217], the clavicle [234], the scapula [235, 236] or the labrum [204]. Furthermore, of the models reviewed in this study, some were only compared with literature results [194, 196], others against in vitro studies [206, 211], but the majority was not validated [79, 201].

There are some approaches to validate a FEM against experimental data, such as measuring displacements [204] and strains distributions [169, 235] or by comparing deformed shapes [169]. Anderson *et al.* [237] and Henninger *et al.* [238] present review articles that discuss methods for model verification and validation.

A summary of the geometric data acquisition technique, material properties, boundary conditions and validation procedures of some FEM of the intact and implanted shoulder is presented in Table 4.3.

Table 4.3. Finite element model process of some recent FEM of the intact and implanted shoulder.

Authors	Geometric Acquisition	Material Properties	Boundary Conditions	Validation
Favre *et al.* [196] 2012	Scapula: *in vitro* CT-scan Humerus: literature data	Bone: isotropic linear-elastic Soft tissues: Neo-Hookean hyperelastic incompressible	Muscle forces: estimated from multi-body model; Glenohumeral elevation in scapular plane	Against literature results
Walia *et al.* [194] 2013	Literature data	Bone: rigid Cartilage: Neo-Hookean hyperelastic incompressible	Humerus: fixed in sagittal plane and laterally unconstrained	Against literature results
Inoue *et al.* [201] 2013	*In vivo* CT-scan	Muscle and tendons: non-linear elastic Articular cartilage: linear elastic	Scapula: fixed	Against literature results
Hwang *et al.* [206] 2014	Bones: micro CT-scan Soft tissue: Boolean operations	Bone: rigid Cartilages: isotropic elastic Labrum: transversely isotropic Neo-Hookean hyperelastic incompressible LHBT: transversely isotropic hyperelastic	Humerus: in 30°abduction in scapular plane, neutral rotation; humeral translation	Against in vitro results
Suárez *et al.* 2012 [211]	Implant and bone substitute: modelled	Bone substitute: homogeneous, linear, isotropic	Metal back/bone: perfectly bonded Humeral head/PE inlay: Coulomb friction, μ=0.05 Implant/bone substitute: Coulomb friction, μ=0.6	Against in vitro results
Zhang *et al.* [79] 2013	Bones: *in vivo* CT-scan Implant component: digitizing	Scapula, cement and humeral head component: isotropic linear elastic Glenoid implant: viscoelastic-plastic Humeral component: rigid	Cement/implant and cement/bone: perfectly bonded Glenoid/humeral implants: Coulomb friction, μ=0.07	No
Patel *et al.* [208] 2014	Scapula: *in vitro* CT-scan	Scapula: isotropic linear elastic	Scapula: fixed at medial border and acromion; Bone/cement, cement/implant, bone/metal: fully bonded	No
Patel *et al.* [216] 2015	Scapula: *in vitro* CT-scan	Scapula: isotropic linear elastic	Scapula: fixed at medial border and acromion; Bone/cement, cement/implant, bone/metal: fully bonded	No

4.3 Building the Intact and Implanted FE Shoulder Models

4.3.1 Geometric Data Acquisition

The developed FEM of the intact and implanted shoulder uses fourth generation composite structures, namely a left humerus and scapula, from Sawbones®.

The composite humerus was scanned with a Roland PicZa 3D Laser Scanner (resolution (1.4 × 1.4) mm). The external surface acquired was adapted with CATIA© (V5.21©Dassault Systèmes) [170]. Subsequently, the model of the humeral external geometry was obtained and a volume generated. The cortical thickness of the proximal and distal humerus has around 6 mm [239], while the cortical thickness of the humeral head has nearly 1.3 mm [171]. The cortical bone structure was subtracted to the original body, to create the trabecular bone volume.

For the humeral cartilage (present only in the intact model), a constant thickness of 0.95 mm was assumed, being in accordance with literature [171] and with the average observed in different CT scans. Figure 4.1 presents the composite model of the humerus and the CAD models developed, as external and internal geometries.

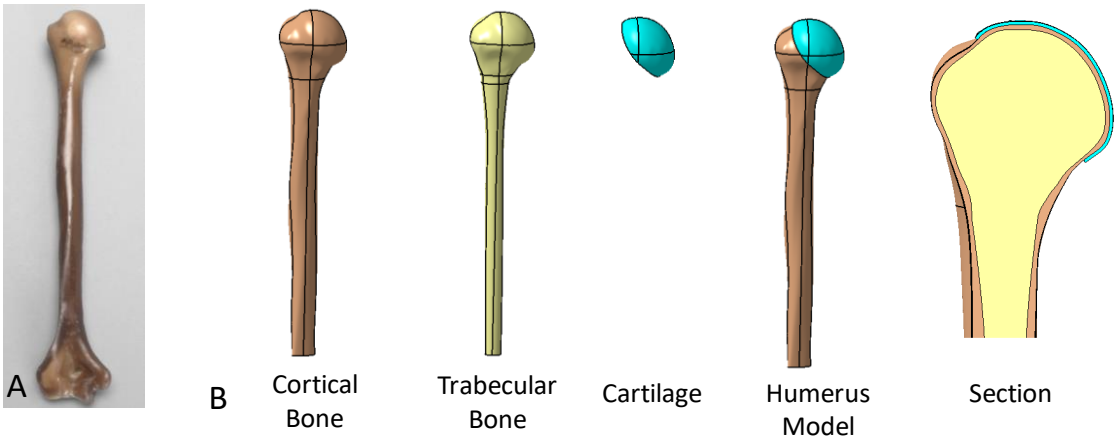

Figure 4.1. A: Fourth generation composite left humerus from Sawbones®. B: CAD model developed.

The composite bone model of the scapula was scanned with a ZScanner 700 (Zcorporation), and the external surface acquired was adapted with CATIA© [170]. Subsequently, the model of the scapular external geometry was obtained and a volume generated. The glenoid cavity was modelled with a cortical thickness of 1 mm, in average. The trabecular bone volume was assumed to exist in the glenoid cavity, coracoid process, acromion and axillary border.

Concerning the glenoid cartilage (present only in the intact model), a constant thickness of 0.95 mm was assumed, being in accordance with literature [171], and typically observed

in different CT scans. Figure 4.2 shows the composite model of the scapula and the CAD models developed. The inferior glenohumeral ligament (IGHL) was designed to replicate the elastic used in the experimental model, thus having a thickness of 1.2 mm, in average. It is only present in the intact shoulder model. The CAD model of the intact shoulder is presented in Figure 4.3.

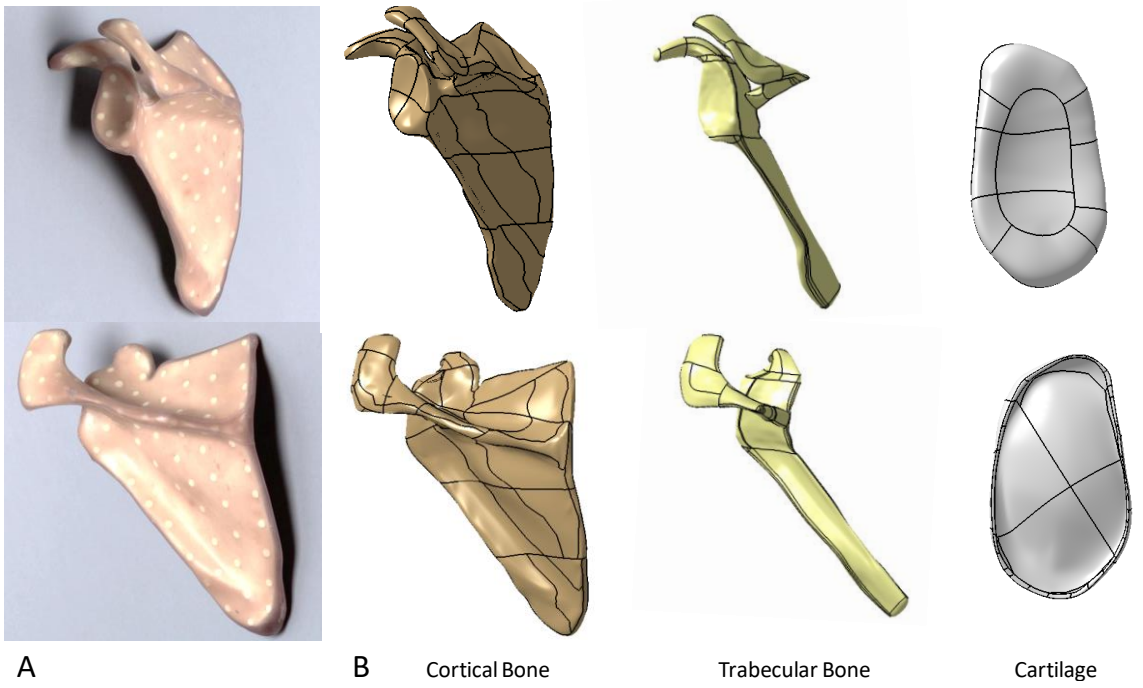

Figure 4.2. A: Fourth generation composite left scapula from Sawbones®. B: CAD model developed.

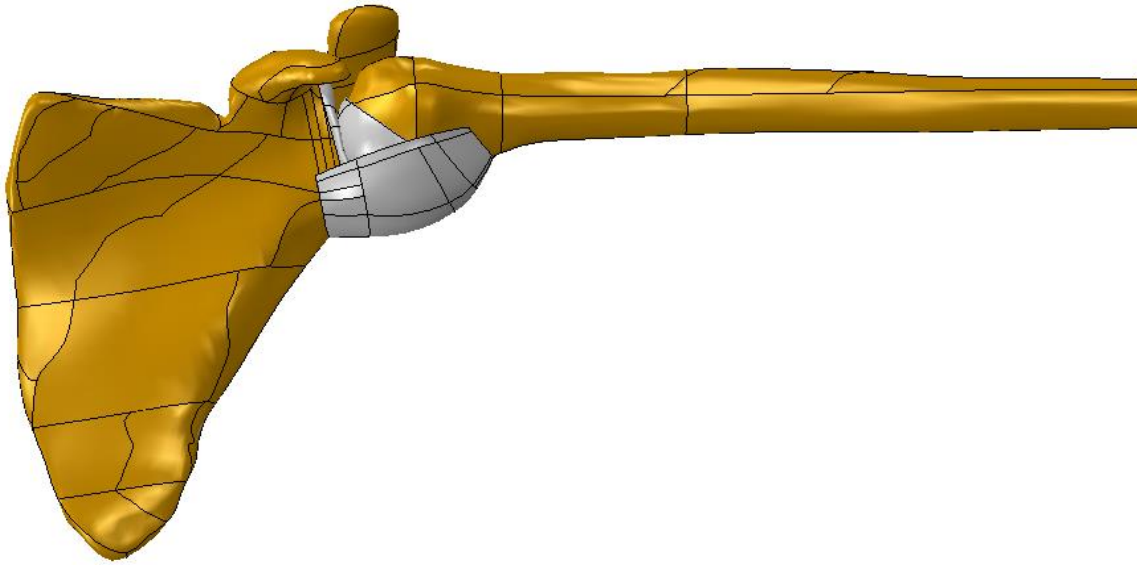

Figure 4.3. CAD model of the intact shoulder developed in this thesis.

The shoulder model was implanted with a Comprehensive® Total Shoulder System, from Biomet®, comprising a humeral implant and a glenoid implant.

The humeral implant has three components: the stem, the head and the taper adaptor. The humeral stem serves to fix the humeral implant to the humeral bone, as it is introduced into the central canal of the humerus; the humeral head is the top of the implant, and substitutes the head of the humeral bone; the humeral head taper adaptor serves to connect the stem to the head of the implant. The stem is made of titanium, having a layer of porous titanium (Regenerex® Porous Titanium) in its superior region, intended to provide a higher biologic fixation between implant and bone. The implant head is made of CoCrMo alloy, and the humeral head taper adaptor of Ti6Al4V alloy. The stem used is a mini size, measuring (8 × 83) mm; and the humeral head has a size of (46 × 24 × 47) mm. The humeral head taper adaptor has a diameter of 22.5 mm and a thickness of 7.7 mm. Figure 4.4 shows all components, as well as the CAD models developed. For FEM simplification, the humeral head taper adaptor and the humeral head were modelled together; and the humeral stem and the humeral head were then considered as a single body, with titanium material properties.

Figure 4.4. Humeral components of the Comprehensive® Shoulder System, BIOMET® and the corresponding CAD models. A: Mini Length Humeral Stem; B: Versa-DialTM Humeral Head; C: Humeral Head Taper Adaptor;

The glenoid implant has two components: the base and the central peg. The glenoid base has a curved back, with an anatomic pear shape, and it substitutes the cartilage and labrum and has three periphery pegs for fixation and a central hole; the central peg serves for implant fixation and is fixed to the central hole of the base. The glenoid base in made of Ultra-High Molecular Weight Polyethylene (UHMWPE), and its hole is metallic; the central peg is made of titanium, with a layer of Regenerex® Porous Titanium. The glenoid base has 37 mm long and a thickness of 4 mm at the centre. Figure 4.5 shows the components of the glenoid implant, as well as the CAD models developed. For FEM simplification, the glenoid base was considered all-UHMWPE and its posterior region was smoothed.

The whole CAD model of the Comprehensive® Shoulder System is in Figure 4.6.

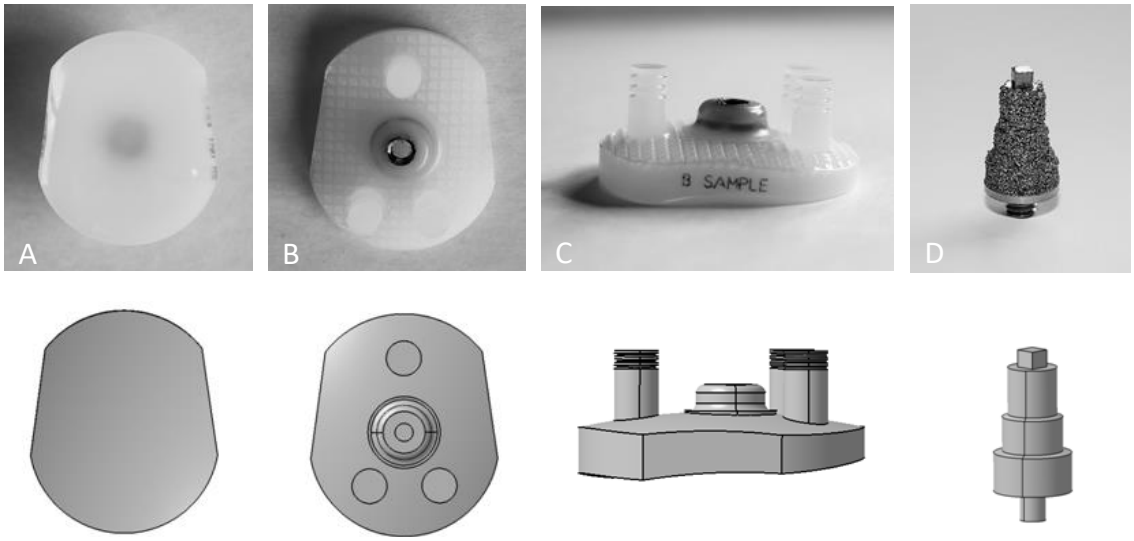

Figure 4.5. Glenoid components of the Comprehensive® Shoulder System, BIOMET® and the corresponding CAD models. A, B, C: Modular Hybrid® Glenoid Base; D: Regenerex® Modular Hybrid Glenoid Central Peg.

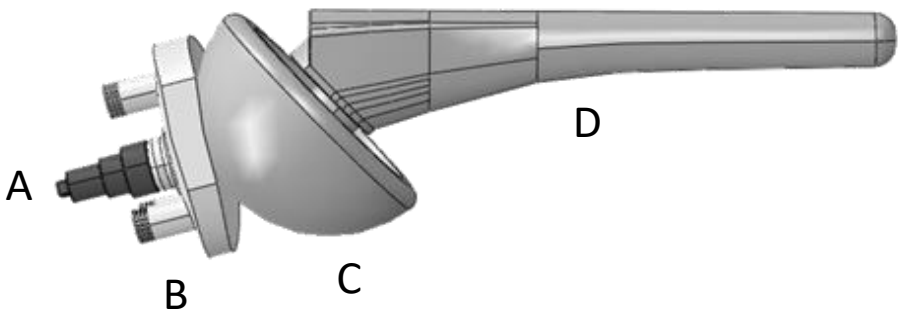

Figure 4.6. CAD of the Comprehensive® Shoulder System, BIOMET®. A: Regenerex® Modular Hybrid Glenoid Central Peg; B: Modular Hybrid® Glenoid Base; C: Versa-Dial™ Humeral Head; D: Humeral Stem.

The virtual arthroplasty was performed following the press-fit surgical technique, as in the experimental arthroplasty. As Figure 4.7 suggests, the virtual arthroplasty accurately represents the real scenario experimentally observed. We developed the CAD models and the virtual arthroplasty with CATIA© (V5.21©Dassault Systèmes).

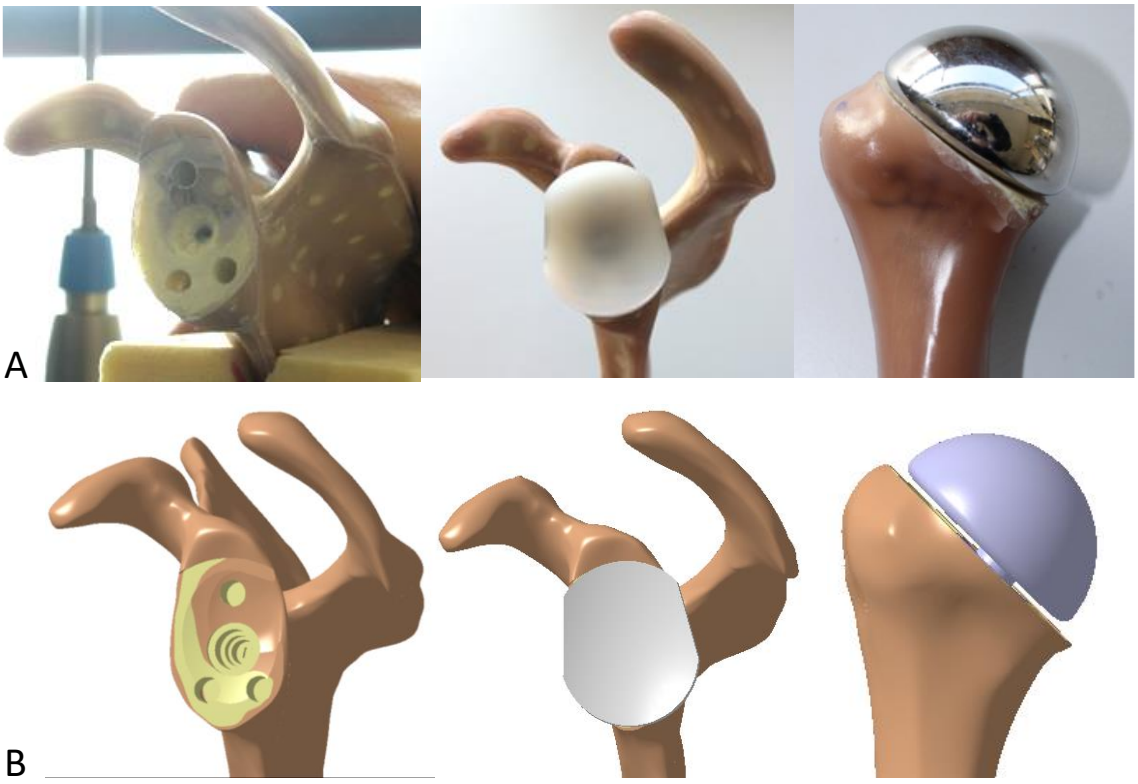

Figure 4.7. Total shoulder arthroplasty performed experimentally (A) and virtually (B).

4.3.2 Material Property Assignment

All components of the intact and implanted shoulder models were considered with isotropic linear elastic behaviour, similarly to other studies [196, 240]. Table 4.4 presents the material properties applied, which are similar with those used in the *in vitro* shoulder models (see Chapter 3), so that the FEMs can be further validated against the experiments. The composite bones properties were defined according with Sawbones® [165].

Table 4.4. Material properties used in the FEM of the intact and implanted shoulder model.

Structure	Young Modulus	Poisson ratio
Composite cortical bone	16.7 GPa	0.3
Composite trabecular bone	0.155 GPa	0.3
Silicone (cartilage)	625 MPa	0.08
Elastomer (IGHL)	3 MPa	0.09
Titanium (humeral component and glenoid post)	110 GPa	0.3
Polyethylene (glenoid component)	1 GPa	0.4

4.3.3 Boundary Conditions

To reproduce the in vitro shoulder models previously developed (see Chapter 3), the CAD models were positioned according with the experimental apparatus. The scapula was fixed in the inferior angle and in the superior margin; while a point of the humeral base was fixed to simulate the influence of the external load.

In both FEMs developed, the cortical bone and trabecular bone of the humerus were bonded together permanently; the same was done with the scapula.

In the intact model, the cortical humerus and the humeral cartilage were bonded together permanently; the same was done with the scapula. The IGHL extremities were bonded permanently to the cortical bone of the humerus and of the scapula. A Coulomb contact condition, with a friction coefficient $\mu = 0.2$ between the two cartilage structures (made of silicone in the in vitro model), was assumed. The same was considered for the contact condition between the IGHL and the humeral and scapular cartilage (in case they interact). The small-sliding formulation was adopted, as there was little sliding between the silicone structures on the in vitro model. As indicated in Chapter 3, the elasticity modulus of the elastomer (simulating the IGHL) equals approximately 3.5 MPa, and it suffered an elongation of 16.7 mm. Thus, in the FEM developed, we added a pre-tension of 1.5 MPa to the IGHL.

In the implanted model, the prosthesis components were bonded together permanently to their adjacent bone. A Coulomb contact condition, with a friction coefficient of $\mu = 0.1$ [228] between the humeral head component and the glenoid component was assumed, and the small-sliding formulation was adopted. Abaqus CAE (V6.12©Dassault Systèmes) was the solver used. Figure 4.8 and Figure 4.9 highlight the boundary conditions and the muscles lines of action of the intact and implanted models developed, respectively.

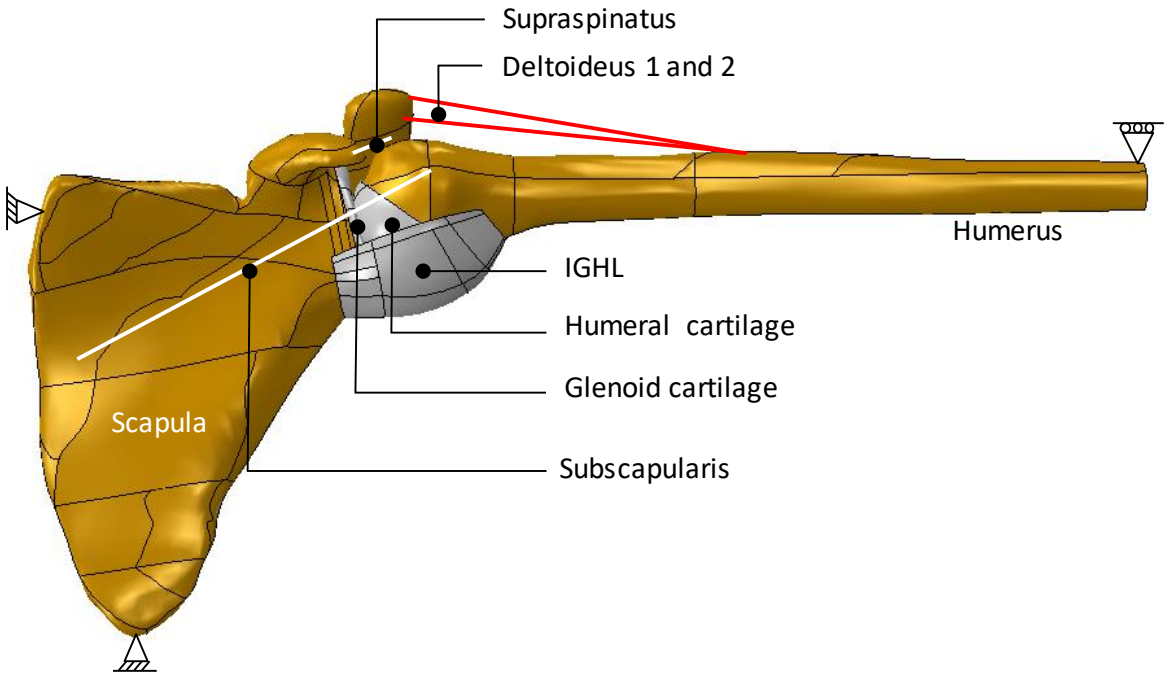

Figure 4.8. Intact shoulder model developed, in 90° abduction.

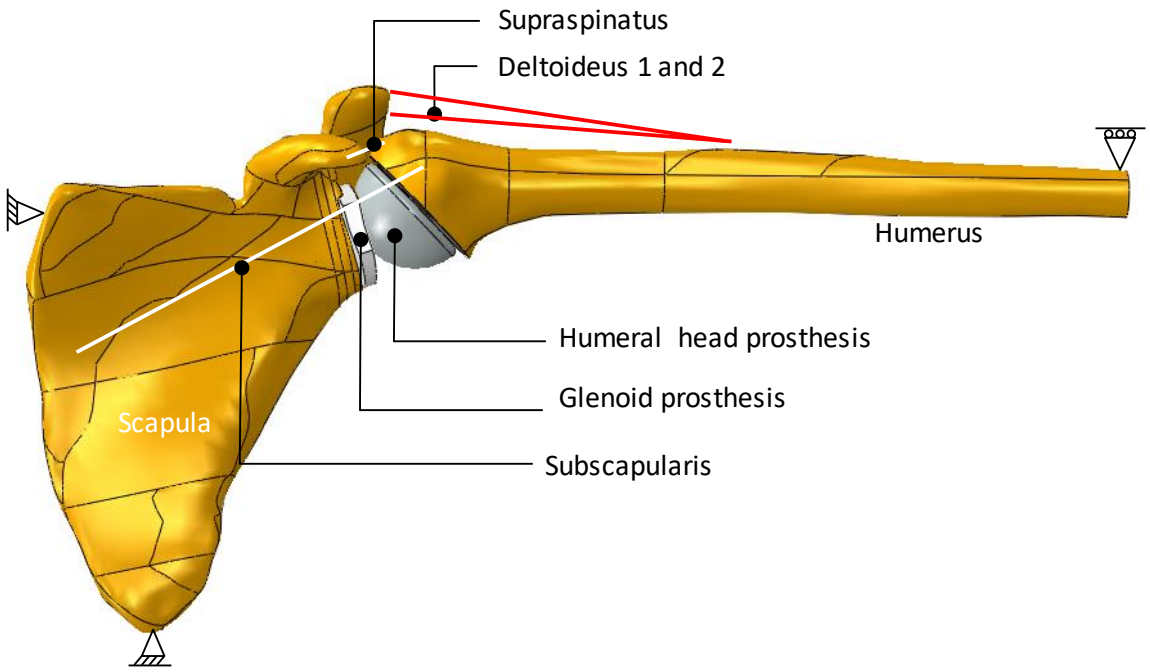

Figure 4.9. Implanted shoulder model developed, in 90° abduction.

4.4 Finite Element Mesh

4.4.1 Mesh Sensitivity Analysis[1]

Regardless of the growing number of FEM applied on the study of shoulder biomechanics [196, 206, 217, 240, 241] or shoulder prosthesis [179, 213, 242, 243], Burkhart *et al.* [233] claim, in a recent review article, that there is a clear lack of studies concerning mesh quality, energy balance and validation methods in this field of studies. The importance of the element type in FEM was analysed previously and presented the importance of this factor in the results [233, 244]. Another important point of the FEM, in the last forty decades of analysis in biomechanics, is the validation of models [245], and the importance of the models accuracy to represent the real world variability. Since FEM of human features must be as accurate as possible, it is important to give attention to mesh sensitivity analysis, when the validation of models is difficult, or impossible. Another important factor in FEM simulation is the boundary conditions to represent the real scenario, and thus the most critical situation should be considered.

In this sense, we used the CAD models of the fourth-generation composite left humerus from Sawbones® and its cartilage, to construct a preliminary FEM with the goal of performing a mesh sensitivity analysis.

The bone and cartilage structures were considered isotropic linear elastic. For trabecular bone model, the relationship between Young's modulus and bone density was established [217]. For the humeral head, bone density was the mean value of trabecular body mass density [246]. Humeral cartilage and glenoid cartilage densities equal the value used by Gatii *et al.* [204], on the development and validation of a FEM of the superior glenoid labrum. Table 4.5 presents all material properties used.

Table 4.5. Material properties used in the mesh convergence analysis.

Structure	Young Modulus	Poisson ratio
Cortical bone	16.5 GPa	0.3
Trabecular bone	124 MPa	0.3
Cartilage	66 MPa	0.08

[1] Based on: Bola, Ana M., Ramos, A. and Simões, J. A, "Sensitivity analysis for finite element modeling of humeral bone and cartilage", Biomaterials and Biomechanics in Bioengineering, Vol. 3, No. 2 (2016) 071-084

We note that the material properties indicated in Table 4.5 differ from those in Table 4.4 because the mesh sensitivity analysis was performed in an early stage of the study, and material properties available in literature were used. However, the FEM built for model validation considers the same material properties as the ones of Sawbones®.

FE meshes of cortical and trabecular bones and of cartilage were developed and analysed independently from each other. In all meshes, the maximum gap between mesh and geometry was made equal to 0.5 mm.

Eighteen models for each structure were constructed with different mesh densities. Tetrahedral linear elements, also used by others [217], having three degrees of freedom per node, were chosen, since they can be used under frictionless conditions [247], as in the present case. Ramos and Simões [244], on their study with a realistic model of a proximal femur, did not observe substantial differences between simulations obtained with first and second order tetrahedral and hexahedral elements. However, they verified that hexahedral quadratic elements appeared to be more stable and less influenced by mesh refinement.

To evaluate the created meshes, the average aspect ratio (AAR), and corresponding standard deviations (SD) were accessed. The criteria adopted to establish the degree of acceptance of the meshes considers that the percentage of elements with aspect ratio greater than 3 should remain below 5% [233].

The FEM of both bones were fixed distally, and the cartilage fixed laterally. For each mesh, compression tests were carried out simulating the application of a GH-JRF during 90° arm abduction with external load. GH-JRF was applied in a node at the top of the models and the results were analysed at two nodes in each model (see Figure 4.10). The appropriate mesh sizes for each structure were then identified. A scheme of the mesh selection process is presented in our published article on this topic.

It is important to assess the results in two different regions because bones are not regular structures, thus, one should evaluate if different regions of a bone can be represented by the same mesh size.

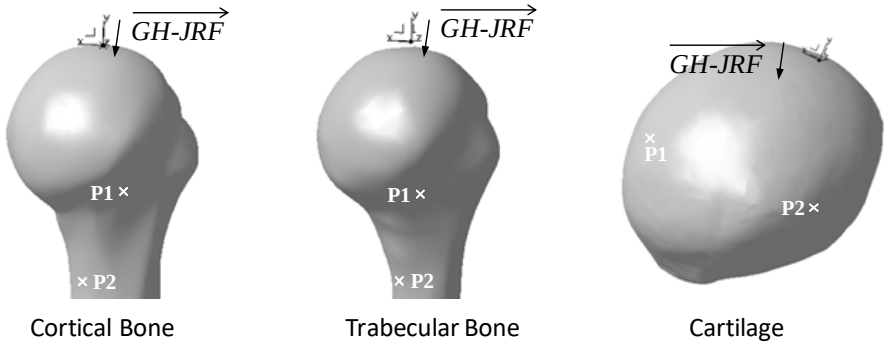

Figure 4.10. Location of the GH-JRF and of the points analysed.

GH-JRF was determined with the multi-body model of the intact shoulder in Chapter 2. It was concluded that with 2 kgf it is necessary more synergism between muscles to perform movement and results were unsatisfactory when compared with literature [132]. Thus, an external load of 1 kgf was considered and the corresponding GH-JRF determined ((472, -1250) N, Cartesian coordinated system). GH-JRF is of the order of magnitude of reaction forces determined by Bergmann *et al.* [132] and Nikooyan *et al.* [102] in their experiments with an instrumented prosthesis, in forward flexion and abduction, for patients holding an external load of 2 kgf and suffering from osteoarthritis. It is important to note that anthropometry differences and shoulder osteoarthritis influence forces measured [132, 248].

The AAR of al meshes are within the interval classified as good ($1 \leq AR \leq 2.5$), with cartilage meshes presenting higher AARs. All cortical and trabecular bone meshes have a percentage of bad elements smaller than 5%. The same was not observed with the humeral cartilage, since models with a mesh size of 2.5 mm and 3 mm presented a percentage of bad elements of 7.7% and 14.6%, respectively, whereby these were not considered in the mesh refinement analysis.

Displacement results of cortical and trabecular bones are represented in the graphs A and B of Figure 4.11, and for the humeral cartilage in the graph of Figure 4.12. For both bones, the displacement at points P1 and P2 presents similar behaviour. This means, on the one hand, that different regions of the same bone can be represented by the same mesh size. On the other hand, different bone types are represented by different size meshes. Regarding cartilage, the displacement behaviour is similar with that observed for cortical and trabecular bone (see Figure 4.12).

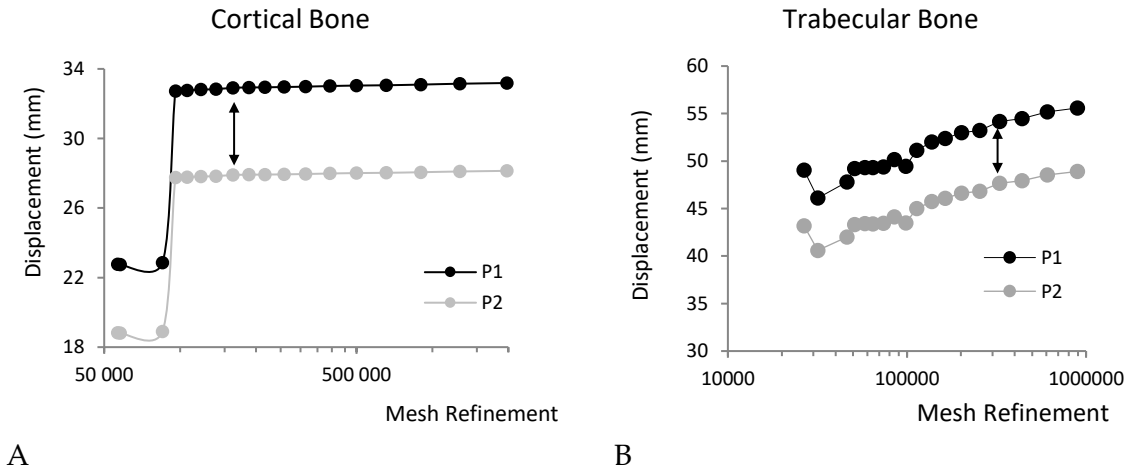

A B

Figure 4.11. Displacement versus mesh refinement, for cortical bone (A) and trabecular bone (B).

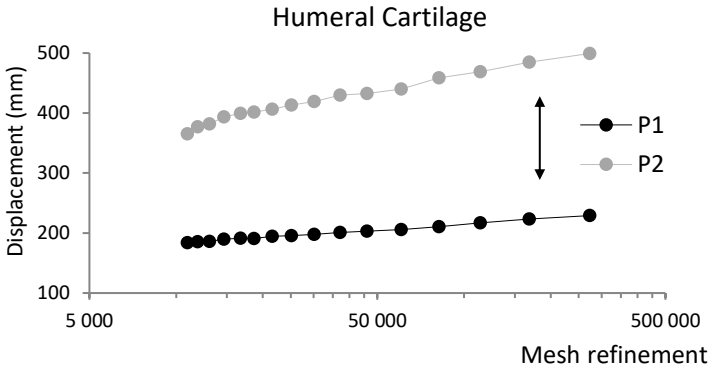

Figure 4.12. Displacement versus mesh refinement, for humeral cartilage.

Thus, mesh sizes of 1.5 mm, 0.8 mm and 0.6 mm have good quality to represent the biomechanical behaviour of cortical bone, trabecular bone and cartilage, respectively, as they present small AARs.

4.4.2 Intact Model

The mesh sizes were determined in the sensitivity analysis performed earlier. Still, for smaller computational times, a maximum element size of 3 mm was assumed far from the joint. The intact shoulder model was built with linear tetrahedral elements of type C3D4 (4 nodes, 3 degrees of freedom per node). It has a total of (142 615) nodes and (641 019) elements, making a total of (427 845) degrees of freedom. To evaluate the produced meshes, the AAR of each mesh was accessed. As before, the criteria assumed to establish the degree of acceptance of the meshes deliberates that the percentage of elements with aspect ratio (AR) higher than 3 should remain below 5% [233]. Table 4.6 gathers the features of the meshes developed.

Table 4.6. FE mesh features of the intact shoulder model.

Structure	Elements	Nodes	NDOF	AAR	AR > 3 (%)
Humeral cortical bone	53 344	14 891	44 673	1.66	0.55
Humeral trabecular bone	325 310	61 709	185 127	1.59	0.01
Scapular cortical bone	92 393	25 219	75 657	1.80	2.79
Scapular trabecular bone	101 332	20 783	62 349	1.63	0.43
Humeral cartilage	42 723	12 518	37 554	1.65	0.30
Glenoid cartilage	17 795	4 931	14 793	2.02	7.10
Ligament	8 122	2 564	7 692	1.78	0.79

Overall, the structures developed have small AAR. The smallest corresponds to the humeral trabecular bone mesh (1.59) and the highest to the glenoid cartilage mesh (2.02). This mesh has nearly 7% of its elements with an AR greater than 3 and, according with the criteria adopted, a new mesh with different mesh density should have been developed. However, the poor elements with such higher aspect ratio are mainly located at the periphery of the structure, having small influence on the global results. For this reason, the mesh was used. The FE meshes developed for each structure are presented in Figure 4.13 and the region of interest of the intact shoulder model is represented in Figure 4.14.

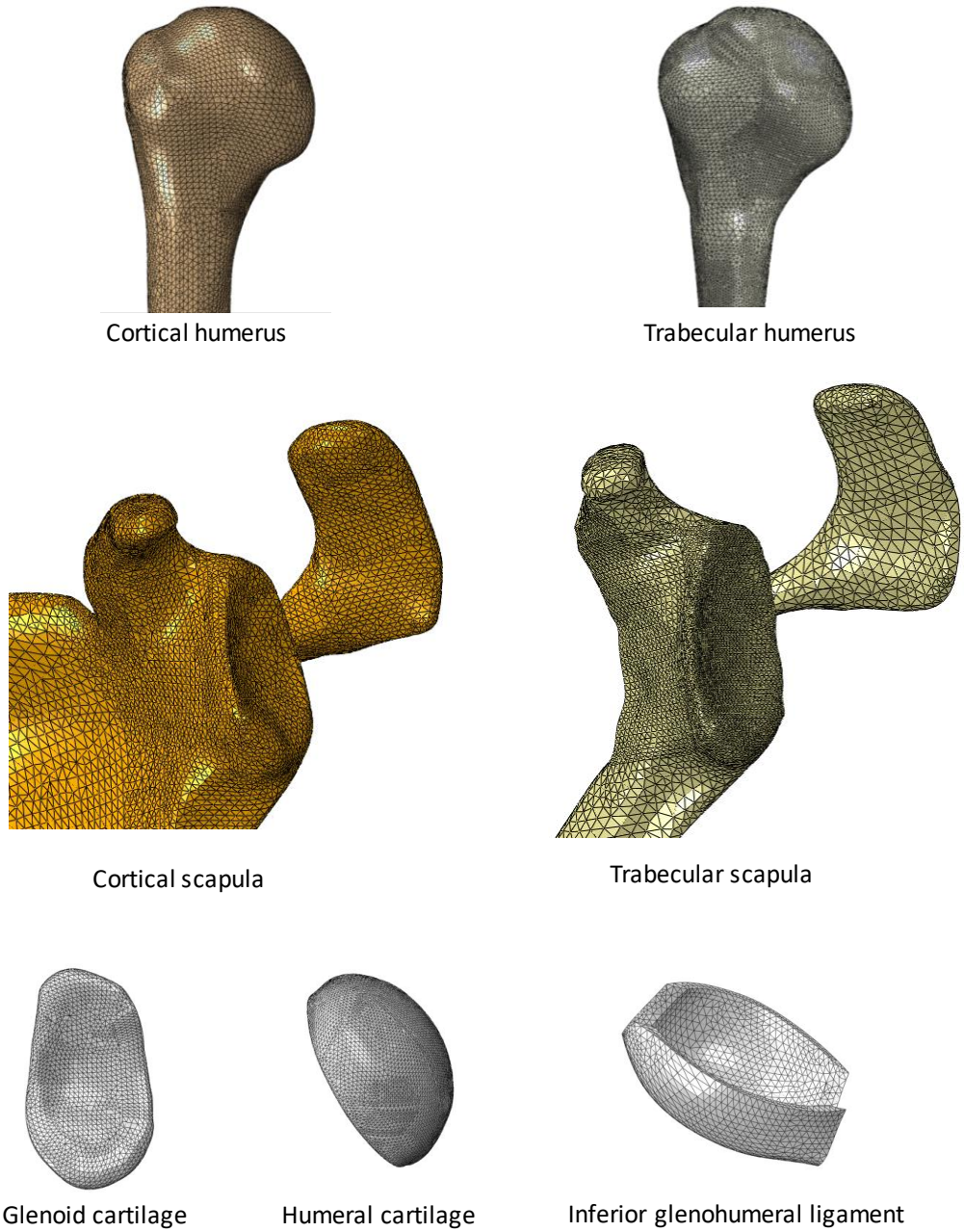

Figure 4.13. FE meshes of the several structures of the intact shoulder model.

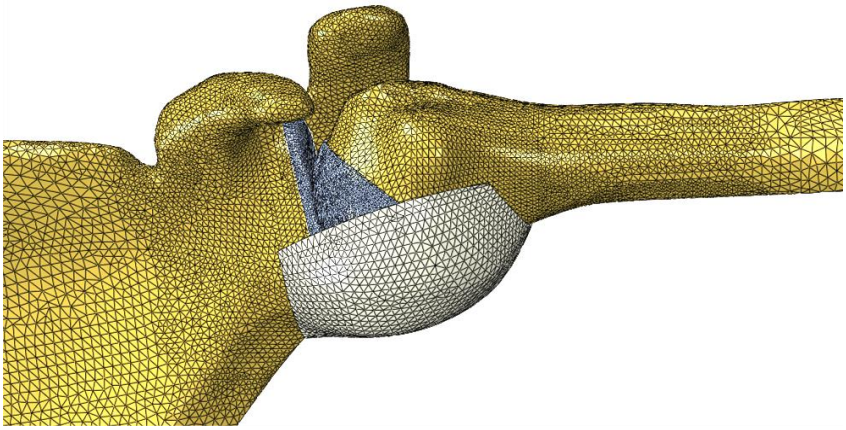

Figure 4.14. FE meshes of the intact shoulder model.

4.4.3 Implanted Model

As with the intact shoulder model, the mesh sizes are equal to those determined in the mesh sensitivity analysis performed, and 3 mm size was considered far from the joint. The implanted shoulder model was also built with linear tetrahedral elements of type C3D4, with (168 856) nodes and (796 871) elements, making a total of (506 568) degrees of freedom.

The meshes were evaluated via the AAR, presented in Table 4.7, and overall have small AAR. The smallest corresponds to the humeral trabecular bone (1.64), and the highest to the humeral cortical bone (1.85). The smallest percentage of elements with AAR higher than 3 correspond to the humeral trabecular bone (0.81) and the highest to the humeral cortical bone (4.03%). Figure 4.15 presents the FE meshes developed for each structure, and Figure 4.16 presents the region of interest of the implanted shoulder model.

Table 4.7. FE mesh features of the implanted shoulder model developed in this study.

Structure	Elements	Nodes	NDOF	AAR	AR > 3 (%)
Humeral cortical bone	39 550	11 167	33 501	1.85	4.03
Humeral trabecular bone	230 003	44 868	134 604	1.64	0.81
Scapular cortical bone	100 755	26 738	80 214	1.77	2.11
Scapular trabecular bone	225 779	44 383	133 149	1.67	1.52
Glenoid Central Peg	39 594	8 093	24 279	1.71	3.92
Glenoid PE component	78 962	16 558	49 674	1.72	1.69
Humeral component (head + stem)	69 926	14 160	42 480	1.71	1.18

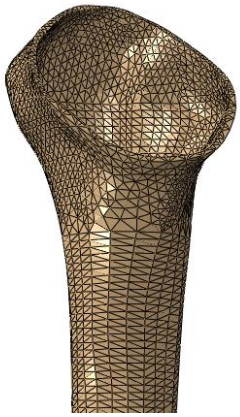

Cortical humerus

Trabecular humerus

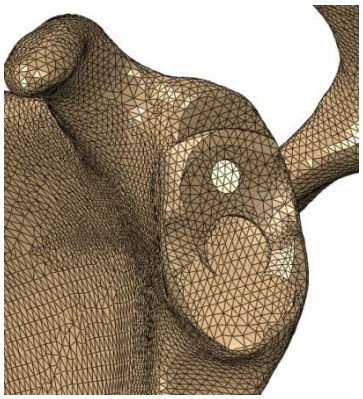

Cortical scapula

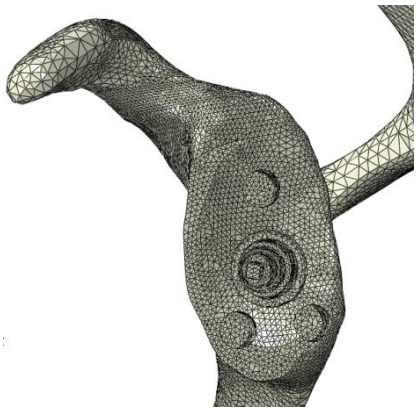

Trabecular scapula

Humeral implant

Central Peg

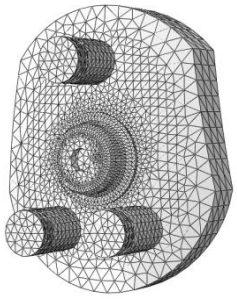

Glenoid Base

Figure 4.15. FE meshes of the several structures of the implanted shoulder model.

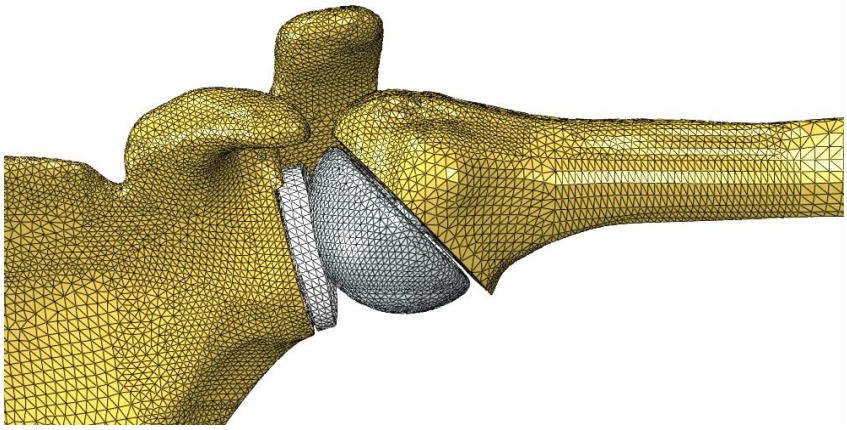

Figure 4.16. FE mesh of the implanted shoulder model.

4.5 FEM Validation

4.5.1 Validation of the Intact Model

The anterior, posterior, and superior views of the experimental and numerical models of the intact shoulder are represented in Figure 4.17. The pictures help to compare the positions of both models. Despite some minor geometrical differences between the composite scapula and the CAD model, the numerical model is a proper representation of the experimental model. We considered that the bone structures and soft tissues were appropriately positioned to mimic a 90° abduction of the joint.

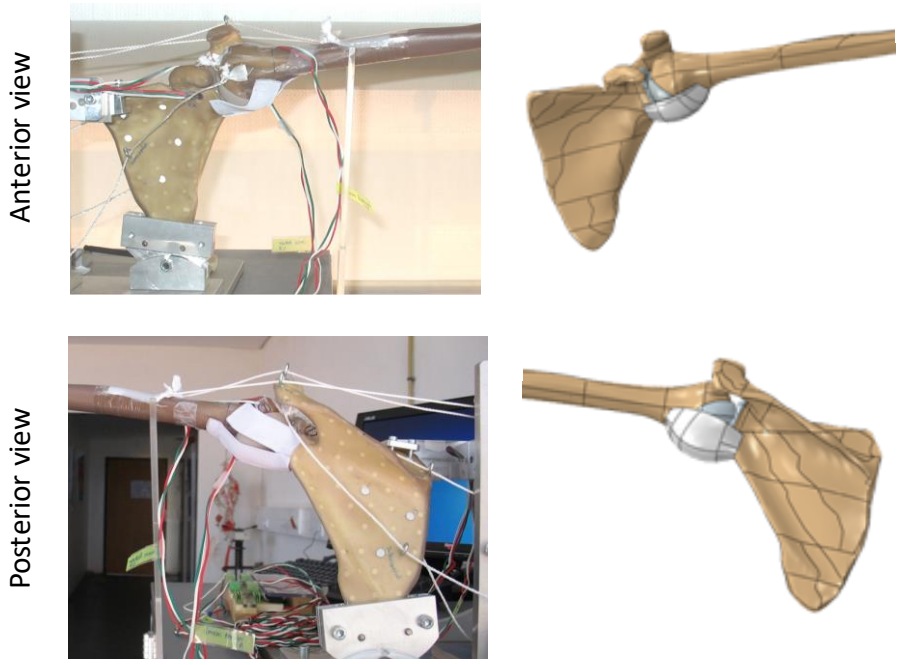

Figure 4.17. Comparison between the experimental and numerical models of the intact shoulder.

With the FEM constructed, it is mandatory to evaluate the quality of its numerical predictions. Therefore, the mean muscular forces applied in the experimental model (see Table 4.8) were applied in the numerical model. The principal strains obtained with the two models were compared. The numerical predictions were evaluated at nearly the same location as the experimental ones.

Table 4.8. Muscle actions applied experimentally in the intact model.

Muscle	Deltoideus 1	Deltoideus 2	Subscapularis	Infraspinatus	Supraspinatus
Mean Force (N)	110.92	112.54	168.14	88.90	67.08
Standard Deviation	0.76	1.39	0.97	0.43	0.10

4.5.2 Validation of the Implanted Model

The anterior, posterior and superior views of the experimental and numerical models of the implanted shoulder are represented in Figure 4.18. The pictures help to relate the positions of both models. It is fair to say that the developed numerical model of the implanted shoulder is an accurate representation of the developed experimental model, and it was correctly positioned to mimic the 90° abduction simulated.

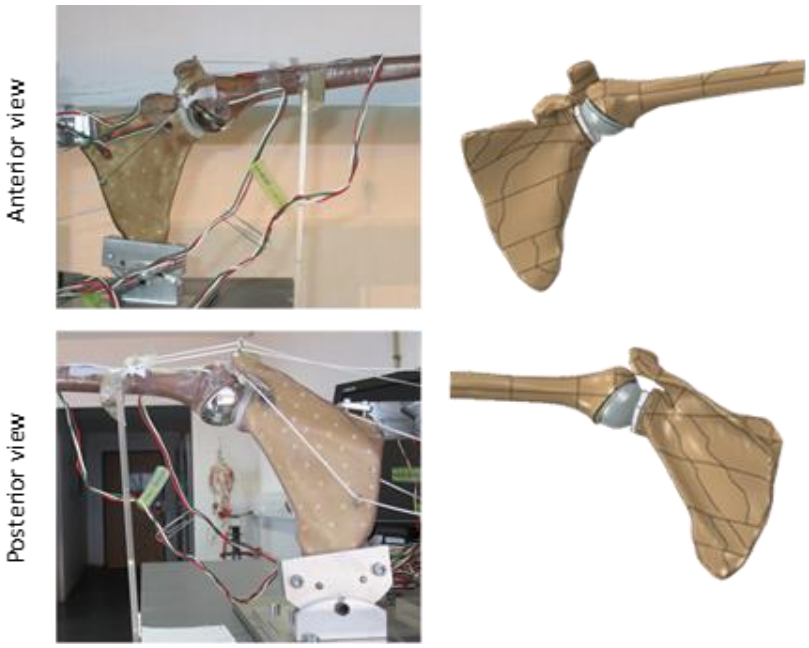

Figure 4.18. Comparison between the experimental and numerical models of the implanted shoulder.

After constructing the FE model of the implanted shoulder, it is necessary to evaluate the quality of the numerical predictions to establish the degree of confidence of the model developed. Therefore, the mean muscular forces used in the experimental model of the implanted shoulder were used in the FEM developed (see Table 4.9), and the principal strains obtained with the two models were compared. The numerical predictions were evaluated at nearly the same location as the experimental ones.

Table 4.9. Muscle actions applied experimentally in the implanted model.

Muscle	Deltoideus 1	Deltoideus 2	Subscapularis	Infraspinatus	Supraspinatus
Mean Force (N)	110.41	111.35	166.74	88.80	68.86
Standard Deviation	1.46	1.99	1.84	2.00	2.50

4.6 Results

The maximum and minimum principal strains at the intact shoulder, experimentally measured and numerically predicted, are represented in the graph of Figure 4.19.

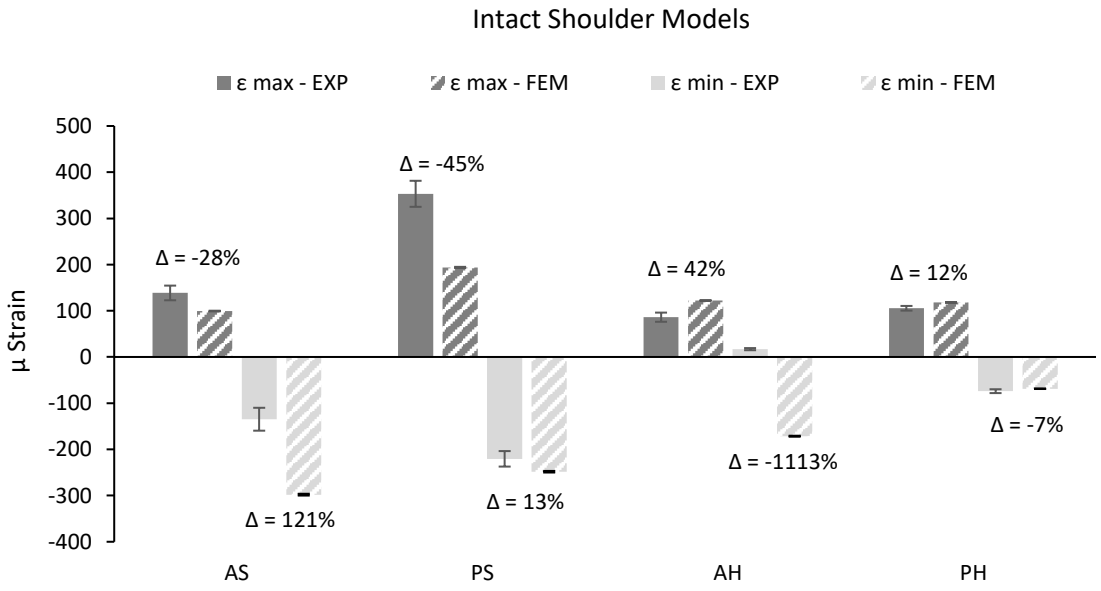

Figure 4.19. Comparison between principal strains at the experimental and numerical models of the intact shoulder. AS/PS: Anterior/Posterior Scapula; AH/PH: Anterior/Posterior Humerus.

Generally, the FE model developed underestimates the maximum principal strains at the glenoid side, and overestimates at the humeral side. The smallest differences between the measured and calculated results are found at the anterior glenoid (rosette AS) and at the posterior humerus (rosette PH), with differences of 28% and 12%, respectively. The posterior glenoid region (rosette PS) and the anterior humeral region (rosette AH) have differences of 45% and 42%, correspondingly.

Regarding the minimum principal strains, the numerical model overestimates the strains at the scapula and at the anterior humerus, being underestimating at the posterior humerus. The minimum differences are at the posterior glenoid and at the posterior humerus, with differences of 13% and 7%, respectively. The highest predictions are at the anterior glenoid (121%) and at the anterior humerus (1113%).

It is important to notice that the minimum principal strain predicted by rosette AH is a negative value, while the one measured in the experimental model is positive, despite of very small. This may indicate some difference in the positioning of the humerus in the FEM.

To evaluate the correspondence between the measured and the calculated results, a linear regression analysis was performed (without rosette AH, due to the different signal between the experimental and the numerical minimum principal strain values), and is presented in the graph of Figure 4.20. The regression slope and the correlation coefficient R^2 were equal to (0.956) and to (0.860), respectively, indicating a good agreement between the experimental and the FE strains. The intercept equals (60.5), and it is due to the considerable difference observed between the measured and predicted strain results in the scapular side.

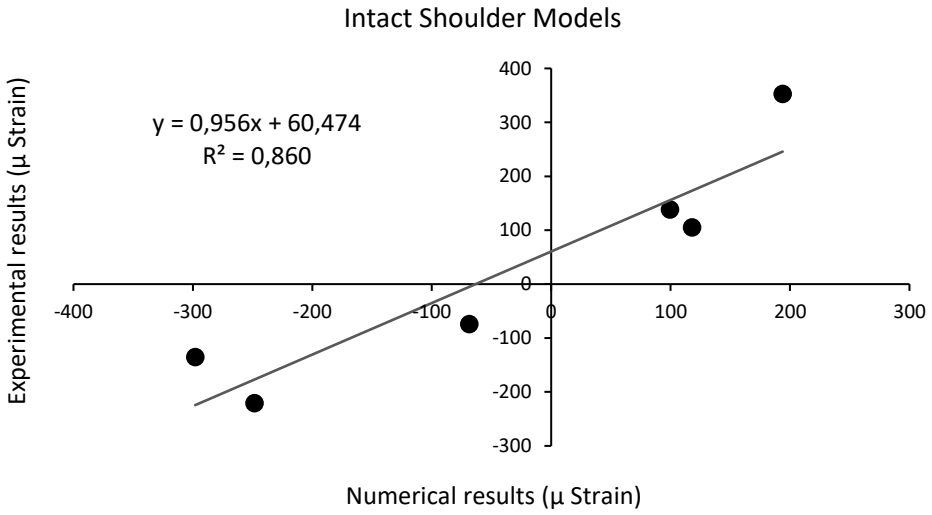

Figure 4.20. Linear regression analysis of the experimental and numerical results.

The maximum and minimum principal strains at the implanted model, experimentally measured and numerically predicted, are represented in the graph of Figure 4.21.

Generally, the numerical model overestimates the maximum principal strains in the whole model, except in the posterior humerus (rosette PH), where a 32% decrease in strain is observed. The highest difference was registered at the posterior humerus (+ 57%), and the smallest at the anterior humerus (+ 4%).

Regarding the minimum principal strains, the FE model is also overestimating the results in all regions. The highest prediction was observed at the posterior glenoid region (738%), and the smallest at the posterior humerus (11%). We notice that at the anterior glenoid region (rosette AS), the minimum principal strains measured and predicted have different signals, meaning that in the numerical model the scapula is suffering high compressions where it should be suffering a small traction. This may indicate a difference in the positioning of the numerical model relative to the experimental. This was only observed in this rosette.

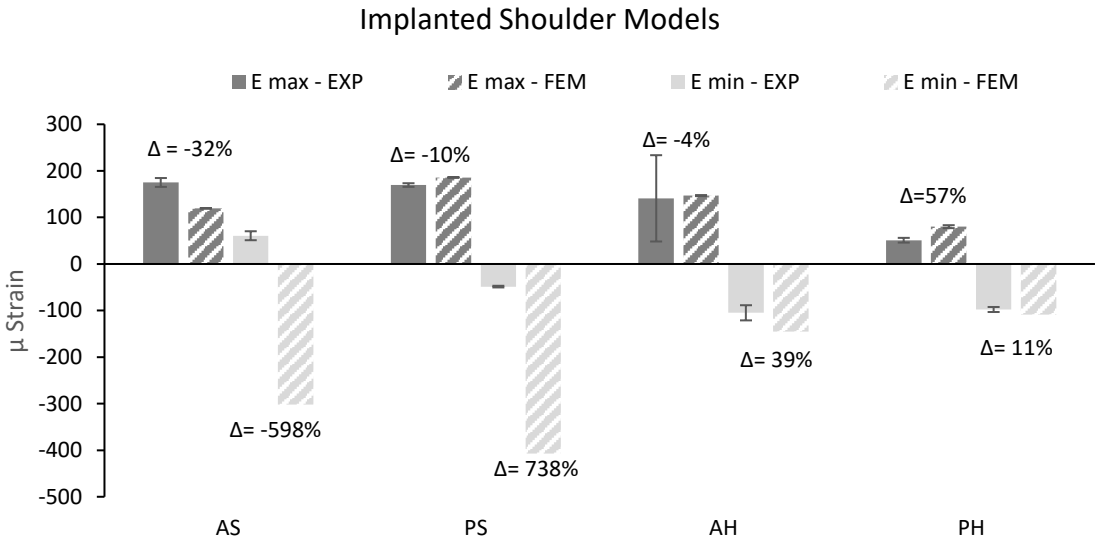

Figure 4.21. Comparison between principal strains at the experimental and numerical models of the implanted shoulder. AS/PS: Anterior/Posterior Scapula; AH/PH: Anterior/Posterior Humerus.

To evaluate the correspondence between the measured and the predicted results, a linear regression analysis was performed, as is represented in the graph of Figure 4.22. Due to the different signal between the experimental and the numerical minimum principal strain values of rosette AS, this rosette was not considered. In addition, since there is a 738% increase in the minimum principal strains predicted by the model in rosette PS, this result was not considered in the linear regression analysis.

The regression slope and the correlation coefficient R^2 were equal to (0.852) and to (0.986) respectively, indicating an acceptable agreement between the experimental and the FE strains.

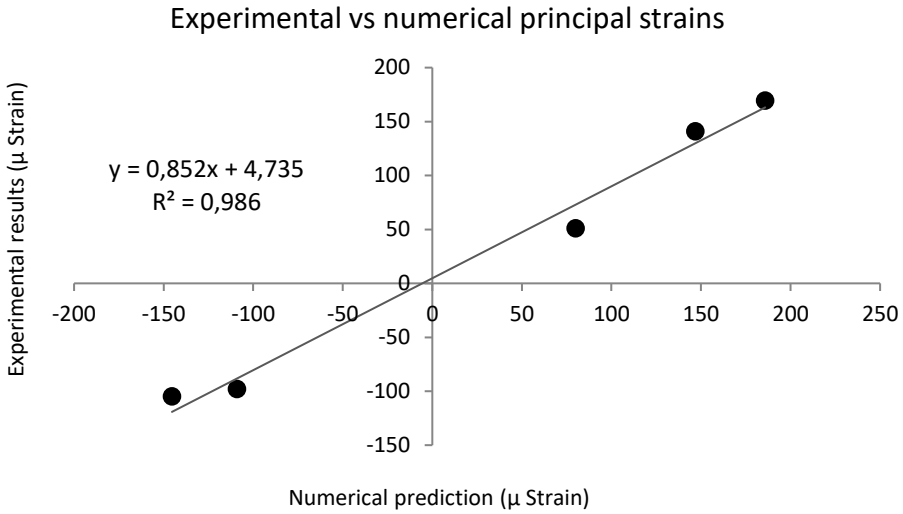

Figure 4.22. Linear regression analysis of the experimental and numerical results.

It should be noted that the position adopted by the bone structures has a major influence in the strain distribution at the joint. Small positioning differences, and consequently differences on the contact area between the several structures, leads to strain differences at the cortical and trabecular bones.

This influence proved to be important, and it was necessary to guarantee greater stability in the experimental systems, thus translating into a same zone of contact between the different components for each experimental test carried out.

When comparing the FEM results and the experimental results, we verify that the correlation coefficient R^2 is a high value in the implanted model (0.986), being smaller in the intact model (0.860), which may be related to the fact that the implanted system is more rigid than the intact due to the weight of the humeral prosthesis. This makes it easier to ensure the same position of the joint structures between each trial, which corroborates the importance that must be given in fulfilling the correct placement of the bone structures.

4.7 Discussion

The purpose of this study was to develop and validate two finite elements models of the shoulder, the most unstable joint of the human body. One is a 3D representation of the intact shoulder, and the other of the implanted shoulder. The intact model is composed by

the humerus and scapula bone structures and their soft tissue, as well as the IGHL. The implanted model is composed by the humerus and scapula bone structures and by the Comprehensive® Total Shoulder System, from BIOMET®. Both models take into account the influence of the four most important muscles in abduction (deltoideus, infraspinatus, supraspinatus, subscapularis), according with literature and with a multi-body model previously developed (see Chapter 2).

The FEM were successfully validated against the experimental models previously developed (see Chapter 3). Maximum and minimum principal strains were compared. The correlation between the models was expressed as a percentage of the Root-Mean-Square-Error (%RMSE) of the difference between the highest and smallest principal strain values measured. Having in mind the complexity of the shoulder joint and the number of components added on the models, the high correlation coefficients (0.860 and 0.986), and %RMSE of 22% and 20% for the intact and implanted models, respectively, suggests reasonable agreement between predicted and measured values. The validation means that it will be possible to evaluate certain areas of the shoulder where it is impossible to obtain information with the experimental models.

Several authors performed validation of biomechanical models, by comparing measured strains with predicted maximum and minimum principal strains [217, 249–251]. However, as far as we know, no model with both the humerus and the scapula has been experimentally validated, so it is difficult to perform direct comparisons with literature. Nevertheless, we can relate with the study of Gupta *et al.* [235] and of Varghese *et al.* [217]. Gupta *et al.* [235], developed and validated a 3D FE model of a human scapula, achieving correlation coefficients between 0.89 and 0.97. Varghese *et al.* [217] developed and validated FE models of long bones, including the humerus, obtaining correlation coefficients between 0.64 e 0.99. Our results relate with those in the sense that the correlation coefficient is of the same order of magnitude. But stronger comparisons cannot be performed, as our models consider two bone structures and different loading and boundary conditions.

The other purpose of the present study was to perform a sensitivity analysis of finite element meshes of bone and cartilage, to fill a gap established in literature. It is focused on the humerus and considers cortical and trabecular bone and its cartilage. The results obtained suggest that mesh sizes depend on aspects like geometry and size of the surface or type of material attributed to the model. Thus, cortical and trabecular bone, as well as cartilage, may not be correctly represented by meshes of the same size. The study points out that 1.5 mm, 0.8 mm and 0.6 mm are appropriate mesh sizes for modelling cortical bone, trabecular bone and cartilage.

In literature, there are many FEM of the humerus and of the shoulder devoted to study topics like bone remodelling [243], stress and strain distributions at the humerus [217, 240], glenohumeral stability [196] or osteoarthritic joints [139]. Unfortunately, only few authors provide details on the developed meshes, and thus comparison of new models with existing

ones is short. In the study of Maldonado *et al.* [240], bone is treated as inhomogeneous, and CT density information is used. On the contrary, our model considers each bone structure as homogeneous and with higher Young modulus. The other major difference between the two models relies on the type and number of elements used to build the FEM: Maldonado *et al.* [240] used only (58 048) eight-node brick elements.

In another study on a computed-tomography based FEM of long bones, Varghese *et al.* [217] used tetrahedral linear elements and made a convergence analysis. Element sizes of 2, 3 and 4 mm were evaluated and the authors considered 3 mm to be the optimal mesh size. However, based on the mesh convergence results of our study, a mesh size of 3 mm is considered large to correctly represent the geometry of bone structures. In yet another study [196], shoulder bone and cartilage models were developed with tetrahedral quadratic elements. Unfortunately, no details on mesh size, number of elements, nodes nor degrees of freedom are given and comparison cannot be accomplished.

4.8 Conclusions

Being able to build FE shoulder models which replicate the anatomy and biomechanics of the joint, and that allows us to trust on the results obtained, is not trivial. Furthermore, to build FE models that can replicate the experimental data obtained, with accuracy, is a challenge, as they must be constructed as identical as possible to the experimental ones. Thus, achieving results that are both repeatable and representative of the real anatomical scenario, in the two conditions studied, and with such a complex system, is a hard task.

Many factors influence the success of the FEM constructed, such as the development of CAD models that truly replicate all the structures considered (bones, cartilage, ligaments and prosthesis components); the placement of all structures in the right position; the origin an insertion sites of the muscles considered; the material properties used; and the inherent relationship of all these structures. These facts together made the development of the intact and implanted FEM a difficult assignment to accomplish.

Nonetheless, a FEM of the intact shoulder, and a FEM of the implanted shoulder were developed, and validated against experimental data obtained earlier. The numerical models developed replicate the experimental models previously constructed, which are presented in detail in Chapter 3.

The models will allow us to evaluate the influence that a prosthesis has on strain distribution at the humerus and at the scapula.

Chapter 5

Numerical Results and Clinical Predictions

5.1 Introduction

In the first chapter of this thesis, it became clear that glenoid loosening is one of the major causes of failure in TSA and that the standard of care is the use of all-polyethylene cemented glenoid components [63, 252, 253], with pegged implants performing better than keeled implants [64, 65, 254]. However, loosening of the glenoid remains an issue that is far from being resolved [54, 55, 57].

Several aspects are believed to be related with loosening of the glenoid implant [57], but implant/fixation-related factors such as failure at the implant/cement interface [255], bone necrosis due to the high amount of heat released in the curing of the PMMA, fatigue failure and fragmentation suffered by the PMMA layer [81] are some of the most significant. To overcome the fixation-related issues, uncemented or limited-cementing techniques have been adopted and component designs have evolved with the goal of reducing the problems found.

Cementing fixation of the humeral stem is the most used technique with excellent results. Nevertheless, concerns regarding the cement have appeared and in accordance with Seitz *et al.* [256] those may be justified with earlier experiences in cemented hip and knee arthroplasties in young patients. Because of this, uncemented humeral fixation has become more frequent but loosening and subsidence have been observed [257, 258], which is a concern.

In the present chapter, the clinical outcomes of the Modular Hybrid® Glenoid Component and of the humeral stem of the Comprehensive® Total Shoulder System (Biomet®) were discussed and compared with the principal stress/strain distributions predicted by the finite element model of the implanted shoulder, developed in Chapter 4. Micromotions of the glenoid and humeral component were determined and related with clinical findings.

5.2 Clinical Outcomes

5.2.1 Glenoid Component

A retrospective study comparing the clinical outcomes of TSA when performed with a hybrid glenoid component (cemented peripheral polyethylene pegs and uncemented central post) and with a conventional cemented all-polyethylene pegged glenoid component was performed by Gulotta *et al.* [60]. The patients were followed during 3.2 years, in average, and radiographs were evaluated at a minimum follow up of 2 years after surgery. The conventional all-PE implant used was a Bio-Modular® Shoulder System and the hybrid component was the Modular Hybrid® Glenoid Component (used in this work), both from Biomet®. The two implants have a curved back with an anatomic pear shape. The difference between the two is the titanium post at the centre of the hybrid component.

Ten patients with a hybrid glenoid component were randomly chosen to undertake a CT-scan, so that the presence or absence of bone growing onto the central titanium post could be observed. Axial and coronal views were analysed in 8 well-defined regions and the implant was considered solidly fixed if bone ongrowth was observed in more than 6 regions. After the evaluation, all hybrid glenoids analysed were considered firmly fixed.

An example of an axial and coronal CT-scan obtained for one implanted shoulder is presented in Figure 5.1. In this case, the authors could identify new bone next to the central titanium post in all regions, except in region number 6 (see Figure 5.1, B).

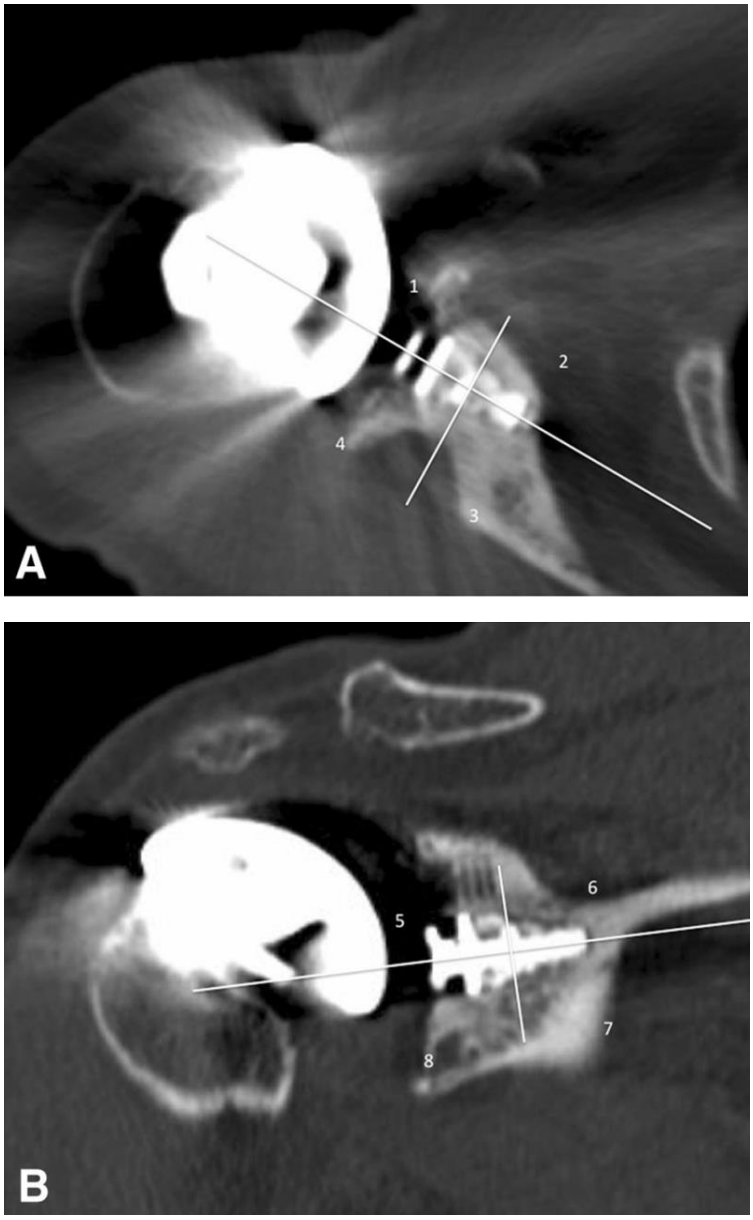

Figure 5.1. CT-scan of a right shoulder implanted with a hybrid glenoid component: axial (A) and coronal (B) views. The several regions of interest are identified [60].

Despite the fact that all ten CT-scans evaluated confirmed that the glenoid component was solidly fixed to the surrounding bone, Gulotta *et al.* [60] did not find major differences between the outcome results of the two glenoid components regarding radiolucent line scores, outcome scores at final follow up, complication rates and reoperation rates. The only complication registered in the hybrid component group was posterior instability (one patient). Nine months after surgery, the patient suffered a reoperation and it was possible to observe new bone around the central post.

5.2.2 Humeral Component

The first study to analyse the clinical outcomes of the Comprehensive® Humeral mini stem (Biomet) was performed by Jost *et al.* [44]. The study started by focusing on the results of the Bio-Modular mini stem (Biomet) in 40 shoulders, but the humeral implant was later updated to the Comprehensive® Humeral mini stem (used in this thesis), being employed in 15 shoulders. The first stem had a size between 52 mm and 66 mm, while the second had a size of 83 mm. The most important difference between both humeral implants was the head-shaft angle (55° in the first and 45° in the last). The follow-up of the study lasted a minimum of 2 years and the outcome results demonstrated improved range-of-motion, improved abduction and improved internal and external rotation, with no implant-related post-operative complications. The authors claim that the results obtained are comparable to those of conventional-length humeral components. Regarding radiographic findings, the authors identified radiolucent lucent lines with less than 1 mm in 11 patients (identified in Figure 5.2 B), but none were progressive at later follow-up. Besides, no signs of subsidence or of changes in position were observed [44].

Recently, Schnetzke *et al.* [259] presented a radiographic analysis of 52 patients implanted with an uncemented short-stem humeral implant (Aequalis Ascend Monolithic; Tornier, Grenoble, France) which can be considered in the same category as the Comprehensive Humeral Stem used in this work. Figure 5.3 illustrates frequent radiographic evidences observed on the study. The zones labelled M1 and L2 present the most significate differences 26 months after operation, namely cortical thinning and osteopenia (mild loss of bone mass) in zone M1 in 82.7% of cases, and spot welds (new bone linking the gap between the endosteal surface and the stem) in 71.2% of cases. A smaller amount (11.5%) of condensation lines was observed around the tip of the humeral stem. The authors point out that the radiologic evidences of bone adaptation are signs of stress shielding. Nevertheless, at a minimum of 2 years of follow-up, no signs of loosening, subsidence or osteolysis were observed. Similar results were obtained in a previous study by the same authors [260].

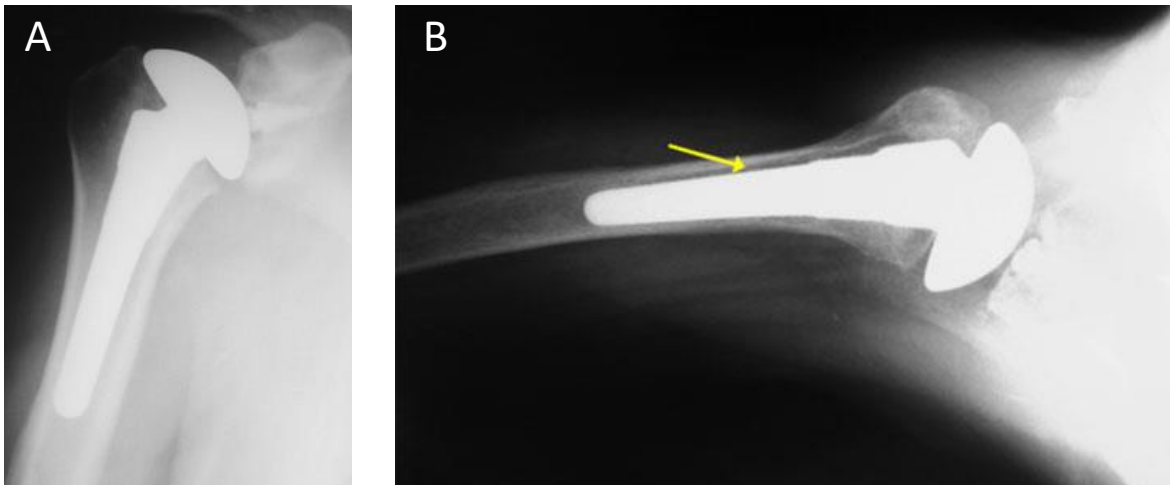

Figure 5.2. Uncemented mini-stem humeral component post-operatively. In (B) a radiolucent lucent line is identified. Adapted from [44].

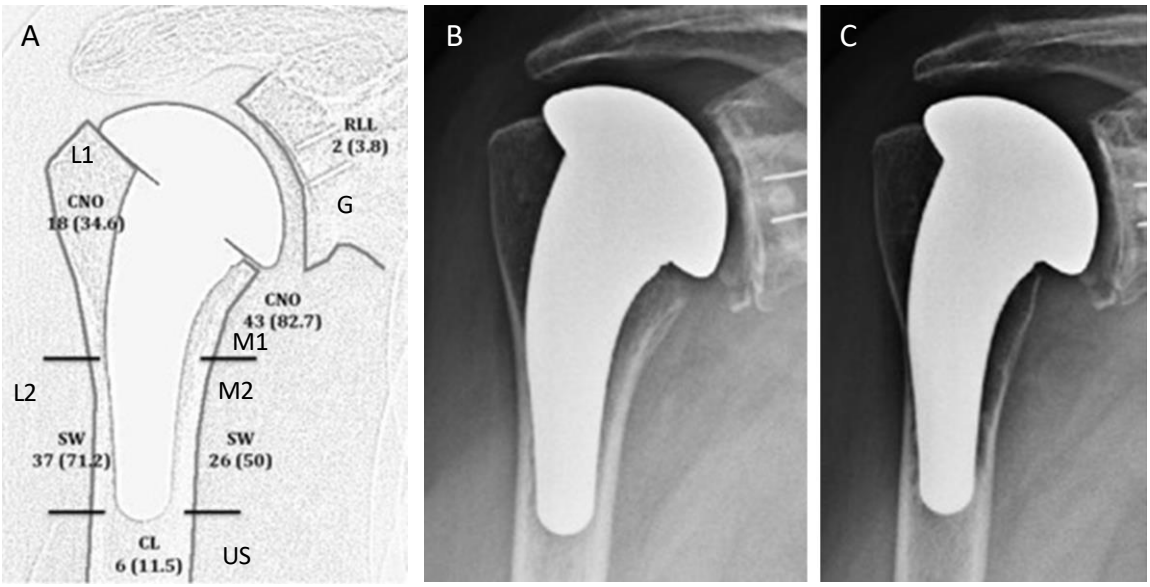

Figure 5.3. Uncemented mini-stem humeral component. A: schematic representation showing the most frequent radiologic bone adaptations in each zone (number (%)). Labels: M – medial, L – lateral, US - under stem, G – glenoid, CL - condensation line, CNO - cortical thinning and osteopenia, RLL - radio- lucent line, SW - spot weld. B: Radiograph shortly after operation; C: radiograph 26 months after operation. (right shoulder). Adapted from [259].

5.3 Materials and Methods

5.3.1 Intact Shoulder Model

On a first stage, the FEM of the intact shoulder was evaluated. Stress and strain distribution at the trabecular bone structures were accessed, as well as the general behaviour of the cartilage and of the inferior glenohumeral ligament.

5.3.2 Implanted Shoulder Model

The implanted shoulder model was the focus of this chapter. As the present goal is the study of bone behaviour when implanted with prosthesis, bone material properties were chosen to be close to the ones of real bone structures.

The cortical and trabecular bone materials of the humerus continued to be considered isotropic linear elastic, as Peng *et al.*[261] found little difference between the behaviour of a femur when assigned with isotropic and orthotropic material properties. Given that the femur and the humerus are long bones, we assume that the same conclusions can be applied in our study. Regarding the scapula, its cortical bone was considered an isotropic linear elastic material, similarly to other models [213, 262]. Concerning the trabecular bone, since it is known to be highly anisotropic [263], and there has been an effort to model it accordingly [207, 215], we assumed anisotropic linear elastic material properties.

The material properties of the bone structures used are stated in Table 5.1 and the material properties of the prosthesis components were stated in Table 4.4.

Table 5.1. Material properties of the bone structures.

Structure	Young Modulus	Poisson ratio
Cortical humerus	16.5 GPa	0.3
Trabecular humerus	124 MPa	0.3
Cortical scapula	16 GPa	0.3
Trabecular scapula	E_{11} = 342 MPa E_{22} = 213 MPa E_{33} = 194 MPa $G_{12} = G_{13} = G_{23}$ = 100 MPa	$\nu_{12} = \nu_{13} = \nu_{23} = 0.26$

5.3.2.1 Define the Critical Condition

To understand the principles of failure of uncemented shoulder prosthesis, it is mandatory to define the most critical mechanical condition for implant fixation. In this condition, the bone will suffer the highest stresses ultimately compromising arthroplasty

procedure success. In this sense, the joint behaviour was compared in three abduction positions: 45°, 60° and 90°, assuming the same muscle insertion sites and that the prosthesis components are perfectly bonded to the surrounding bone. All boundary conditions equal those of the validated FEM (see Chapter 4, section 4.3.3).

The muscular actions applied in each abduction position were determined with the multi-body model presented in Chapter 2 and are in Table 5.2 (same for Table 3.3 for the 90° abduction).

Table 5.2. Muscle actions applied in the pre-clinical testing.

	Muscle	Deltoideus 1	Deltoideus 2	Subscapularis	Infraspinatus	Supraspinatus
Abduction 45°	Force (N)	95	95	119	53	43
Abduction 60°		116	116	145	70	53
Abduction 90°		150	150	225	120	90

5.3.2.2 Post-Operative Scenarios

Two post-operative scenarios were developed and the most critical mechanical condition identified previously was considered in each.

In the first post-operative scenario, the FEM simulated a short-term condition accomplished considering a Coulomb friction between the prosthesis components and the surrounding bone structure. The friction coefficient of porous-coated metals was assumed equal to $\mu = 0.88$ in accordance with [264]. The friction coefficient of the smooth metal surface was considered nearly half of the former value, being similar to the friction coefficient of the polyethylene. All friction coefficients considered in the analysis are stated in Table 5.3.

The several shoulder prosthetic components where friction is present, emphasizing the different materials used, are represented in Figure 5.4.

Table 5.3. Interface conditions.

Friction coefficient	Surface pairs
0.30	Glenoid prosthesis / Glenoid bone
0.88	Glenoid central post / Glenoid trabecular bone Porous surface of humeral component / Humeral bone
0.40	Smooth surface of humeral component / Humeral bone

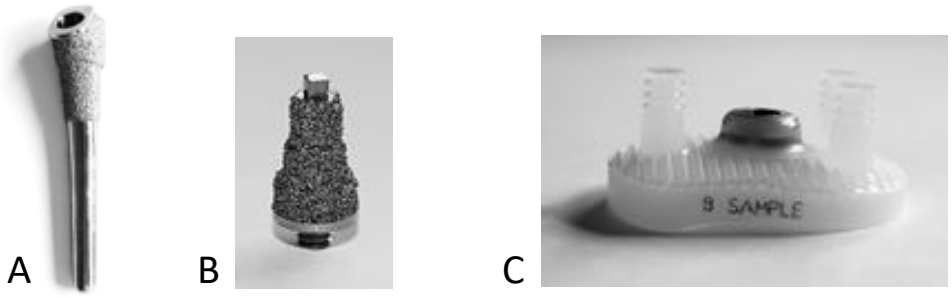

Figure 5.4. The prosthesis components: (A) humeral stem, (B) glenoid central post, (C) glenoid base. The porous–coated surfaces are present at (A) and (B); the smooth metal surface is present at (A); and the polyethylene is present at (C).

Originally, the boundary condition at the base of the humeral shaft was a symmetry constraint about a plane of constant z coordinate (ZSYMM: U3 = UR1 = UR2 = 0). However, in the presence of friction the model became unstable and failed to deliver a solution. To overcome this, the boundary condition was modified to a constraint on all translational degrees of freedom (pinned: U1 = U2 = U3 = 0).

In the second post-operative scenario, the FEM simulated a long-term condition with the prosthesis and the surrounding bone tissue perfectly bonded to each other. The boundary condition at the base of the humeral shaft is the same as in the previous model so to evaluate them under the same physical scenario.

5.3.2.3 Clinical Predictions and Post-Operative Scenarios

The clinical outcomes available in literature correspond to short/medium-term outcome results, as presented in section 5.2. For this reason, comparison between the clinical outcomes and the simulated short-term post-operative condition was performed to infer if the FEM can predict bone behaviour at this stage. The comparison was based on principal strain and stress distribution inside the trabecular bone and on micromotions at the bone/implant interface analysed at the short-term post-operative condition (when friction is present). Micromotions were calculated in two nodes at each side of the interface bone/implant for the most critical position.

In the glenoid component, micromotions were assessed around the central and peripheral pegs at the coronal and axial planes, as indicated in Figure 5.5. The several regions of interest of the central fixation post are identified with letters (A), (B) and (C) (A1, A2; B1, B2; C1, C2 indicate the periphery where micromotions were determined). The periphery fixation pegs are identified as (P1), (P2) and (P3).

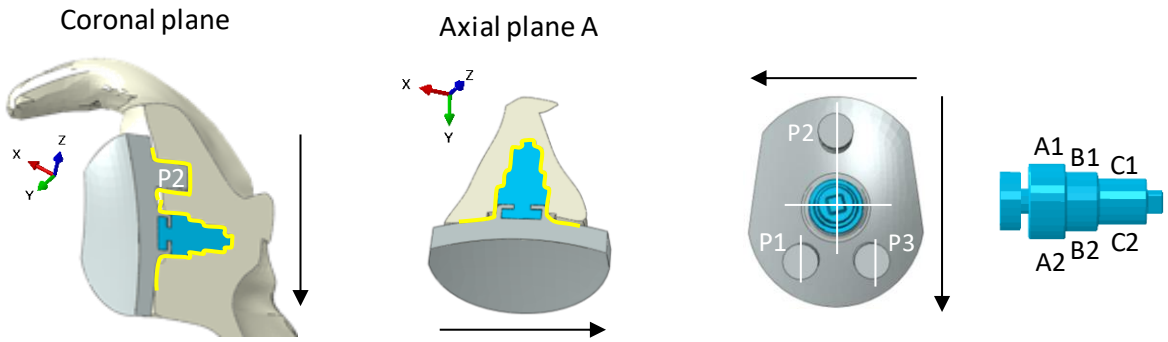

Figure 5.5. Glenoid cavity and prosthesis details. Micromotions were determined on bone/implant periphery, indicated by the yellow lines. The arrows indicate in which direction those were determined.

In the humeral component, micromotions were accessed at the anterior, posterior, lateral and medial directions, as indicated in Figure 5.6.The humeral implant was divided into (D) and (E) regions: region (D) corresponds to the superior region of the prosthesis and region (E) to the inferior region.

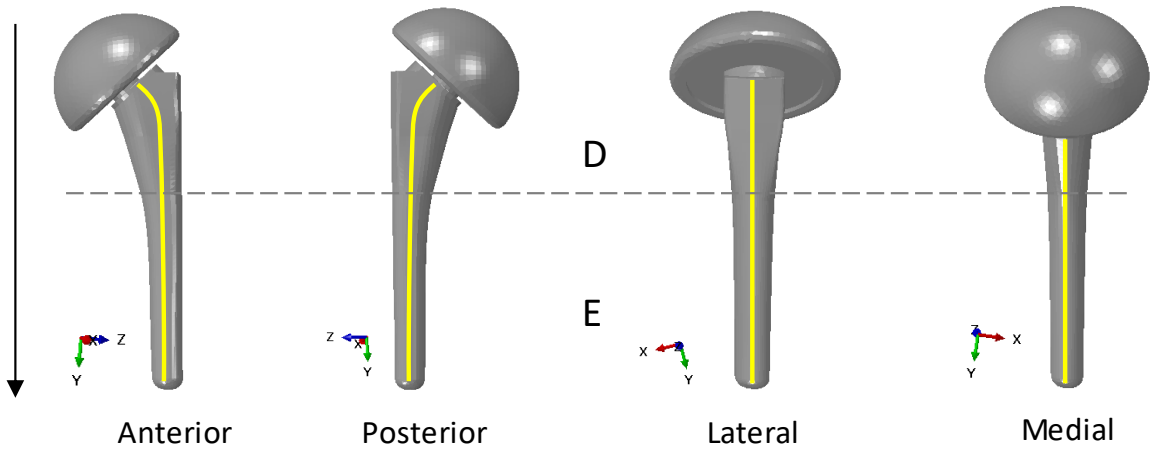

Figure 5.6. Humeral prosthesis. Micromotions were determined on bone/implant periphery, indicated by the yellow lines. The arrows indicate in which direction those were determined.

5.4 Results

5.4.1 Intact Shoulder Model

The maximum (A) and minimum (B) principal stress distribution on the trabecular bone of the shoulder joint, when under a 90° abduction, is presented on Figure 5.7.

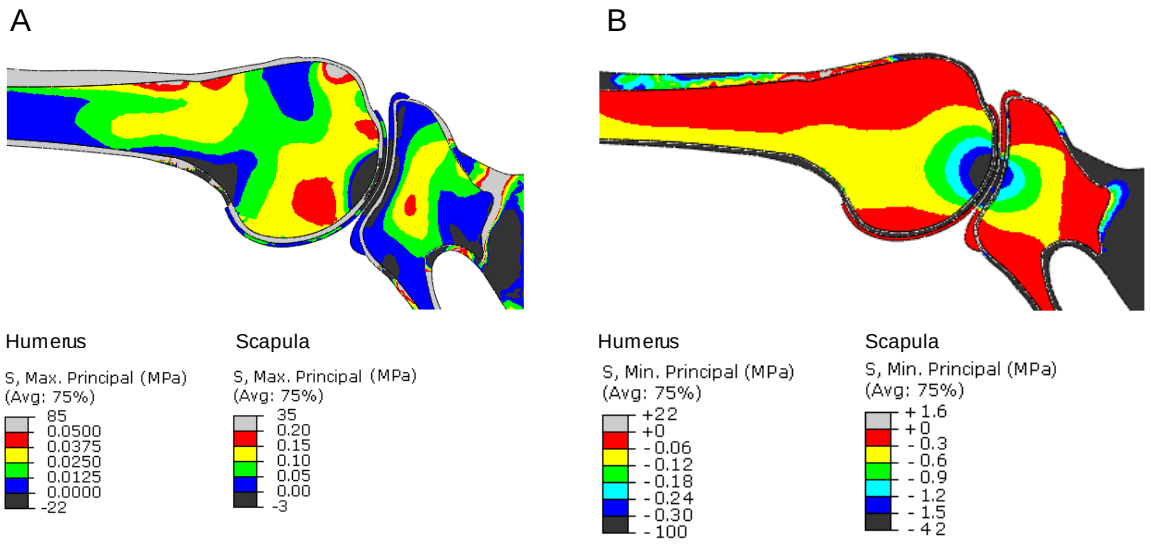

Figure 5.7. Maximum (A) and minimum (B) principal stress distribution on the intact joint.

The glenoid cavity is under higher tensile and compressive stresses than those of the humerus, being concentrated closer to the contact region between both bone structures. The smaller volume and the less bone density of the glenoid justifies the differences observed.

On the humeral side, the maximum principal stresses are distributed through the entire proximal humerus, while the higher minimum principal stresses are located on the humeral head.

Most of the studies that evaluate the stress distribution on the intact/implanted scapula focus their attention on Von Mises stress distribution. However, we are not interested in the failure phenomena but on the global comparison of stresses before and after prosthesis implantation, and in this sense maximum and minimum principal stresses are more appropriate. Nevertheless, to compare our result with literature ones, the Von Mises stresses were accessed for the intact scapula. In the glenoid region those are between (0.05, 2) MPa, being of the same order of magnitude of the ones determined by Gupta *et al.* [265] ((0.05, 4) MPa) under similar modelling conditions.

Regarding the maximum (A) and minimum (B) principal strain distribution inside the joint, those are presented on Figure 5.8.

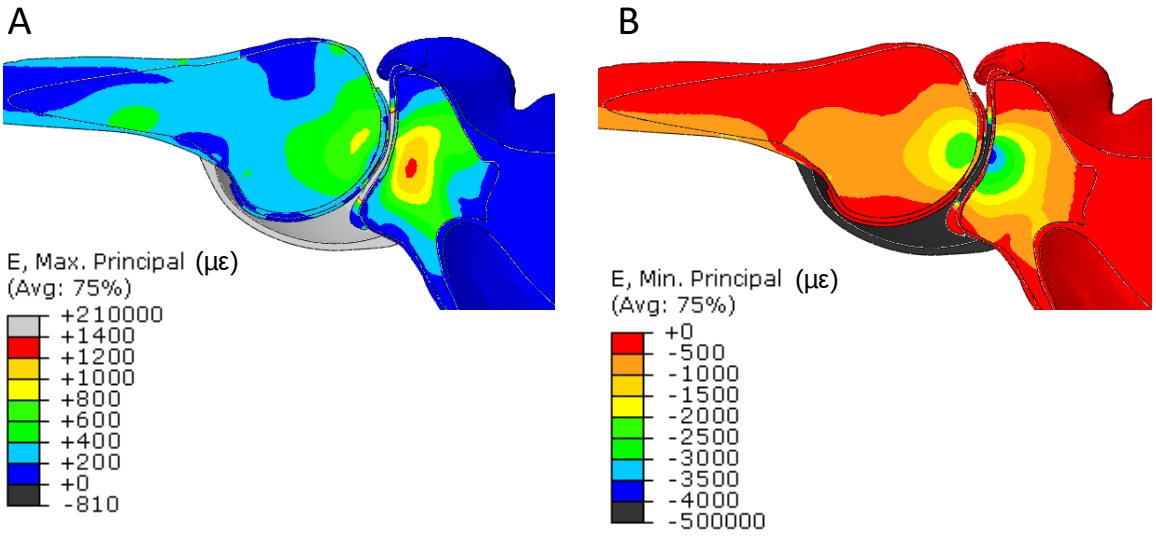

Figure 5.8. Maximum (A) and minimum (B) principal strain distribution inside the trabecular bone of the intact joint.

Strains are distributed on the humeral head and on the glenoid cavity, reaching higher principal strains on the glenoid side than on the humeral side ((1200, 1400) με) vs (800, 1000) με; and (-3500 -4000 με) vs (-2000, -3000) με, respectively).

The highest compressive strains are close to the contact region between the glenoid and the humeral head, and the majority of strains are between (-500, -2500) με, being inside the interval of normal physiological bone deformation ((-200, -2500) με) [186]. The same was observed with the tensile strains, whose majority are between (800, 1000) με. This indicates that the developed FEM is correctly representing the behaviour of the intact joint.

The contact region between the cartilage of both bones is represented in Figure 5.9.

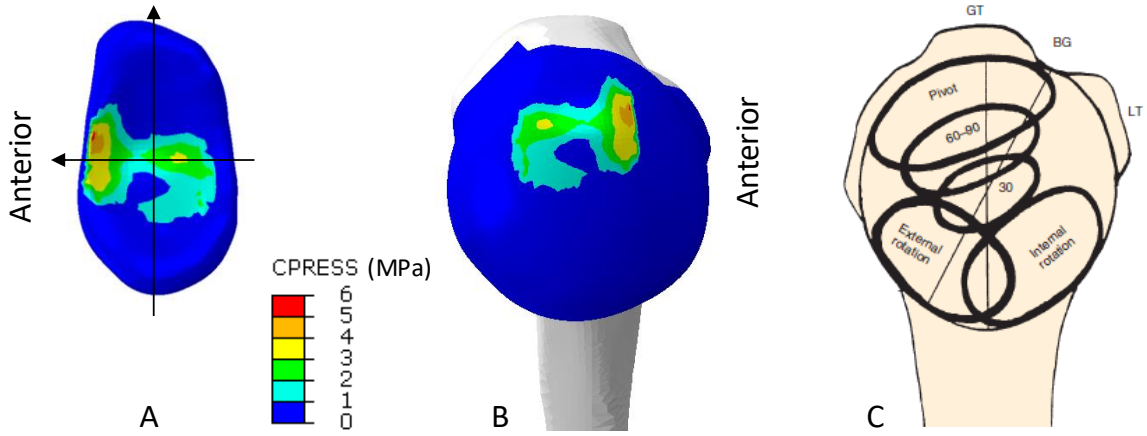

Figure 5.9. Glenohumeral joint contact regions. Figure (C) was adapted from [3].

On the glenoid, the contact is performed on the central region of the cartilage (Figure 5.9 A), with the peak pressure located anteriorly (red area). On the humerus, the contact is performed in the superior region of the cartilage (Figure 5.9 B).

Throughout the years, many strategies have been developed to determine glenohumeral contact patterns [266–268], but its quantification in *in vivo* systems remains a challenge. Despite some contradictory results [267, 268], Massimini *et al.* [268] point out that the glenohumeral contact area on the glenoid side is mainly on the anterior region, which is in accordance with our findings. However, Bey *et al.* [267] determined that the contact area is mainly in the posterior region. There are several reasons than can justify the different outcomes of each study, such as the aetiology of the study (*in vivo* vs *in vitro*), the type of movement performed (abduction on the scapular plane or in the coronal plane, for instance), the healthy conditions of the rotator cuff muscles, and others.

Regarding the contact area on the humerus, it is pointed to be closer to the greater tuberosity [3, 266] and our results are in accordance with literature, as illustrated on Figure 5.9 (C).

Regarding the IGHL, it was considered in the study due to its importance in high angle motions, like 90° abduction (as referred before). With the help of the other ligaments (not considered in the study) and of the rotator cuff muscles, the IGHL works to keep the humeral head on the glenoid cavity, preventing humeral dislocation as the arm moves. We observed that the ligament was responsible for keeping the peak glenohumeral contact on the anterior side of the glenoid, as we performed the same numerical simulation without the ligament for the sake of comparison and observed that the peak contact point moved towards the posterior region on the glenoid cartilage, while having little influence on the interval of stress and strain observed. Notwithstanding, we choose to build the implanted shoulder model without the influence of the IGHL since it is cut during the TSA procedure and sutured after prosthesis insertion, altering its performance.

5.4.2 Define the Critical Condition

The abduction angle influenced the location of the contact point between the two prosthesis components, as illustrated in Figure 5.10. The contact point moved toward the centre of the glenoid prosthesis with increasing abduction angles, staying in a postero-superior region when in 90° abduction. The contact pressures also augmented with increasing angles. In what concerns the joint reaction force at the base of the humeral bone, it is similar between all abduction positions considered (≈ 28 N).

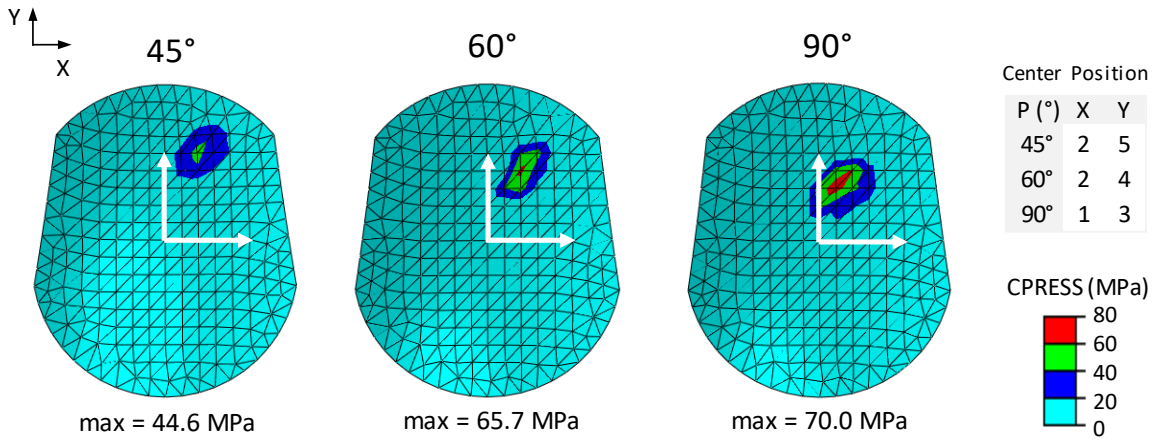

Figure 5.10. Contact pressure at the glenoid prosthesis at 45°, 60° and 90° abduction.

To define the most critical mechanical condition for implant fixation, the principal stresses and strains distributions at the trabecular bone were analysed in the three positions considered, assuming the prosthesis components are perfectly bonded to the surrounding bone. The distribution of principal stresses inside the trabecular bone is represented in Figure 5.11. The highest tensile and compressive values are located on the posterior aspect of the glenoid component, particularly around the holes for fixation of the glenoid implant, and they augment as the abduction angle augments. In the 90° abduction, the highest tensile stresses are between (-1.6, -6) MPa and the highest compressive stresses are between (1.5, 2) MPa. The humeral trabecular bone generally suffers smaller stresses and these are more prominent on the humeral head cut at the 90° abduction, as indicated by the arrow in the figure.

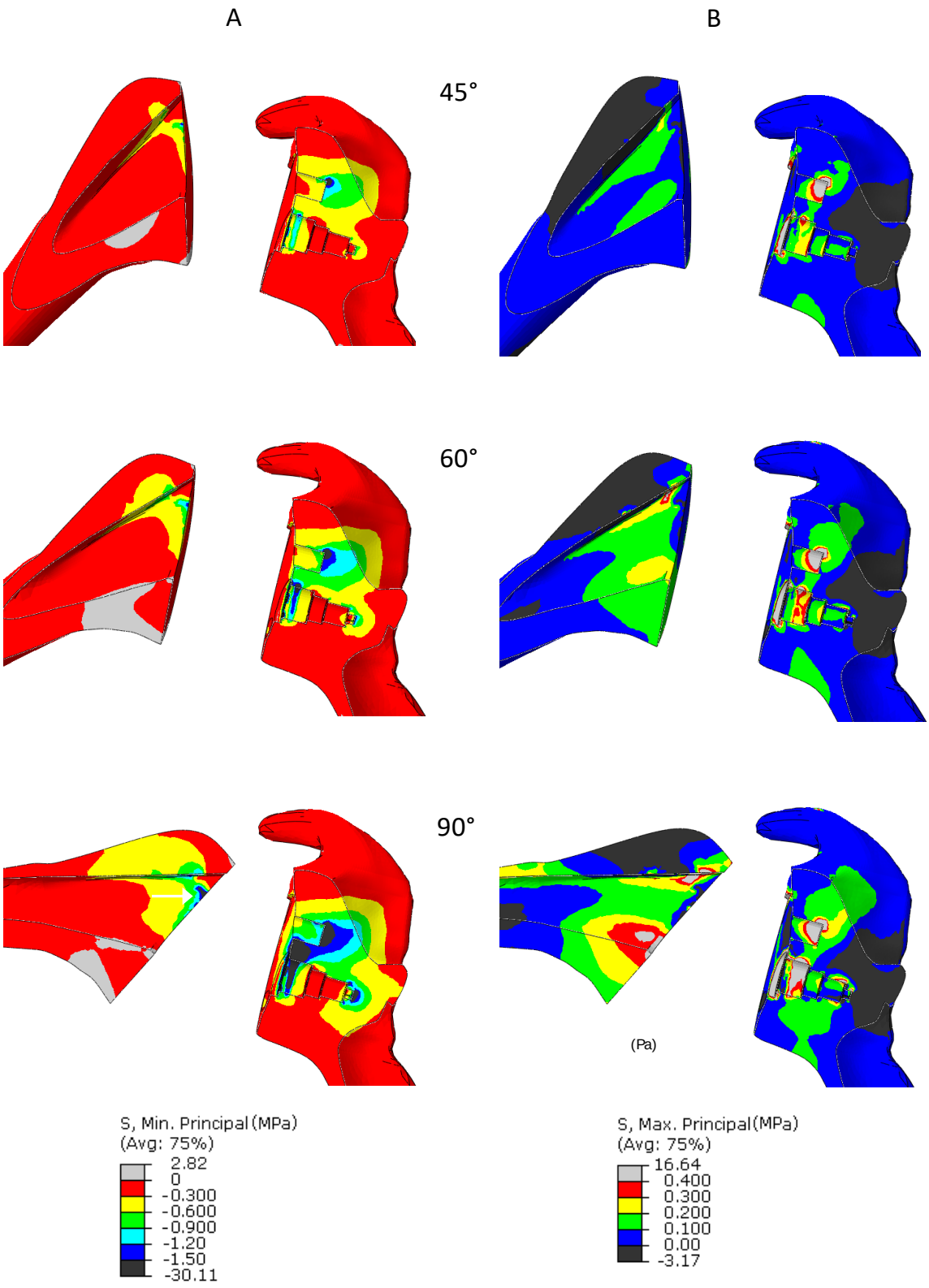

Figure 5.11. Compressive (A) and tensile (B) principal stresses in the three positions analysed. The prosthesis components and the cortical bone were omitted for a clearer representation.

The principal strains (tensile and compressive) for the three positions analysed are represented on Figure 5.12. On the entire joint, the highest compressive strains are comprised between (-4500, -7000) με. Closer to the humeral head cut they increase as the arm is abducted and the peak values are registered medially. On the glenoid side, the compressive strains also augment for higher abduction angles, being high around the superior and centre holes for implant fixation.

The peak tensile strains are comprised between (3000, 5000) με (Figure 5.12 B). On the humeral side, the joint presents critical regions closer to the humeral head cut that are higher at 90° abduction. On the glenoid side, the joint presents critical regions around the holes for prosthesis fixation, especially at the superior and central holes, since the contact between the humeral component and the glenoid component takes place at the upper/posterior region of the glenoid component in all abduction positions considered.

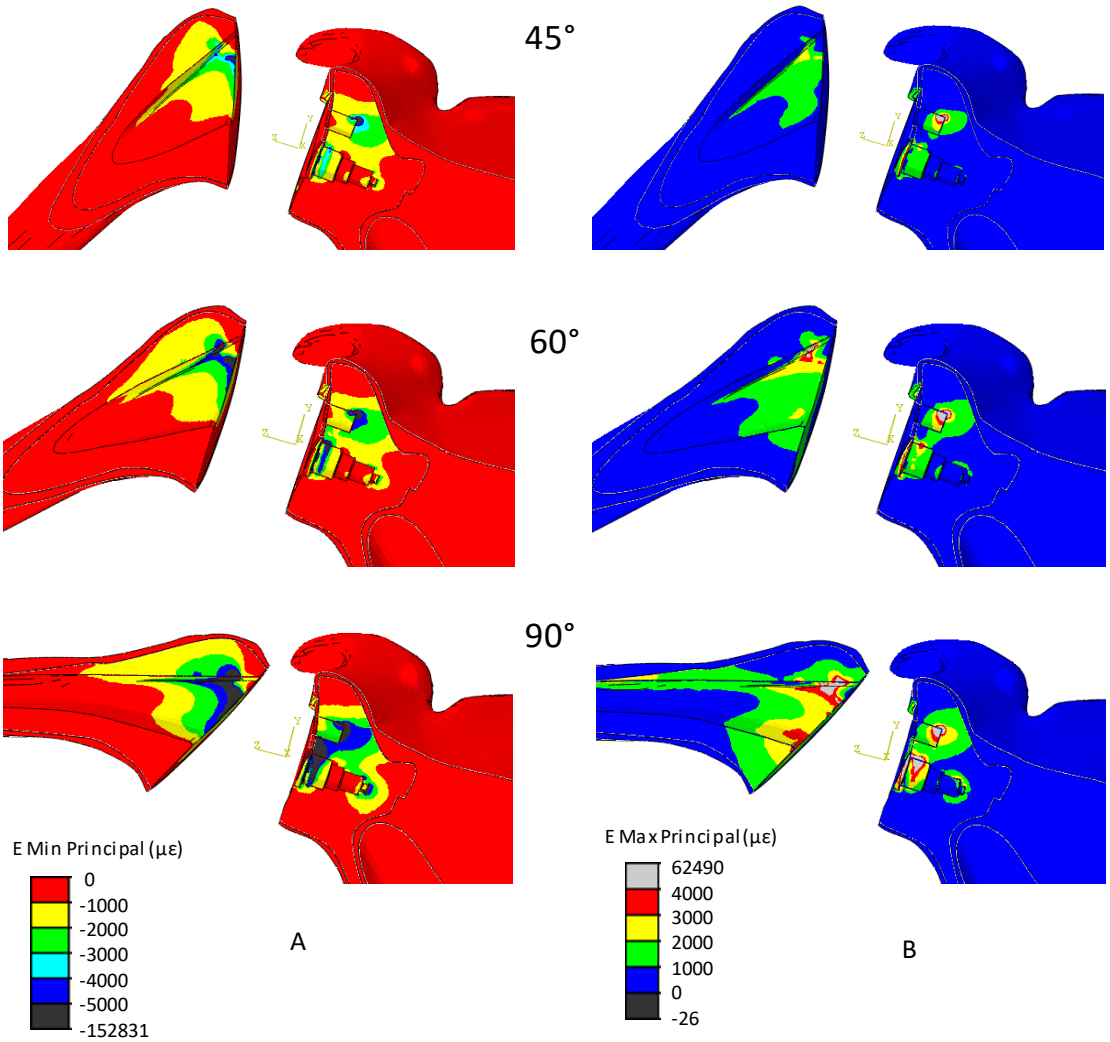

Figure 5.12. Minimum (A) and maximum (B) principal strains in the three positions analysed. The prosthesis components were assumed perfectly bonded to the surrounding bone.

5.4.2.1 Conclusions

To define the most critical condition for implant fixation we started by performing an analysis of strain/stress distribution at the cortical and trabecular bone for the three abduction angles considered (45°, 60°, 90°). From the analysis performed, the most critical condition for the shoulder is during high abduction angles (90° in the present case). For a further quantitative comparison, the principal strains and stresses were determined at the periphery of the superior and central holes of the glenoid bone (Figure 5.13) and at the periphery of the humeral head, on the medial and lateral margins (Figure 5.14).

As illustrated (Figure 5.13), compressive strains and stresses are more significate than tensile ones in all regions analysed. Particularly, strains/stresses are higher on the superior fixation hole (upper and base periphery) and on region A1, close to the central fixation post. It is clear that as the abduction angle augments, tensile and compressive stresses also augment, confirming that the critical position for the shoulder corresponds to the 90° abduction, being in accordance with literature [132]. The same was observed in the humerus, where the lateral periphery suffers higher stresses/strains than the medial one.

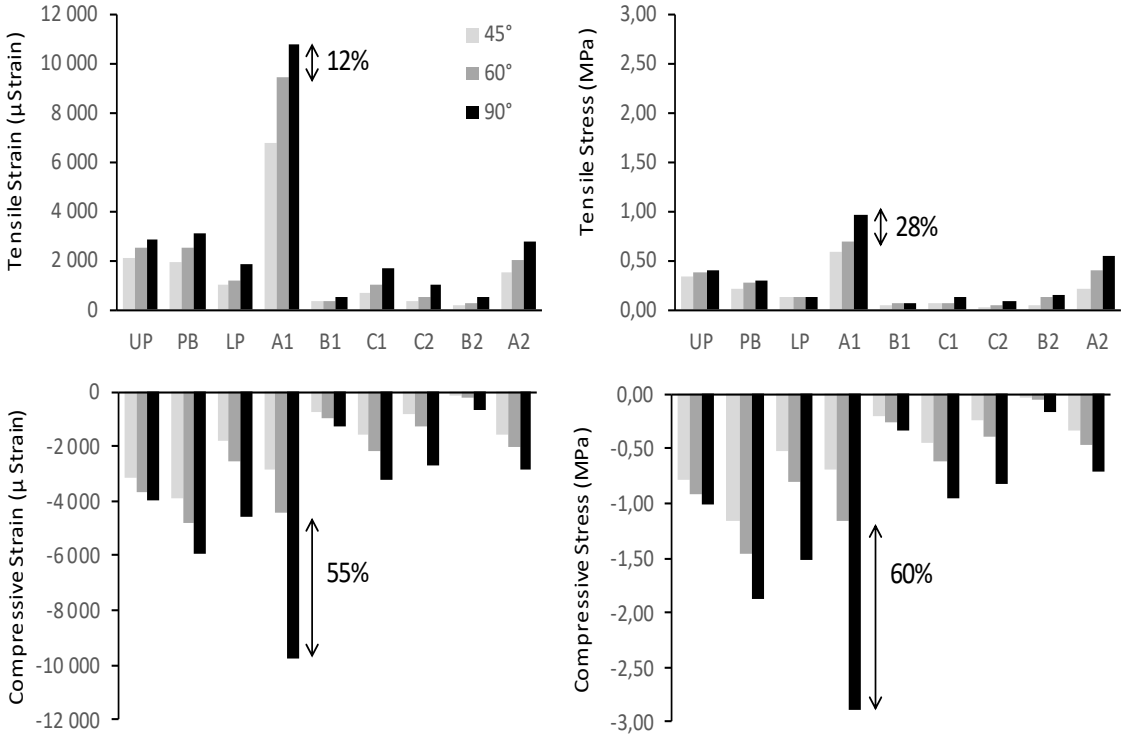

Figure 5.13. Tensile and compressive strains/stresses determined on the glenoid. UP: upper periphery; PB: peg base periphery; LP: lower periphery of the superior fixation hole; A1, A2, B1, B2, C1, C2: periphery of the central fixation post (see Figure 5.5 for further details).

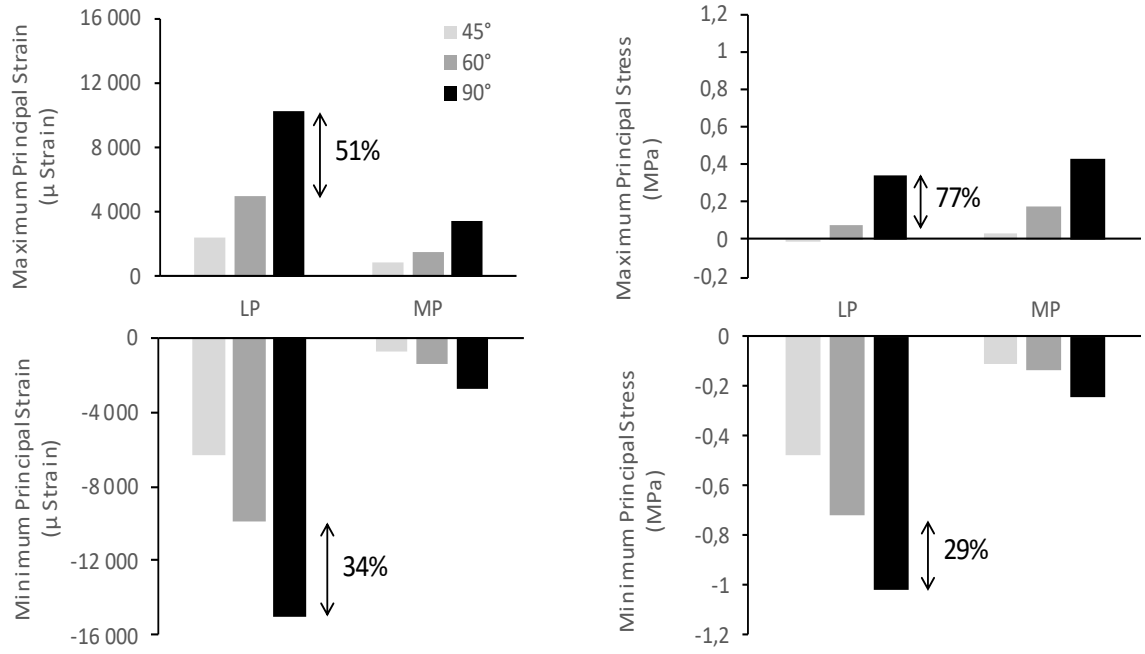

Figure 5.14. Principal strains and stresses determined on the humerus. LP: lateral periphery; MP: medial periphery.

5.4.3 Clinical Predictions and Short-Term Post-Operative Scenario

5.4.3.1 Glenoid Component

The only clinical outcomes of the Comprehensive® Total Shoulder System (Biomet®) available in literature are those presented previously [60] (see section 5.2) and according with the authors there was new bone next to the central titanium post in nearly all regions.

The axial and coronal planes of the referred CT-scan (right shoulder) and the tensile (A) and compressive (B) strains predicted by the FEM on the short-term post-operative condition, for the same planes of interest, are presented in Figure 5.15. The glenoid cavity was divided into axial and coronal planes and the several regions of interest were identified (numbered from 1 to 4 in the axial plane, and from 5 to 8 in the coronal plane), after [60].

The majority of the tensile strains (green area) and compressive strains (yellow area) are inside the range considered of normal physiologic bone loading, which according to Roberts *et al.* [186] is (≈ 200, 2500) με. This indicates that the modular Hybrid® glenoid post used in this study seems to be a viable option for glenoid fixation as bone density is maintained within normal values and so is bone integrity [186].

Close to the fixation holes there are tensile strains (yellow areas) and compressive strains (green areas) inside the interval (2500, 4000) με, meaning that in those regions there is a tendency for bone hypertrophy with density augmentation [186]. Some critical regions where strains are between (4000, 25 000) με are also observed (red areas in A and blue areas in B). This indicates that the trabecular bone is under very high compressive/tensile forces,

and when strain repeatedly exceeds 4000 με, as in region 3, bone becomes at risk for stress fractures which is a possible cause of loosening [269] and lack of bone ongrowth [186].

Finite element model predictions for the short-term post-operative condition are similar with the clinical outcomes [60] for the glenoid component, as bone was identified on the central post in all regions, except in one. Furthermore, the ten CT-scans analysed in the study [60] showed evidenced of bone ongrowth around the fixations pegs.

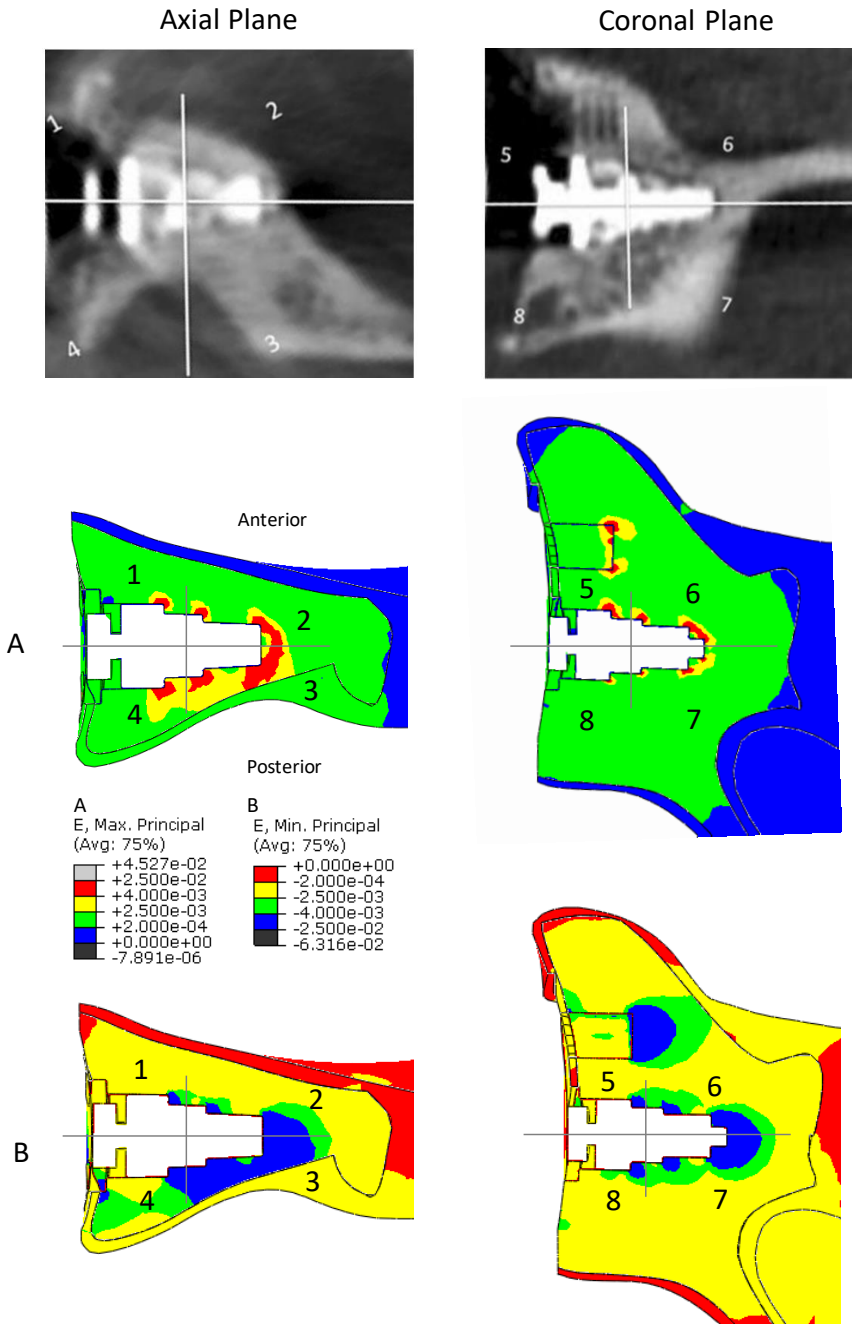

Figure 5.15 CT-scans (adapted from [60]) and the tensile (A) and compressive (B) strains on the short-term post-operative condition.

5.4.3.2 Humeral Component

Even though clinical results of the humeral component of the Comprehensive Shoulder System are available in literature [44], the authors did not compare radiographic evidences nearly after surgery and at the final follow up, so the prosthesis influence on the surrounding bone structure is hard to evaluate. For this reason, the numeric predictions will be compared with the clinical results of the Aequalis Ascend Monolithic humeral prosthesis (taken 26 months after surgery [259]), as it can be considered in the same category as the Comprehensive Humeral Stem.

The tensile (A) and compressive (B) strains predicted by the FEM, on the short-term post-operative condition, are presented on Figure 5.16, as well as the referred CT-scan. The humerus was divided into medial (M1 and M2), lateral (L1 and L1) and under stem (US) regions in accordance with Nagels *et al.* [270], as exposed. The differences between both prostheses are easily identifiable since the Comprehensive Humeral Component stem is longer and thinner than that of the Aequalis Ascend, but both are considered short-stem prosthesis.

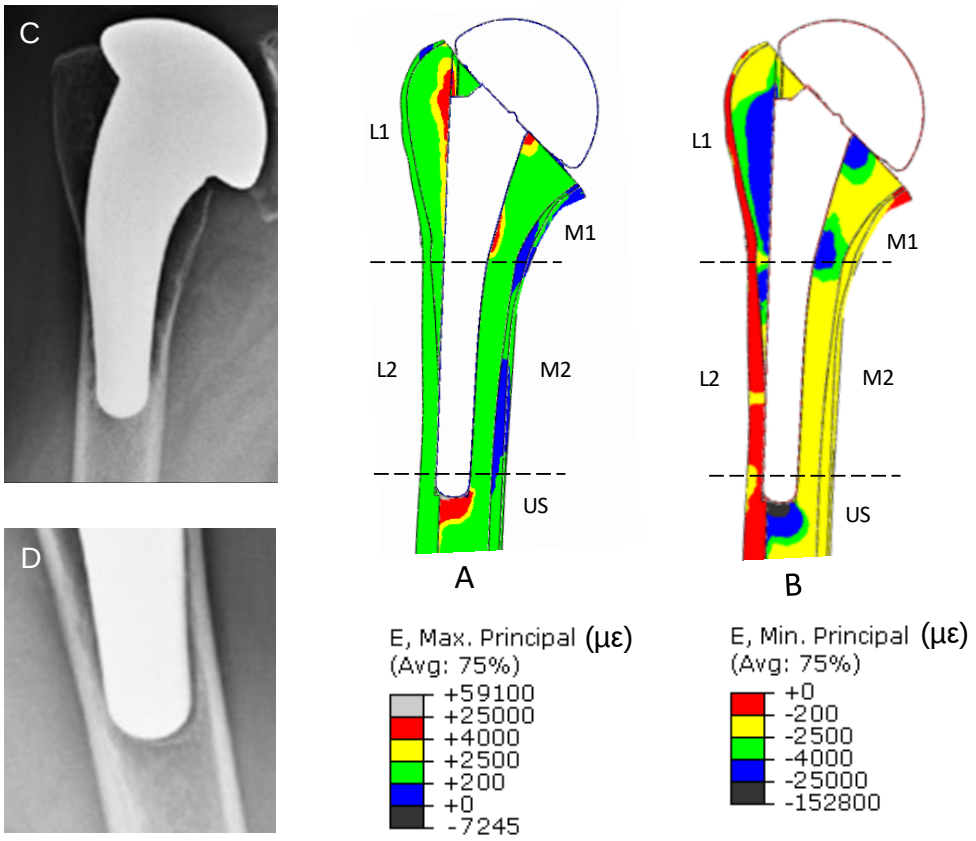

Figure 5.16 CT-scans (adapted from [259]) and the tensile (A) and compressive (B) strains on the short-term post-operative condition.

On the trabecular humerus, the majority of the tensile (A) and compressive (B) strains are inside the interval considered of normal physiologic bone loading ((≈ 200, 2500) με, green and yellow areas, respectively) [186].

In region L1, bone becomes at risk for stress fractures by fatigue failure close to the interface bone/implant, when strain equals (4000, 25 000) με (blue and red areas in image (B) and (A), respectively). However, bone remodelling can also occur in nearby areas for strains inside the interval (2500, 4000) με (green and yellow areas in image (B) and (A), respectively) [186]. Clinically, Schnetzke *et al.* [259] identified cortical thinning and mild bone loss in region L1 in 34.6% of the shoulders evaluated. The FEM previews cortical thinning on the same region, since compressive strains are inside the interval (0, 200) με (red area in image B) for the cortical bone, which means that here the bone is not suffering enough stimulus for bone remodelling. The lack of new bone close to the implant may lead to loosening and micromotion of the humeral component [269].

The behaviour previewed by the FEM for region L1 is also previewed for region M1. This is partially in accordance with the clinical findings of Schnetzke *et al.* [259], as mild bone loss is observed on the trabecular humerus, and cortical thinning is previewed by the model. In region L2, cortical thinning is previewed by the FEM, being observed on the CT-scan of Figure 5.16.

In region US, there are areas where trabecular bone is considered at risk of spontaneous fractures since compressive strains exceed 25 000 με. There are also areas where principal strains promote bone hypertrophy, with bone density augmentation. This may be related with the condensation lines around the tip of the stem as observed in Figure 5.16 (D), being considered a sign of stress shielding. Despite the lack of a secure "tip-fill" of the humeral component that could indicate subsidence, clinically this was not observed in the majority of the studies [259, 260], being observed in only 1 case in the study of Morwood *et al.* [271].

With what was exposed we conclude that the implanted FEM of the short-term post-operative condition predicts bone behaviour when implanted with a total shoulder prosthesis. Thus, we are confident that the FEM of the long-term post-operative condition can likewise preview the joint behaviour. The numerical results on the long-term will be compared with the short-term condition to illustrate joint behaviour evolution.

5.4.4 Long-Term Post-Operative Scenario

5.4.4.1 Glenoid Component

Once bone completely bonds into the prosthesis components (long-term post-operative condition) (see Figure 5.17), the tensile strains (A) and compressive strains (B) inside the glenoid cavity are mainly between (200, 2500) με in both axial and coronal planes. This indicates that on the long-term the glenoid prosthesis is well fixed to the surrounding bone tissue and that bone integrity is maintained despite the presence of the implant.

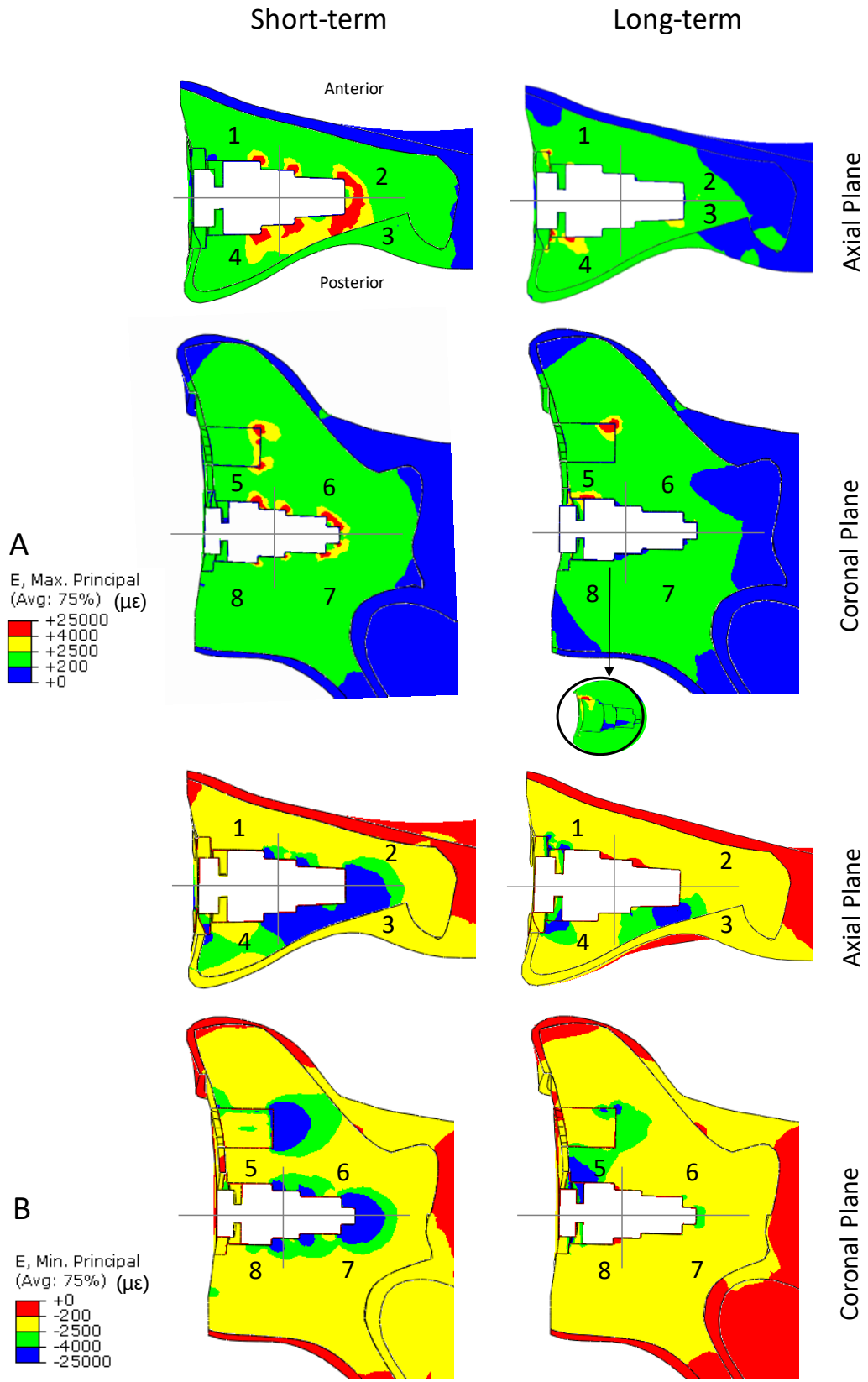

Figure 5.17 Tensile (A) and compressive (B) strain distribution on the glenoid cavity for the short-term and long-term post-operative conditions.

On the axial plane the high tensile strains (A) observed in the short-term, mainly in region 3, were not observed in the long-term. Still, there are some peak values ((2500, 25 000) με) observed in some small areas (see region 4). On the contrary, the compressive strains (B) registered between (2500, 25 000) με on the short-term (see region 3 and 4) were observed in a smaller area on the long term. This indicates that even after the prosthesis completely bonds into the surrounding bone structure, there are regions were bone density augmentation can be observed (green area) and others where fatigue failure can occur (blue area). Besides, In regions 1 and 2, close to the central fixation hole, compressive strains are smaller than -200 με (red area), meaning that bone is not being sufficiently stimulated for bone remodelling to happen [186].

On the coronal plane, fixation areas with high tensile (A) and compressive (B) strain distribution are identified around the superior fixation peg and around the central fixation post, especially on posterior/superior regions, similarly to what was observed in the short-term condition. Tensile (A) and compressive (B) strains surpass 4000 με in some small areas around the fixation holes, meaning that on the long-term there are still possibility of bone fractures due to stress, even if in small regions.

Overall, the long-term post-operative numerical model previews that the glenoid prosthesis component will be well fixed on the surrounding bone tissue, with bone ingrowth around some areas of the central and periphery fixation pegs. Nevertheless, there are some small regions where bone suffers high tensile and compressive strains close to the fixation holes. It is possible that in those areas bone resorption with fatigue failure will be observed. Still, the results indicate that the prosthesis used is a possible option for uncemented fixation.

Based on the results, we point out that the critical areas around the central fixation post could be avoided with the use of a flat design.

5.4.4.2 Humeral Component

The tensile (A) and compressive (B) strain distribution on the short-term and long-term post-operative conditions, for the trabecular humerus, is presented in Figure 5.18.

On the long-term, when bone is completely bonded to the humeral prosthesis, most tensile (A) and compressive (B) strains are within the interval of normal physiologic bone loading, where bone integrity is maintained ((200, 2500) με) [186] (green and yellow areas, respectively).

On region L1 there are still areas of concern, mainly regarding compressive strains (blue area) where bone can suffer fatigue collapse [186]. Nevertheless, bone remodelling with bone density increase can also be observed (green area).

It is interesting to notice that on the short-term (region L1) the region where bone collapse may occur (blue area) is a region where bone remodelling may be observed on the

long-term (green area). This could indicate that if bone has the capability to withstand strain on the short-term, there is a possibility that on the long-term it can regenerate and become stronger.

It is important to remember that in region L1 and M1 the stem has a porous surface that can promote bone ingrowth around it and this design feature could be important for a proper humeral component fixation without cement.

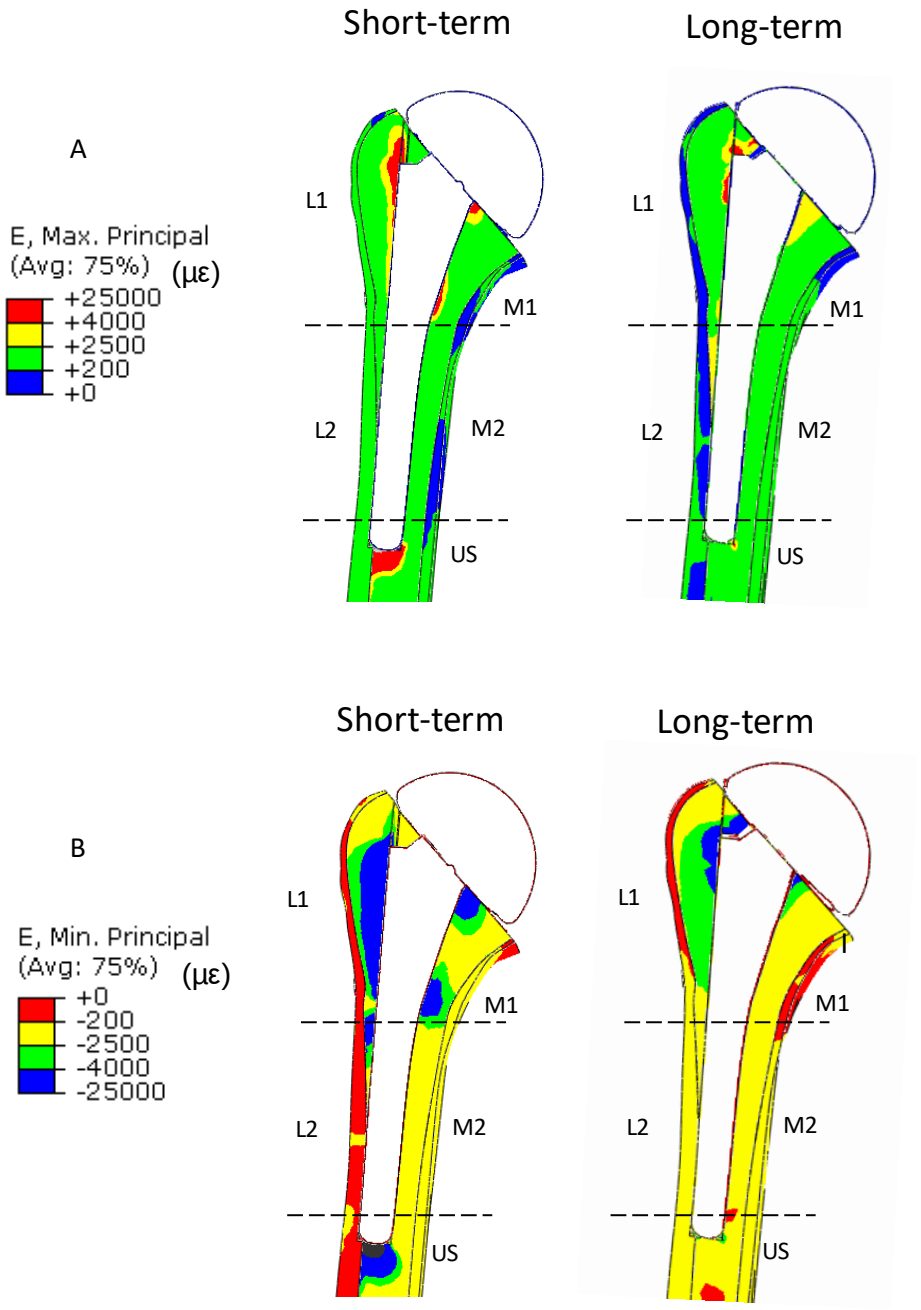

Figure 5.18 Tensile (A) and compressive (B) strain distribution on the trabecular humerus for the short-term and long-term post-operative conditions.

5.4.5 Stress Distribution on the Short and Long Term

The stress distribution on the trabecular bone of the humerus and of the glenoid cavity is represented in Figure 5.19. The short and long-term post-operative conditions are represented.

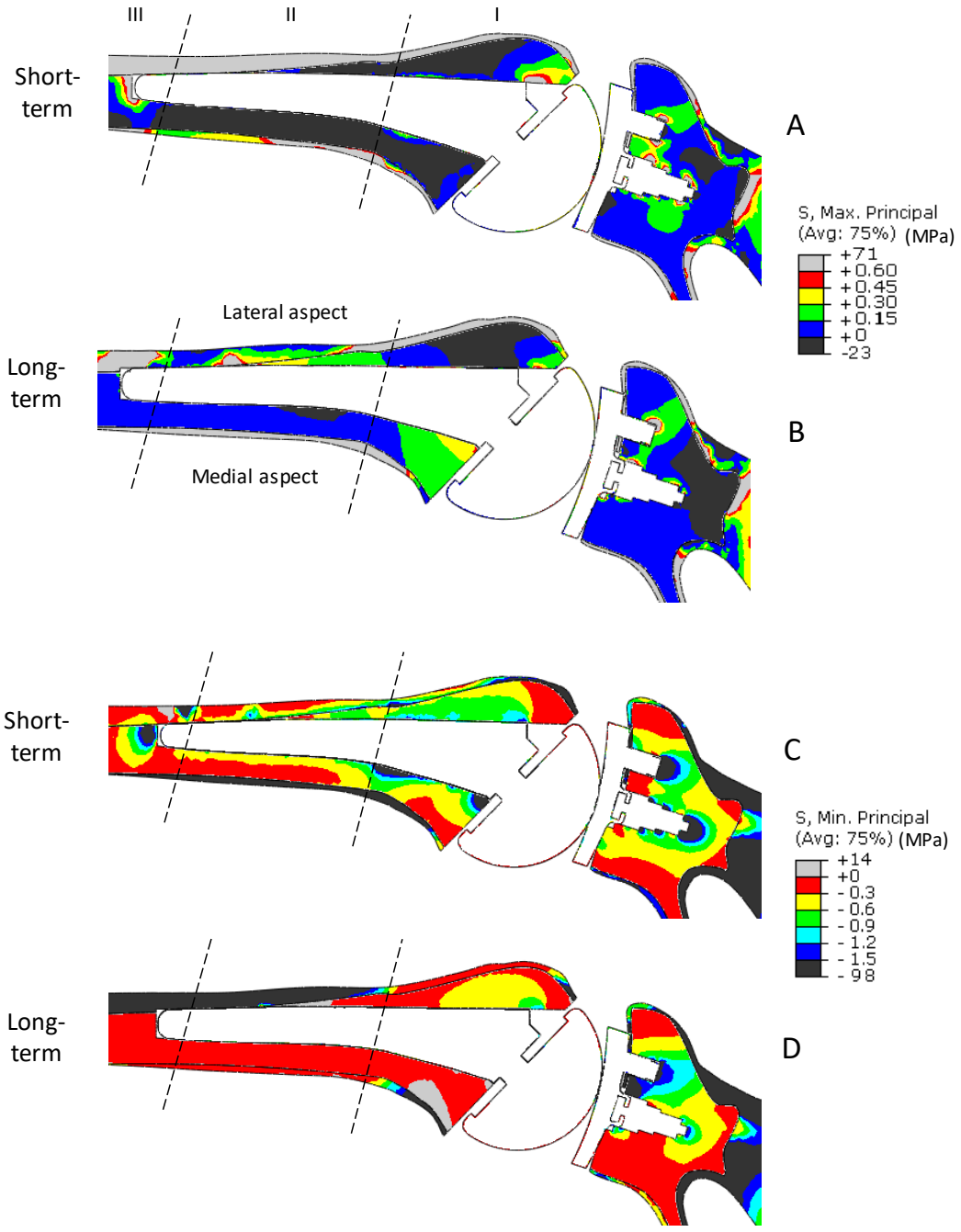

Figure 5.19 Maximum (A, B) and minimum (C, D) stress distribution on the trabecular humerus for the short-term and long-term post-operative conditions.

On the short-term post-operative condition, when there is friction between the humeral prosthesis and the surrounding bone, the trabecular bone shaft suffers mainly compressive forces (see Figure 5.19, C), with the maximum values located close to the tip of the prosthesis stem (region III) and on the medial aspect of region I (black area, (-1.2, -8) MPa. On the long term, minimum principal stresses on the trabecular bone diminishes (highest values (-0.6, -0.9) MPa), but are still more significate than maximum stresses, which is expected, since the joint is mainly under compression when under a 90° abduction.

On the glenoid side, maximum principal stresses on the short-term (Figure 5.19, A) are between (0.45, 5) MPa, being concentrated around small areas of the central and superior fixation posts. A similar behaviour is observed with the minimum principal stresses, that is, the highest values are located on specific areas around the central and superior fixation post, being between the interval (-1.2, -7) MPa (black areas).

When the prosthesis is perfectly bonded to the surrounding bone tissue (long-term condition), the highest maximum (see Figure 5.19, B) and minimum (see Figure 5.19, D) principal stresses occupy smaller areas of the trabecular bone, still around the fixation posts.

The areas of higher stress concentration (on the short and long terms) correspond to the regions of high strain distribution, where bone may fracture and ongrowth may not be observed. As referred before, this is in accordance with what was clinically observed for the glenoid and for the humerus.

5.4.6 Bone Interface Micromotions

5.4.6.1 Glenoid Component Interface

Micromotions of the central fixation post in the axial and coronal planes are presented in the graph of Figure 5.20. The several regions of the fixation post are identified.

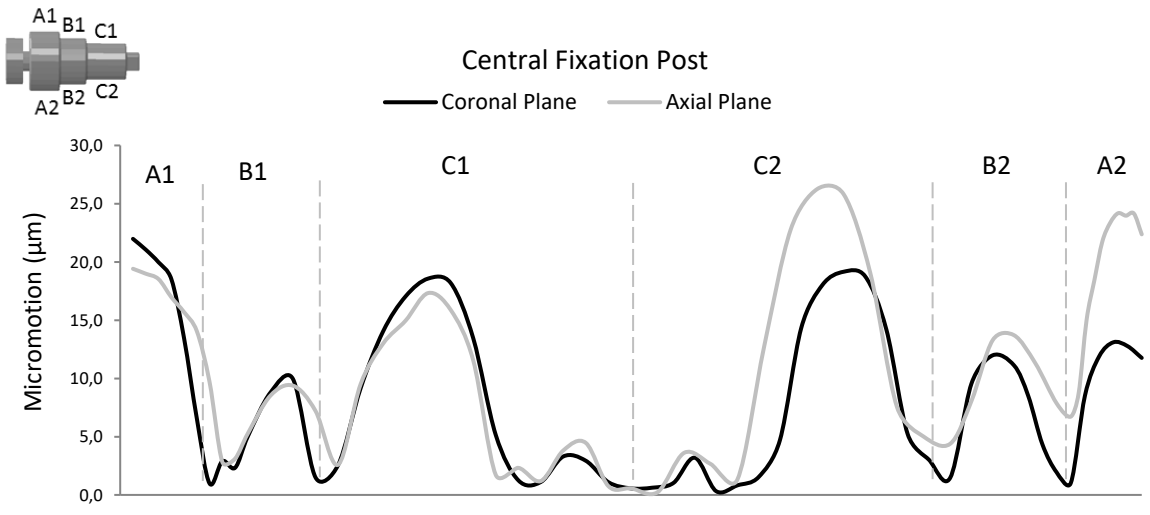

Figure 5.20 Micromotions of the central fixation post at the coronal and axial planes.

On the coronal plane, micromotions have a symmetric distribution around the periphery of the fixation post, and it was observed that the several micromotion components (x, y, z) are similar between each other (Cartesian axis in Figure 5.5). The highest values are observed in regions A1, C1 and C2, being close to 20 μm.

On the axial plane, micromotion distribution around the periphery of the central fixation post is not symmetric and a clear increase of the micromotions in regions A2, B2 and C2 in all (x, y, z) components was observed. The highest values are observed in regions C2 and A2, being close to 25 μm. The results also show that micromotion distribution on regions A1, B1, and C1 are similar in both coronal and axial planes.

The range of micromotions observed on the central fixation post does not surpasses 30 μm on the regions analysed, being inside the interval considered optimum for bone ingrowth/ongrowth [272]. This is in accordance with the observations of Gulotta *et al.* [60], since the authors observed bone ingrowth in all CT-scans analysed. This indicates that the porous coated central post is a good option for glenoid component fixation.

The micromotions of the polyethylene fixation pegs in the coronal plane are presented in the graph of Figure 5.21.

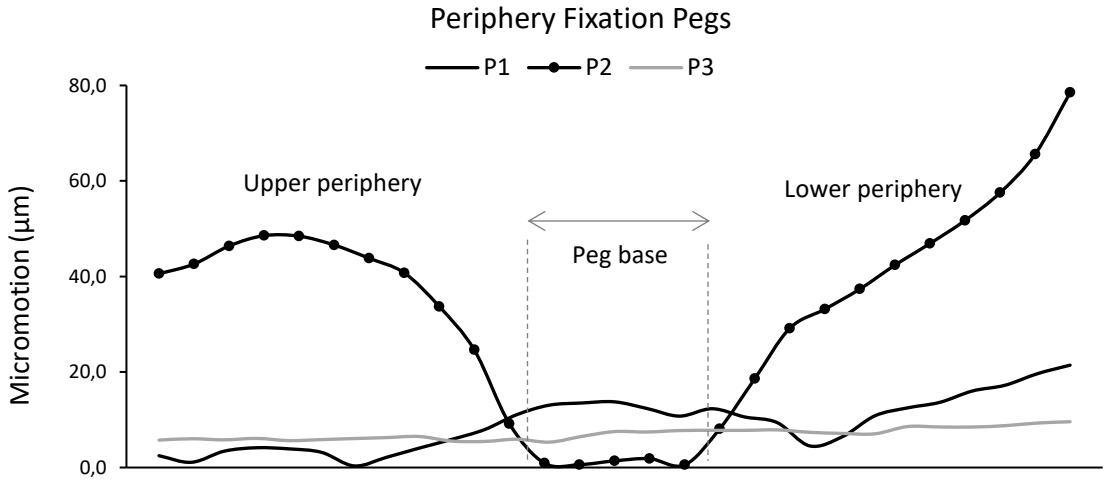

Figure 5.21 Micromotions of the periphery fixation pegs on the coronal plane.

Outside the base of the three pegs the superior fixation peg (P2) presents micromotions higher than those of the inferior pegs (P1 and P3), being in its majority higher than 20 μm.

At P2, micromotions are higher for (y) component, meaning that there is a major tendency of prosthesis rotation in the medial/lateral direction. Regarding components (x) and (z), their micromotions are small and similar between them. At the peg base, micromotions are nearly zero, which indicates that it tends to rotate in the medial/lateral direction, and thus trabecular bone prevents the peg from moving forward. It is evident

that micromotion distribution is nearly symmetric along its periphery.

Peg P1 presents small micromotions in the entire peg periphery, being smaller than 15 μm, which indicates that the peg tends to move in the lateral/medial direction.

Peg P3 presents micromotions smaller than 10 μm in its entire periphery. Along the peg base, micromotions are also higher than zero, meaning that P3 also tends to move in the lateral/medial direction (as P1).

The range of micromotions observed on the periphery pegs is smaller than 80 μm, being the largest measured at the superior peg (P2), while in the inferior fixation pegs the largest values are close to 10 μm and to 20 μm for pegs P3 and P1, respectively. Micromotions are inside the interval considered optimal for bone ingrowth/ongrowth [272], which means that bone ingrowth can occur in those areas. Additionally, the higher micromotions observed on the top periphery peg and the smaller on the bottom may indicate a tendency to the so-called rocking horse phenomenon that is related to glenoid loosening. However, the also smaller micromotions of the central fixation post (< 30 μm) indicate that the glenoid component is well fixed in that region, which will limit the glenoid component loosening.

5.4.6.2 Humeral Component Interface

Micromotions of the humeral stem implant, on the anterior, posterior, medial and lateral aspects (see Figure 5.6) are presented in the graph of Figure 5.22.

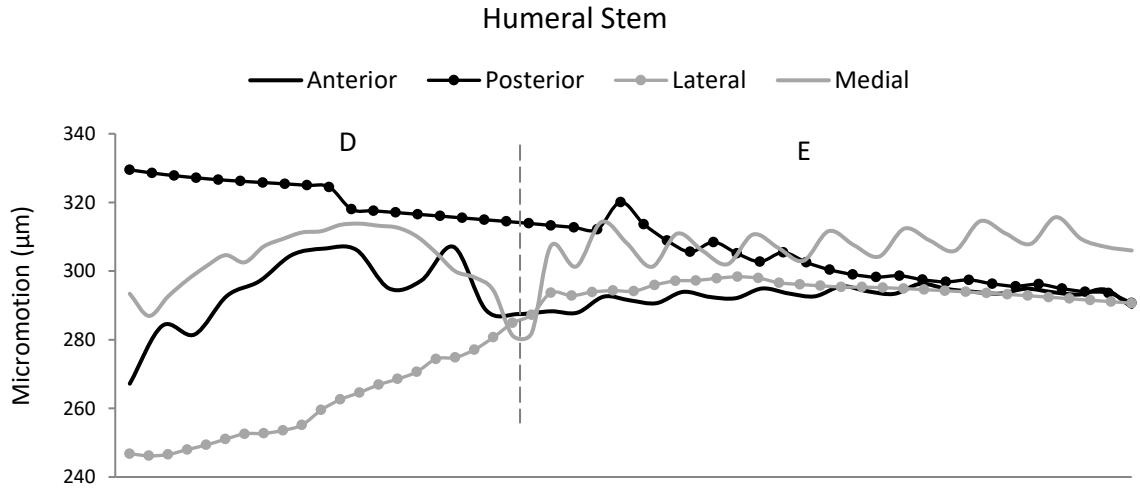

Figure 5.22 Micromotions of the humeral implant along the stem.

There are clear differences on the micromotion distribution of regions (D) and (E) (see Figure 5.6). In region (D), micromotion distribution is similar between the anterior and

medial aspects, differing between the lateral and posterior ones. The highest micromotions are observed posteriorly (≈ 325 μm) while the smallest are observed laterally (≈ 250 μm). In region E, micromotion distribution is similar between all different aspects analysed. Particularly, micromotions are comparable anteriorly and laterally, being close to 295 μm; and medially and posteriorly, staying between (300, 320) μm. According with literature [273], humeral stem micromotions are too high to allow bone ingrowth around its entire surface.

Micromotions in component (y) are the largest (between (250, 350) μm) and are always positive, meaning that the prosthesis is prone to subsidence along the intramedullary canal, allowing the humerus to sink down the canal. This is in accordance with what has been observed on uncemented humeral prosthesis by several authors [85, 256, 257].

Component (x) ranges between (-90, 60) μm, being always positive laterally and anteriorly; always negative medially; and with positive and negative regions posteriorly.

Component (z) ranges between (-100, 60) μm, being positive in all aspects for region D, and negative in most of region E. The sinusoidal behaviour observed along region E, present in all aspects, is due to micromotions of components (x) and (z).

The combination between strains higher than the range of normal physiologic bone loading observed around the humeral stem (see Figure 5.18) and of micromotions higher than 150 μm, may obstruct the formation of new bone, allowing the implant to subside inside the shaft, as observed clinically (see Figure 5.2).

These results indicate that our numeric model is in accordance with what has been observed clinically for the uncemented humeral component.

5.5 Discussion

The main purpose of the present study was to analyze the numerical results of the FEM of the implanted shoulder (stress/strain distribution and micromotions), and to compare those with the clinical outcomes available in literature. Another goal was the comparison of strain distribution at the bone structures before and after prosthesis implantation.

The FEM of the implanted shoulder considers the material properties close to those of real bone structures. Two modelling conditions were considered: a short/medium-term post-operative condition and a long-term post-operative condition. The first considers the existence of friction between the several prosthesis components and the surrounding bone tissue, allowing a closer comparison with the clinical outcomes available in literature [60]. The second considers the several prosthesis components perfectly bonded to the surrounding bone tissue, allowing us to predict the long-term behaviour of the implanted prosthesis.

On the glenoid, evidence of critical regions mainly at the posterosuperior area of the cavity is pronounced. The central post does not present any deformation due to its high

stiffness, which may lead to the strain-shielding effect on the surrounding bone, which on its turn has been related to loosening of the glenoid component. Regardless of this, our numerical results are in accordance with the clinical outcomes of Gulotta *et al.* [60], since the distribution of strain in most of the glenoid cavity is within the interval considered as normal physiological loading ($(\approx 200, 2500)\ \mu\varepsilon$), meaning that the modular Hybrid® glenoid post used is a possible option for uncemented glenoid fixation, as it will not obstruct the integrity of bone density inside the cavity.

As far as we know, the clinical study of Gulotta *et al.* [60] is the only one presenting the outcomes of the use of a Comprehensive® Total Shoulder System (Biomet®) with a modular Hybrid® glenoid component. However, other clinical reports of modern glenoid components that are non-cemented [85, 274–276] or minimally cemented [58, 74, 277] evidence the low risk of glenoid loosening that these designs seem to provide and are in accordance with those of Gulotta *et al.* [60]. Most of those designs are built totally in polyethylene, with the central fixation post having flanges for bone integration and a central titanium core to provide stiffness. One such design will be considered on the next chapter of this thesis and for this reason the present discussion will not address those clinical studies.

In addition, the relative motion between bone and implant (micromotion) is a major question that must be considered regarding implant fixation. Leucht *et al.* [272] showed bone formation on an unloaded environment and a dramatic increase when micromotion was present (150 μm). However, bone ingrowth does not always takes place around porous-surfaced implants [60] and it may not occur when micromotions are larger than 150 μm [273]. Despite of any known optimum micromotion range for bone ingrowth/ongrowth, some suggest an interval between (20, 150) μm.

Recently, using FEM, Wahab *et al.* [215] determined maximum micromotions of 20.7 μm, 18.3 μm and 23.3 μm at bone/cement interface in centric, superior-anterior and superior-posterior loading conditions, on a four pegged all-PE implant, respectively. These results are similar to ours, but comparisons must be performed carefully, as there are several conditions of the study that differ from ours, such as loading scenarios, the use of cement and of an all-PE glenoid component.

Suárez *et al.* [211] have developed FEM studies on micromotion of cementless glenoid components and the relationship with conforming designs and prosthesis positioning has been suggested [262]. However, the author focused the study on a metal-backed implant with a central metallic fixation screw and comparison with our model is difficult to perform.

The first experimental study with all-PE glenoid components having a centrally fluted peg (Anchor Peg Glenoid, DePuy Orthopaedics) and considering three different fixation methods was developed by Wiater *et al.* [278]. Interference-fit (also called press-fit), hybrid cement (cemented on the periphery pegs and uncemented on the central peg) and fully cemented were the methods considered. The results obtained suggest that addition of

cement on the peripheral pegs does not significantly improve initial fixation when compared with interference-fit technique.

The glenoid component has been at the centre of discussion around prosthesis fixation in TSA [55, 56, 279], but the humeral implant has also raised doubts on his own [257, 258]. To try to overcome those, several developments have occurred in humeral component fixation [256, 280] and on humeral stem design [45, 53], as seen in Chapter 1. Nevertheless, loosening and movement of uncemented humeral components with standard stem sizes is a reality [257]. In the study of Sanchez-Sotelo *et al.* [257] more than half of the humeral components (55.6%) were considered at risk for loosening.

The use of short-stem humeral components has been promising [44, 259, 260], with better clinical outcomes than those of standard-stem sizes. Jost *et al.* [44] presented, in 2011, the first clinical outcomes of short-stem humeral implants with the review of 40 Biomodular Shoulder Components and of 15 Comprehensive Shoulder Systems, both from Biomet Inc. (Warsaw, Ind) (as the one used in this thesis). The FEM of the implanted shoulder developed in our study was made considering inclination of the stem, after observing that the humeral stem was introduced with some degree of tilting in the *in vitro* arthroplasty performed in our laboratory. It was interesting to note that there was a 5% incidence of humeral stem inclination on the shoulders analysed by Jost *et al.* [44] and that this degree of inclination did not seem to affect the outcome results. Subsidence and changes in implant position were not observed.

Schnetzke *et al.* [259], on a clinical study with an Aequalis Ascend Monolithic Humeral Component, claim that the results obtained with a short-stem component are better than those obtained with a standard stem size, as loosening, subsidence and osteolysis were not identified on the radiographic analysis at 2 years after surgery, despite the presence of cortical thinning and loss of bone density (82.7% in the medial region, close to the humeral calcar), which are considered signs of stress shielding. These results are in accordance with our findings, since the FEM could preview cortical thinning and bone loss in similar areas than those observed clinically. However, the bulk humeral stem used by Schnetzke *et al.* [259] promotes load transfer mainly in regions L1 and M1, while the Comprehensive Humeral Stem presents higher stresses mainly at region M1.

Recently, Morwood *et al.* [271] performed a comparative study between proximally coated and uncoated short-stem humeral implants and analysed its influence on the clinical outcomes. The mean follow-up study of 27.3 months revealed that uncoated stems seem to be at greater risk for loosening, being in accordance with the study of Casagrande *et al.* [281]. In our study, the humeral prosthesis used is coated on the proximal region and the high stress and strain distribution at the base of the implant could indicate subsidence, observed in only 1 shoulder (2.9% of a total of 34) in the clinical study of Morwood *et al.* [271]. Unfortunately, no radiographic images are available for comparison with the results numerically obtained with the FEM regarding loos of bone density and cortical thinning.

Nonetheless, strain distribution in most of the proximal humerus is within the interval considered as normal physiological loading, indicating that the proximally coated short-stem component is an option for uncemented humeral fixation, as it will not obstruct the integrity of bone density.

Micromotions of the humeral component are higher than 250 μm in all aspects (anterior, posterior, medial and lateral) and are probably too higher to allow bone ingrowth [273] on the regions analysed. This indicates the likelihood of subsidence of the prosthesis, but this effect was not observed clinically in proximally coated implants [44, 259, 260]. One possible explanation could be related with the friction coefficients considered to simulate the contact between the humeral stem and the trabecular bone. Additional studies would have to be performed to evaluate if the use of different friction coefficients could replicate better the micromotion of the humeral component. No studies on this issue where found in literature.

5.5 Conclusions

The FEM developed simulates the behaviour of a shoulder joint implanted with an anatomical total shoulder implant, with a porous coated central fixation post for glenoid fixation and with a porous-coated short-stem humeral component.

The results of the FEM agree with what is observed clinically, especially for the glenoid component, allowing us to preview the joint behaviour on the short/medium-term and on the long-term. However, we should point out that micromotions of the humeral component are not in accordance with clinical observations for short-stem implants, as micromotions determined with the FEM indicate the possibility of subsidence and this phenomenon was not observed clinically, even though bone loss and cortical thining are observed both clinically and numerically. This may be related with numerical conditions adopted on the FEM, mainly related with the friction condition considered.

The FEM can be considered a pre-clinical test to analyse the performance of shoulder implants, as will be discussed in the next chapter.

Chapter 6

Pre-Clinical Test to Discriminate Shoulder Performance

6.1 Introduction

Joint prosthesis are used at a global scale and thousands are implanted in the most developed countries every year [187, 282]. With the popularity of hip and knee replacements, shoulder arthroplasty has been gaining space and many prosthesis concepts and designs have appeared on the market, as discussed in Chapter 1.

Despite the good results that some designs present, glenoid loosening is still pointed as a major concern in anatomic shoulder arthroplasty, in both cemented and uncemented procedures. Furthermore, the use of uncemented humeral fixation in standard-stem implants led to humeral fracture upon impaction and loosening, which ultimately may lead to subsidence or proximal migration of the humeral component [256, 257]. Meanwhile, uncemented short-stem humeral implants have appeared [259, 260], presenting better clinical outcomes than the standard stems, with no signs of subsidence. Nonetheless, to try to avoid these and other implant-related problems, the prostheses need to be properly tested before entering the market.

As seen in Chapter 1, arthroplasty registers are the most used tool to evaluate prosthesis efficacy but at the expenses of patients' health, as those studies are conducted after prosthesis implantation and problems are mainly detected after many years of use. This brings to the table several complications to the patients, since a revision surgery is eventually needed. Besides, financial issues are added to the equation as a primary arthroplasty surgery is an expensive procedure, but so it is a revision one.

Nevertheless, prostheses are being tested before marketed and have been classified as class III medical devices by the European Union, meaning that there are a series of regulations (see Directive 93/42/CEE for further details) that a prosthesis must fulfil before it can be used in clinical practice. These regulations aim at ensuring prostheses safety but, in accordance with Prendergast and Maher [283], they do not evaluate prostheses efficacy, not being able to detect problems leading to an unsuccessful surgery.

Although new shoulder prostheses are being introduced on the medical market assuring better success rates, the reality shows that there continue to exist prostheses withdrawn. One such example is the SMR L2 Metal-Back Glenoid Component (Lima Orthopaedics), discontinued in 2012 after presenting higher than expected revision rates (https://www.tga.gov.au/alert/smr-l2-metal-back-glenoid-component-used-shoulder-replacements, accessed 29/July/2017). Early this year (February 2017), the Comprehensive Reverse Shoulder System (Zimmer Biomet) was recalled from market after presenting high fracture rates (https://www.fda.gov/MedicalDevices/Safety/ListofRecalls/ucm541862.htm, accessed 29/July/2017). These and other recent cases corroborate our conviction that the directives applied are not evaluating the efficacy of joint replacement prostheses and that robust pre-clinical testing is mandatory. Due to the implications of this problem on public health, it is imperative to understand and evaluate the causes of failure of shoulder

prosthesis to find the most reliable solutions. Thus, the main goal of this thesis was to develop a pre-clinical test that can predict shoulder prosthesis performance on the short/medium-term and on the long-term after implantation.

6.2 A New Fixation Post

On this chapter, a new central fixation post (called *PE-fixation-post*) (see Figure 5.1 (B)), was used to verify that the pre-clinical test purposed is sensitive to small differences in implant design and that the test can predict implant performance. The *PE-fixation-post* is built in polyethylene with a central titanium core and is an option of the Comprehensive Total Shoulder System (Biomet) used in this research. Surgeons are free to choose between the *PE-fixation-post* and the porous titanium fixation post (*Ti-fixation-post*) based on their experience, on host trabecular bone conditions and by personal preferences.

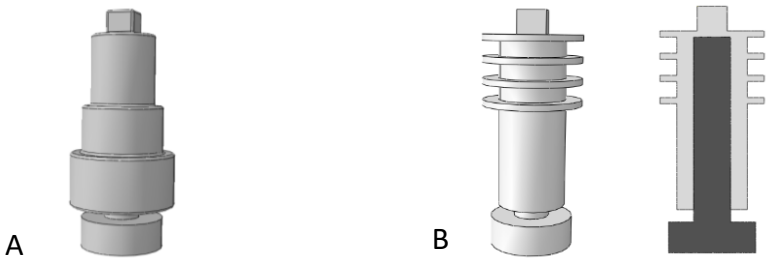

Figure 6.1. Central fixation posts used to test the pre-clinical test purposed. A: porous titanium post; B: polyethylene post, with evidence of the titanium core.

The influence of the *PE-fixation-post* will be discussed next. Stress and strain distribution will be compared with clinical findings and the long- and short-term results will be presented. Subsequently, the results will be compared with those obtained with the *Ti-fixation-post* (presented in Chapter 5) to prove that the pre-clinical test purposed can predict implant performance, even with small differences in prosthesis designs.

6.2.1 Clinical Outcomes

Wilde *et al.* [274] analysed, for the first time, the clinical and radiographic outcome results of 34 shoulders implanted with a fully uncemented pegged glenoid component and with a fully uncemented humeral component (Anchor Peg Glenoid Component, Global Advantage Humeral Prosthesis, DePuy, Warsaw, IN, USA). The patients were followed during a mean of 28.3 months (short-term analysis). All parameters evaluated preoperatively increased after surgery and there were no signs of loosening in 88% of the

observed cases. Additionally, signs of bone ingrowth were identified in 79% of cases. Figure 6.2 (A) presents a CT-scan that shows bone ingrowth around the central fixation post and around the superior fixation peg. Figure 6.2 (B) shows an example were loosening and the lack of bone ingrowth around the central fixation peg is evident.

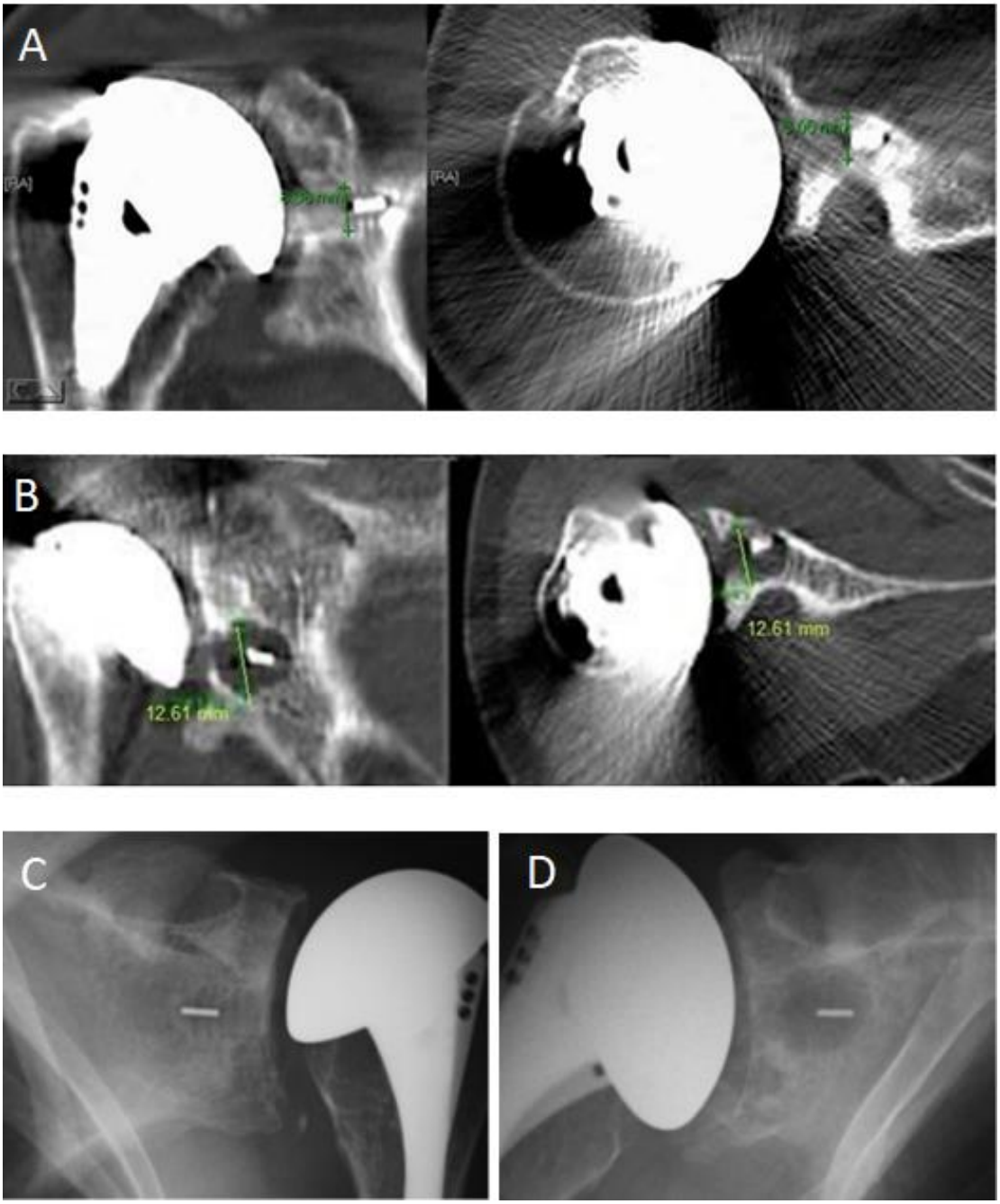

Figure 6.2. CT-scan of shoulders implanted with the Anchor Peg Glenoid Component. A and B adapted from [274]; C and D adapted from [70]. A and C present bone ingrowth around the flanges of the central post, not observed on B and D.

Other authors [70, 74, 277] have used the Anchor Peg Glenoid Component with cement on the peripheral fixation pegs and without cement on the central post. Churchill *et al.* [70] reviewed 20 shoulders and at the 5-year follow-up (medium-term analysis) 75% of them presented bone around the flanges of the central fixation post. Figure 6.2 (C and D) presents examples of CT-scans analysed in the study of Churchill *et al.* [70], where bone ingrowth was observed between the flanges in case (C) and no bone was observed in case (D). Vidil *et al.* [277] analysed 26 shoulders during a mean of 4 years. Postoperatively, shoulder motion measurements improved and 1 year after surgery 81% presented tissue integration and bone ingrowth around the central post. In yet another study, Groh *et al.* [74] identified evidence of bone ingrowth in 29% of the cases revised.

Parks et at. [58] performed a short- to medium-term follow-up study with the Affiniti CortiLoc Glenoid Component (Tornier, Inc., Edina, MN, USA), finding evidence of bone ingrowth around the central peg on 88.2% the cases reviewed.

In 2015, Noyes *et al.* [284] presented the longest average follow-up study (5- to 10-years, middle-term results) using a partially cemented glenoid component (DePuy Global Advantage, DePuy, Warsaw, IN, USA). The analysis was performed in 42 patients. At the final follow up, the average forward elevation and external rotation improved (from 107° to 137° and from 30° to 37°, respectively) and a 97% survivorship rate was observed. Bone ingrowth around the fluted central peg, with no lucent lines, was observed in 81% of the implants. Unfortunately, no radiographic images were available in [284].

6.3 Numerical Results

The FEM of the implanted shoulder, presented in Chapter 4, was used considering the *PE-fixation-post* in place of the *Ti-fixation-post*. All boundary and loading conditions were kept unchanged and the material properties of the new fixation post are in Table 6.1

Table 6.1. Material properties of the *PE-fixation-post*.

Structure	Young Modulus (GPa)	Poisson ratio
Titanium	110	0.3
Polyethylene	1	0.4

6.3.1 Clinical Predictions and Short-Term Post-Operative Scenario

The axial and coronal planes of a CT-scan of the Anchor Peg Glenoid Component of the study of Vidil *et al.* [277], and the maximum (A) and minimum principal (B) strain

distributions predicted by the FEM, on the short-term post-operative condition, for the same planes of interest, is presented on Figure 6.3. The several regions of interest were identified (numbered from 1 to 4 in the axial plane, and from 5 to 8 in the coronal plane), similarly to [60].

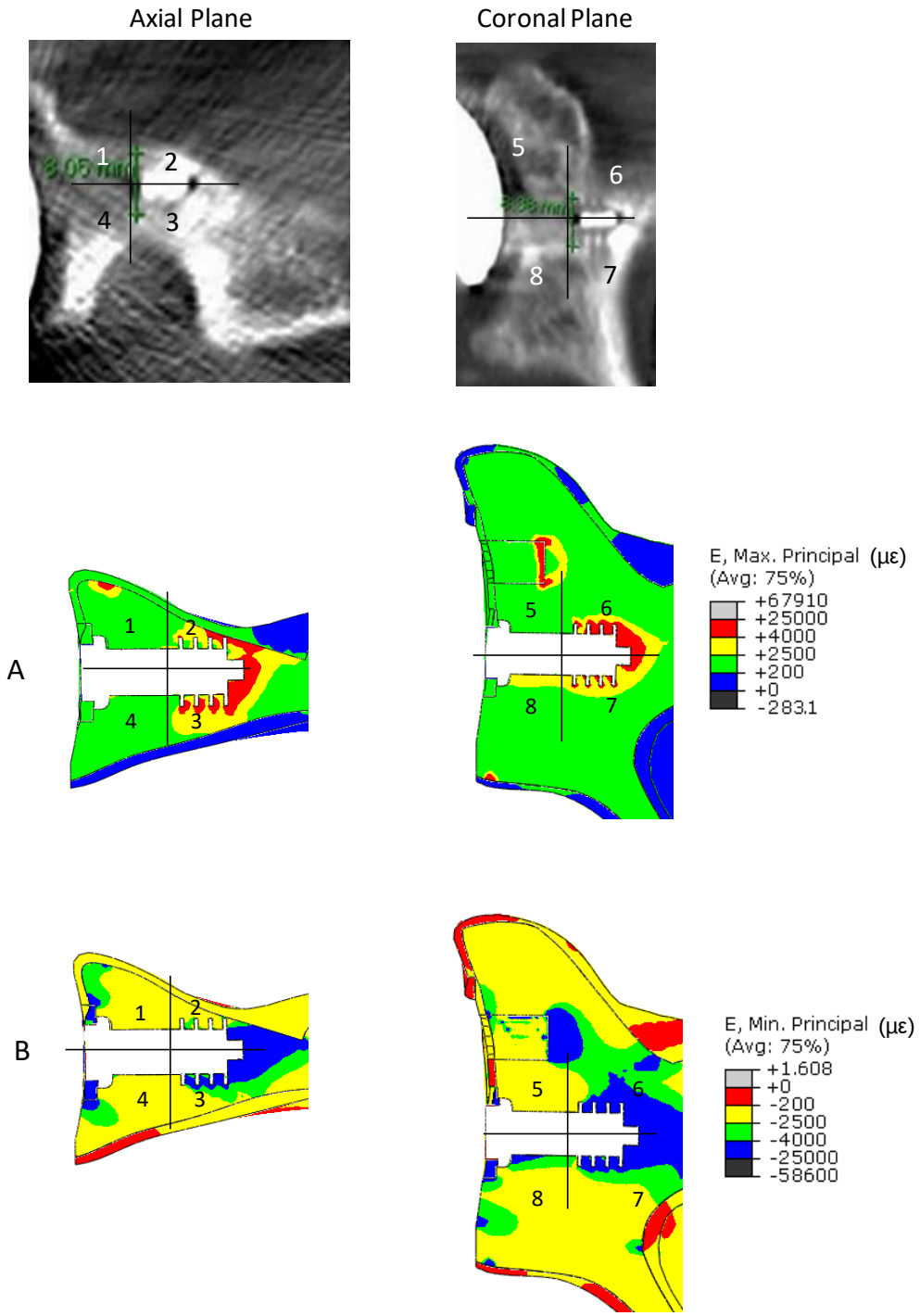

Figure 6.3. CT-scans (adapted from [274]) and the maximum (A) and minimum (B) principal strains on the short-term post-operative condition.

On the axial plane, the CT-scan shows evidences of bone ingrowth around and between the flanges of the central fixation post, especially on region 2 and 3, where strains are between (2500, 4000) με (yellow area in (A) and green area in (B)). Nevertheless, there are also regions were strains are higher ((4000, 25 000) με) (red area in (A) and blue area in (B)) and bone collapse may be observed [186].

On the coronal plane, the CT-scan shows evidence of bone ingrowth around and between the flanges of the *PE-fixation-post* and around the superior fixation peg (region 5). Maximum principal (A) and minimum principal (B) strain distribution is similar to that of the axial plane, that is: some areas prone to bone ingrowth and others to bone collapse, mainly located on regions 6 and 7. The model also previews bone density augmentation around the *PE-fixation-post* in region 8, being in accordance with what was observed on the CT-scan in the same region, as a brighter area is observed around the central post, indicating the presence of denser bone. On the superior fixation peg (region 5), strain distribution is such that bone density augmentation may be observed, as well as bone collapse due to fatigue. This is in accordance with the observed in the CT-scan of Figure 6.3, where there is a clear periphery of higher bone density around the fixation peg.

In the remaining cavity, strain distribution is inside the interval of normal physiologic bone loading ((≈ 200, 2500) με [186]), but there are smaller areas where bone remodelling with density augmentation and bone collapse due to fatigue may be observed.

Strain distribution that can promote bone remodelling with density augmentation ((2500, 4000) με) is clinically related with the evidence of bone around the fixation pegs. This has been observed in all clinical studies related with uncemented or minimally cemented all polyethylene glenoid components. De Wilde *et al.* [274] on the evaluation of fully uncemented glenoid components found no signs of loosening on 30 patients (88%), and found evidences of one or more bone flanges at the central post in 27 patients (79%). Parks *et al.* [58] found evidences of bone around the periphery of the flanges of the central post and increased radiodensity in between those flanges in 38 shoulders (50%). In 38.2% of cases evidences of bone around the central peg where found, but no signs of increased radiodensity between the flanges. In only 9 shoulders (11.8%) there was bone density decrease and osteolysis around the central post. Vidil *et al.* [277] found complete bone integration around the peg flanges of the central post in 21 shoulders (78%) and only peripheral bone integration in four. In yet another study, Groh *et al.* [74] found 24 shoulders (29%) with evidences of bone between the flanges of the central post and no signs of radiolucency were observed.

Strain areas where bone collapse is possible to be observed ((4000, 25 000) με) can be clinically related with the existence of radiolucent lines around the fixation pegs. De Wilde *et al.* [274] found radiolucency in only 4 patients, while Parks *et al.* [58] found 62 shoulders (81.6%) with no or small evidences of radiolucent lines (grade 0 or 1 according with [285]) and 14 shoulders (18.4%) with clear to severe evidences of radiolucent lines (graded 2 to 5

according with [285]). In another similar study, Vidil *et al.* [277] found radiolucent lines in 3 shoulders (11%).

The numerical predictions of the FEM show that even though there are regions where strain distribution is such that there is a possibility of bone collapse due to fatigue, there are also other areas where strains may promote bone remodelling with density augmentation, especially close to and around the central and superior fixation pegs. As demonstrated, this is in accordance with the clinical observations that indicate bone ingrowth between and around the flanges of the central fixation post, but also regions of radiolucency. According with the analysis, the developed pre-clinical test can simulate the behaviour of the bone structure as observed clinically, and indicates that the *PE-fixation-post* seems to be an option for uncemented glenoid fixation in total shoulder arthroplasty, with encouraging short/medium-term post-operative results.

6.3.2 Long-Term Post-Operative Scenario

To simulate the long-term post-operative scenario, the FEM was altered so that the prosthesis and the surrounding bone tissue were considered perfectly bonded to each other, with no friction condition between the interface bone/implant.

The strain distribution at the trabecular bone on the long-term is presented in Figure 6.4. The same figure also presents the strain distribution on the short-term, for comparison.

On the long-term, the maximum (A) and minimum (B) principal strains inside the glenoid are mainly between (200, 2500) με in both axial and coronal planes (green area in (A) and yellow area in (B)). Still, on the axial plane, high ((2500, 25 000) με) maximum (A) and minimum (B) principal strains are observed close to the flanges of the central post (region 2 and 3) where bone remodelling (yellow area in (A) and green area in (B)) or bone collapse (red area in (A) and blue area in (B)) can occur [186]. These strain distributions were present also on the short-term condition, but in larger areas. On the long-term, particularly on region 4, there is an area (red area) where minimum principal strains are smaller than -200 με, meaning that bone is not sufficiently stimulated and resorption can be observed [186]. On the coronal plane, critical minimum principal strains close to the central post were identified, where bone remodelling and bone collapse can be observed.

The predictions of the FEM indicate that the *PE-fixation-post* is a good option for prosthesis fixation and that bone integrity is preserved despite the implant. In literature, the longest clinical follow-up of a bone-ingrowth all-polyethylene glenoid component was performed by Noyes *et al.* [284]. The average follow-up was of nearly 7 years (medium-term study) and 97% survivorship rate was determined, with 81% of the implants presenting bone ingrowth around the flanges of the central peg with no lucent lines.

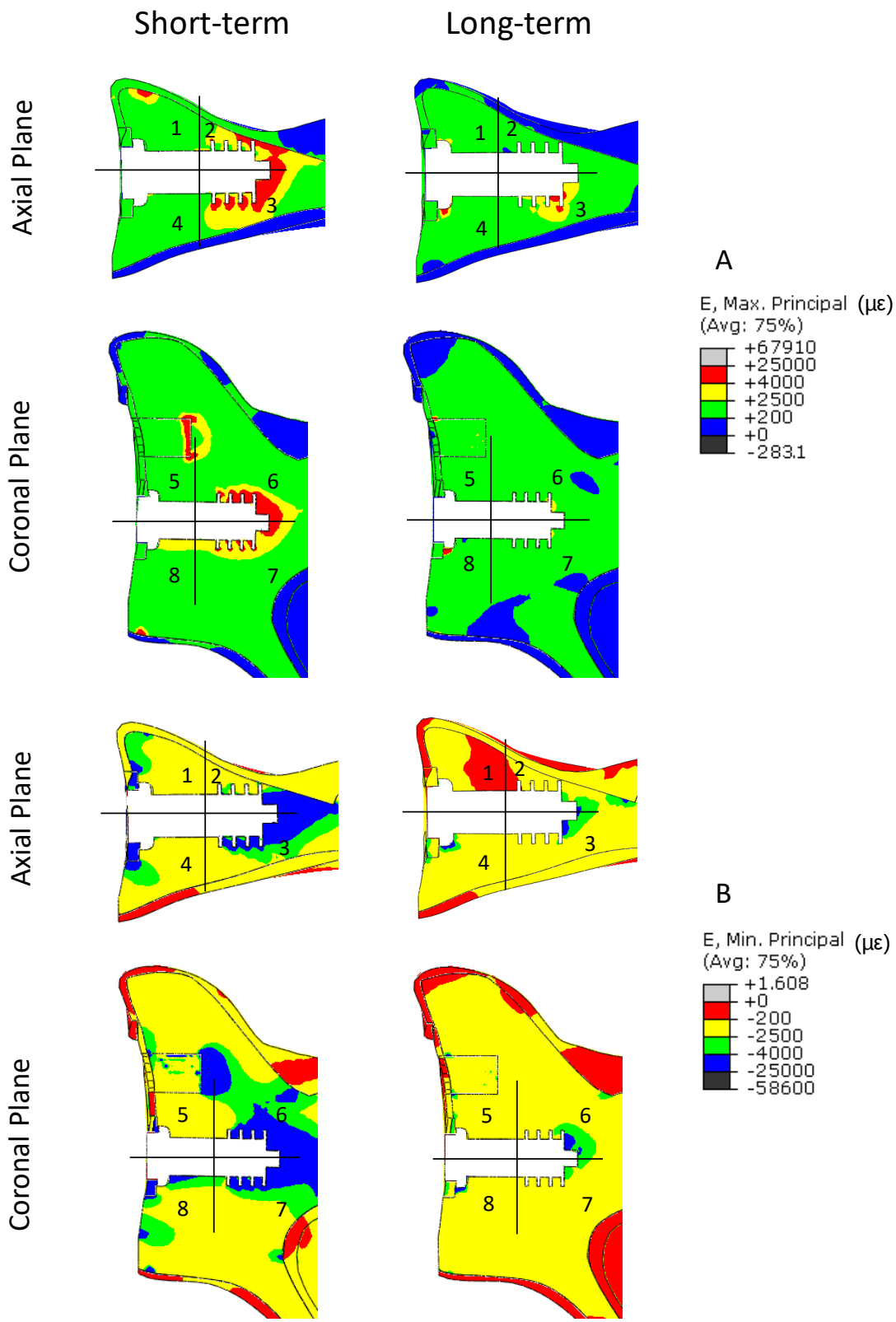

Figure 6.4. Maximum principal (A) and minimum principal (B) strain distribution on the glenoid cavity for the short-term and long-term post-operative conditions.

6.3.3 Stress Distribution on the Short and Long Term

The stress distribution of the trabecular bone, on the intact and implanted glenoid, is shown in Figure 6.5. The short- and long-term post-operative conditions are represented.

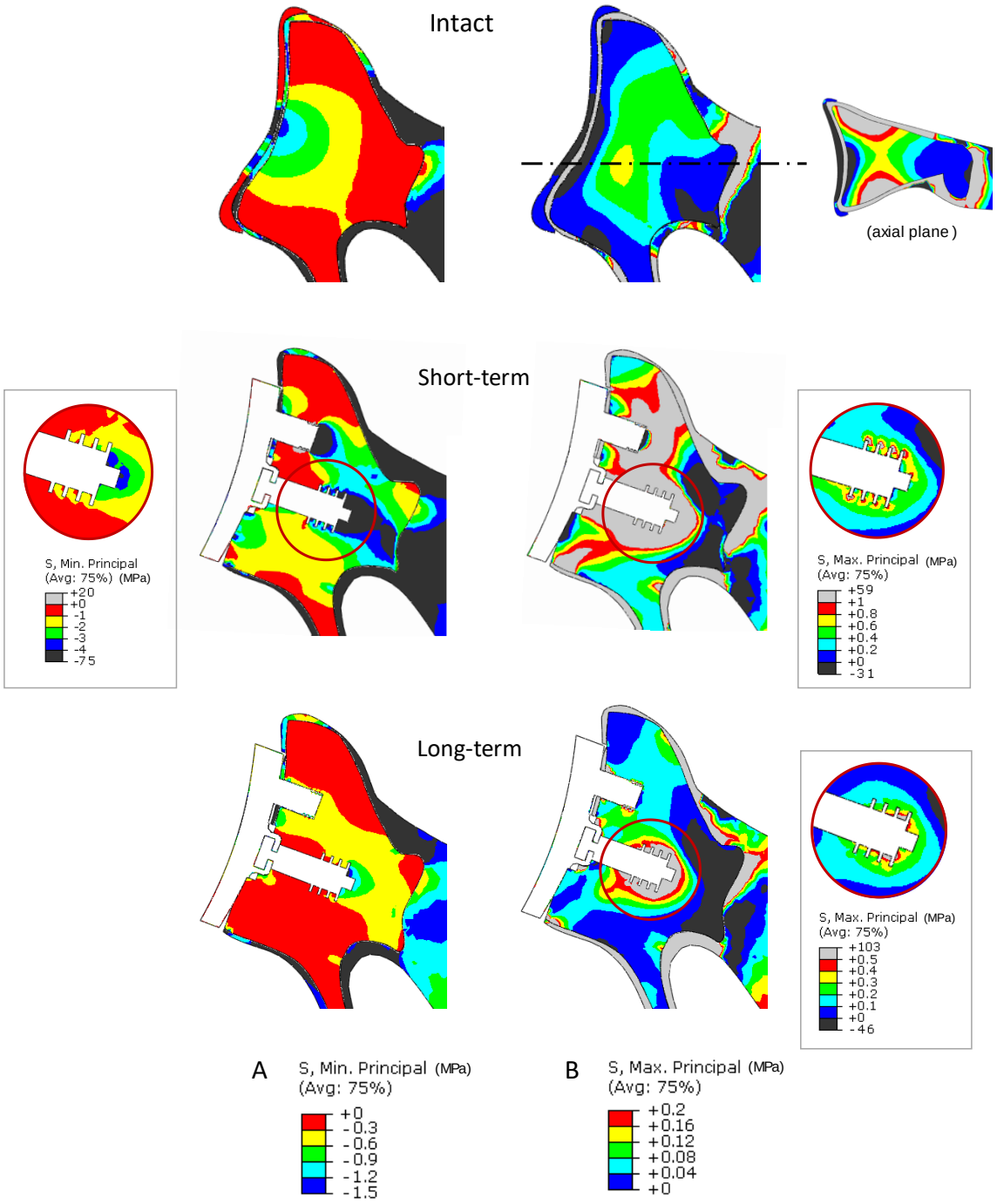

Figure 6.5. Minimum (A) and maximum (B) principal stress distribution on the glenoid cavity for the intact, short-term and long-term post-operative conditions, at the coronal plane.

On the intact glenoid, the maximum principal stresses (Figure 6.5, B) are mainly between (0, 0.16) MPa. However, as shown by the detail of the axial plane, stresses are higher closer to the anterior and posterior regions of the cavity. The minimum principal stresses (Figure 6.5, A) are mainly between (0, -1.5) MPa.

After the glenoid component is implanted (Figure 6.5, short-term) the trabecular bone presents maximum principal stresses (B) higher than when intact. Around the flanges of the central peg, stress can reach 1 MPa (and higher). Regarding the minimum principal stresses (A), those are mainly in the same interval as in the intact condition, but around the fixation pegs they can reach between (-1, -4) MPa. This behaviour indicates that the stress shielding phenomenon seems to be prevented with the use of an all-polyethylene pegged glenoid component with central flanges, and bone is stimulated to promote bone growth. This is a good indicative of the possible success of the glenoid prosthesis, since stress distribution before and after prosthesis implantation should be similar. The predictions of the FEM are in accordance with the clinical outcomes discussed earlier, that confirms bone ingrowth around the peg flanges in most all short-term studies.

On the long-term post-operative condition (Figure 6.5, long-term), the interval of stress distribution previewed by the FEM is equal to that of the intact condition for both maximum (B) and minimum (A) principal stresses, except around the flanges of the central *PE-fixation-post*, where maximum principal stresses can reach 0.5 MPa. This indicates that on the long-term the trabecular bone suffers stresses that allow bone integrity and density augmentation around the central fixation post, and that despite the implant, stresses are in the same interval as in the intact condition, which is desirable to bone integrity. These results are in agreement with what was observed by Noyes *et al.* [284] on their medium-term study (5- to 10-years follow-up): 81% of bone ingrowth around the flanges of the central fixation post. Longer follow-up studies are preferable for comparison with the FEM prediction, but longer studies are not available yet.

6.3.4 Porous-surfaced fixation post vs all-polyethylene fixation post

The pre-clinical test purposed can predict shoulder implants performance on the short- and long-terms. The numerical results it presents are in accordance with clinical findings available in literature, especially concerning bone ingrowth around the central fixation post. In the present section, the short-term numerical predictions obtained for both central fixation posts analyzed is presented in Figure 6.6 for comparison. On the *Ti-fixation-post*, regions of bone ingrowth ((2500, 4000) με) and of bone collapse ((4000, 25000) με) are found around the entire structure. On the contrary, those are concentrated mainly at the flanges of the *PE-fixation-post* (regions identified with numbers 2, 3, 6 and 7 in Figure 6.6). This suggests that the *Ti-fixation-post* is a better option since it allows new bone to grow around its entire porous surface, promoting better implant fixation.

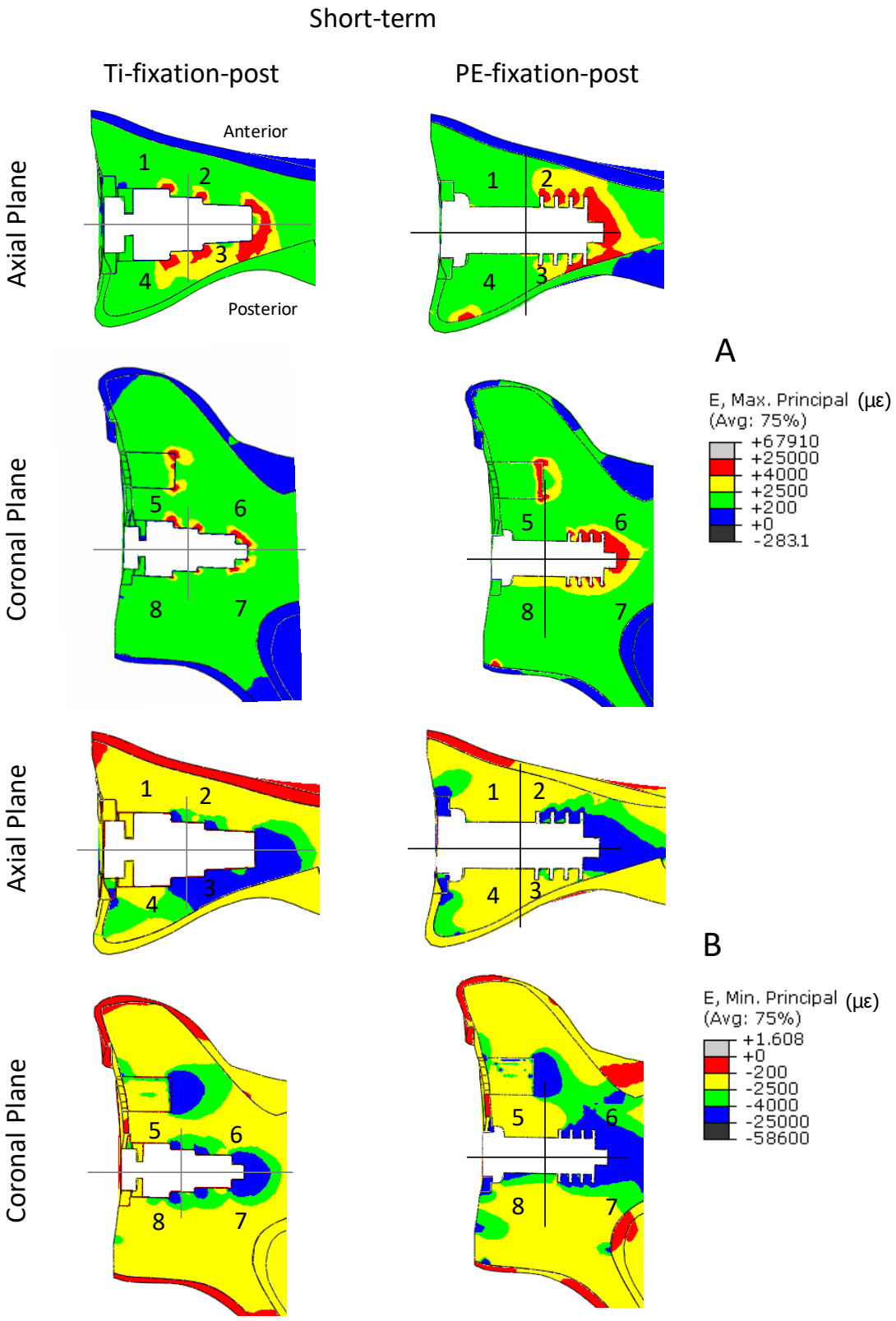

Figure 6.6. Comparison between strain distribution on the short-term for the central fixation posts analysed. A: maximum principal strains; B: minimum principal strains.

The strain distribution on the cortical bone surface was determined at the periphery of the glenoid cavity for the intact model and for the two implanted models. It is represented on the graph of Figure 6.7. The intact model shows to distinct regions of high strain distribution, that appear on the posterior and anterior sides of the cortical bone. When the implant is present, strains are mainly on the posterior side.

The presence of the IGHL on the inferior region does not seem to have a major influence on strain, as maximum and minimum principal strains are similar between the three models evaluated. Regarding the strain distribution in the model with the *Ti-fixation-post*, they are closer to the strain distribution of the intact model, which is an indicative that the use of porous titanium seems to be a better solution for implant fixation.

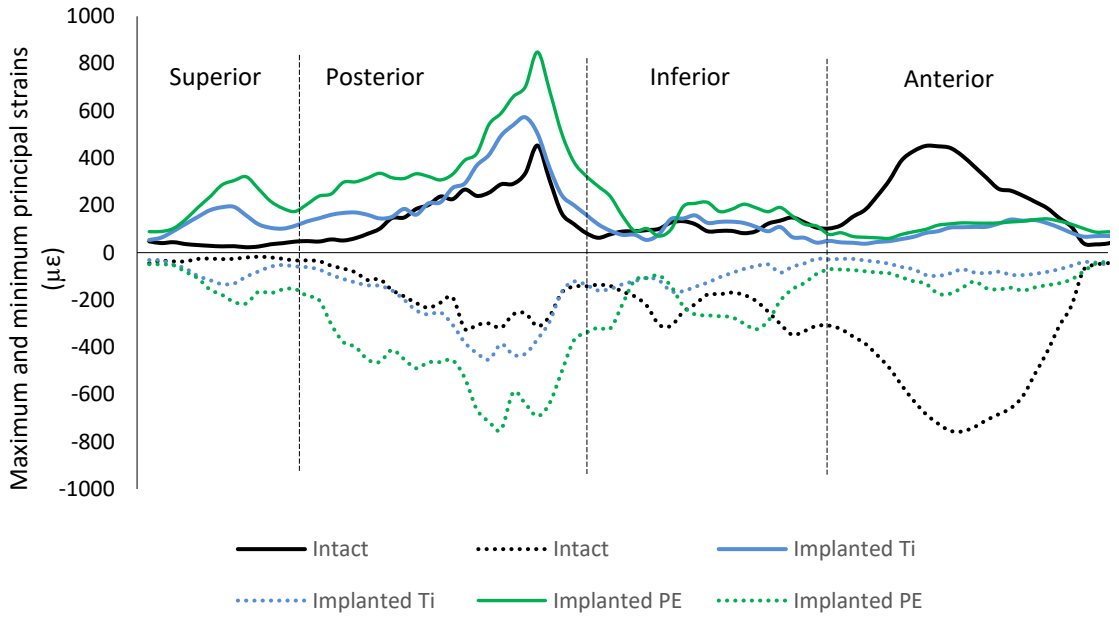

Figure 6.7. Maximum and minimum principal strain distribution on the cortical surface of the glenoid component on the intact and implanted models.

6.4 The Purposed Pre-Clinical Test

Pre-clinical testing of shoulder implants can be accomplished by means of laboratory bench testing, animal experimentation and computational modelling, that combine to form a pre-clinical testing platform [283]. In the present thesis, we propose a pre-clinical test based on computational modelling.

The Comprehensive Total Shoulder System (Biomet©) was used, comprising a humeral steam, a humeral head, a glenoid base and central fixation post. The humeral implant was designed for the uncemented procedure and the glenoid implant for the minimally

cemented procedure. However, some clinicians use similar glenoid components with the uncemented technique and so it was chosen in the development of the pre-clinical test.

To develop a computational pre-clinical test to infer on the short- and long-term performance of an anatomical total shoulder prosthesis, we purpose the following procedure:

1. When building the CAD models of the several bone structures, consider appropriate models, especially on the glenoid cavity, since the material properties of the trabecular bone structure differ greatly from those of the cortical bone structure;

2. Test the implanted joint with the several bone structures placed on a 90° abduction, as this is considered, and verified, the most critical position for the loaded shoulder;

3. Consider the influence of the following muscles: deltoideus (2 muscle segments), supraspinatus, infraspinatus and subscapularis (1 muscle segment for each rotator cuff muscle), as these are considered, and verified, the most important muscles in shoulder abduction;

4. Use the subsequent muscle forces: deltoideus 300 N (150 N for each segment), subscapularis 225 N, infraspinatus 120 N, supraspinatus 90 N, that were calculated by means of a multi-body model of the intact shoulder, and agree with literature;

5. To validate the FEM developed, an *in vitro* model of the intact and implanted joint should be built with synthetic bone structures, placed in a 90° abduction and loaded with the same muscle forces. Strain-gage sensors should be placed on the anterior and posterior sides of the glenoid cavity and of the proximal humerus, so that strain predicted by the FEM can be compared with strain determined experimentally. We suggest 3 strain gages on the anterior and on the posterior regions of the glenoid, close to the implant, so that the influence of the peripherical fixation pegs could be assessed. On the humeral side, we suggest 1 strain gages at each aspect (anterior, posterior, lateral and medial) close to the humeral head cut, and 2 closer to the tip of the humeral shaft, on the anterior and lateral aspects, since the humeral shaft could be implanted in valgus or varus position, as observed clinically (see Figure 6.8).

6. To simulate the short-term post-operative condition, consider friction between all bone /implant interfaces;

7. To simulate the long-term post-operative condition, consider all bone/implant interfaces perfectly bonded with each other;

8. Analyse stress/strain distribution at the trabecular bone structures to identify the main areas of bone ingrowth/ongrowth and of bone loss.

9. When friction is present, analyse micromotions of prosthetic components to evaluate if their magnitude can help to promote or to suppress bone ingrowth/ongrowth.

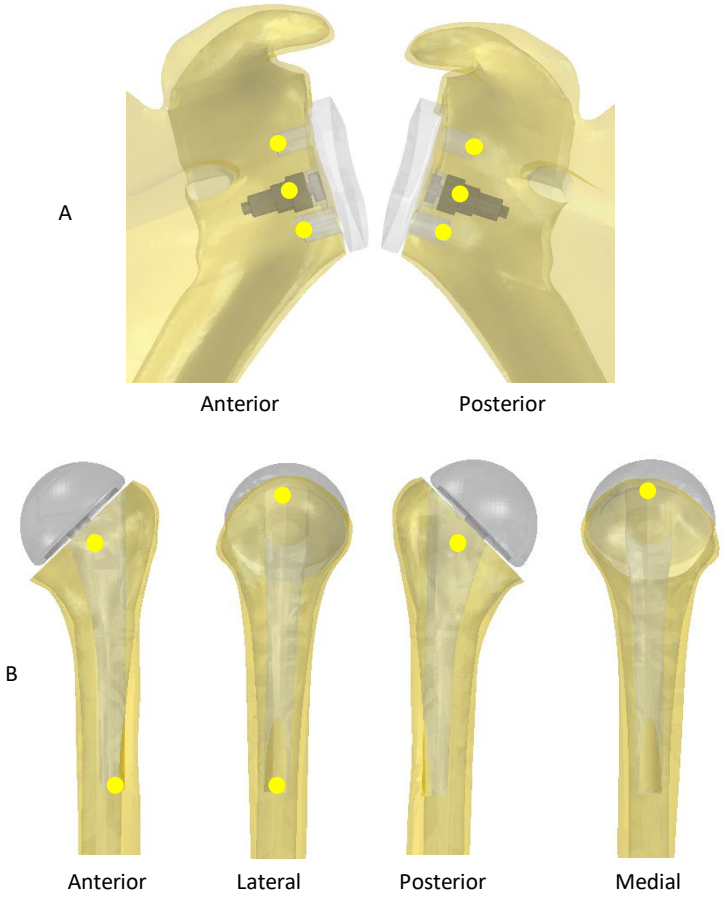

Figure 6.8. Suggested positions for the strain gages on the scapula (A) and humerus (B). The several aspects are shown.

6.5 Conclusion

The results of the FEM using the new central fixation post are in accordance with the clinical findings. This confirms that the pre-clinical test developed can predict shoulder implant performance with small design differences and that the strategy used for the development of the pre-clinical test can be employed on the study of other shoulder implants before *in vivo* clinical trials.

Chapter 7

Conclusions and Future Developments

7.1 Conclusions

In a general way, the objective of developing a pre-clinical test to preview the short- and long-term performance of anatomical total shoulder prostheses, was achieved.

For the pre-clinical test purposed, experimental and numerical models of the intact and implanted shoulder were developed and the numerical results were compared with the clinical data available. Our results are in accordance with the clinical evidences of bone in/ongrowth around the fixation pegs of the glenoid implant and in some areas of the humeral stem implant. The Comprehensive Total Shoulder System (Biomet©) was used, comprising a humeral stem (with a proximally coated porous-surface), a humeral head, a glenoid base and two central fixation posts (one in titanium porous-coated and one in polyethylene with titanium core). The uncemented technique it was chosen for the pre-clinical test development.

To define the pre-clinical test, we initially determined which movement is considered critical for the shoulder joint. The literature was analysed and despite the few studies on this matter, we concluded that the most critical movement for the shoulder is when loaded in abduction/adduction. The construction of the pre-clinical test included the modelling of shoulder muscle actions using a multibody model of the intact shoulder, with the goal of determining the muscle-force contribution during the adduction/abduction movement. This allowed us to evaluate the importance of the muscles and to identify the most relevant ones (deltoideus, subscapularis, supraspinatus, infraspinatus, trapezius and levator scapulae). The muscle forces determined were posteriorly used in the implanted models of the joint. This raises the question of whether the equilibrium of forces determined with the multibody model would be altered by the presence of a prosthesis. Nevertheless, anatomical shoulder prostheses, as the one used in this study, are designed not to alter the rotation centre of the shoulder joint and thus it is expected that the equilibrium of forces would be maintained. Even though this study does not bring novelty, it was relevant for our understanding of joint functioning and of the complex relationship between all structures composing it.

The study comprised the development of experimental models of the intact and implanted shoulder joint using composite bone structures and an anatomical shoulder prosthesis. The construction of a shoulder simulator that could hold the bone structures in the appropriate position (90°abduction) was also accomplished. The validation of both intact and implanted FEM using strain gage data was successful, but in future validation studies of other implants more sensors should be used.

The pre-clinical test developed is based on a FEM of the implanted shoulder joint. One of the most important aspects in the development of (any) FEM is that it should replicate, as accurately as possible, the corresponding experimental model, so that the validation can be successful. As referred before, FEM validation was achieved, but the correct positioning

of the bone structures was a challenge overcome, since the model under study comprises two bone structures with a high degree of freedom, and its positioning to replicate the experimental model was a somewhat demanding process.

For the FEM model to replicate the clinical results it is necessary that the interactions between the prostheses and the surrounding bone are correctly defined. This means that it is necessary to consider the several phases of prosthesis fixation into the bone, being that the clinical short-term scenario differs from that of the long-term, as it is observed in several clinical studies through CT-scan evaluation. Thus, two scenarios were analysed: a short-term condition where friction is considered on the bone/implant interface, and a long-term condition without friction. This distinction is a fundamental aspect in the FEM of implanted joints, since the results revealed to be very distinct between each other and the frictionless condition differs from what is clinically observed on short-term CT-scan analysis. This differs from what is usually done in other studies, where much of the FEM models, maybe for simplicity, do not consider friction between the several components. In those cases, the studies can only indicate long-term tendencies of prosthesis behaviour. However, it is mandatory to understand the short-term behaviour, as it is in this period that an appropriate prosthesis fixation will be determined. Nevertheless, we should ask ourselves what is considered a "short-term" post-operative period, since the rehabilitation is not only related with the type of prosthesis used but also, and maybe more important, with host bone quality, with the muscular structure conditions and with the willingness of the patient to actively participate in the entire rehabilitation process.

By comparison between the clinical predictions available in literature for the short-term condition and the results obtained by the FEM (particularly stress/strain distribution and prostheses micromotions), we conclude that the developed model allows the prediction of the short-term behaviour of the prostheses studied, specially of the glenoid component, since the micromovement of the humeral prosthesis were high, which was not expected in a porous-coated prosthesis. More specifically, the model can predict zones of bone growth, which agree with the clinical findings. On the long-term, the model previews that the prosthesis is well-fixed to the surrounding bone, with most strains being inside the interval considered of normal physiological loading. Since the glenoid component used in this study is relatively new, there are no available clinical studies on the long-term post-operative condition for comparison with our results.

The study included the analysis of the behaviour of two distinct central fixation posts, one in porous titanium and other in polyethylene. The pre-clinical test developed made the distinction between the two components regarding stress/strain distribution. The results suggest that the titanium fixation post allows that the strain distribution inside the glenoid cavity and at the cortical periphery to be closer to the observed in the intact model.

7.2 Future Developments

It is intended that the tools developed in the scope of this thesis can be used and improved in future studies. In this sense, the following developments are purposed:

- Improve the experimental system developed to allow dynamic analysis and to include a cumulative damage mechanism;

- Perform FE analysis with the pre-clinical test developed using different implant fixation types, such as cemented and hybrid, so to study all fixation types used clinically;

- Use the pre-clinical test developed to study a larger group of shoulder prostheses, mainly those well- established on the market, to verify if the pre-clinical test purposed can help to identify the best and worst prosthesis;

- Improve the pre-clinical teste developed including the possibility to study damage through the existence of a cumulative damage mechanism.

Bibliography

[1] L. S. Lippert, "Shoulder Joint," in *Clinical Kinesiology and Anatomy*, Fourth Edi., Philadelphia: F. A. Davis Company, 2006.

[2] G. M. Gartsman and T. B. Edwards, "Evolution of Shoulder Arthroplasty," in *Shoulder Arthroplasty*, First Edit., Philadelphia: Sauders, Elsevier, 2008.

[3] E. Itoi, B. F. Morrey, and K. An, "Biomechanics of the Shoulder," in *The Shoulder - volume 1*, Fourth Edi., C. A. Rockwood Jr. and F. A. Matsen III, Eds. Philadelphia: Sauders, Elsevier, 2009.

[4] M. McKinley and V. D. O'Loughlin, "Articulations," in *Human Anatomy*, Third edit., New York: McGraw-Hill, 2012.

[5] P. K. Levangie and C. C. Norkin, "The Shoulder Complex," in *Joint Structure and Function: a comprehensive analysis*, Third Edit., Philadelphia: F. A. Davis Company, 2001.

[6] L. S. Lippert, "Shoulder Girdle," in *Clinical Kinesiology and Anatomy*, Fourth Edi., Philadelphia: F. A. Davis Company, 2006.

[7] M. McKinley and V. D. O'Loughlin, "Appendicular Muscles," in *Human Anatomy*, Thirth Edi., New York: McGraw-Hill, 2012.

[8] H. Mcguinness, *Anatomy & Physiology therapy basics*, Fourth Edi. Hodder Education, 2010.

[9] L. S. Lippert, "Articular System," in *Clinical Kinesiology and Anatomy*, Fourth Edi., Philadelphia: E. A. Davis Company, 2006.

[10] J. M. Soucie, C. Wang, A. Forsyth, S. Funk, M. Denny, K. E. Roach, and D. Boone, "Range of motion measurements: reference values and a database for comparison studies," *Haemophilia*, vol. 17, no. 3, pp. 500–507, 2011.

[11] J. Aizawa, T. Masuda, T. Koyama, K. Nakamaru, K. Isozaki, A. Okawa, and S. Morita, "Three-dimensional motion of the upper extremity joints during various activities of daily living," *J. Biomech.*, vol. 43, no. 15, pp. 2915–2922, 2010.

[12] S. Namdari, G. Yagnik, D. D. Ebaugh, S. Nagda, M. L. Ramsey, G. R. Williams, and S. Mehta, "Defining functional shoulder range of motion for activities of daily living," *J. shoulder Elb. Surg.*, vol. 21, no. 9, pp. 1177–1183, 2012.

[13] T. J. Grewal and C. R. Dickerson, "A novel three-dimensional shoulder rhythm definition that includes overhead and axially rotated humeral postures," *J. Biomech.*, vol. 46, no. 3, pp. 608–611, 2013.

[14] X. Xu, J. hua Lin, and R. W. McGorry, "A regression-based 3-D shoulder rhythm," *J. Biomech.*, vol. 47, no. 5, pp. 1206–1210, 2014.

[15] V. T. Inman, J. B. Saunders, and L. C. Abbott, "Observations on the function of the shoulder joint," *J. Bone Jt. Surg.*, vol. XXVI, no. 26–A, pp. 1–30, 1944.

[16] K. W. Farmer, J. W. Hammond, W. S. Queale, E. Keyurapan, and E. G. Mcfarland, "Shoulder Arthroplasty versus Hip and Knee Arthroplasties," *Clin. Orthop. Relat. Res.*, no. 455, pp. 183–189, 2006.

[17] R. A. Brand, M. A. Mont, and M. M. Manring, "Biographical sketch: Themistocles Gluck (1853-1942)," *Clin. Orthop. Relat. Res.*, vol. 469, no. 6, pp. 1525–1527, 2011.

[18] M. Bankes and R. Emery, "Pioneers of shoulder replacement: Themistocles Gluck and Jules

Emile Péan," *J. Shoulder Elb. Surg.*, vol. 4, no. 4, pp. 259–262, 1995.

[19] L. U. Bigliani, R. H. Cofield, E. L. Flatow, H. Fukuda, R. J. Hawkins, F. A. Matsen III, D. S. Morrison, C. A. Rockwood Jr., and R. F. Warren, "Charles Neer: On the giant of the shoulder," *J. Shoulder Elb. Surg.*, vol. 18, no. 3, pp. 333–338, 2009.

[20] C. S. Neer, "Articular replacement for the humeral head," *J. Bone Joint Surg. Am.*, vol. 37–A, no. 2, pp. 215–228, 1955.

[21] C. S. Neer, "Replacement Arthroplasty for Glenohumeral Osteoarthritis," *J. Bone Jt. Surg.*, vol. 56–A, pp. 1–13, 1974.

[22] M. J. Sandow, H. David, and S. J. Bentall, "Hemiarthroplasty vs total shoulder replacement for rotator cuff intact osteoarthritis: how do they fare after a decade?," *J. Shoulder Elb. Surg.*, vol. 22, no. 7, pp. 877–885, 2013.

[23] J. Clinton, A. K. Franta, T. R. Lenters, D. Mounce, and F. A. Matsen, "Nonprosthetic glenoid arthroplasty with humeral hemiarthroplasty and total shoulder arthroplasty yield similar self-assessed outcomes in the management of comparable patients with glenohumeral arthritis," *J. Shoulder Elb. Surg.*, vol. 16, no. 5, pp. 534–538, 2007.

[24] M. Pfahler, F. Jena, L. Neyton, F. Sirveaux, and D. Molé, "Hemiarthroplasty versus total shoulder prosthesis: results of cemented glenoid components," *J. Shoulder Elb. Surg.*, vol. 15, no. 2, pp. 154–163, 2006.

[25] A. C. Nwakama, R. H. Cofield, B. F. Kavanagh, and J. F. Loehr, "Semiconstrained total shoulder arthroplasty for glenohumeral arthritis and massive rotator cuff tearing," *J. Shoulder Elb. Surg.*, vol. 9, no. 4, pp. 302–307, 2000.

[26] J. D. Zuckerman, A. J. Scott, M. A. Gallagher, and N. York, "Hemiarthroplasty for Cuff Tear Arthropathy," *J. Shoulder Elb. Surg.*, vol. 9, no. 3, pp. 169–172, 2000.

[27] J. W. Sperling, R. H. Cofield, and C. M. Rowland, "Neer Hemiarthroplasty and Neer Total Shoulder Arthroplasty in Patients Fifty Years Old or Less . Long-Term Results," *J. Bone Jt. Surg.*, vol. 80, no. 4, pp. 464–473, 2010.

[28] E. L. Flatow and A. K. Harrison, "A history of reverse total shoulder arthroplasty," *Clin. Orthop. Relat. Res.*, vol. 469, no. 9, pp. 2432–2432, 2011.

[29] E. Baulot, F. Sirveaux, and P. Boileau, "Grammont's Idea: The Story of Paul Grammont's Functional Surgery Concept and the Development of the Reverse Principle," *Clin. Orthop. Relat. Res.*, vol. 469, no. 9, pp. 2425–2431, 2011.

[30] R. Jazayeri and Y. W. Kwon, "Evolution of the reverse total shoulder prosthesis," *Bull. NYU Hosp. Jt. Dis.*, vol. 69, no. 1, pp. 50–55, 2011.

[31] P. Grammont, P. Trouilloud, J. P. Laffay, and X. Deries, "Etude et réalisation d'une nouvelle prothèse d'épaule," *Rhumatologie*, vol. 39, no. 10, pp. 407–418, 1987.

[32] A. T. J. A. Karelse, D. N. Bhatia, and L. F. De Wilde, "Prosthetic component relationship of the reverse Delta III total shoulder prosthesis in the transverse plane of the body," *J. Shoulder Elb. Surg.*, vol. 17, no. 4, pp. 602–607, 2008.

[33] G. Mattiassich, L. L. Marcovici, R. M. Krifter, R. Ortmaier, P. Wegerer, and A. Kroepfl, "Delta III reverse shoulder arthroplasty in the treatment of complex 3- and 4-part fractures of the proximal humerus: 6 to 42 months of follow up," *BMC Musculoskelet. Disord.*, vol. 14, no. 1, pp. 1–10, 2013.

[34] P. Boileau, D. J. Watkinson, A. M. Hatzidakis, and F. Balg, "Grammont reverse prosthesis: design, rationale, and biomechanics," *J. Shoulder Elb. Surg.*, vol. 14, no. 1 Suppl S, p. 147S–161S, 1991.

[35] F. Sirveaux, L. Favard, D. Oudet, D. Huquet, G. Walch, and D. Molé, "Grammont inverted total shoulder arthroplasty in the treatment of glenohumeral osteoarthritis with massive rupture of the cuff," *J. Bone Jt. Surg.*, vol. 86, no. 3, pp. 388–395, 2004.

[36] P. Boileau, D. Watkinson, A. M. Hatzidakis, and I. Hovorka, "Neer Award 2005: The Grammont reverse shoulder prosthesis: results in cuff tear arthritis, fracture sequelae, and revision arthroplasty," *J. Shoulder Elb. Surg.*, vol. 15, no. 5, pp. 527–540, 2006.

[37] F. A. Grassi, L. Murena, F. Valli, and R. Alberio, "Six-year experience with the Delta III reverse shoulder prosthesis," *J. Orthop. Surg. (Hong Kong)*, vol. 17, no. 2, pp. 151–156, 2009.

[38] M. Frankle, S. Siegal, D. R. Pupello, A. Saleem, M. Mighell, and M. Vasey, "The Reverse Shoulder Prosthesis for Glenohumeral Arthritis Associated with Severe Rotator Cuff Deficiency," *J. Bone Jt. Surg.*, vol. 87–A, no. 8, pp. 1697–1705, 2005.

[39] N. A. Virani, M. Harman, K. Li, J. Levy, D. R. Pupello, and M. A. Frankle, "In vitro and finite element analysis of glenoid bone/baseplate interaction in the reverse shoulder design," *J. shoulder Elb. Surg.*, vol. 17, no. 3, pp. 509–521, 2008.

[40] G. Huri, F. Familiari, and E. G. McFarland, "Treatment options for rotator cuff tear arthropathy," *Semin. Arthroplasty*, vol. 25, no. 1, pp. 13–16, 2014.

[41] M. P. Baker and L. A. Crosby, "Cuff tear arthropathy is best treated with a reverse total shoulder arthroplasty," *Semin. Arthroplasty*, vol. 25, no. 1, pp. 7–12, 2014.

[42] C. S. Neer, K. C. Watson, and F. J. Stanton, "Recent experience in total shoulder replacement," *J. Bone Joint Surg. Am.*, vol. 63–A, no. 3, pp. 319–337, 1982.

[43] P. Boileau and G. Walch, "The three-dimensional geometry of the proximal humerus. Implications for surgical technique and prosthetic design," *J. Bone Joint Surg. Br.*, vol. 79, pp. 857–865, 1997.

[44] P. W. Jost, J. S. Dines, M. H. Griffith, M. Angel, D. W. Altchek, and D. M. Dines, "Total Shoulder Arthroplasty Utilizing Mini-Stem Humeral Components: Technique and Short-Term Results," *HSS J.*, vol. 7, no. 3, pp. 213–217, 2011.

[45] L. Harmer, T. Throckmorton, and J. W. Sperling, "Total shoulder arthroplasty: are the humeral components getting shorter?," *Curr. Rev. Musculoskelet. Med.*, vol. 9, no. 1, pp. 17–22, 2016.

[46] O. Levy and S. A. Copeland, "Cementless surface replacement arthroplasty (Copeland CSRA) for osteoarthritis of the shoulder," *J. shoulder Elb. Surg.*, vol. 13, no. 3, pp. 266–271, 2004.

[47] K. L. Jensen, "Humeral resurfacing arthroplasty: rationale, indications, technique, and results," *Am. J. Orthop.*, vol. 36, no. 12 Suppl 1, pp. 4–8, 2007.

[48] H. Mullett, O. Levy, D. Raj, T. Even, R. Abraham, and S. A. Copeland, "Copeland surface replacement of the shoulder: results of an hydroxyapatite-coated cementless implant in patients over 80 years of age," *J. Bone Jt. Surg. - Br. Vol.*, vol. 89–B, no. 11, pp. 1466–1469, 2007.

[49] C. L. Getz and M. L. Ramsey, "Resurfacing Shoulder Arthroplasty," *Shoulder Arthroplast.*, pp. 39–47, 2012.

[50] O. Levy and S. a Copeland, "Cementless surface replacement arthroplasty of the shoulder. 5- to 10-year results with the Copeland mark-2 prosthesis," *J. Bone Joint Surg. Br.*, vol. 83, no. 2, pp. 213–221, 2001.

[51] B.-T. S. Fevang, S. H. L. Lygre, G. Bertelsen, A. Skredderstuen, L. I. Havelin, and O. Furnes, "Pain and function in eight hundred and fifty nine patients comparing shoulder hemiprostheses, resurfacing prostheses, reversed total and conventional total prostheses," *Int. Orthop.*, vol. 37, no. 1, pp. 59–66, 2013.

[52] G. Pape, T. Bruckner, M. Loew, and F. Zeifang, "Treatment of severe cuff tear arthropathy with the humeral head resurfacing arthroplasty: Two-year minimum follow-up," *J. Shoulder Elb. Surg.*, vol. 22, no. 1, pp. 1–7, 2013.

[53] R. S. Churchill and G. S. Athwal, "Stemless shoulder arthroplasty—current results and designs," *Curr. Rev. Musculoskelet. Med.*, vol. 9, no. 1, pp. 10–16, 2016.

[54] G. C. Mallo, L. Burton, M. Coats-Thomas, S. D. Daniels, N. J. Sinz, and J. J. P. Warner, "Assessment of painful total shoulder arthroplasty using computed tomography arthrography," *J. Shoulder Elb. Surg.*, vol. 24, no. 10, pp. 1507–1511, 2015.

[55] N. Bonnevialle, B. Melis, L. Neyton, L. Favard, D. Molé, G. Walch, and P. Boileau, "Aseptic glenoid loosening or failure in total shoulder arthroplasty: Revision with glenoid reimplantation," *J. Shoulder Elb. Surg.*, vol. 22, no. 6, pp. 745–751, 2013.

[56] M. Schrumpf, T. Maak, S. Hammoud, and E. V. Craig, "The glenoid in total shoulder arthroplasty," *Curr. Rev. Musculoskelet. Med.*, vol. 4, no. 4, pp. 191–199, 2011.

[57] A. Karelse, A. Van Tongel, T. Van Isacker, B. Berghs, and L. De Wilde, "Parameters influencing glenoid loosening," *Expert Rev. Med. Devices*, vol. 13, no. 8, pp. 773–784, 2016.

[58] D. L. Parks, D. J. Casagrande, M. A. Schrumpf, S. M. Harmsen, T. R. Norris, and J. D. Kelly, "Radiographic and clinical outcomes of total shoulder arthroplasty with an all-polyethylene pegged bone ingrowth glenoid component: Prospective short- to medium-term follow-up," *J. Shoulder Elb. Surg.*, vol. 25, no. 2, pp. 246–255, 2016.

[59] D. Pinkas, B. Wiater, and J. M. Wiater, "The Glenoid Component in Anatomic Shoulder Arthroplasty," *AAOS Now*, vol. 23, no. 5, pp. 317–326, 2015.

[60] L. V. Gulotta, K. L. Chambers, R. F. Warren, D. M. Dines, and E. V. Craig, "No Differences in Early Results of a Hybrid Glenoid Compared With a Pegged Implant," *Clin. Orthop. Relat. Res.*, vol. 473, no. 12, pp. 3918–3924, 2015.

[61] J. F. Gonzalez, G. B. Alami, F. Baque, G. Walch, and P. Boileau, "Complications of unconstrained shoulder prostheses," *J. Shoulder Elb. Surg.*, vol. 20, no. 4, pp. 666–682, 2011.

[62] F. Montoya, P. Magosch, B. Scheiderer, S. Lichtenberg, P. Melean, and P. Habermeyer, "Midterm results of a total shoulder prosthesis fixed with a cementless glenoid component," *J. Shoulder Elb. Surg.*, vol. 22, no. 5, pp. 628–635, 2013.

[63] P. Boileau, C. Avidor, S. G. Krishnan, G. Walch, J. F. Kempf, and D. Molé, "Cemented polyethylene versus uncemented metal-backed glenoid components in total shoulder arthroplasty: A prospective, double-blind, randomized study," *J. Shoulder Elb. Surg.*, vol. 11, no. 4, pp. 351–359, 2002.

[64] L. Fink Barnes, B. O. Parsons, and E. Flatow, "Pegged or keeled glenoid component use: Which is it?," *Semin. Arthroplasty*, vol. 25, no. 4, pp. 246–249, 2014.

[65] T. B. Edwards, J. E. Labriola, R. J. Stanley, D. P. O'Connor, H. A. Elkousy, and G. M.

Gartsman, “Radiographic comparison of pegged and keeled glenoid components using modern cementing techniques: A prospective randomized study,” *J. Shoulder Elb. Surg.*, vol. 19, no. 2, pp. 251–257, 2010.

[66] G. M. Gartsman, H. A. Elkousy, K. M. Warnock, T. B. Edwards, and D. P. O’Connor, “Radiographic comparison of pegged and keeled glenoid components,” *J. Shoulder Elb. Surg.*, vol. 14, no. 3, pp. 252–257, 2005.

[67] I. Szabo, F. Buscayret, T. B. Edwards, C. Nemoz, D. P. O’Connor, P. Boileau, and G. Walch, “Radiographic comparison of two glenoid preparation techniques in total shoulder arthroplasty,” *Clin. Orthop. Relat. Res.*, no. 431, pp. 104–110, 2005.

[68] R. S. Churchill, R. S. Boorman, E. V Fehringer, and F. a Matsen, “Glenoid cementing may generate sufficient heat to endanger the surrounding bone,” *Clin. Orthop. Relat. Res.*, vol. 6500, no. 419, pp. 76–79, 2004.

[69] M. A. Wirth, D. L. Korvick, C. J. Basamania, F. Toro, T. B. Aufdemorte, and C. A. Rockwood, “Radiologic, mechanical, and histologic evaluation of 2 glenoid prosthesis designs in a canine model,” *J. Shoulder Elb. Surg.*, vol. 10, no. 2, pp. 140–148, 2001.

[70] R. S. Churchill, C. Zellmer, H. J. Zimmers, and R. Ruggero, “Clinical and radiographic analysis of a partially cemented glenoid implant: Five-year minimum follow-up,” *J. Shoulder Elb. Surg.*, vol. 19, no. 7, pp. 1091–1097, 2010.

[71] D. L. Parks, D. J. Casagrande, M. A. Schrumpf, S. M. Harmsen, T. R. Norris, and J. D. Kelly, “Radiographic and clinical outcomes of total shoulder arthroplasty with an all-polyethylene pegged bone ingrowth glenoid component: prospective short- to medium-term follow-up,” *J. Shoulder Elb. Surg.*, no. 615912, pp. 1–10, 2015.

[72] R. M. Arnold, R. R. High, K. T. Grosshans, C. W. Walker, and E. V. Fehringer, “Bone presence between the central peg’s radial fins of a partially cemented pegged all poly glenoid component suggest few radiolucencies,” *J. Shoulder Elb. Surg.*, vol. 20, no. 2, pp. 315–321, 2011.

[73] M. A. Wirth, R. Loredo, G. Garcia, C. A. Rockwood, C. Southworth, and J. P. Iannotti, “Total Shoulder Arthroplasty with an All-Polyethylene Pegged Bone-Ingrowth Glenoid Component,” *J. Bone Jt. Surg.*, vol. 94, no. 3, pp. 260–267, 2012.

[74] G. I. Groh, “Survival and radiographic analysis of a glenoid component with a cementless fluted central peg,” *J. Shoulder Elb. Surg.*, vol. 19, no. 8, pp. 1265–1268, 2010.

[75] J. L. Franklin, W. P. Barrett, S. E. Jackins, and F. A. 3rd Matsen, “Glenoid loosening in total shoulder arthroplasty. Association with rotator cuff deficiency,” *J. Arthroplasty*, vol. 3, no. 1, pp. 39–46, 1988.

[76] F. Matsen, M. Wirth, S. Lippitt, and C. Rockwood, “Glenohumeral Arthritis and Its Management,” in *The Shoulder - volume 1*, Fourth., Saunders, 2009, p. 1105.

[77] C. Anglin, U. P. Wyss, and D. R. Pichora, “Mechanical testing of shoulder prostheses and recommendations for glenoid design.,” *J. Shoulder Elb. Surg.*, vol. 9, no. 4, pp. 323–31, 2000.

[78] V. M. Wang, R. Krishnan, O. F. C. Ugwonali, E. L. Flatow, L. U. Bigliani, and G. A. Ateshian, “Biomechanical evaluation of a novel glenoid design in total shoulder arthroplasty,” *J. Shoulder Elb. Surg.*, vol. 14, no. 1 SUPPL., pp. 129–140, 2005.

[79] J. Zhang, C. Yongpravat, H. M. Kim, W. N. Levine, L. U. Bigliani, T. R. Gardner, and C. S. Ahmad, “Glenoid articular conformity affects stress distributions in total shoulder

arthroplasty," *J. shoulder Elb. Surg.* /, vol. 22, no. 3, pp. 350–356, 2013.

[80] J. C. J. Webb and R. F. Spencer, "The role of polymethylmethacrylate bone cement in modern orthopaedic surgery," *J. Bone Joint Surg. Br.*, vol. 89, no. 7, pp. 851–857, 2007.

[81] R. Vaishya, M. Chauhan, and A. Vaish, "Bone cement," *J. Clin. Orthop. Trauma*, vol. 4, no. 4, pp. 157–163, 2013.

[82] S. Gheduzzi, J. J. C. Webb, and A. W. Miles, "Mechanical characterisation of three percutaneous vertebroplasty biomaterials," *J. Mater. Sci. Mater. Med.*, vol. 17, no. 5, pp. 421–426, 2006.

[83] W. N. Levine and S. Aviles, "Total Shoulder Replacement: Humeral Component Technique," in *Shoulder Arthroplasty*, L. U. Bigliani and E. L. Flatow, Eds. Springer, 2005, pp. 21–36.

[84] P. Raiss, T. B. Edwards, A. Deutsch, A. Shah, T. Bruckner, M. Loew, P. Boileau, and G. Walch, "Radiographic Changes Around Humeral Components in Shoulder Arthroplasty," vol. 54, pp. 1–9, 2014.

[85] W. H. S. Jr, P. Marinello, and J. Styron, "The cemented humerus and non-cemented glenoid: The optimal hybrid solution for total shoulder arthroplasty," *Semin. Arthroplasty*, vol. 27, no. 2, pp. 98–103, 2016.

[86] C. Kolling, B. R. Simmen, G. Labek, and J. Goldhahn, "Key factors for a successful National Arthroplasty Register," *J. Bone Joint Surg. Br.*, vol. 89, no. 12, pp. 1567–1573, 2007.

[87] H. Rahme, M. B. Jacobsen, and B. Salomonsson, "The Swedish Elbow Arthroplasty Register and the Swedish Shoulder Arthroplasty Register: two new Swedish arthroplasty registers," *Acta Orthop. Scand.*, vol. 72, no. 2, pp. 107–112, 2001.

[88] J. V Rasmussen, B. S. Olsen, B.-T. S. Fevang, O. Furnes, E. T. Skytta, H. Rahme, B. Salomonsson, K. D. Mohammed, R. S. Page, and A. J. Carr, "A review of national shoulder and elbow joint replacement registries," *J. shoulder Elb. Surg.*, vol. 21, no. 10, pp. 1328–1335, 2012.

[89] I. H. Klintberg, K. Lind, T. Marlow, and U. Svantesson, "Western Ontario Osteoarthritis Shoulder (WOOS) index: a cross-cultural adaptation into Swedish, including evaluation of reliability, validity, and responsiveness in patients with subacromial pain," *J. Shoulder Elb. Surg.*, vol. 21, no. 12, pp. 1698–1705, 2012.

[90] A. Nordqvist, "Trends - what to the rigistries tell us? Swedish registry example," Malmö, Sweden, 2012.

[91] U. Lillkrona, A. Mordqist, H. Rahme, and B. Salomonsson, "The Swedish Shoulder Arthroplasty Register. An analysis of 255 re-operations on arthroplasties reported to the register," 2007.

[92] National Joint Replacement Registry, "Shoulder Arthroplasty Annual Report 2015," 2015.

[93] N. N. Z. O. Association, "THE NEW ZEALAND JOINT REGISTRY. Sixteen Year Report. January 1999 to December 2014," 2014.

[94] National Joint Registry, "12th Annual Report 2015. National Joint Registry for England, Wales, Northern Ireland and the Isle of Man. Surgical data to 31 december 2014," 2015.

[95] Sociedade Portuguesa de Ortopedia e Traumatologia, "Registo Português de Artroplastias - Relatório Anual 2013," 2013.

[96] L. Favard, D. Katz, M. Colmar, T. Benkalfate, H. Thomazeau, and S. Emily, "Total shoulder arthroplasty - arthroplasty for glenohumeral arthropathies: results and complications after a minimum follow-up of 8 years according to the type of arthroplasty and etiology," *Orthop. Traumatol. Surg. Res.*, vol. 98, no. 4 Suppl, pp. S41-47, 2012.

[97] T. K. Kiet, B. T. Feeley, M. Naimark, T. Gajiu, S. L. Hall, T. T. Chung, and C. B. Ma, "Outcomes after shoulder replacement: Comparison between reverse and anatomic total shoulder arthroplasty," *J. Shoulder Elb. Surg.*, vol. 24, no. 2, pp. 179–185, 2015.

[98] J. E. Biemond, R. Aquarius, N. Verdonschot, and P. Buma, "Frictional and bone ingrowth properties of engineered surface topographies produced by electron beam technology," *Arch. Orthop. Trauma Surg.*, vol. 131, no. 5, pp. 711–718, 2011.

[99] B. Salomonsson, "Latest results from the Swedish Shoulder Arthroplasty Register 2012," 2012.

[100] J. Yang, K. Abdel-Malek, and K. Nebel, "Reach envelope of a 9-degree-of-freedom model of the upper extremity," *Int. J. Robot. Autom.*, vol. 20, no. 4, 2005.

[101] M. Sundberg, L. Lidgren, Annette-W-Dahl, and O. Robertsson, "The Swedish Knee Arthroplasty Register - Annual Report 2013," 2013.

[102] A. A. Nikooyan, H. E. J. Veeger, P. Westerhoff, B. Bolsterlee, F. Graichen, G. Bergmann, and F. C. T. van der Helm, "An EMG-driven musculoskeletal model of the shoulder," *Hum. Mov. Sci.*, vol. 31, no. 2, pp. 429–447, 2012.

[103] P. Favre, R. Sheikh, S. F. Fucentese, and H. A. C. Jacob, "An algorithm for estimation of shoulder muscle forces for clinical use," *Clin. Biomech. (Bristol, Avon)*, vol. 20, no. 8, pp. 822–833, 2005.

[104] D. Blana, J. G. Hincapie, E. K. Chadwick, and R. F. Kirsch, "A musculoskeletal model of the upper extremity for use in the development of neuroprosthetic systems," *J. Biomech.*, vol. 41, no. 8, pp. 1714–1721, 2008.

[105] M. Masjedi and L. D. Duffell, "Dynamic analysis of the upper limb during activities of daily living: comparison of methodologies," *Proc. Inst. Mech. Eng. H.*, vol. 227, no. 12, pp. 1275–1283, 2013.

[106] A. J. Schnorenberg, B. A. Slavens, M. Wang, L. C. Vogel, P. A. Smith, and G. F. Harris, "Biomechanical model for evaluation of pediatric upper extremity joint dynamics during wheelchair mobility," *J. Biomech.*, vol. 47, no. 1, pp. 269–276, 2014.

[107] A. Terrier, X. Larrea, V. Malfroy Camine, D. P. Pioletti, and A. Farron, "Importance of the subscapularis muscle after total shoulder arthroplasty," *Clin. Biomech.*, vol. 28, no. 2, pp. 146–150, 2013.

[108] R. E. Debski, J. A. Weiss, W. J. Newman, S. M. Moore, and P. J. McMahon, "Stress and strain in the anterior band of the inferior glenohumeral ligament during a simulated clinical examination," *J. Shoulder Elb. Surg.*, vol. 14, no. 1 SUPPL., pp. 24–31, 2005.

[109] N. J. Drury, B. J. Ellis, J. A. Weiss, P. J. McMahon, and R. E. Debski, "Finding consistent strain distributions in the glenohumeral capsule between two subjects: Implications for development of physical examinations," *J. Biomech.*, vol. 44, no. 4, pp. 607–613, 2011.

[110] D. Karlsson and B. Peterson, "Towards a model for force predictions in the human shoulder," *J. Biomech.*, vol. 25, no. 2, pp. 189–199, 1992.

[111] F. C. T. van der Helm, "A finite element musculoskeletal model of the shoulder

mechanism," *J. Biomech.*, vol. 27, no. 5, pp. 551–569, 1994.

[112] B. P. A. Garner and M. G. Pandy, "Musculoskeletal model of the upper limb based on the visible human male dataset," *Comput. Methods Biomech. Biomed. Engin.*, vol. 4, pp. 93–126, 2001.

[113] I. Charlton, "A model for the prediction of the forces at the glenohumeral joint," University of Newcastle, Newcastle Upon Tyne, UK, 2003.

[114] K. R. S. Holzbaur, W. M. Murray, and S. L. Delp, "A model of the upper extremity for simulating musculoskeletal surgery and analyzing neuromuscular control," *Ann. Biomed. Eng.*, vol. 33, no. 6, pp. 829–840, 2005.

[115] C. R. Dickerson, D. B. Chaffin, and R. E. Hughes, "A mathematical musculoskeletal shoulder model for proactive ergonomic analysis," *Comput. Methods Biomech. Biomed. Engin.*, vol. 10, no. 6, pp. 389–400, 2007.

[116] F. C. T. van der Helm, "Analysis of the kinematic and dynamic behavior of the shoulder mechanism," *J. Biomech.*, vol. 27, no. 5, pp. 527–550, 1994.

[117] A. A. Nikooyan, H. E. J. Veeger, E. K. J. Chadwick, M. Praagman, and F. C. T. Van Der Helm, "Development of a comprehensive musculoskeletal model of the shoulder and elbow," *Med. Biol. Eng. Comput.*, vol. 49, no. 12, pp. 1425–1435, 2011.

[118] R. Happee and F. C. T. Van der Helm, "The control of shoulder muscles during goal directed movements, an inverse dynamic analysis," *J. Biomech.*, vol. 28, no. 10, pp. 1179–1191, 1995.

[119] M. Praagman, E. K. J. Chadwick, F. C. T. van der Helm, and H. E. J. Veeger, "The relationship between two different mechanical cost functions and muscle oxygen consumption," *J. Biomech.*, vol. 39, no. 4, pp. 758–765, 2006.

[120] B. Bolsterlee, D. H. E. J. Veeger, and E. K. Chadwick, "Clinical applications of musculoskeletal modelling for the shoulder and upper limb," *Med. Biol. Eng. Comput.*, vol. 51, no. 9, pp. 953–963, 2013.

[121] L. J. Holmberg and A. Klarbring, "Muscle decomposition and recruitment criteria influence muscle force estimates," *Multibody Syst. Dyn.*, vol. 28, no. 3, pp. 283–289, 2012.

[122] W. Blajer, A. Czaplicki, K. Dziewiecki, and Z. Mazur, "Influence of selected modeling and computational issues on muscle force estimates," *Multibody Syst. Dyn.*, vol. 24, no. 4, pp. 473–492, 2010.

[123] M. Damsgaard, J. Rasmussen, S. T. Christensen, E. Surma, and M. de Zee, "Analysis of musculoskeletal systems in the AnyBody Modeling System," *Simul. Model. Pract. Theory*, vol. 14, no. 8, pp. 1100–1111, 2006.

[124] A. Terrier, M. Aeberhard, Y. Michellod, P. Mullhaupt, D. Gillet, A. Farron, and D. P. Pioletti, "A musculoskeletal shoulder model based on pseudo-inverse and null-space optimization," *Med. Eng. Phys.*, vol. 32, no. 9, pp. 1050–1056, 2010.

[125] P. O. Lemieux, N. Hagemeister, P. Tétreault, and N. Nuño, "Influence of the medial offset of the proximal humerus on the glenohumeral destabilising forces during arm elevation: a numerical sensitivity study," *Comput. Methods Biomech. Biomed. Engin.*, vol. 16, no. 1, pp. 103–111, 2013.

[126] M. Voinescu, D. P. Soares, R. M. Natal Jorge, A. Davidescu, and L. J. Machado, "Estimation of the forces generated by the thigh muscles for transtibial amputee gait," *J. Biomech.*, vol.

45, no. 6, pp. 972–977, 2012.

[127] P. O. Lemieux, P. Tétreault, N. Hagemeister, and N. Nuño, "Influence of prosthetic humeral head size and medial offset on the mechanics of the shoulder with cuff tear arthropathy: A numerical study," *J. Biomech.*, vol. 46, no. 4, pp. 806–812, 2013.

[128] A. D. Nimbarte, Y. Sun, M. Jaridi, and H. Hsiao, "Biomechanical loading of the shoulder complex and lumbosacral joints during dynamic cart pushing task," *Appl. Ergon.*, vol. 44, no. 5, pp. 841–849, 2013.

[129] J. Rasmussen, M. Damsgaard, and M. Voigt, "Muscle recruitment by the min/max criterion - a comparative numerical study," *J. Biomech.*, vol. 34, no. 3, pp. 409–415, 2001.

[130] P. Westerhoff, F. Graichen, A. Bender, A. Rohlmann, and G. Bergmann, "An instrumented implant for in vivo measurement of contact forces and contact moments in the shoulder joint," *Med. Eng. Phys.*, vol. 31, no. 2, pp. 207–213, 2009.

[131] P. Westerhoff, F. Graichen, A. Bender, A. Halder, A. Beier, A. Rohlmann, and G. Bergmann, "In vivo measurement of shoulder joint loads during activities of daily living," *J. Biomech.*, vol. 42, no. 12, pp. 1840–1849, 2009.

[132] G. Bergmann, F. Graichen, A. Bender, A. Rohlmann, A. Halder, A. Beier, and P. Westerhoff, "In vivo gleno-humeral joint loads during forward flexion and abduction," *J. Biomech.*, vol. 44, no. 8, pp. 1543–1552, 2011.

[133] C. Y. Scovil and J. L. Ronsky, "Sensitivity of a Hill-based muscle model to perturbations in model parameters," *J. Biomech.*, vol. 39, no. 11, pp. 2055–2063, 2006.

[134] G. Bergmann, F. Graichen, A. Bender, M. Kääb, A. Rohlmann, and P. Westerhoff, "In vivo glenohumeral contact forces - measurements in the first patient 7 months postoperatively," *J. Biomech.*, vol. 40, no. 10, pp. 2139–2149, 2007.

[135] J. Rasmussen, M. de Zee, S. Tørholm, and M. Damsgaard, "Comparison of a musculoskeletal shoulder model with in-vivo joint forces," in *International Society of Biomechanics 11th Congress : Abstracts*, 2007.

[136] G. Wu, F. C. T. van der Helm, H. E. J. (DirkJan) Veeger, M. Makhsous, P. Van Roy, C. Anglin, J. Nagels, A. R. Karduna, K. McQuade, X. Wang, F. W. Werner, and B. Buchholz, "ISB recommendation on definitions of joint coordinate systems of various joints for the reporting of human joint motion —Part II: shoulder, elbow, wrist and hand," *J. Biomech.*, vol. 38, no. 5, pp. 981–992, 2005.

[137] S. Carbes, "Shoulder Rhythm," Aalborg, Denmark: AnyBody Technology A/S, 2011.

[138] J. Wickham, T. Pizzari, K. Stansfeld, A. Burnside, and L. Watson, "Quantifying 'normal' shoulder muscle activity during abduction," *J. Electromyogr. Kinesiol.*, vol. 20, no. 2, pp. 212–222, 2010.

[139] P. Büchler, N. A. Ramaniraka, L. R. Rakotomanana, J. P. Iannotti, and A. Farron, "A finite element model of the shoulder: application to the comparison of normal and osteoarthritic joints," *Clin. Biomech.*, vol. 17, no. 9–10, pp. 630–639, 2002.

[140] A. E. Kedgley, G. A. Mackenzie, L. M. Ferreira, D. S. Drosdowech, G. J. W. Ling, K. J. Faber, and J. A. Johnson, "The effect of muscle loading on the kinematics of in vitro glenohumeral abduction," *J. Biomech.*, vol. 22, no. 10, pp. 2953–2960, 2007.

[141] P. Favre, H. A. C. Jacob, and C. Gerber, "Changes in shoulder muscle function with humeral position: a graphical description," *J. shoulder Elb. Surg.*, vol. 18, no. 1, pp. 114–121,

2009.

[142] T. Yanagawa, C. J. Goodwin, K. B. Shelburne, J. E. Giphart, M. R. Torry, and M. G. Pandy, "Contributions of the individual muscles of the shoulder to glenohumeral joint stability during abduction," *J. Biomech. Eng.*, vol. 130, no. 2, pp. 1–9, 2008.

[143] D. Baumgartner, D. Tomas, L. Gossweiler, W. Siegl, G. Osterhoff, and B. Heinlein, "Towards the development of a novel experimental shoulder simulator with rotating scapula and individually controlled muscle forces simulating the rotator cuff," *Med. Biol. Eng. Comput.*, vol. 52, no. 3, pp. 293–299, 2014.

[144] C. M. Bono, R. Renard, R. G. Levine, and a S. Levy, "Effect of displacement of fractures of the greater tuberosity on the mechanics of the shoulder," *J. Bone Joint Surg. Br.*, vol. 83, no. 7, pp. 1056–1062, 2001.

[145] U. Onder, M. Blauth, F. Kralinger, and W. Schmoelz, "Shoulder joint abduction motion test bench: A new shoulder test bench for in vitro experiments with active muscle force simulation," *Biomed. Tech.*, vol. 57, no. 3, pp. 163–168, 2012.

[146] M. Apreleva, I. M. Parsons, J. J. P. Warner, F. H. Fu, and S. L. Y. Woo, "Experimental investigation of reaction forces at the glenohumeral joint during active abduction," *J. Shoulder Elb. Surg.*, vol. 9, no. 5, pp. 409–417, 2000.

[147] A. E. Kedgley, G. a Mackenzie, L. M. Ferreira, J. a Johnson, and K. J. Faber, "In vitro kinematics of the shoulder following rotator cuff injury," *Clin. Biomech. (Bristol, Avon)*, vol. 22, no. 10, pp. 1068–1073, 2007.

[148] A. E. Kedgley, G. A. Mackenzie, L. M. Ferreira, D. S. Drosdowech, G. J. W. King, K. J. Faber, and J. A. Johnson, "Humeral head translation decreases with muscle loading," *J. Shoulder Elbow Surg.*, vol. 17, no. 1, pp. 132–138, 2008.

[149] B. J. Jun, J. P. Iannotti, M. H. McGarry, J. C. Yoo, R. J. Quigley, and T. Q. Lee, "The effects of prosthetic humeral head shape on glenohumeral joint kinematics: a comparison of non-spherical and spherical prosthetic heads to the native humeral head," *J. Shoulder Elbow Surg.*, vol. 22, no. 10, pp. 1423–1432, 2013.

[150] J.-D. Werthel, A. Hooke, T. Hatta, E. Wagner, K.-N. An, B. Elhassan, and J. Sperling, "Changes in Glenohumeral Muscle Moment Arms Following Reverse Shoulder Arthroplasty: a Biomechanical Study," 2015. [Online]. Available: http://prgmobileapps.com/AppUpdates/ors2015/Abstracts/abs1850.html.

[151] M. Schamblin, R. Gupta, B. Y. Yang, M. H. McGarry, W. C. McMaster, and T. Q. Lee, "In vitro quantitative assessment of total and bipolar shoulder arthroplasties: A biomechanical study using human cadaver shoulders," *Clin. Biomech.*, vol. 24, no. 8, pp. 626–631, 2009.

[152] R. W. Nyffeler, R. Sheikh, T. S. Atkinson, H. A. C. Jacob, P. Favre, and C. Gerber, "Effects of glenoid component version on humeral head displacement and joint reaction forces: An experimental study," *J. Shoulder Elb. Surg.*, vol. 15, no. 5, pp. 625–629, 2006.

[153] M. Krämer, A. Bäunker, M. Wellmann, C. Hurschler, and T. Smith, "Implant impingement during internal rotation after reverse shoulder arthroplasty. The effect of implant configuration and scapula anatomy: A biomechanical study," *Clin. Biomech.*, vol. 33, pp. 111–116, 2016.

[154] J. W. Giles, G. D. G. Langohr, J. A. Johnson, G. S. Athwal, R. M. Hand, U. L. Centre, and S. Joseph, "The rotator cuff muscles are antagonists after reverse total shoulder arthroplasty," *J. Shoulder Elb. Surg.*, vol. 25, no. 10, pp. 1592–1600, 2016.

[155] L. R. North, M. A. Hetzler, M. Pickell, J. T. Bryant, K. J. Deluzio, and R. T. Bicknell, "Effect of implant geometry on range of motion in reverse shoulder arthroplasty assessed using glenohumeral separation distance," *J. Shoulder Elb. Surg.*, vol. 24, no. 9, pp. 1359–1366, 2015.

[156] N. A. Virani, A. Cabezas, S. Gutiérrez, B. G. Santoni, R. Otto, and M. Frankle, "Reverse shoulder arthroplasty components and surgical techniques that restore glenohumeral motion," *J. Shoulder Elb. Surg.*, vol. 22, no. 2, pp. 179–187, 2013.

[157] R. A. Glennie, J. W. Giles, J. A. Johnson, G. S. Athwal, and K. J. Faber, "An in vitro study comparing limited to full cementation of polyethylene glenoid components," *J. Orthop. Surg. Res.*, vol. 10, pp. 142–148, 2015.

[158] W. W. Flint, G. S. Lewis, H. B. Wee, B. J. Bryce, and A. D. Armstrong, "Glenoid cement mantle characterization using micro-computed tomography of three cement application techniques," *J. Shoulder Elb. Surg.*, vol. 25, no. 4, pp. 572–580, 2016.

[159] J. P. Iannotti, K. E. Lappin, C. L. Klotz, E. W. Reber, and S. W. Swope, "Liftoff resistance of augmented glenoid components during cyclic fatigue loading in the posterior-superior direction," *J. Shoulder Elb. Surg.*, vol. 22, no. 11, pp. 1530–1536, 2013.

[160] C. Sukjamsri, D. M. Geraldes, T. Gregory, F. Ahmed, D. Hollis, S. Schenk, A. Amis, R. Emery, and U. Hansen, "Digital volume correlation and micro-CT: An in-vitro technique for measuring full-field interface micromotion around polyethylene implants," *J. Biomech.*, vol. 48, no. 12, pp. 3447–3454, 2015.

[161] A. M. T. Choo, R. H. Hawkins, B. K. Kwon, and T. R. Oxland, "The effect of shoulder arthroplasty on humeral strength: An in vitro biomechanical investigation," *Clin. Biomech.*, vol. 20, no. 10, pp. 1064–1071, 2005.

[162] P. Favre, J. Seebeck, P. A. E. Thistlethwaite, M. Obrist, J. G. Steffens, A. R. Hopkins, and P. A. Hulme, "In vitro initial stability of a stemless humeral implant," *Clin. Biomech.*, vol. 32, pp. 113–117, 2016.

[163] N. Maurel, A. Diop, J. Grimberg, and S. Elise, "In vitro biomechanical analysis of glenoids before and after implantation of prosthetic components," *J. Biomech.*, vol. 35, no. 8, pp. 1071–1080, 2002.

[164] A. Diop, N. Maurel, J. Grimberg, and O. Gagey, "Influence of glenohumeral mismatch on bone strains and implant displacements in implanted glenoids. An in vitro experimental study on cadaveric scapulae," *J. Biomech.*, vol. 39, no. 16, pp. 3026–3035, 2006.

[165] SAWBONES ® Pacific Research Laboratories, "Brochure: Biomechanical Test Materials." Vashon, WA, 2014.

[166] P. Grover, C. Albert, M. Wang, and G. F. Harris, "Mechanical Characterization of Fourth Generation Composite Humerus," *J. Eng. Med.*, vol. 225, no. 12, pp. 1169–1176, 2011.

[167] M. P. Gardner, A. C. M. Chong, A. G. Pollock, and P. H. Wooley, "Mechanical evaluation of large-size fourth-generation composite femur and tibia models," *Ann. Biomed. Eng.*, vol. 38, no. 3, pp. 613–620, 2010.

[168] T. Goswami, V. Patel, D. J. Dalstrom, and M. J. Prayson, "Mechanical evaluation of fourth-generation composite femur hybrid locking plate constructs," *J. Mater. Sci. Mater. Med.*, vol. 22, no. 9, pp. 2139–2146, 2011.

[169] S. M. Moore, B. Ellis, J. A. Weiss, P. J. McMahon, and R. E. Debski, "The glenohumeral capsule should be evaluated as a sheet of fibrous tissue: A validated finite element model,"

Ann. Biomed. Eng., vol. 38, no. 1, pp. 66–76, 2010.

[170] C. Relvas, A. Ramos, A. Completo, and J. A. Simões, "Accuracy control of complex surfaces in reverse engineering," *Int. J. Precis. Eng. Manuf.*, vol. 12, no. 6, pp. 1035–1042, 2011.

[171] J. A. Fox, B. J. Cole, A. A. Romeo, A. K. Meininger, J. M. Williams, R. E. Glenn, J. Bicos, J. K. Hayden, and C. B. Dorow, "Articular Cartilage Thickness of the Humeral Head: An Anatomic Study," *Orthopedics*, vol. 31, no. 3, pp. 1–6, 2008.

[172] S. G. Gapps, "Total Shoulder Arthroplasty - Biomechanical Testing of the Fixation of a New Glenoid Design," Biomet Orthopedics, Inc., Warsaw, IN, 2007.

[173] BIOMET® Orthopedics Inc., "Brochure: Comprehensive® Total Shoulder System. Featuring Comprehensive® Access Glenoid Instrumetation. Surgical Technique," 2012.

[174] J. P. Iannotti, E. E. Spencer, U. Winter, D. Deffenbaugh, and G. Williams, "Prosthetic positioning in total shoulder arthroplasty," *J. Shoulder Elb. Surg.*, vol. 14, no. 1 SUPPL., pp. 111–121, 2005.

[175] G. R. Williams, K. L. Wong, M. D. Pepe, V. Tan, D. Silverberg, M. L. Ramsey, A. Karduna, and J. P. Iannotti, "The effect of articular malposition after total shoulder arthroplasty on glenohumeral translations, range of motion, and subacromial impingement," *J. Shoulder Elb. Surg.*, vol. 10, no. 5, pp. 399–409, 2001.

[176] A. Terrier, S. Ramondetti, F. Merlini, D. D. Pioletti, and A. Farron, "Biomechanical consequences of humeral component malpositioning after anatomical total shoulder arthroplasty," *J. Shoulder Elb. Surg.*, vol. 19, no. 8, pp. 1184–1190, 2010.

[177] P. Favre, B. Moor, J. G. Snedeker, and C. Gerber, "Influence of component positioning on impingement in conventional total shoulder arthroplasty," *Clin. Biomech.*, vol. 23, no. 2, pp. 175–183, 2008.

[178] J. P. Landau and H. R. Hoenecke, "Genetic and biomechanical determinants of glenoid version: Implications for glenoid implant placement in shoulder arthroplasty," *J. Shoulder Elb. Surg.*, vol. 18, no. 4, pp. 661–667, 2009.

[179] C. Yongpravat, H. M. Kim, T. R. Gardner, L. U. Bigliani, W. N. Levine, and C. S. Ahmad, "Glenoid implant orientation and cement failure in total shoulder arthroplasty: a finite element analysis," *J. Shoulder Elb. Surg.*, vol. 22, no. 7, pp. 940–947, 2013.

[180] B. Couteau, P. Mansat, R. Darmana, M. Mansat, and J. Egan, "Morphological and mechanical analysis of the glenoid by 3D geometric reconstruction using computed tomography," *Clin. Biomech. (Bristol, Avon)*, vol. 15 Suppl 1, no. 1, pp. S8-12, 2000.

[181] P. Mansat and N. Bonnevialle, "Morphology of the normal and arthritic glenoid," *Eur. J. Orthop. Surg. Traumatol.*, vol. 23, no. 3, pp. 287–299, 2013.

[182] H. Azevedo, R. Duarte, J. A. F. Ferreira, M. Mesnard, and A. Ramos, "Desenvolvimento de um simulador da articulação temporomandibular," in *10º Congresso Nacional de Mecânica Experimental*, 2016, pp. 109–110.

[183] A. Ramos, R. J. Duarte, and M. M. Strain, "Strain induced in the condyle by self-tapping screws in the Biomet alloplastic temporomandibular joint: a preliminary experimental study," *Int. J. Oral Maxillofac. Surg.*, vol. 44, no. 11, pp. 1376–1382, 2015.

[184] P. J. McMahon, R. E. Debski, W. O. Thompson, J. J. Warner, F. H. Fu, and S. L. Woo, "Shoulder muscle forces and tendon excursions during glenohumeral abduction in the scapular plane.," *J. Shoulder Elbow Surg.*, vol. 4, no. 3, pp. 199–208, 1995.

[185] A. Roozbazar, G. W. Bosker, and M. E. Richerson, "A theoretical model to estimate some ergonomic parameters from age, height and weight," *Ergonomics*, vol. 22, no. 1, pp. 43–58, 1979.

[186] W. E. Roberts, S. S. Huja, and J. A. Roberts, "Bone modeling: Biomechanics, molecular mechanisms, and clinical perspectives," *Semin. Orthod.*, vol. 10, no. 2, pp. 123–161, 2004.

[187] Australian Orthopaedic Association, "National Joint Replacement Registry. Analysis of state & territory health data all arthroplasty. Supplementary Report 2013," Adelaide, 2013.

[188] New Zealand Joint Registry, "The New Zealand Joint Registry - Fifteen Year Report - January 1999 to December 2013," 2013.

[189] J. S. Day, E. Lau, K. L. Ong, G. R. Williams, M. L. Ramsey, and S. M. Kurtz, "Prevalence and projections of total shoulder and elbow arthroplasty in the United States to 2015," *J. Shoulder Elb. Surg.*, vol. 19, no. 8, pp. 1115–1120, 2010.

[190] A. Terrier, A. Reist, A. Vogel, and A. Farron, "Effect of supraspinatus deficiency on humerus translation and glenohumeral contact force during abduction," vol. 22, pp. 645–651, 2007.

[191] A. F. Viehöfer, C. Gerber, P. Favre, E. Bachmann, and J. G. Snedeker, "A larger critical shoulder angle requires more rotator cuff activity to preserve joint stability," *J. Orthop. Res.*, vol. 34, no. 6, pp. 961–968, 2016.

[192] P. Favre, C. Gerber, and J. G. Snedeker, "Automated muscle wrapping using finite element contact detection," *J. Biomech.*, vol. 43, no. 10, pp. 1931–1940, 2010.

[193] B. K. Moor, M. Rothlisberger, D. A. Muller, M. A. Zumstein, S. Bouaicha, M. Ehlinger, and C. Gerber, "Age, trauma and the critical shoulder angle accurately predict supraspinatus tendon tears," *Orthop. Traumatol. Surg. Res.*, vol. 100, no. 5, pp. 489–494, 2014.

[194] P. Walia, A. Miniaci, M. H. Jones, and S. D. Fening, "Theoretical Model of the Effect of Combined Glenohumeral Bone Defects on Anterior Shoulder Instability : A Finite Element Approach Geometric Data for Model," *J. Orthop. Res.*, vol. 31, pp. 601–607, 2013.

[195] P. Favre, "A model to study active shoulder motion and stability," PhD Thesis - ETH ZURICH, 2011.

[196] P. Favre, M. Senteler, J. Hipp, S. Scherrer, C. Gerber, and J. G. Snedeker, "An integrated model of active glenohumeral stability," *J. Biomech.*, vol. 45, no. 13, pp. 2248–2255, 2012.

[197] P. Favre, J. G. Snedeker, and C. Gerber, "Numerical modelling of the shoulder for clinical applications," *Philos. Trans. A. Math. Phys. Eng. Sci.*, vol. 367, no. 1895, pp. 2095–2118, 2009.

[198] I. Wakabayashi, E. Itoi, H. Sano, Y. Shibuya, R. Sashi, H. Minagawa, and M. Kobayashi, "Mechanical environment of the supraspinatus tendon: a two-dimensional finite element model analysis," *J. Shoulder Elb. Surg.*, vol. 12, no. 6, pp. 612–617, 2003.

[199] H. Sano, I. Wakabayashi, and E. Itoi, "Stress distribution in the supraspinatus tendon with partial-thickness tears: An analysis using two-dimensional finite element model," pp. 100–105, 2006.

[200] C. R. Adams, M. a Baldwin, P. J. Laz, P. J. Rullkoetter, and J. E. Langenderfer, "Effects of rotator cuff tears on muscle moment arms: a computational study," *J. Biomech.*, vol. 40, no. 15, pp. 3373–3380, 2007.

[201] A. Inoue, E. Chosa, K. Goto, and N. Tajima, "Nonlinear stress analysis of the supraspinatus

tendon using three-dimensional finite element analysis," *Knee Surg. Sports Traumatol. Arthrosc.*, vol. 21, no. 5, pp. 1151–1157, 2013.

[202] N. Seki, E. Itoi, Y. Shibuya, I. Wakabayashi, H. Sano, R. Sashi, H. Minagawa, N. Yamamoto, H. Abe, K. Kikuchi, K. Okada, and Y. Shimada, "Mechanical environment of the supraspinatus tendon: three-dimensional finite element model analysis," *J. Orthop. Sci.*, no. 13, pp. 348–353, 2008.

[203] B. J. Ellis, R. E. Debski, S. M. Moore, P. J. McMahon, and J. A. Weiss, "Methodology and sensitivity studies for finite element modeling of the inferior glenohumeral ligament complex," *J. Biomech.*, vol. 40, no. 3, pp. 603–612, 2007.

[204] C. J. Gatti, J. D. Maratt, M. L. Palmer, R. E. Hughes, and J. E. Carpenter, "Development and validation of a finite element model of the superior glenoid labrum," *Ann. Biomed. Eng.*, vol. 38, no. 12, pp. 3766–3776, 2010.

[205] N. J. Drury, B. J. Ellis, J. a Weiss, P. J. McMahon, and R. E. Debski, "The impact of glenoid labrum thickness and modulus on labrum and glenohumeral capsule function," *J. Biomech. Eng.*, vol. 132, no. 12, p. 121003–1/7, 2010.

[206] E. Hwang, J. E. Carpenter, R. E. Hughes, and M. L. Palmer, "Shoulder Labral Pathomechanics with Rotator Cuff Tears," *J. Biomech.*, vol. 47, no. 7, pp. 1733–1738, 2014.

[207] B. Couteau, P. Mansat, E. Estivalèzes, R. Darmana, M. Mansat, and J. Egan, "Finite element analysis of the mechanical behavior of a scapula implanted with a glenoid prosthesis.," *Clin. Biomech. (Bristol, Avon)*, vol. 16, no. 7, pp. 566–75, Aug. 2001.

[208] R. J. Patel, T. M. Wright, and Y. Gao, "Load transfer after cemented total shoulder arthroplasty," *J. Shoulder Elb. Surg.*, vol. 23, no. 10, pp. 1553–1562, 2014.

[209] P. Mansat, J. Briot, M. Mansat, and P. Swider, "Evaluation of the glenoid implant survival using a biomechanical finite element analysis: Influence of the implant design, bone properties, and loading location," *J. Shoulder Elb. Surg.*, vol. 16, no. 3S, p. 79S–83S, 2007.

[210] A. Terrier, P. Büchler, and A. Farron, "Influence of glenohumeral conformity on glenoid stresses after total shoulder arthroplasty," *J. Shoulder Elbow Surg.*, vol. 15, no. 4, pp. 515–520, 2006.

[211] D. R. Suárez, W. Nerkens, E. R. Valstar, P. M. Rozing, and F. van Keulen, "Interface micromotions increase with less-conforming cementless glenoid components," *J. Shoulder Elb. Surg.*, vol. 21, no. 4, pp. 474–482, 2012.

[212] A. Terrier, V. Brighenti, D. P. Pioletti, and A. Farron, "Importance of polyethylene thickness in total shoulder arthroplasty: A finite element analysis," *Clin. Biomech.*, vol. 27, no. 5, pp. 443–448, 2012.

[213] S. Gupta, F. C. T. van der Helm, F. van Keulen, F. C. T. Van Der Helm, and F. Van Keulen, "Stress analyses of cemented glenoid prosthesis in Total Shoulder Arthroplasty," *J. Biomech.*, vol. 37, no. 11, pp. 1777–1786, 2004.

[214] G. B. Sharma, R. E. Debski, P. J. McMahon, and D. D. Robertson, "Effect of glenoid prosthesis design on glenoid bone remodeling: Adaptive finite element based simulation," *J. Biomech.*, vol. 43, no. 9, pp. 1653–1659, 2010.

[215] A. H. A. Wahab, M. R. A. Kadir, M. N. Harun, T. Kamarul, and A. Syahrom, "Number of pegs influence focal stress distributions and micromotion in glenoid implants: a finite element study," *Med. Biol. Eng. Comput.*, vol. 55, no. 3, pp. 439–447, 2017.

[216] R. J. Patel, L. Gulotta, T. M. Wright, and Y. Gao, "Effects of osteoarthritis on load transfer after cemented total shoulder arthroplasty," *J. Shoulder Elb. Surg.*, vol. 24, no. 3, pp. 407–415, 2015.

[217] B. Varghese, D. Short, R. Penmetsa, T. Goswami, and T. Hangartner, "Computed-tomography-based finite-element models of long bones can accurately capture strain response to bending and torsion," *J. Biomech.*, vol. 44, no. 7, pp. 1374–1379, 2011.

[218] G. Campoli, B. Bolsterlee, F. van der Helm, H. Weinans, and A. a Zadpoor, "Effects of densitometry, material mapping and load estimation uncertainties on the accuracy of patient-specific finite-element models of the scapula," *J. R. Soc. Interface*, vol. 11, no. 93, p. 20131146, 2014.

[219] H. H. Rachmat, D. Janssen, W. J. Zevenbergen, G. J. Verkerke, R. L. Diercks, and N. Verdonschot, "Generating finite element models of the knee: How accurately can we determine ligament attachment sites from MRI scans?," *Med. Eng. Phys.*, vol. 36, no. 6, pp. 701–707, 2014.

[220] J. D. J. Webb, S. S. Blemker, S. S. L. Delp, J. D. J. Webb, S. S. Blemker, and S. S. L. Delp, "3D finite element models of shoulder muscles for computing lines of actions and moment arms," *Comput. Methods Biomech. Biomed. Engin.*, vol. 17, no. 8, pp. 829–837, 2014.

[221] S. Gupta and F. C. T. van der Helm, "Load transfer across the scapula during humeral abduction," *J. Biomech.*, vol. 37, no. 7, pp. 1001–1009, 2004.

[222] H. Graichen, "Validation of cartilage volume and thickness measurements in the human shoulder with quantitative magnetic resonance imaging," *Osteoarthr. Cartil.*, vol. 11, no. 7, pp. 475–482, 2003.

[223] M. T. Nieminen, J. Töyräs, M. S. Laasanen, J. Silvennoinen, H. J. Helminen, and J. S. Jurvelin, "Prediction of biomechanical properties of articular cartilage with quantitative magnetic resonance imaging," *J. Biomech.*, vol. 37, no. 3, pp. 321–328, 2004.

[224] P. Büchler and A. Farron, "Benefits of an anatomical reconstruction of the humeral head during shoulder arthroplasty: a finite element analysis," *Clin. Biomech.*, vol. 19, no. 1, pp. 16–23, 2004.

[225] J. S. Bauer, I. Sidorenko, D. Mueller, T. Baum, A. S. Issever, F. Eckstein, E. J. Rummeny, T. M. Link, and C. W. Raeth, "Prediction of bone strength by (micro)CT and MDCT-based finite-element-models: How much spatial resolution is needed?," *Eur. J. Radiol.*, vol. 83, no. 1, pp. e36–e42, 2014.

[226] G. N. Hounsfield, "Computed medical imaging," *Physiol. or Med.*, 1979.

[227] G. B. Sharma and D. D. Robertson, "Adaptive scapula bone remodeling computational simulation: Relevance to regenerative medicine," *J. Comput. Phys.*, vol. 244, pp. 312–320, 2013.

[228] D. R. Suárez, H. Weinans, and F. Van Keulen, "Bone remodelling around a cementless glenoid component," *Biomech. Model. Mechanobiol.*, vol. 11, no. 6, pp. 903–913, 2012.

[229] E. Dall'Ara, D. Barber, and M. Viceconti, "About the inevitable compromise between spatial resolution and accuracy of strain measurement for bone tissue: A 3D zero-strain study," *J. Biomech.*, vol. 47, no. 12, pp. 2956–2963, 2014.

[230] J. A. Weiss, J. C. Gardiner, B. J. Ellis, T. J. Lujan, and N. S. Phatak, "Three-dimensional finite element modeling of ligaments: technical aspects," *Med. Eng. Phys.*, vol. 27, no. 10, pp. 845–

861, 2005.

[231] J. J. García and D. H. Cortés, "A biphasic viscohyperelastic fibril-reinforced model for articular cartilage: Formulation and comparison with experimental data," *J. Biomech.*, vol. 40, no. 8, pp. 1737–1744, 2007.

[232] J. S. Bell, C. P. Winlove, C. W. Smith, and H. Dehghani, "Modeling the steady-state deformation of the solid phase of articular cartilage," *Biomaterials*, vol. 30, no. 31, pp. 6394–6401, 2009.

[233] T. a Burkhart, D. M. Andrews, and C. E. Dunning, "Finite element modeling mesh quality, energy balance and validation methods: a review with recommendations associated with the modeling of bone tissue," *J. Biomech.*, vol. 46, no. 9, pp. 1477–1488, 2013.

[234] Z. Li, M. W. Kindig, J. R. Kerrigan, R. W. Kent, and J. R. Crandall, "Development and validation of a subject-specific finite element model of a human clavicle," *Comput. Methods Biomech. Biomed. Engin.*, vol. 16, no. 8, pp. 819–829, 2013.

[235] S. Gupta, F. C. van der Helm, J. C. Sterk, F. van Keulen, and B. L. Kaptein, "Development and experimental validation of a three-dimensional finite element model of the human scapula," *Proc. Inst. Mech. Eng. H.*, vol. 218, no. 2, pp. 127–142, 2004.

[236] N. Maurel, A. Diop, and J. Grimberg, "A 3D finite element model of an implanted scapula: Importance of a multiparametric validation using experimental data," *J. Biomech.*, vol. 38, no. 9, pp. 1865–1872, 2005.

[237] A. E. Anderson, B. J. Ellis, and J. a Weiss, "Verification, validation and sensitivity studies in computational biomechanics," *Comput. Methods Biomech. Biomed. Engin.*, vol. 10, no. 3, pp. 171–184, 2007.

[238] H. B. Henninger, S. P. Reese, A. E. Anderson, and J. A. Weiss, "Validation of computational models in biomechanics," *Proc. Inst. Mech. Eng. H.*, vol. 224, no. 7, pp. 801–812, 2010.

[239] J. Mather, J. C. MacDermid, K. J. Faber, and G. S. Athwal, "Proximal humerus cortical bone thickness correlates with bone mineral density and can clinically rule out osteoporosis," *J. Shoulder Elb. Surg.*, vol. 22, no. 6, pp. 732–738, 2013.

[240] Z. M. Maldonado, J. Seebeck, M. O. W. W. Heller, D. Brandt, P. Hepp, H. Lill, and G. N. Duda, "Straining of the intact and fractured proximal humerus under physiological-like loading," *J. Biomech.*, vol. 36, no. 12, pp. 1865–1873, 2003.

[241] S. S. Metan, P. Krishna, and G. C. Mohankumar, "FEM Model an effective tool to evaluate Von Mises stresses in shoulder joint and muscles for adduction and abduction," *Procedia Mater. Sci.*, vol. 5, pp. 2090–2098, 2014.

[242] A. R. Hopkins, U. N. Hansen, A. A. Amis, M. Taylor, N. Gronau, and C. Anglin, "Finite element modelling of glenohumeral kinematics following total shoulder arthroplasty," *J. Biomech.*, vol. 39, no. 13, pp. 2476–2483, 2006.

[243] C. Quental, J. Folgado, P. R. Fernandes, and J. Monteiro, "Medical Engineering & Physics Bone remodelling analysis of the humerus after a shoulder arthroplasty," *Med. Eng. Phys.*, vol. 34, no. 8, pp. 1132–1138, 2012.

[244] A. Ramos and J. A. Simões, "Tetrahedral versus hexahedral finite elements in numerical modelling of the proximal femur," *Med. Eng. Phys.*, vol. 28, no. 9, pp. 916–924, 2006.

[245] M. Taylor and P. J. Prendergast, "Four decades of finite element analysis of orthopaedic devices: Where are we now and what are the opportunities?," *J. Biomech.*, vol. 48, no. 5, pp.

767–778, 2015.

[246] M. J. Tingart, J. Lehtinen, D. Zurakowski, J. J. P. Warner, and M. Apreleva, "Proximal humeral fractures: regional differences in bone mineral density of the humeral head affect the fixation strength of cancellous screws," *J. Shoulder Elbow Surg.*, vol. 15, no. 5, pp. 620–624, 2006.

[247] S. C. Tadepalli, A. Erdemir, and P. R. Cavanagh, "Comparison of hexahedral and tetrahedral elements in finite element analysis of the foot and footwear," *J. Biomech.*, vol. 44, no. 12, pp. 2337–2343, 2011.

[248] P. Westerhoff, F. Graichen, A. Bender, A. Halder, A. Beier, A. Rohlmann, and G. Bergmann, "In vivo measurement of shoulder joint loads during walking with crutches," *Clin. Biomech.*, vol. 27, no. 7, pp. 711–718, 2012.

[249] A. Ramos, R. J. Duarte, C. Relvas, A. Completo, and J. A. Simões, "The influence of acetabular bone cracks in the press-fit hip replacement: Numerical and experimental analysis," *Clin. Biomech.*, vol. 28, no. 6, pp. 635–641, 2013.

[250] B. Helgason, F. Taddei, H. Pálsson, E. Schileo, L. Cristofolini, M. Viceconti, and S. Brynjólfsson, "A modified method for assigning material properties to FE models of bones," *Med. Eng. Phys.*, vol. 30, no. 4, pp. 444–453, 2008.

[251] F. Taddei, E. Schileo, B. Helgason, L. Cristofolini, and M. Viceconti, "The material mapping strategy influences the accuracy of CT-based finite element models of bones: an evaluation against experimental measurements," *Med. Eng. Phys.*, vol. 29, no. 9, pp. 973–979, 2007.

[252] S. S. Hasan, J. M. Leith, B. Campbell, R. Kapil, K. L. Smith, and F. A. Matsen, "Characteristics of unsatisfactory shoulder arthroplasties," *J. Shoulder Elb. Surg.*, vol. 11, no. 5, pp. 431–441, 2002.

[253] G. Walch, P. Boileau, J.-F. Gonzalez, G. B. Alami, F. Baque, G. Walch, and P. Boileau, "Complications of unconstrained shoulder prostheses," *J. Shoulder Elb. Surg.*, vol. 20, pp. 666–682, 2011.

[254] T. J. Fox, A. Cil, J. W. Sperling, J. Sanchez-Sotelo, C. D. Schleck, and R. H. Cofield, "Survival of the glenoid component in shoulder arthroplasty," *J. Shoulder Elb. Surg.*, vol. 18, no. 6, pp. 859–863, 2009.

[255] J. Sarah, G. Sanjay, S. Sanjay, A. Carolyn, R. Emery, A. Andrew, and H. Ulrich, "Failure mechanism of the all-polyethylene glenoid implant," *J. Biomech.*, vol. 43, no. 4, pp. 714–719, 2010.

[256] W. H. Seitz, "Humeral Component Fixation," *Semin. Arthroplasty*, vol. 19, no. 1, pp. 64–73, 2008.

[257] J. Sanchez-sotelo, T. W. Wright, S. W. O. Driscoll, R. H. Cofield, and C. M. Rowland, "Radiographic Assessment of Uncemented Humeral Components in Total Shoulder Arthroplasty," vol. 16, no. 2, pp. 180–187, 2001.

[258] T. E. Harris, C. M. Jobe, and Q. G. Dai, "Fixation of proximal humeral prostheses and rotational micromotion," *J. Shoulder Elb. Surg.*, vol. 9, no. 3, pp. 205–210, 2000.

[259] M. Schnetzke, S. Coda, P. Raiss, G. Walch, and M. Loew, "Radiologic bone adaptations on a cementless short-stem shoulder prosthesis," *J. Shoulder Elb. Surg.*, vol. 25, no. 4, pp. 650–657, 2016.

[260] M. Schnetzke, S. Coda, G. Walch, and M. Loew, "Clinical and radiological results of a

cementless short stem shoulder prosthesis at minimum follow-up of two years," *Int. Orthop.*, vol. 39, no. 7, pp. 1351–1357, 2015.

[261] L. Peng, J. Bai, X. Zeng, and Y. Zhou, "Comparison of isotropic and orthotropic material property assignments on femoral finite element models under two loading conditions," *Med. Eng. Phys.*, vol. 28, no. 3, pp. 227–233, 2006.

[262] D. R. Suárez, J. C. van der Linden, E. R. Valstar, P. Broomans, G. Poort, P. M. Rozing, and F. van Keulen, "Influence of the positioning of a cementless glenoid prosthesis on its interface micromotions," *Proc. Inst. Mech. Eng. H.*, vol. 223, no. 7, pp. 795–804, 2009.

[263] I. Kalouche, J. Crépin, S. Abdelmoumen, D. Mitton, G. Guillot, and O. Gagey, "Mechanical properties of glenoid cancellous bone," *Clin. Biomech.*, vol. 25, no. 4, pp. 292–298, 2010.

[264] Zimmer, "Trabecular Metal Technology™. The Best Thing Next to Bone™," 2006.

[265] S. Gupta, F. C. T. Van Der Helm, and F. Van Keulen, "The possibilities of uncemented glenoid component - A finite element study," *Clin. Biomech.*, vol. 19, no. 3, pp. 292–302, 2004.

[266] N. Yamamoto, E. Itoi, H. Abe, H. Minagawa, N. Seki, Y. Shimada, and K. Okada, "Contact between the glenoid and the humeral head in abduction, external rotation, and horizontal extension: A new concept of glenoid track," *J. Shoulder Elb. Surg.*, vol. 16, no. 5, pp. 649–656, 2007.

[267] M. J. Bey, S. K. Kline, R. Zauel, P. A. Kolowich, and T. R. Lock, "In vivo measurement of glenohumeral joint contact patterns," *EURASIP J. Adv. Signal Process.*, vol. 2010, pp. 2–7, 2010.

[268] D. F. Massimini, J. J. P. Warner, and G. Li, "Glenohumeral joint cartilage contact in the healthy adult during scapular plane elevation depression with external humeral rotation," *J. Biomech.*, vol. 47, no. 12, pp. 3100–3106, 2014.

[269] M. Taylor and K. E. Tanner, "Fatigue failure of cancellous bone: a possible cause of implant migration and loosening," *J. Bone Joint Surg. Br.*, vol. 79, no. 2, pp. 181–182, 1997.

[270] J. Nagels, M. Stokdijk, and P. M. Rozing, "Stress shielding and bone resorption in shoulder arthroplasty," *J. Shoulder Elb. Surg.*, vol. 12, no. 1, pp. 35–39, 2003.

[271] M. P. Morwood, P. S. Johnston, and G. E. Garrigues, "Proximal ingrowth coating decreases risk of loosening following uncemented shoulder arthroplasty using mini-stem humeral components and lesser tuberosity osteotomy," *J. Shoulder Elb. Surg.*, vol. 26, no. 7, pp. 1246–1252, 2017.

[272] P. Leucht, J. Kim, R. Wazen, J. A. Currey, A. Nanci, B. Brunski, and J. A. Helms, "Effect of mechanical stimuli on skeletal regeneration around implants," *Bone*, vol. 40, no. 4, pp. 919–930, 2008.

[273] S. Goodman and P. Aspenberg, "Effect of amplitude of micromotion on bone ingrowth into titanium chambers implanted in the rabbit tibia," *Biomaterials*, vol. 13, no. 13, pp. 944–948, 1992.

[274] L. De Wilde, N. Dayerizadeh, F. De Neve, C. Basamania, and A. Van Tongel, "Fully uncemented glenoid component in total shoulder arthroplasty," *J. Shoulder Elb. Surg.*, vol. 22, no. 10, pp. 1–7, 2013.

[275] G. Merolla and G. Merolla, "Total shoulder arthroplasty with a second- generation tantalum trabecular metal-backed glenoid component: Clinical and radiographic outcomes at a mean follow-up of 38 months," *bone Jt. J.*, vol. 98–B, 2016.

[276] M. D. Budge, E. M. Nolan, M. H. Heisey, K. Baker, and J. M. Wiater, "Results of total shoulder arthroplasty with a monoblock porous tantalum glenoid component: A prospective minimum 2-year follow-up study," *J. Shoulder Elb. Surg.*, vol. 22, no. 4, pp. 535–541, 2013.

[277] A. Vidil, P. Valenti, F. Guichoux, and J. H. Barthas, "CT scan evaluation of glenoid component fixation: A prospective study of 27 minimally cemented shoulder arthroplasties," *Eur. J. Orthop. Surg. Traumatol.*, vol. 23, no. 5, pp. 521–525, 2013.

[278] J. E. Moravek, M. D. Kurdziel, K. C. Baker, and J. M. Wiater, "Biomechanical Evaluation of All-Polyethylene Pegged Bony Ingrowth Glenoid Fixation Techniques on Implant Micromotion," *Am. J. Orthop.*, no. June, pp. E211–E216, 2016.

[279] S. Urgery, I. Ncorporated, A. Papadonikolakis, N. Mb, and M. Fa, "Failure of the Glenoid Component in Anatomic Total Shoulder Arthroplasty," *J. Bone Jt. Surg.*, vol. 95–A, pp. 2205–2212, 2013.

[280] R. B. Litchfield, M. D. McKee, R. Balyk, S. Mandel, R. Holtby, R. Hollinshead, D. Drosdowech, S. E. Wambolt, S. H. Griffin, and R. McCormack, "Cemented versus uncemented fixation of humeral components in total shoulder arthroplasty for osteoarthritis of the shoulder: A prospective, randomized, double-blind clinical trial-A JOINTs Canada Project," *J. Shoulder Elb. Surg.*, vol. 20, no. 4, pp. 529–536, 2011.

[281] D. J. Casagrande, D. L. Parks, T. Torngren, M. A. Schrumpf, S. M. Harmsen, T. R. Norris, and J. D. K. Ii, "Radiographic evaluation of short-stem press-fit total shoulder arthroplasty : short-term follow-up," *J. Shoulder Elb. Surg.*, vol. 25, no. 7, pp. 1163–1169, 2016.

[282] National Joint Registry, "National Joint Registry for England, Wales Northen Ireland and Isle of Man. 12th Annual Report," 2015.

[283] P. J. Prendergast and S. a. Maher, "Issues in pre-clinical testing of implants," *J. Mater. Process. Technol.*, vol. 118, no. 1–3, pp. 337–342, 2001.

[284] M. P. Noyes, B. Meccia, and E. E. Spencer, "Five- to ten-year follow-up with a partially cemented all-polyethylene bone-ingrowth glenoid component," *J. Shoulder Elb. Surg.*, vol. 24, no. 9, pp. 1458–1462, 2015.

[285] M. D. Lazarus, K. L. Jensen, C. Southworth, and F. a Matsen, "The radiographic evaluation of keeled and pegged glenoid component insertion," *J. Bone Joint Surg. Am.*, vol. 84–A, no. 7, pp. 1174–1182, 2002.